Disease-associated Balanced Chromosomal Rearrangements:

Molecular characterisation of two cases with a review of the impact of published cases in human genetic research

Louise Harewood

Thesis submitted for the degree of Doctor of Philosophy

University of Edinburgh

MRC Human Genetics Unit

December 2005

Abstract

Disease-associated balanced chromosomal rearrangements (DBCRs) are large-scale alterations in normal genomic sequence, which occur without copy number change in a phenotypically abnormal individual. Complete ascertainment of published DBCRs was attempted via recursive searches of the literature. 775 cases were identified with 1672 breakpoints and 406 different phenotypes. Physical mapping of DBCR breakpoints has elucidated the genetic basis of Mendelian disorders in 29 cases and was the first indication of a subsequently verified disease locus in a further 30 cases. Two interesting DBCR cases, which had no cell-lines or fixed cell suspensions, were available for study: Case 1 had a t(2;12)(p25.1;q23.3) translocation associated with upper limb peromelia and lower limb phocomelia; case 2 had a t(1;2)(q41;p25.3) associated with lethal bilateral renal adysplasia. Archival paraffin embedded tissue sections were available for both cases. A fluorescent *in-situ* hybridisation (FISH) method was developed to enable physical mapping on dissociated nuclei from these sections. In case 1, the 2p25 breakpoint was found to interrupt the *ROCK2* gene, which, on the basis of the phenotype of null mice, was considered to be a poor candidate for the peromelia/phocomelia phenotype. The 12q23.3 breakpoint lay 0-25 kb from the 5′ end of the *CMKLR1* gene, which encodes a chemokine-like receptor, the sole ligand for which is encoded by the retinoic acid responsive gene, *RARRES2*. Site and stage-specific expression of both the receptor and the ligand in the developing limb bud suggested that *CMKLR1* was a good candidate for a causative gene. A phenotypically similar case was screened for mutations in *CMKLR1* and a candidate regulatory region, but none could be identified. A mouse model is being

developed to further elucidate the developmental role of this gene. In case 2, the 2p25.3 breakpoint mapped to a gap in the genome sequence. No good candidate gene could be identified in the vicinity of this gap. The breakpoint at 1q41 interrupted the *USH2A* gene, homozygous null mutations in which cause a well-characterised disorder with retinal degeneration and deafness but no kidney abnormalities. The only other transcript in this gene-poor region was *ESRRG*, encoding a nuclear steroid hormone receptor family member. Esrrg showed expression in the ureteric bud and collecting ducts of the developing kidney of mouse embryos. This gene appeared to be a very good candidate, although no point mutations, deletions or protein abnormalities could be detected in six cases of lethal renal adysplasia or four families with dominant renal adysplasia. DBCRs continue to provide an excellent resource for the discovery of new Mendelian phenotypes and are opening new avenues of investigation in experimental developmental biology.

Acknowledgements

Sincerest thanks to all those that have helped throughout the three years of this PhD. Special thanks go to David FitzPatrick for all his support and for letting me do things my own way and to Jude Fantes for the innumerable FISH discussions. Thanks also to Ann Hever for the numerous cups of tea and 'quick pints' after work, to Jacqui Ramsay for keeping me sane in the lab and to everyone else who has made the last few years bearable and sometimes even fun!

This PhD would not have been possible without the unfluctuating support of my family: thanks to my parents for always believing in me, to Guy for giving me the determination to beat him at everything, and to Liz - things may not have always been good but what are sisters for if not to make life hell?! Thanks also to Nana for the milky coffee and eternal support and to Naomi and Simon for allowing me to live in rent free luxury for the last few months - I shall be forever indebted.

Finally, to those that did not make it to see this. You are always in my thoughts and I can only hope that you would have been proud.

List of Figures

List of Tables

Abbreviations

AER	Apical ectodermal ridge
ALMS	Alstrom syndrome
AMV-RT	Avian Myeloblastosis Virus Reverse Transcriptase
AT	Ataxia telangiectasia
BAC	Bacterial Artificial Chromosome
bp	Base pairs
BCIP	5-bromo-4-chloro-3-indolyl phosphate
BSA	Bovine Serum Albumin
CCD	Charge Couple device
CdCS	Cri-du-chat syndrome
CdLS	Cornelia de Lange syndrome
cDNA	Complementary DNA
CGH	Comparative genomic hybridisation
Chr	Chromosome
cM	Centimorgan
CMKLR1	Chemokine like receptor 1
CMT1A	Charcot-Marie-Tooth type 1A disease
CO_2	Carbon dioxide
DAPI	4',6-Diamidino-2-phenylindole
DBCR	Disease associated chromosomal rearrangement
DEPC	Diethyl cyanophosphonate
der	Derived chromosome
dHPLC	Denaturing high performance liquid chromatography
Dig	Digoxigenin
DMD	Duchenne muscular dystrophy
DMSO	Dimethyl sulfoxide
DNA	DeoxyRibonucleic Acid
dNTPs	deoxynucleotide triphosphates (A-adenine, G-guanine, C-cytosine, T-thymine)
dpc	Days post *coitum*
DSB	Double strand break
DTT	Dithiothreitol
dUTP	deoxyuridine-triphosphate
ECR	Evolutionary conserved regions
EDTA	Ethylenediaminetetraacetic acid
ERE	Estrogen response element
ERRE	Estrogen related response element
ES	Embryonic stem
ESRRG	Estrogen related receptor gamma
EST	Expressed sequence tag
EtOH	Ethanol
FGF	Fibroblast growth factor
FISH	Fluorescent *In-Situ* Hybridisation
FITC	Fluorescein isothiocyanate
G-band	Giemsa-band

HCl	Hydrochloric acid
HIV	Human immunodeficiency virus
HNPP	Hereditary neuropathy with liability to pressure palsies
HP-AP	Human placental alkaline phosphatase
HR	Homologous recombination
IHC	Immunohistochemistry
ILS	Isolated lissencephaly
Kb	Kilobases
KCl	Potassium Chloride
LCL	Lymphoblastoid Cell Line
LCR	Low copy repeat
Lmbr1	Limb region 1
M	Molar
Mb	Megabase
MDS	Miller-Dieker syndrome
MeOH	Methanol
$MgCl_2$	Magnesium Chloride
mRNA	Messenger Ribonucleic Acid
NaCl	Sodium Chloride
NAHR	Non allelic homologous recombination
NaOAc	Sodium Acetate
NaOH	Sodium Hydroxide
NBT	Nitro blue tetrazolium chloride
NHEJ	Non-homologous end joining
OMIM	Online Mendelian inheritance in man
PAC	P1 derived Artificial Chromosome
PATRR	Palindromic AT-rich repeats
PBS	Phosphate buffered saline
PCR	Polymerase Chain Reaction
PD	Proximodistal
PFA	Paraformaldehyde
PPARs	Peroxisome proliferator-activated receptors
PPD	Preaxial polydactyly
PZ	Progress zone
RA	Retinoic acid
RFLP	Restriction fragment length polymorphism
RNA	Ribonucleic Acid
RNAi	RNA Interference
RT-PCR	Reverse Transcriptase Polymerase Chain Reaction
RTS	Rubinstein-Taybi syndrome
SDS	Sodium Dodecyl Sulphate
SHH	Sonic hedgehog
SIV	Simian immunodeficiency virus
SMS	Smith-Magenis syndrome
SNP	Single Nucleotide Polymorphism
SSC	Saline-Sodium Citrate
ssDNA	Single-stranded DNA
Ssq	Sasquatch

TBE buffer	Tris/Borate/EDTA buffer
TE	Tris/EDTA buffer
Tm	Melting temperature
YAC	Yeast Artificial Chromosome
ZPA	Zone of polarising activity

Author's Declaration

I declare that I am the sole author of this thesis and that it contains no material that has been accepted for the award of any other degree or diploma in any university.

To the best of my knowledge and belief this thesis contains no material previously published by any other person except where due acknowledgement has been made.

Louise Harewood

December 2005

1: Introduction

1.1. Chromosomal Abnormalities

Human chromosomal abnormalities occur in many different forms and can be inherited from either parent (familial) or may occur during gametogenesis or in the early mitotic divisions that follow fertilisation (*de novo* (new) abnormalities).

All chromosomal abnormalities can be placed into two broad groups: numerical, involving the gain or loss of whole chromosomes, and structural, in which the chromosomes have undergone rearrangement. These groups are not exclusive and individuals can possess abnormalities from both groups. The most common constitutional numerical abnormality is Down syndrome, which involves the gain of a whole chromosome 21 (OMIM 190685). This is known as a trisomy syndrome as there are three copies of a chromosome, instead of the normal two. There are only two other autosomal (i.e. not chromosome X or Y) trisomies that are commonly compatible with live births; these involve chromosomes 13 (Patau syndrome) and 18 (Edwards syndrome). Both are extremely severe phenotypes with over 90 % of children reported to die within the first year of life, the median age of death being around 10 days [1].

No other full autosomal trisomies are viable to birth, although mosaic trisomies can occur for chromosomes such as 8, 16 and 22. Trisomies for most other autosomes result in miscarriage, accounting for between 35 % and 41 % of all spontaneous abortions [2;3] . Trisomies for chromosomes 1 or 19 are rarely observed, even in miscarried embryos. This is thought to be due to the particularly high gene density of these autosomes.

Constitutional autosomal monosomies (one copy of a chromosome instead of two) are very rarely viable. Numerical abnormalities of the X and Y chromosomes are generally much better tolerated than for the autosomes.

Structural abnormalities are caused by the occurrence of breaks or recombinations in the DNA, leading to the normal sequence of the chromosomes being altered. The different types of structural rearrangements will be discussed in more detail in section 1.4.

1.2. DNA Breakage and Repair

1.2.1. Breakage in Somatic Cells

Chromosome breaks occur as a result of double strand breaks (DSBs) in the genomic DNA. These breaks differ from other types of DNA damage in that they affect both strands of the DNA helix and there is therefore no undamaged strand to use as a template for repair. DSBs can occur as a direct result of damage from mutagens such as chemicals or radiation or can occur spontaneously due to errors in replication as the cell passes through the cell cycle. An example of this can be seen in bacterial cells, where single strand breaks have been shown to cause the collapse of a replication fork and the formation of a DSB [4]. It has been estimated that at least 1 % of single strand breaks escape repair in normal human cells and this results in around 50 DSBs per cell per cell cycle [5].

DSBs are clearly detrimental to proper genome duplication and eukaryotic cells have developed extensive checkpoints to prevent damaged cells from starting DNA replication (the G1/S checkpoint), from continuing through replication (the

intra S checkpoint) or initiating mitosis (the G2/M checkpoint) [6]. The biological consequences of errors in these checkpoints can be seen in the human syndrome, ataxia telangiectasia (AT). This is characterised by a high incidence of chromosomal translocations and frequent malignancies in lymphoid cells. Cells in individuals with AT have errors in several of these checkpoint mechanisms, allowing damaged cells to continue through replication and onto mitosis.

Correctly functioning cell cycle checkpoints will detect any broken chromosome ends and will, where possible, repair them. This is generally performed by capping the end with a telomere or by rejoining any broken ends. If this is successful, the cell can then pass through the checkpoints and continue to mitosis. However, errors in this process can produce chromosomes that have no centromere (acentric) or with two centromeres (dicentric). These will not segregate in a stable manner through mitosis and will subsequently be lost.

Even chromosomes with a single centromere and stable mitotic transmission may have gained or lost genomic material or the broken ends of the wrong chromosomes may have been re-joined. This is how somatic structural abnormalities can arise.

1.2.2. Breaks during Meiosis

Although DSBs are potentially detrimental to the genomic integrity and survival of cells in mitosis, they do occur normally during processes such as DNA replication, immune system development and meiosis. Recombination between homologous chromosomes in meiosis is essential for the generation of genetic diversity and proper chromosome segregation and is a central event in almost all

organisms [7]. In meiosis, DSBs are generally repaired via homologous recombination, although non-homologous end joining can also occur.
The absence of meiotic recombination in yeast cells results in the erroneous segregation of homologues and production of aneuploid gametes, giving rise to progeny that are either inviable or defective [8].

1.2.2.1. Meiotic DSB Repair by Homologous Recombination

The majority of the information on DSB repair in meiosis has come from studies in the yeast *Saccharomyces cerevisiae* or *Schizosaccharomyces pombe* but the process appears to be well conserved in eukaryotes [9].

Meiotic recombination is initiated by the formation of DSBs by the topoisomerase II-like protein Spo11 and at least nine other gene products [10]. The repair of these lesions results in the formation of connections, or crossovers, between homologous chromosomes. The 5′ ends of the strands are resected to produce 3′ ended single strands, which can then invade a homologous DNA duplex, generally a homologous chromosome. This results in the formation of a displacement loop (D-loop), which anneals to the non-invading strand. DNA synthesis occurs and a structure is formed containing two Holliday junctions. Cleavage of these by DNA endonucleases results in recombinant molecules in which the flanking DNA sequences have either been retained (non-crossover or parental) or have been exchanged between the homologous chromosomes or sister chromatids (crossover or non-parental). The type of molecule produced is dependent on the orientation of the cleavage of each of the Holliday junctions, as these can be resolved by cleaving either the inner or outer strands. If both junctions are cleaved in the same orientation,

there will be no crossover, whereas a crossover will occur if the two cleavage events are in different orientations (see figure 1.1).

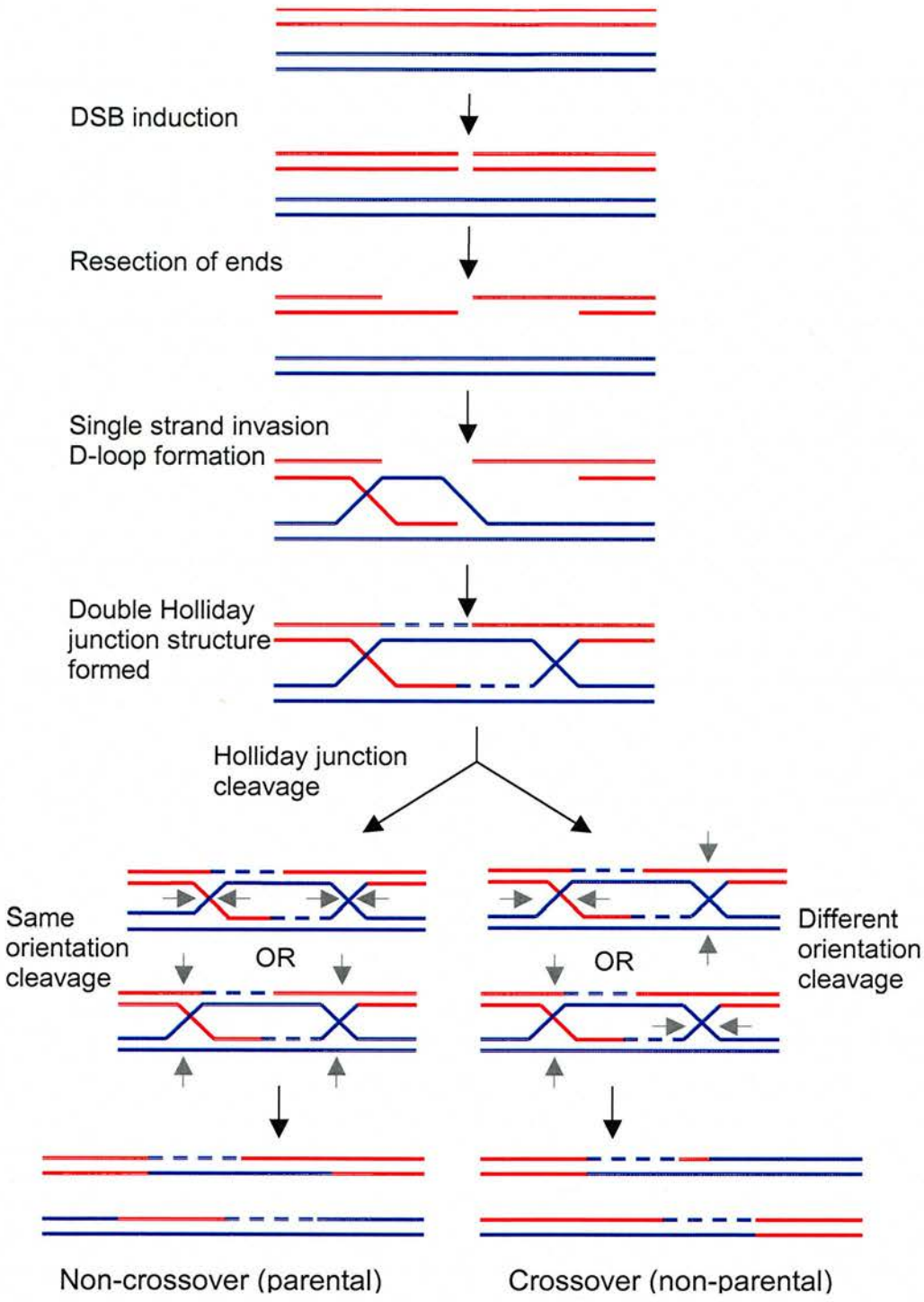

Figure 1.1. Homologous recombination.

Red lines indicate the DNA strands in which the DSB occurs. Blue lines indicate the homologous DNA that serves as a template for repair. Grey arrows indicate the cleavage of the Holliday junctions. See text for details.

1.2.2.2. Non-Homologous End Joining in Meiosis

Homologous recombination is the principal DSB repair mechanism during meiosis but non-homologous end joining (NHEJ) can also occur, albeit at a lower frequency. Studies in yeast have shown that proteins required for NHEJ are present at much lower concentrations in meiotic cells than in mitotic cells, reducing the capacity of NHEJ in cells undergoing meiosis [11].

NHEJ is a more prominent mechanism in mitotic cells and will be discussed in more detail in section 1.2.3.2.

1.2.3. Mitotic DSB Repair

1.2.3.1. Mitotic Homologous Recombination

Homologous recombination (HR) occurs in both mitosis and meiosis and the mechanisms are similar. DSBs occurring as a result of damage to the cell are repaired in largely the same way as those induced by Spo11. However, to ensure the greatest number of recombination events in meiosis the template used for repair is generally a homologous chromosome [12]. The opposite seems to be true in mitotic cells, where the sister chromatid will be used, where possible, in order to minimise variation [13]. The number of crossover events occurring in the recombinant molecules also seems to be reduced in mitotic cells, with crossovers occurring between 100 to 1000 times less frequently that during meiosis [14]. Again, this is most likely to allow the DSB to be repaired as conservatively as possible.

1.2.3.2. Non-Homologous End Joining

Whereas, homologous recombination appears to be the primary DSB repair mechanism in yeast cells, higher eukaryotes, including mammals, preferentially employ non-homologous end joining (NHEJ) over HR [15]. NHEJ results in the ligation of broken ends, irrespective of the level of sequence homology and is a relatively error-prone mechanism that can result in the addition or deletion of nucleotides around the breakpoints. Three NHEJ mechanisms, namely re-ligation, fill in and deletion, are outlined in figure 1.2. With re-ligation, the complementary broken ends of the DNA are merely re-joined, resulting in a perfect repair of the sequence. The fill in and deletion mechanisms both occur after regions of microhomology on the broken ends (one or several bases pairs) become misaligned. If the misalignment results in gaps, the nucleotides are filled in using the other strand as a template, if an overlap of the ends occurs, the excess bases are removed, resulting in a deletion. Deletion is the most common type of misrepair in both yeast and mammalian cells, with deletions extending in both directions from the DSB site [16]. The occurrence of several DSBs in the same cell can result in the wrong ends being re-joined and structural chromosomal rearrangements such as translocations and inversions can be produced (see section 1.4).

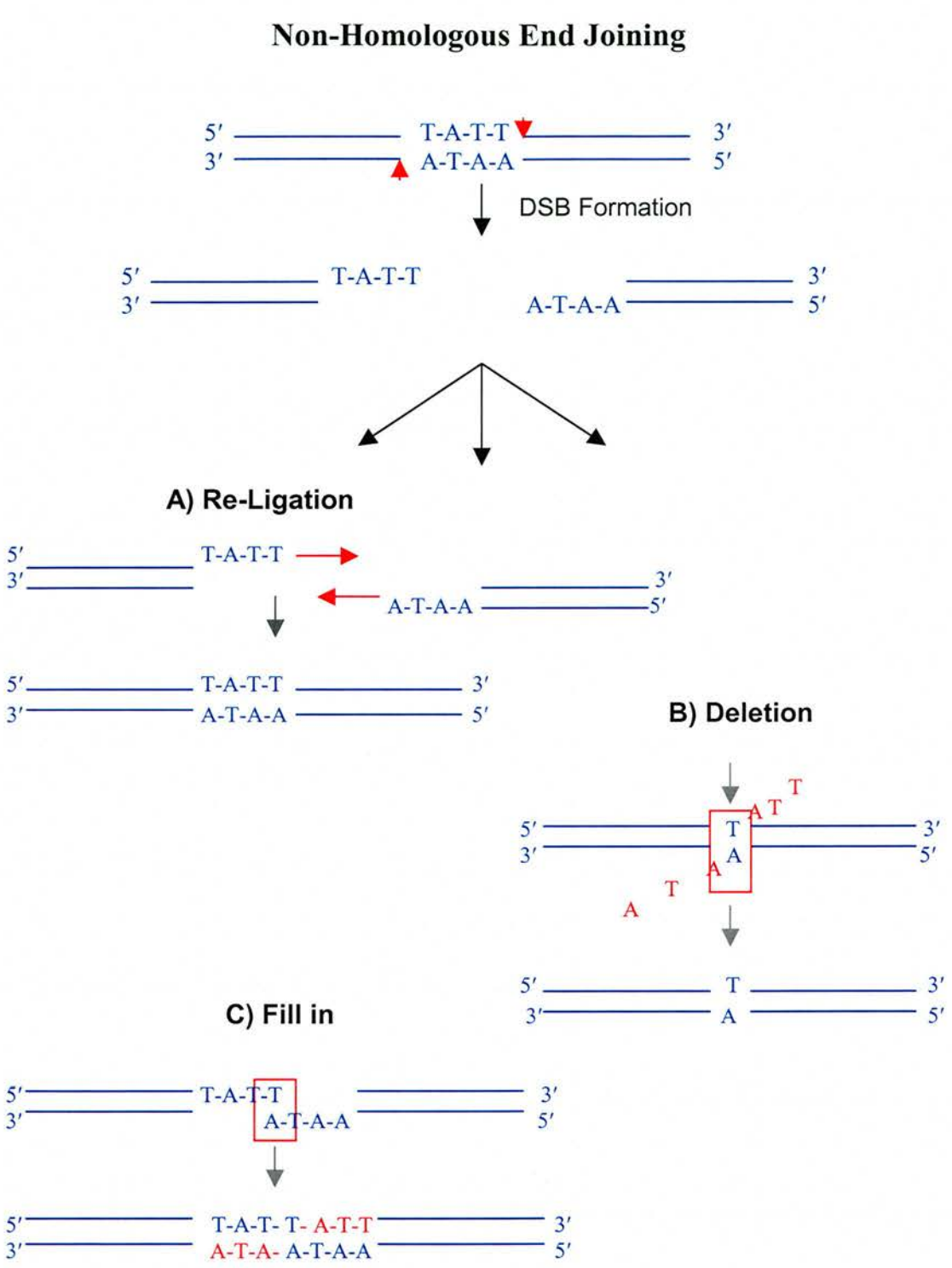

Figure 1.2. Non-Homologous End Joining.

Three mechanisms of non-homologous end joining showing: A) non-erroneous repair via re-ligation, B) nucleotide deletion and C) the addition of nucleotides. See text for details.

1.3. Genome Architecture

Although rare, the breakpoints of some structural chromosomal abnormalities have been shown to cluster within specific genomic regions [17], suggesting that the breaks do not occur at random. Although this may be partly explained by certain genomic regions being haplo- or triplo-lethal, it also suggests that there are regions of the genome that are unstable and thereby predisposed to rearrangements. This instability suggests an underlying structure, or architecture, of the genome that can mediate the production of chromosomal rearrangements via DSB repair mechanisms. Some examples are outlined below.

1.3.1. Non-Homologous End Joining and Palindromic Repeats

The most common recurrent abnormality in humans is the constitutional balanced translocation between chromosomes 11 and 22, the t(11;22)(q23;q11). Carriers of this translocation do not, in general, show a phenotype and it is often only identified after the birth of an offspring that has inherited an unbalanced product.

Children that inherit the derived chromosome 22 (der(22)) have a disorder known as supernumerary der(22) syndrome, recently re-named Emanuel syndrome (OMIM 609029) after Dr. Beverly Emanuel, one of the first to describe the disorder [18]. These children have a partial trisomy of chromosomes 22 and 11 and show a distinctive phenotype consisting of severe mental retardation, ear anomalies, cleft or high arched palate, head, heart and kidney abnormalities.

The breakpoints on both chromosomes 11 and 22 were cloned from 40 independent t(11;22) families and found to lie within palindromic AT-rich repeats

(PATRRs) [19;20], which are predicted to form hairpin or cruciform structures. Sequencing of the chromosome 11 PATRR in normal individuals showed that it was 445 bp long and consisted of a nearly perfect palindromic sequence and thereby formed a symmetrical hairpin. Further mapping of this region led to the discovery that the breakpoints were located at the tip of the hairpin, which is sensitive to cleavage by nucleases [21]. If this cleavage occurs on both strands, a DSB can occur.

This led Kurahashi *et al* [22] to suggest that the initiating step in the formation of the t(11;22) translocation may be a double stranded DNA break mediated by the hairpin-nicking activity. If two DSBs occur in the same cell, a translocation can be generated by non-homologous end joining (NHEJ). This has also been shown in experiments using Saccharmyces cerevisiae where translocations occur after the induction of two DSBs on different chromosomes [23].

The 22q11 region that is involved in the recurrent t(11;22) translocation has been labelled a 'hotspot' for chromosomal rearrangements with as many as 1 in 3000-4000 live births having a deletion, duplication or translocation involving that region [24]. As well as being involved in the t(11;22), the palindromic 22q11 region is also involved in the recurrent t(17;22), which is associated with neurofibromatosis type 1, the non-recurrent t(4;22) [25] and the ependymoma-associated t(1;22). As with chromosome 11, breakpoints on the partner chromosomes at 17q11 and 4q35 were also found to be within a palindromic repeat, although the 1p21.2 breakpoint did not appear to be. This may suggest that translocations occur between chromosomal regions that have similar characteristics, such as the ability to form palindromic hairpins or cruciform structures, but not necessarily sequence homology [26].

1.3.2. Homologous Recombination and Low Copy Repeats

The 22q11 breakpoint of the recurrent t(11;22) localises to one of the low copy repeats (LCRs) that have been identified on chromosome 22 [27;28]. LCRs, also known as segmental duplications or duplicons, are estimated to make up approximately 5-10 % of the human genome [29]. They usually consist of blocks of DNA between 10 and 400 kb in size, with over 97 % sequence identity and are thought to have arisen through duplication of genomic segments [30].

LCRs are unevenly distributed throughout the genome and are often clustered in pericentromeric and subtelomeric regions. The reason for this is unknown but it may be that these regions have a greater tolerance for the introduction of new genetic material or suppressed recombination [31]. However, several LCRs have only been identified by mapping rearrangement breakpoints, so there may well be further, currently unidentified, LCRs dispersed throughout the genome.

LCRs facilitate both inter- and intra-chromosomal rearrangements through non-allelic homologous recombination (NAHR). NAHR between LCRs that are on the same chromosome and lie in the same orientation will cause deletions and duplications, whereas those in the opposite orientation can produce inversions. If NAHR occurs between LCRs on different chromosomes, reciprocal translocations can occur [32].

NAHR has been shown over recent years to be a major mechanism in human disease, with many diseases resulting from recurrent DNA rearrangements between unstable genomic regions (see table 1.1). These diseases have been termed 'Genomic Disorders' and are defined as "conditions that result from DNA rearrangements due to regional genomic architecture" [33].

Table 1.1: A table of Genomic Disorders

Disorder	Inheritance	OMIM[1]	Chromosome Band	Gene	Rearrange-ment
Alpha-thalassemia	AD	141800	16p13.3	*HBA*	del
Angelman syndrome	AD	105830	15q11.2-q13	*UBE3A*	del
Bartter syndrome type 3	AR	607364	1p36	*CLCNKB*	del
Beta-Thalassemia	AR	141900	11p15.5	*HBB*	del
Charcot-Marie-Tooth, Type 1A	AD	118220	17p12	*PMP22*	dup
Congenital adrenal hyperplasia due to 21-hydroxylase deficiency	AR	201910	6p21.3	*?*	del
CYP2D6 pharmacogenetic trait	AR	124030	22q13.1	*CYP2D6*	del/dup
DiGeorge/VCFS	AD	188400/ 192430	22q11.2	*TBX1*	del
Emery-Dreifuss muscular dystrophy	XL	310300	Xq28	*EMD*	del/dup/inv
Facioscapulohumeral muscular dystrophy	AD	158900	4q35	*?*	del
Gaucher Disease	AR	231000	1q21	*GBA*	del
Haemophilia A	XL	306700	Xq28	*F8*	inv
Hereditary neuropathy with liability to pressure palsies (HNPP)	AD	162500	17p12	*PMP22*	del
Hyperaldosteronism, familial, type 1	AD	103900	8q21	*CYP11B1/ CYP11B2*	dup
Ichthyosis, X-linked	XL	308100	Xp22.32	*STS*	del
Incontinentia Pigmenti	XL	308300	Xq28	*IKK-Gamma*	del
Kabuki syndrome[2]	AD	147920	8qp22-p23.1		dup
Mucopolysaccharidosis II (Hunter syndrome)	XL	309900	Xq28	*IDS*	inv/del
Nephronophthisis 1	AR	256100	2q13	*NPHP1*	del
Neurofibromatosis type 1	AD	162200	17p11.2	*NF1*	del
Nonobstructive spermatogenic failure	YL	415000	Yq11.2	*DBY, USP9Y, AZF1*	del
Pituitary dwarfism 1	AR	262400	17q23.3	*GH1*	del
Polycystic kidney disease 1	AD	601313	16p13.3	*PKD1*	
Prader-Willi syndrome	AD	176270	15q11.2-q13	*SNRPN, NDN*	del
Red/Green coulourblindness	XL	303800/ 303900	Xq28	*RCP/ GCP*	del
Shwachman-Diamond syndrome[3]	AR	260400	7q11.21	*SBDS*	
Smith-Magenis syndrome	AD	182290	17p11.2	*RAI1*	del
Sotos syndrome[4]	Sporadic	117550	5q35	*NSD1*	del

Spinal muscular atrophy, type 1	AR	253300	5q13.2	*SMN1*	inv/dup
Split-hand/foot malformation 3[5]	Unknown	600095	10q24	*SHFM3*	dup
Williams-Beuren syndrome	AD	194050	7q11.23	*ELN, LIMK1, CYNL2*	del/inv

AD - Autosomal dominant, AR - Autosomal recessive, XL - X-linked, YL - Y-linked
del - deletion, dup - duplication, inv – inversion

[1]OMIM - http://www.ncbi.nlm.nih.gov/entrez/query.fcgi?db=OMIM
[2] [34], [3] [35], [4] [36], [5] [37]
All others: [38]

One genomic region that has been extensively studied is 17p11.2-p12. This region is gene rich and highly unstable and is rearranged in a variety of structural abnormalities that are associated with diseases such as Charcot-Marie-Tooth type 1A disease (CMT1A) (OMIM 118220), hereditary neuropathy with liability to pressure palsies (HNPP) (OMIM 162500), Smith-Magenis syndrome (SMS) (OMIM 182290) and the more recently described dup(17)(p11.2p11.2) syndrome [39;40].

CMT1A is caused by duplication of an approximately 1.4 Mb region on chromosome 17p12. Deletion of the same region causes another disease, namely HNPP. This 1.4 Mb region is flanked by two LCRs that are approximately 24 kb in size and lie in the same orientation on the chromosome. The duplication or deletion of this region is due to the LCRs acting as substrates for NAHR [41].

The same LCR/NAHR mechanism also causes Smith Magenis and the dup(17)(p11.2p11.2) syndromes. Again, these are caused by the deletion (SMS) or duplication (dup(17)) of the same approximately 4 Mb genomic region on 17p11.2. This region is flanked by two LCRs (~260 kb and ~190 kb) and there is a third positioned in the middle in the opposite orientation. Smaller deletions have also been identified in SMS with breakpoints within this middle LCR [42].

The breakpoints of non-recurrent abnormalities have also been found to associate with LCRs. A study looking at unusual sized deletions and reciprocal translocations with breakpoints in the proximal part of chromosome 17p showed that 64 % of deletion breakpoints in 17p11.2 mapped within LCRs, whereas only 13 % of translocation breakpoints were within an LCR. However, they did find that 63 % of translocation breakpoints from the region mapped within, or immediately adjacent to, the centromere [43]. This may be due to instability caused by variations in heterochromatin condensation.

Another study of non-recurrent rearrangements, this time involving the 22q11 region, showed that 57 % (8/14) of translocation breakpoints mapped within LCRs and all of the breakpoints on partner chromosomes mapped to the most telomeric bands [44]. After performing a literature search, Spiteri *et al* also stated that 57 % of 22q11.2 translocations involved the most telomeric bands of random partner chromosomes and 39 % of reciprocal translocations involving any chromosomes had one breakpoint within a telomeric band [45].

This suggests that there is an increased frequency of rearrangements involving 22q11.2 and a telomeric band of another chromosome, as opposed to a random distribution over all chromosome bands. It also appears that telomeric regions are more prone to rearrangements in general. As stated previously, this may be due to these areas having a greater tolerance for the introduction or deletion of genetic material. It is possible that the deletion or rearrangement of more proximal areas would be detrimental to survival or development.

The involvement of centromeres, telomeres and pericentromeric regions in both recurrent and non-recurrent rearrangements suggests that genome architecture consists of much more than just LCRs or palindromic AT-rich repeats. Although non-allelic homologous recombination (NAHR) and non-homologous end joining (NHEJ) have been discussed in detail here, these are unlikely to be the only mechanisms that facilitate chromosomal rearrangements. The study of further recurrent and non-recurrent abnormalities is likely to identify further features of genome architecture and elucidate new rearrangement mechanisms.

1.4. Structural Chromosomal Abnormalities

The type of structural abnormality that occurs in a cell is dependent on the number of chromosome breaks and whether they occur in one or more chromosomes. If one break occurs, the result will generally be a terminal deletion as the end is capped with a telomere. However, if the break occurs within the centromeric region, an isochromosome can be formed, containing either both long or both short arms. The exact mechanism of isochromosome formation is unknown but it has been proposed that they are caused by either misdivision of the centromere or sister chromatid exchange [46;47].

If two breaks are on the same chromosome, the segment between them can be deleted, inverted, or in some cases, duplicated. Ring chromosomes can also be formed in which the broken ends of the same chromosome join together to create a circular structure, with the loss of the end pieces. Breaks in the arms of different chromosomes can also result in deletions as well as translocations. The latter can be

reciprocal (or balanced) where the material from one chromosome joins onto the other and vice versa, resulting in no apparent loss of genetic material; or unbalanced, where part of one or both of the chromosomes is lost.

As the number of breaks increase, so does the possible complexity of the abnormalities. When more than two breaks occur, insertions can also happen, where a section of one chromosome is inserted elsewhere into the genome, whether it be into the same chromosome or a different one.

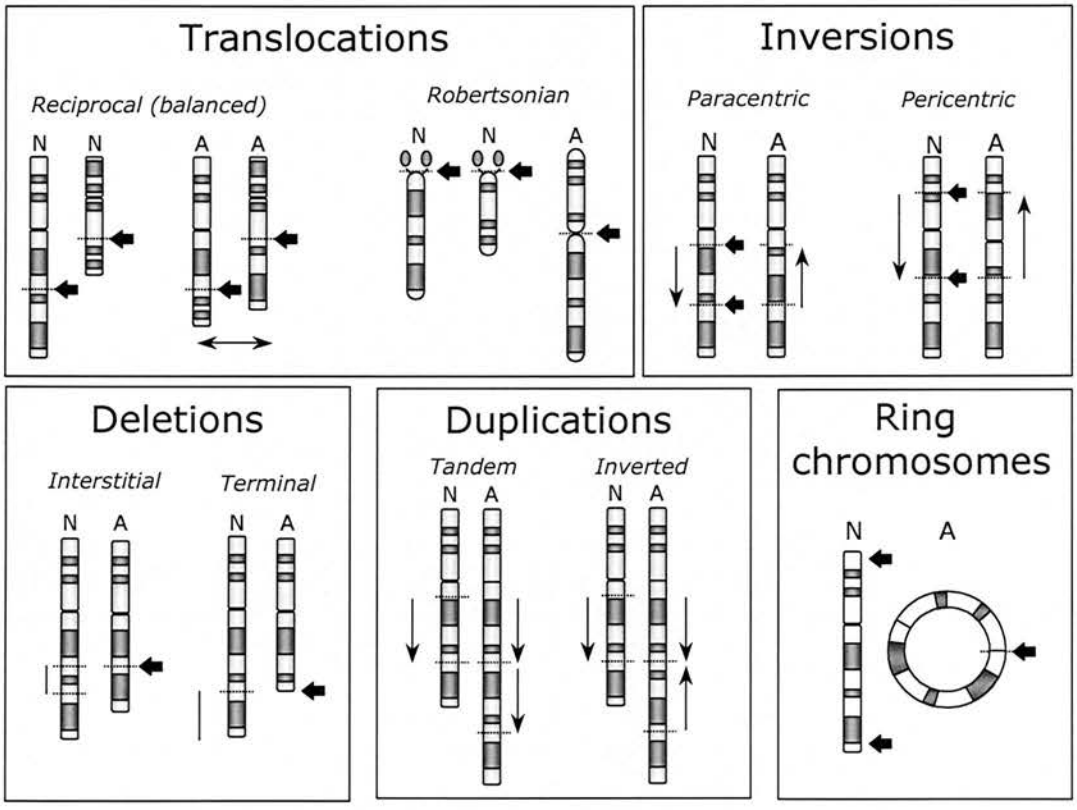

Figure 1.3. Structural chromosomal rearrangements.

A figure showing different types of structural chromosomal rearrangements. Filled arrows indicate the location of the breakpoints. Long arrows indicate the orientation of the chromosome fragment, bars the deleted regions. N indicates the normal chromosome, and A the abnormal.

1.4.1. Balanced/Unbalanced Structural Rearrangements

All chromosome abnormalities can be placed into two broad groups, unbalanced and balanced. Unbalanced structural rearrangements are those in which there is a gain or loss of genetic material as compared to a prototypical diploid human genome, for example, deletions, duplications and ring chromosomes. Balanced abnormalities on the other hand, have no apparent change in the amount of genetic material, although some rearrangement has occurred.

Unbalanced chromosome abnormalities tend to be associated with a phenotype, which can often be severe or fatal. This is not surprising as a number of genes may be lost or, more rarely, duplicated as a result of the rearrangement.

One example of an unbalanced phenotype is cri-du-chat (cat cry) syndrome (CdCS) (OMIM 123450). This is thought to be one of the more common deletion phenotypes with an incidence of approximately 1 in 20,000 to 1 in 50,000 births [48]. One of the most characteristic features of the syndrome in newborns is the high-pitched, cat-like cry, hence the name. Other physical features include distinctive head and facial abnormalities, such as a small head (microcephaly), round face, wide set eyes, low set ears, small jaw (micrognathia), and severe mental and psychomotor retardation.

The disorder is caused by a deletion of the short arm of chromosome 5 (5p15.2), which encompasses a number of genes, including the telomerase reverse transcriptase gene (TERT, OMIM 187270), deletion of which is suggested to be involved in the phenotype [49]. The majority of CdCS patients (~80 %) have a *de novo* deletion that can vary in size from those just encompassing band 5p15.2, to deletions of the whole short arm. Approximately 10 % of patients have an

unbalanced rearrangement that has been caused by malsegregation of a parental translocation and the rest occur as a result of rare cytogenetic aberrations [50]. The majority of the deletions seem to occur on the paternally inherited chromosome 5 [51].

The genes that cause CdCS are not known. Mapping of deletions has led to a critical region for CdCS being assigned to the region of 5p15.2-p15.3. Deletions of this region produce the typical phenotype, whilst patients with deletions that do not include 5p15.2 have been reported that do not show classical CdCS or were normal [52]. Molecular analysis has led to the identification of two distinct regions for elements of the CdCS phenotype: one for the cat-like cry in 5q15.3 and another for the facial dysmorphism and the developmental delay in 5p15.2 [53]. It has also been noted that the size of the deletion does not correlate with the level of developmental delay [54].

CdCS is just one example of an unbalanced chromosomal rearrangement being associated with a clinical phenotype. There are many examples with differing levels of chromosomal loss or gain affecting many different regions of the genome.

Individuals with balanced chromosomal rearrangements, such as reciprocal translocations and inversions, can also show an abnormal phenotype, even though there is no apparent loss or gain of genetic material. This suggests that an important gene, or genes, around the breakpoints have somehow been disrupted.

This group of abnormalities are known as disease-associated balanced chromosomal rearrangements (DBCRs). These will be discussed in more detail in chapter 2.

2: Disease-associated Balanced Chromosomal Rearrangements

2.1. Introduction

Balanced chromosomal rearrangements are estimated to occur in approximately 1 in 500 individuals in the general population [55]. A study performed by Warburton *et al*, 1991, looked at 377,357 amniocenteses results from over a 10 year period and found that approximately 1 in 2,000 had a *de novo* reciprocal translocation, 1 in 9,000 a Robertsonian translocation and 1 in 10,000 had a *de novo* inversion. The proportion of these that are disease-related is unknown but the risk of a serious congenital anomaly associated with a rearrangement has been estimated to be around 6.1 % for reciprocal translocations and 9.4 % for inversions [56].

Disease-associated balanced chromosomal rearrangements (DBCRs) have already proved to be instrumental in the mapping of disease loci and positional cloning of disease genes. They have been used to identify a growing number of disease loci, and subsequently disease genes, for a variety of different conditions. Some examples are detailed below.

2.1.1. X-linked Disorders

The first Mendelian disorder to be mapped on the basis of DBCR information was Duchenne muscular dystrophy (DMD). In 1979, Lindenbaum *et al* [57] reported the case of an 8-year girl with DMD and a *de novo* chromosomal abnormality, consisting of an inversion of chromosome X and a reciprocal translocation between

the same chromosome X and chromosome 1. The gene for DMD was already suspected to be on the X chromosome due to the observation that the disease occurred almost exclusively in males and when it segregated through a family, it showed a distinctive X-linked inheritance pattern [58]. The patient in this case was female, which is unusual for X-linked recessive conditions but does occur. 46,XY females or females that have Turner syndrome (monosomy X) can exhibit X-linked recessive disorders if they inherit the X chromosome with the faulty copy of the gene [59]. Cytogenetically normal females can also show the phenotype if the X chromosome that contains the normal copy of the gene is inactivated.

Lindenbaum's patient had a translocation and inversion of chromosome X involving bands Xp11 and Xp21. The presence of the DMD phenotype and the *de novo* rearrangement led the authors to hypothesise that the gene for DMD was located at one of these breakpoints. This hypothesis was supported by reports of three other X;autosome translocations in DMD females with breakpoints at Xp21: In 1977, Greenstein *et al* [60] reported a 16 year old girl with an X;11 translocation, Verellen *et al* (1978) [61] reported an X;21 translocation in a DMD girl and Canki *et al* (1979) [62] reported an X;3 translocation. The number of X;autosome translocations with Xp21 breakpoints continued to increase over the years (e.g.[63-65]) firmly establishing Xp21 as the DMD disease locus.

It was the X;21 patient reported by Verellen [61;66] that proved instrumental in the identification of the DMD gene itself. The 21 breakpoint of this translocation was found to split the large block of ribosomal RNA (rRNA) genes that are present on the short arm of the chromosome [67]. This allowed Ray *et al* [68] to use rRNA gene probes to clone the translocation junction fragments of the derived

chromosomes. The fragment from the X-chromosome portion was found to contain a restriction fragment length polymorphism (RFLP) that was closely linked to the DMD gene. This was subsequently used to test male patients with DMD and some deletions were detected.

The gene causing DMD (also named *DMD*) encodes a protein called dystrophin. The most common phenotype-causing mutations in *DMD* are deletions, which account for approximately 60 % [69]. Other mutations, such as point mutations and duplications, do occur but at a much lower level and generally result in premature termination of translation and hence no viable dystrophin protein being produced.

Translocations and inversions can also disrupt the *DMD* gene in females, resulting in a phenotype if the normal X is inactivated. Although X-inactivation still occurs randomly in these females, it is generally only the cells in which the normal X is inactivated that will survive. If the der(X) is inactivated, the cell will be functionally disomic for the distal part of Xp and monosomic for the part of the chromosome that is translocated to the der(X) as this will also be silenced. It is likely that this genetic imbalance will either cause the cell to undergo apoptosis or the cell will survive but be strongly selected against.

The inactivation of the normal X chromosome will not result in a gross genetic imbalance as both parts of the X chromosome and the autosome will be active. The cell should therefore be genetically balanced, although there is always the possibility of small amounts of material being lost from around the breakpoints.

The method of using phenotypic females with X;autosome translocations to map and clone disease genes was first used for DMD but has since then been used

for other X-linked diseases such as Choroideremia (OMIM 303100) [70], Lowe syndrome (OMIM 309000) [71] and Lissencephaly (OMIM 300067) [72].

2.1.2. Autosomal Dominant Disorders

The DBCR mapping approach has been used for a number of autosomal dominant disorders. As would be expected, these make up a large proportion of the mapped disorders due to the fact that only one copy of the gene needs to be disrupted to produce a phenotype. DBCRs are therefore more often associated with dominant disorders as the rearrangement generally only affects one chromosome of the pair.

One autosomal dominant condition that was mapped using DBCRs is Rubinstein-Taybi syndrome (RTS) (OMIM 180849). This condition is characterised by mental retardation, broad thumbs and toes and facial anomalies [73]. In 1991, Imaizumi and Kuroki [74] reported a teenage girl with RTS and a *de novo* translocation between chromosomes 2 and 16 with breakpoints at p13.3 for both. On the basis of a previous report of an RTS patient with a deletion of 2p, but with no defined breakpoints [75], the authors suggested that the RTS locus was at 2p13.3. Soon after, a 7;16 translocation [76;77] and an inversion of chromosome 16 [78] were reported, both with breakpoints at 16p13.3, the same band as the Imaizumi case. This led to the reassignment of the RTS locus.

In 1995, Petrij *et al* [79] studied the 16p13.3 breakpoints in all three translocations and found that they all mapped within a region containing the CREB binding protein gene (*CBP*), loss of one functional copy of which they proposed to cause the phenotype. They have since preformed further work to conclude that

heterozygous mutation or loss of this gene, even just the C-terminal region, is sufficient to cause RTS [80].

Another disorder in which DBCRs proved vital in the identification of the causative gene was multiple exostoses type 1 (OMIM 133700), a disorder characterised by multiple projections of bone that are capped with cartilage. The gene for the disorder was thought to be on 8q24.1 as the exostoses were identical to those observed in another disorder, Langer-Giedion syndrome (OMIM 150230), which was associated with this chromosomal region.

Again, DBCRs were subsequently reported which confirmed this theory. These included an 8;11 translocation with a breakpoint at 8q24.1 [81] and an 8;13 translocation with a breakpoint at 8q23 [82]. Mapping of the rearrangements in these patients resulted in the identification of a cDNA that spanned the chromosome 8 breakpoints [83]. This was designated the *EXT1* gene.

Since then, mutations and further chromosomal rearrangements have been identified in this gene in patients with both multiple exostoses and Langer-Giedion syndrome, which is thought to be a contiguous gene syndrome caused partly by loss of *EXT1*.

2.1.3. Autosomal Recessive Disorders

The number of autosomal recessive conditions mapped by DBCRs would be expected to be significantly lower than the number of dominant disorders as both copies of a gene need to be disrupted to produce a phenotype. DBCRs, in general, will only disrupt one copy and an independent event is therefore required to affect

the other. Mapping of DBCRs in autosomal recessive conditions can, however, prove fruitful, as evinced by the case of Alstrom syndrome (OMIM 203800).

Alstrom syndrome (ALMS) is a disorder characterised by cone-rod dystrophy, obesity, cardiomyopathy, hearing loss and type 2 diabetes mellitus. The disease locus was initially assigned to chromosome 2p by homozygosity mapping [84] and was then further refined using linkage analysis to the 2p13 region [85]. In 2002, the gene was identified by two independent groups employing different strategies [86;87].

Collin *et al* [88] had previously mapped the gene to within a 14.9 cM region and by performing further recombination and physical mapping, narrowed the interval to 2 cM (around 1.2 Mb). In this region, they found 16 genes and EST clusters. One of these, *KIAA0328*, was expressed in many of the tissues that are affected by ALMS and when they sequenced the DNA of six unrelated ALMS families, they found four frameshift mutations and two nonsense mutations, indicating that this was indeed the *ALMS1* gene.

Hearn *et al* [89] took a different approach. They identified an individual with ALMS who had also inherited a familial translocation between chromosomes 2 and 11. The breakpoints on the chromosome 2 were at 2p13, the ALMS locus, but the mother, from whom he had inherited the rearrangement, did not have the disease, as would be expected in a recessive disorder as only one copy of the gene was disrupted by the rearrangement. This led Hearn *et al* to postulate that the individual was in fact a compound heterozygote and had inherited a translocation disrupting one copy of the *ALMS* gene from his mother and an intragenic mutation in the other copy of the gene from his father.

To determine what gene or genes had been disrupted, Hearn *et al* mapped the translocation breakpoint on chromosome 2 to a 1.7 kb fragment that contained exon 4 and the start of exon 5 of the newly identified *ALMS1* gene. Analysis of the paternal allele revealed frameshift mutation caused by a 2 bp deletion in exon 8 of *ALMS1*, which was predicted to result in premature termination.

The ALMS individual was therefore a compound heterozygote and had both copies of the gene disrupted. Hearn *et al* also analysed other ALMS cases and found mutations in *ALMS1*. They stated that the discovery of six independent mutations, combined with the report by Collin *et al* [90], confirmed that dysfunction of *ALMS1* causes Alstrom syndrome.

This was the first case of an autosomal recessive disease gene being found by mapping DBCRs but it is hoped that there will be more cases in the future. These cases are generally going to be observed when a chromosomal rearrangement is passed through a family. This may interrupt a gene but not be associated with a phenotype until it is inherited along with a mutation on the corresponding allele. If this is the case, the phenotype may appear to be unrelated to the rearrangement. These cases are therefore likely to be missed although, since the report from Hearn *et al*, any rearrangement that has a breakpoint in a previously identified locus may now be mapped.

2.2. How do DBCRs Cause a Phenotype?

A number of hypotheses have been postulated to explain how a DBCR can cause a phenotype, these include (1) the direct interruption of a gene or its *cis*-

regulatory elements leading to a change in function, (2) cryptic deletions at or around the rearrangement breakpoints and (3) alteration of chromatin environment (position effect).

2.2.1. Direct Interruption

There are many examples of DBCRs that have been shown to directly disrupt genes, causing a phenotype. Just a few of these are going to be outlined here.

2.2.1.1. Isolated Lissencephaly

Lissencephaly is a brain malformation characterised by a smooth cerebral surface. It can be associated with other abnormalities, such as abnormal facies in Miller-Dieker syndrome (MDS), or occur on its own (isolated lissencephaly, ILS). 90 % of MDS patients have a deletion of the 17p13.3 region but this is only present in approximately 15 % of patients with ILS [91]. In 1993, Reiner *et al* [92] isolated the *LIS1* gene, haploinsufficiency of which is responsible for the ILS phenotype.

Kurahashi *et al*, 1998 [93], identified a patient with ILS and a *de novo* reciprocal translocation between chromosomes 8 and 17 (t(8;17)(p11.2;p13.3)). The patient did not present with any of the facial features characteristic of MDS. Since the lissencephaly gene was known to be located at 17p13.3, they decided to map the chromosome 17 breakpoint. They found that the breakpoint of the DBCR mapped within intron 1 of the *LIS1* gene, thereby disrupting the 5′ untranslated region of the gene and preventing the production of a functional protein from that allele. The heterozygous loss of the *LIS1* gene is sufficient to cause the ILS phenotype.

2.2.1.2. Holt-Oram syndrome

Holt-Oram syndrome (OMIM 142900) is an autosomal dominant disorder that affects approximately 1 in 100,000 live births [94]. It is characterised by anterior pre-axial limb and cardiac abnormalities and is caused by mutations in the T-box gene, *TBX5*. These can be deletions, nonsense mutations, missense mutations, rearrangements and also insertions [95]. In 1999, Basson *et al* [96] mapped the chromosome 12 breakpoint of a translocation between chromosomes 5 and 12 (t(5;12)(q15;q24)) in a young child with Holt-Oram syndrome. They found that the breakpoint disrupted the *TBX5* gene in the intron following exon 1a and therefore separated exons 2 to 9, the protein encoding exons, from the promoter elements and 5′ untranslated sequences of the gene.

The translocation therefore causes haploinsufficiency of *TBX5*, which is the cause of the Holt-Oram phenotype.

2.2.1.3. Rubinstein-Taybi syndrome

As previously mentioned, the identification of the gene causing Rubinstein-Taybi syndrome (RTS) was identified through mapping DBCRs. Petrij *et al*, 2000 [97], stated that all breakpoints in the six RTS translocations and inversions so far reported mapped to within the 5′ part of the *CBP* gene, within the so called breakpoint cluster region, an intronic region of approximately 13 kb. These disruptions are thought to produce proteins that contain only a small part of the N-terminus of the CBP protein.

One further case with a translocation between chromosomes 2 and 16, t(2;16)(q36.3;p13.3), was found to have a chromosome 16 breakpoint in a different

region, namely between exons 16 and 17. This resulted in a stable protein that was truncated and only about half the normal length. The expression of this along with the protein from the normal allele resulted in the presence of the RTS phenotype in the child. The results from the mapping of these rearrangements suggest that the loss of the C-terminal domains of CBP is sufficient to cause RTS.

2.2.2. Deletions at Rearrangement Breakpoints

Although DBCRs may appear to be balanced by conventional cytogenetics, there may be small changes in the amount of genetic material at or around the breakpoints. There is evidence that cryptic deletions (i.e. those invisible by standard cytogenetics) can occur in as many as two out of three apparently balanced rearrangements [98].

In 2004, Astbury *et al* [99] performed a study to test the hypothesis that deletions of varying sizes occur in DBCRs and that these are a significant cause of the phenotypic abnormalities. They examined 15 patients with seemingly balanced rearrangements and found that nine had deletions ranging in size from 0.8 to 15.3 Mb and involving between 15 and 70 genes. In the remaining six cases, they found that five had a known or putative gene, or genes, disrupted by the rearrangement. The breakpoints in the remaining case did not apparently disrupt any genes.

The data from Astbury *et al* suggests that deletions occur more frequently than gene disruptions in patients with DBCRs. However, of the 15 patients that were examined in this study, two were already known to have a deletion and the remaining 13 were selected as it was believed they were more likely to harbour a deletion on

the basis of their phenotypical findings. The frequency of deletions in patients with DBCRs may therefore be over estimated.

Astbury *et al* [100] showed that deletions can occur at the breakpoints of DBCRs, although the incidence of this has still to be elucidated. However, deletions can also be present that are not at the site of the breakpoint, but some distance away. In 2003, Fantes *et al* [101] reported the case of a young girl with bilateral anophthalmia (the absence of both eyes) and an apparently balanced translocation between chromosome 3 and 11 (t(3;11)(q26.3;p11.2)). Mapping of this translocation led to the discovery of a deletion approximately 740 kb in size that was located around 600 kb from the breakpoint on chromosome 3. None of the genes located around the breakpoint were considered to be good candidates and at the time of mapping, the sequence for the deleted region was incomplete, showing only one annotated gene that was not thought to be involved. *SOX2* was already thought to be a good candidate for the phenotype and although it had previously FISH mapped to the 3q26.3-q27 region, it could no longer be located in the Ensembl genome browser. However, BLAST searches performed using the sheep ortholog of the gene located a series of human BAC clones that covered the *SOX2* gene. These BACs were found to be either fully or partially deleted in the t(3;11) case, suggesting that the bilateral anophthalmia phenotype was due to the direct interruption, by deletion, of the *SOX2* gene.

The phenotype in this case may have been caused by a deletion but this, and subsequently the gene that causes bilateral anophthalmia, were located by mapping the breakpoints of a DBCR.

A study performed by Gribble *et al*, 2005 [102], concerned with looking at any genomic imbalances around, or distant to, DBCR breakpoints, found a high level of rearrangement complexity. Samples were examined using DNA microarrays, at 1 Mb resolution, and array CGH was performed to screen for any imbalances. Of the ten cases studied, three were found to have complex rearrangements at or near the DBCR breakpoints, three were found to have imbalances (one duplication and two deletions) unrelated to the balanced translocations and the remaining four were found to be simple balanced translocations, as originally suspected.

The three cases that proved to be more complex than first expected had multiple rearrangements including inversions and insertions and two involved chromosomes not previously implicated. Two of these three cases also had deletions (approximately 5 Mb and 6 Mb in size) very close to one of the DBCR breakpoints. The third had no detectable imbalance.

This data supports the hypothesis that deletions, or duplications, can accompany an apparently balanced chromosome rearrangement. However, all of the patients that had genetic imbalances had multiple clinical phenotypes, such as learning difficulties, dysmorphic features, epilepsy or autism. These conditions do not follow a Mendelian inheritance pattern and would be expected to be caused by the disruption of many genes. A study of 13 individuals with DBCRs and no discernable phenotypes found no imbalances at the translocation breakpoints. One patient was found to have a deletion of approximately 2 Mb on a chromosome not involved in the rearrangement but this was only found in a transformed cell line and not in genomic DNA from the patient. It was therefore concluded to be an artefact [103].

The results of Gribble *et al* [104] support those of two previous studies looking for submicroscopic deletions or duplications in a subset of patients with learning disability/mental retardation, dysmorphic features and apparently normal chromosomes. A study of 50 patients found deletions in seven cases (14 %) and duplications in five (10 %), approximately 24 % of cases therefore having an imbalance [105]. A similar study of 20 patients discovered three deletions and two duplications (25 % overall) [106]. These figures are comparable with the 30 % of translocation independent imbalances found by Gribble *et al.*

These important studies support the hypothesis that the double stranded breaks which underlie the cytogenetically visible rearrangement may be accompanied by other breakpoints locally or throughout the genome. The complexity of the clinical phenotype may help predict the presence of genomic imbalances in DBCRs. Ideally both physical mapping of the breakpoints and array CGH should be performed in all cases to allow adequate interpretation of the clinical phenotype.

2.2.3. Position Effect

Although the mapping of DBCRs may reveal the direct disruption of a gene, or genes, that results in the accompanied phenotype, this is not always the case. Breakpoints may occur outside the genes themselves and affect their regulation by causing a change in their position within the genome, or occur within one gene and have an effect on another. This phenomenon is known as position effect [107] and can be a major hindrance in the identification of disease genes by mapping DBCRs.

Chromosome rearrangements can alter the transcriptional control of genes in two ways, which may occur independently or in combination. Firstly, the

rearrangement may dissociate the gene's promoter and transcription unit from its *cis*-acting regulatory elements and secondly, the rearrangement may result in an alteration of the chromatin structure, either locally or more globally [108]. Only the first mechanism will be discussed here.

2.2.3.1. Disturbance of long-range regulatory elements

The disturbance of long-range regulatory elements by chromosomal rearrangements has been identified as the basis of a number of human diseases (see table 2.1). One example of this comes from aniridia (the absence of the iris) and other eye related disorders that are caused by a loss of function of one copy of the *PAX6* gene at 11p13. Two cases of aniridia had been described in association with a DBCR in which the chromosome 11 breakpoints were mapped and found to be 125 and 150 kb downstream (3') of *PAX6* [109-111].

Initially this raised the question of whether *PAX6* was the only aniridia gene, as had been suggested by other studies [112], or whether the translocation breakpoints marked the location of another candidate gene in the 11p13 area. The sequence around the breakpoint in one of the cases did suggest the interruption of an exon, leading to the putative assignment of a second aniridia locus (AN2) [113]. In 2002, a novel gene, *ELP4*, was identified directly telomeric to *PAX6*. The translocation breakpoints on both cases were found to map within the final intron of this gene, although heterozygous loss of *ELP4* was shown not to contribute to the aniridia phenotype [114].

It therefore seemed likely that the aniridia phenotype in these cases was due to the disruption of long-range control elements for *PAX6* that are located within the

ELP4 gene. This was clearly shown using mouse-human somatic cell hybrids that were capable of expressing mouse *Pax6* but only expressed human *PAX6* when a normal chromosome 11 was present. The presence of chromosomes from aniridia patients with the *PAX6* transcription unit intact but harbouring a deletion of the distant downstream regulatory elements did not produce expression [115].

The disturbance of long range control elements in humans is most readily recognised when the phenotype is the same as that seen in point mutations or other loss of function mutations in the coding region of the relevant gene. However, the disruption of these elements may cause a different phenotype as the regulation of the gene may only be affected in certain tissues or developmental stages. One example of this was seen with the sonic hedgehog (*SHH*) gene in preaxial polydactyly (PPD).

PPD is one of the most common human congenital limb malformations and the phenotype can vary markedly, from the addition of an extra phalanx (finger bone) to create a triphalangeal thumb, to whole digit duplications and aplasia of the tibia [116].

SHH is only expressed during embryogenesis and plays many important roles in development, especially in the patterning of the early embryo. *SHH* has been shown to be involved in the patterning of the ventral neural tube, the ventral somites and also in the anterior-posterior limb axis. In mouse, *Shh* is transiently expressed in the posterior part of the limb bud, where it sets up a morphogen gradient.

PPD is seen in the mouse mutant Sasquatch (Ssq), which was created by the random insertion of a reporter cassette. This inserted approximately 1 Mb upstream of the *Shh* gene, within intron 5 of the limb region 1 gene (*Lmbr1*) [117]. In this, as well as two other mouse limb mutants with PPD, *Shh* was shown to be expressed in

the anterior, as well as in the usual posterior site [118-120], suggesting that this was the cause of the limb duplication and that the normal control of *Shh* expression in the limb bud has been altered by the insertion [121]. This suggests the existence of a limb regulatory element controlling *Shh* expression located 1 Mb away from the actual gene.

As well as evidence from mouse mutants, there was also evidence from human DBCRs. *Shh* maps to mouse chromosome 5, in a region that is homologous to human chromosome 7q36, the PPD locus. Analysis of a patient with PPD and a *de novo* translocation between chromosomes 5 and 7 (t(5;7)(q11;q36)) showed the 7 breakpoint to lie within intron 5 of the *LMBR1* gene [122]. This is the same region that the Ssq insertion was found to occur.

Another human phenotype was found to involve the *LMBR1* gene, namely acheiropodia, a condition characterised by bilateral congenital amputations of the upper and lower extremities and aplasia of the hands and feet. The locus for this was initially mapped to chromosome 7q36 [123] and then narrowed down, by mapping affected families, to the *LMBR1* gene, with all affected individuals in the studied families showing a deletion of exon 4 [124].

This initially led to the suggestion that the *LMBR1* gene may play an essential role in limb formation, but taken together with the evidence from the Ssq mouse mutant, it seems more likely that the deletion caused a phenotype by deleting regulatory elements of *SHH* that are located within the *LMBR1* gene.

To confirm this theory, this region was sequenced in patients with PPD and no apparent translocations or inversions to see whether there were any mutations that

were sufficient to cause the phenotype. Single point mutations were found in all affected individuals and no non-affected in four families [125].

This shows that point mutations or deletions of a regulatory element located approximately 1 Mb from the gene can have a detrimental effect on development and that this effect can be restricted to a particular tissue type or developmental stage.

Table 2.1. Position Effect Genes in Human Disease

Disorder	Gene	Distance of furthest breakpoint (kb)	3' or 5' side*	Reference
Aniridia	*PAX6*	125	3'	[126]
Blepharophimosos-ptosis-epicanthus inversus syndrome	*FOXL2*	170	5'	[127]
Campomelic dysplasia	*SOX9*	850	5'	[128;129]
Cataract, ocular anterior segment dysgenesis and coloboma	*MAF*	1,000	5'	[130]
Cleidocranial dysplasia (CCD)	*CBFA1*	829	5'	[131]
Facioscapulohumeral dystrophy	*FSHD*	100	3'	[132-134]
Familial adenomatous polyposis (FAP)	*APC*	Unknown	-	[135]
Glaucoma/autosomal dominant iridogoniodysgenesis	*FOXC1*	25/1,200	5'	[136]
Greig cephalopolysyndactyly syndrome	*GLI3*	10	3'	[137]
Haemophilia B	*F9*	-	5'	[138]
Holoprosencephaly (HPE2)	*SIX3*	<200	5'	[139]
Holoprosencephaly (HPE3)	*SHH*	265	5'	[140]
Holt-Oram syndrome (HOS)	*TBX5*	20	3'	[141]
Lactase persistence	*LCT*	15/20	5'	[142]
Lymphedema distichiasis	*FOXC2*	120	3'	[143]
Mesomelic dysplasia and vertebral defects	*Hoxd complex*	60	3'	[144]
Preaxial polydactyly	*SHH*	1,000	5'	[145]
Rieger syndrome	*PITX2*	90	5'	[146]
Saethre-Chotzen syndrome	*TWIST*	260	3'	[147]
Sex reversal	*SRY*	3	5'/3'	[148]
Specific language impairment	*FOXP2*	>680	3'	[149]
Split hand/foot malformation	*SHFM1*	~450	5'/3'	[150]
α-Thalassaemia	*HBA*	18	3'	[151]
γß-Thalassaemia	*HBB*	50	5'	[152]
Van Buchem disease	*SOST*	35	3'	[153]
X-linked deafness	*POU3F4*	900	5'	[154]

*For 3′ breakpoints, the distance refers to that from the breakpoints to the 3′ end of the gene or complex.

2.2.3.2. Position effect and DBCR mapping

Position effect can be a major hindrance when mapping DBCRs with a view to identifying disease genes. If there is already a candidate gene postulated to cause the phenotype and the DBCR breakpoint falls outside of that gene and within another, the presence of another disease locus may be inferred, as with *ELP4* in aniridia. The phenotypes of patients with disrupted elements may also differ from those that have mutations in the coding regions of the gene. This can also lead to speculation that another gene may be involved, disruption of which leads to a slightly different phenotype.

Alternatively, the breakpoint may not actually fall within a gene, making the DBCR seem coincidental and not the cause of the phenotype, when in fact it has disrupted the regulatory elements of a distant gene.

Breakpoints may occur both 5′ and 3′ of the relevant gene and distances can vary from a few kb to over 1 Mb. This can make the identification of new disease genes extremely difficult and problematic as genes from a large area either side of the breakpoints often need to be considered as candidates.

However, even with the afore mentioned difficulties that can be incurred when mapping chromosomal rearrangements, DBCRs have already proved to be an invaluable asset in the identification of both disease loci and disease causing genes.

2.3. DBCR Database

2.3.1. Introduction

Disease-associated balanced chromosome rearrangements (DBCRs) have proven an invaluable resource to the human geneticist for mapping disease loci and the positional cloning of disease genes. In any trait with a significant genetic component they have the potential to identify the causative gene, establish the likely inheritance pattern and elucidate the underlying biological mechanisms. However, chromosomal rearrangements are complex mutational events and the study of individual cases leaves scope for investigators to be misled, as there are a minimum of two breakpoints to be considered in each case. The chance of error may be minimised through judicious use of supporting evidence. This may come from haploinsufficiency maps [155] or genetic linkage data but perhaps the most convincing data comes from the identification of recurrent breakpoints associated with a particular phenotype.

Such information is, however, difficult to access as most DBCRs are not reported, or are reported with inadequate clinical data. A study in Denmark and Southern Sweden showed that of the 216 DBCRs identified in the clinical cytogenetic laboratories in the year 2000, only 25 (12 %) were actually reported in the literature [156].

Even published DBCRs can be difficult to locate as there is no central resource for these analogous to OMIM for non-chromosomal genetic disorders, although initiatives such as the Mendelian Cytogenetics Network database (MCNdb, http://www.mcndb.org/) in Europe and the Developmental Genome Anatomy Project

(http://www.bwhpathology.org/dgap) in the US are attempting to improve ascertainment of unpublished cases and to systemise the phenotypic documentation of DBCRs. However, at the time of initiating the DBCR database, the MCNdb had been offline for some time with no indication of becoming re-accessible.

In order to improve the accessibility of information on these rearrangements, a DBCR database was created to collate all available data into one central, easily accessible and searchable facility. This not only simplifies the identification of DBCRs but also allows some general conclusions to be drawn about rearrangement breakpoints and the worth of breakpoint mapping in disease gene or loci identification.

2.3.2. Aims of the DBCR Database

There are three specific aims of the DBCR database: Firstly, to catalogue clinical, cytogenetic and molecular data on all published DBCR cases and unpublished cases known to us; secondly, where molecular characterisation has been carried out, to review the resolution of the reported mapping and the molecular pathology associated with the breakpoints, and thirdly, to identify predictors for the cases in which DBCR mapping has been unhelpful or misleading.

Every field in the database is searchable so that any similarities in fields such as phenotype, rearrangement, chromosomes involved, chromosome breakpoints, mapping resolution and molecular pathology can be determined. As well as providing information on the phenotype and the rearrangement, each breakpoint is also considered independently as to whether it has been previously implicated in the relevant disorder, to what resolution it has been mapped and if there are any

breakpoint spanning FISH clones, whether a gene has been directly interrupted or found near to a breakpoint, whether any imbalances have been found and further information on the breakpoints, such as whether they occur in light or dark G-bands. Any other relevant information is also extracted from the original papers and noted.

The database provides links, via hyperlinks, to the original data and to information on the phenotype, where applicable, via Online Mendelian Inheritance in Man (OMIM). The accessibility of the database allows data on DBCRs to be easily and comprehensively obtained without the need for numerous literature searches. The existence of a comprehensive, curated, regularly updated database of DBCRs should prove to be invaluable for those interested in studying DBCRs.

2.3.3. Materials and Methods

The DBCRs in the database were obtained through numerous literature searches performed using on-line resources such as Entrez PubMed (http://www.ncbi.nlm.nih.gov/entrez/query.fcgi?db=PubMed) and Online Mendelian Inheritance in Man (OMIM, http://www.ncbi.nlm.nih.gov/omim/). Both text and MeSH term searches were used. The full list of the search terms used is available in appendix 2.4.1. Paper copies of 742/779 (95 %) original papers could be obtained through local sources or the British Library. Each paper was reviewed and the reference list searched for other relevant references. The extracted data was stored in a relational database format using Access 2000 (Microsoft).

The database is currently in the process of being converted to a web-based format to allow open access to the data and should shortly be available through the research pages of Dr. David FitzPatrick, via the MRC Human Genetics Unit website

(http://www.hgu.mrc.ac.uk/Research/Fitzpatrick). The latest version of the database available at the time of writing is included on cd as an appendix.

2.3.3.1. Bioinformatic resources

- OMIM:

  Online Mendelian Inheritance in Man, OMIM (TM). McKusick-Nathans Institute for Genetic Medicine, Johns Hopkins University (Baltimore, MD) and National Center for Biotechnology Information, National Library of Medicine (Bethesda, MD), 2000. World Wide Web URL: http://www.ncbi.nlm.nih.gov/omim/

- Entrez PubMed:

  http://www.ncbi.nlm.nih.gov/entrez/query.fcgi?db=PubMed

- Ensembl Karyoview (v.32 - Jul2005)

  http://www.ensembl.org/Homo_sapiens/karyoview

2.3.3.2. Database Overview

The database was compiled using Microsoft Access 2000. A snapshot of the two linked database forms and the relationship between them can be seen in figures 2.1 and 2.2 respectively.

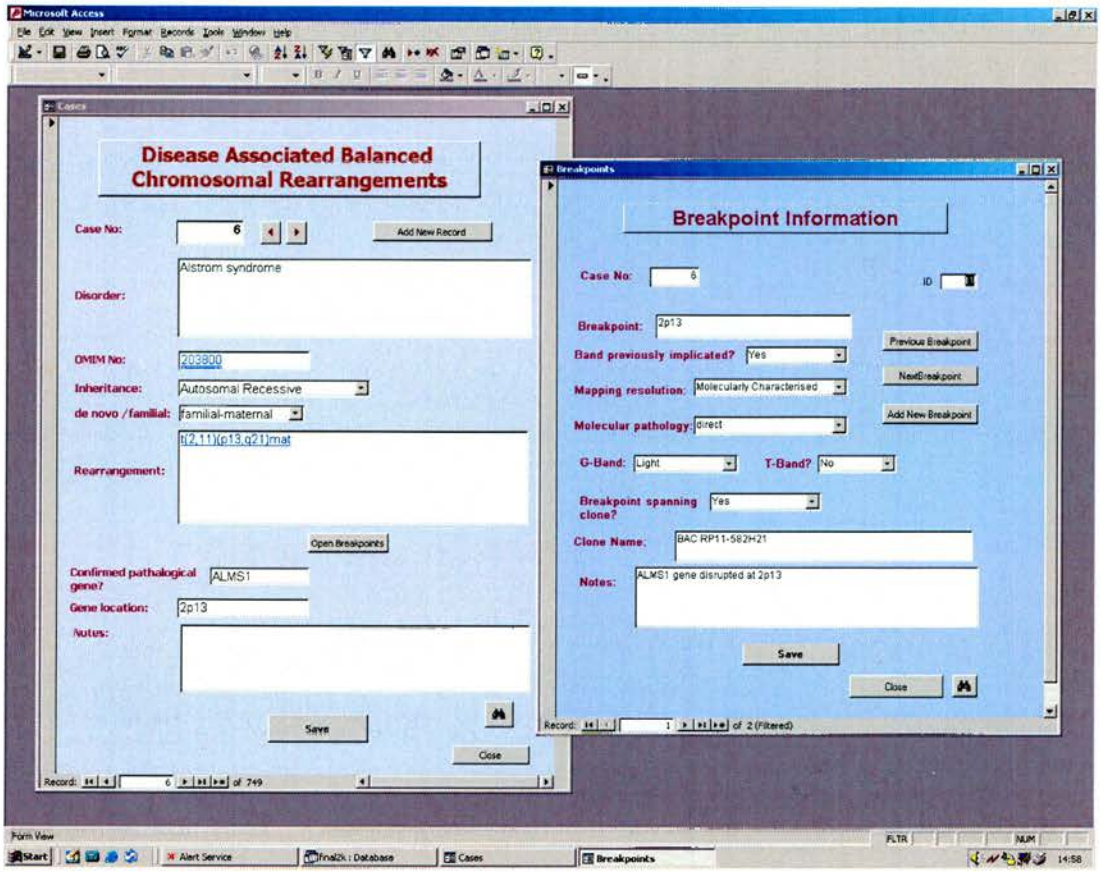

Figure 2.1. A snapshot of the database forms in Microsoft Access

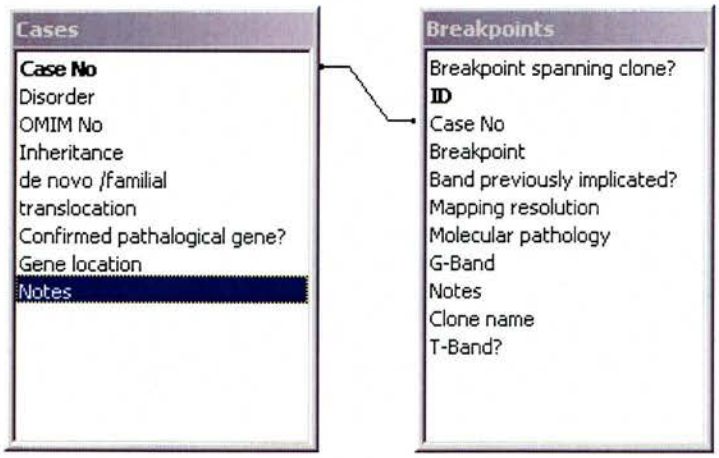

Figure 2.2. Relationship tables for the database.

Microsoft Access relationship tables for the DBCR database showing that the two forms are linked via the individual case number.

2.3.4. Cytogenetic Aspects

919 cases with a cumulative 2023 breakpoints have been entered into the database to date. 396 of these 919 (43 %) DBCRs were apparently *de novo* events. 226/919 (25 %) were inherited; 96/919 (10 %) were maternally derived, 56/919 (6 %) paternally derived and 74/919 (8 %) segregated through multiple generations of a family. The inheritance of the remaining 297/919 (32 %) was unknown, largely due to parental chromosomes being unavailable for analysis.

DBCR breakpoints were observed on every chromosome. 1178/2023 (58 %) of the breakpoints occurred in the gene-rich, light coloured Giemsa-bands (G bands), with 361/2023 (18 %) of these occurring in the T-bands. These are the lightest G-bands and are thought to be the most GC-rich. 426/2023 (21 %) of the breakpoints fell within the relatively gene-poor, dark G-bands and 169/2023 (10 %) were in the centromeric regions of the chromosomes. The remaining 250/2023 (12 %) were either in the heterochromatic regions (24/2023, 1 %), the satellite regions of the acrocentric chromosomes (16/2023, 1 %) or were unknown, predominantly due to G-band misclassification.

552/919 (60 %) of the rearrangements in the database were only reported at the cytogenetic Giemsa-banded (G-banded) level. 181/919 (20 %) have had one or more of the breakpoints physically mapped and only 128/919 (14 %) have had both or all of the breakpoints characterised. This is due to the fact that many of the rearrangements were reported prior to the availability of locus specific FISH and whole genome large insert libraries, which have simplified the high-resolution study of breakpoints. To place the resolutions into broad groups, 1328/2023 (66 %) of the breakpoints were not mapped below the 1 Mb level, 130/2023 (6 %) were mapped to

approximately 250 to 500 kb, 95/2023 (4 %) were to less than 250 kb and 225/2023 (11 %) were to base pair resolution. The mapping resolution of the remaining 245 breakpoints is unknown.

2.3.5. Molecular Pathology

2.3.5.1. Direct gene disruption

There were 48 cases in the database, with 34 different phenotypes, in which the confirmed pathological gene had been directly interrupted by a rearrangement breakpoint. These are listed in table 2.2. 20 of these cases were associated with autosomal dominant conditions, 19 were X-linked and six were either sporadic or unknown. Only two were autosomal recessive.

A further 114 cases in the database had one breakpoint that fell within or in close proximity to the cytogenetic band containing the causative gene for the relevant phenotype but had not been physically mapped. These breakpoints may disrupt the relevant gene or could cause a position effect (see below).

2.3.5.2. Position effects

Breakpoints may occur outside the genes themselves and affect their regulation by causing a change in their position within the genome, or occur within one gene and have an effect on another. This phenomenon is known as position effect (see section 2.2.3) and in most cases known to date results in loss of function of the gene. In the database, there were 27 cases from 15 different disorders that were

stated to be caused by a position effect, with the breakpoints occurring some distance away from the relevant causative gene. These are listed in table 2.2.

2.3.5.3. Microdeletions

As mentioned in section 2.2.2, DBCRs can be associated with deletions at, or distant to, the rearrangement breakpoints. There were six cases in the database, further to those of Astbury *et al* [157] (see section 2.2.2), in which deletions were detected. Five of these had deletions at, or near to, the DBCR breakpoints, encompassing all, or part of, the causative gene (see table 2.2). The sixth, isolated bilateral anophthalmia case [158], had a deletion of approximately 740 kb in size that was located around 600 kb from the translocation breakpoint, resulting in the deletion of *SOX2*.

Case No	Disorder	OMIM Number	Inheritance	*de novo* /familial	Gene name	Gene location	Notes	Gene size* (bases)	Ref
DBCRs in the database that directly interrupt a confirmed pathological gene:									
780	CHARGE syndrome	214800	A D	*de novo*	*CHD7*	8q12.2	Breakpoint between exons 3 and 8 of *CHD7*	188125	[159]
813	Congenital agammaglobulinemia and minor facial abnormalities	601495	A D	*de novo*	*LRRC8*	9q34.13	*LRRC8* gene disrupted	35869	[160]
119	Cornelia de Lange syndrome	122470	A D	*de novo*	*NIPBL*	5q13.1	Breakpoint in intron 1 of *NIPBL*	187314	[161;162]
36	Diamond-Blackfan anaemia (DBA)	205900	A D	*de novo*	*RPS19*	19q13	Breakpoint in 3rd intron of *RPS19*	11494	[163;164]
37	Diamond-Blackfan anaemia (DBA)	205900	A D	unknown	*RPS19*	19q13		11494	[165]
521	Ehlers-Danlos type I (and hypomelanosis of Ito)	130000	A D	unknown	*COL5A1*	9q34.2-q34.3	Breakpoint in intron 24 of *COL5A1*	201087	[166]
811	Familial adenomatous polyposis (FAP)	175100	A D	familial	*APC*	5q21	*APC* gene disrupted	108351	[167]
522	Hereditary neuropathy with liability to pressure palsies (HNPP)	162500	A D	familial	*PMP22*	17p11.2	Breakpoint lies between exons 1a to 3 of *PMP22*	35347	[168]
278	Holt-Oram syndrome	142900	A D	*de novo*	*TBX 5*	12q24.1	Intron 1A of *TBX5* disrupted	54511	[169]
742	Multiple Exostoses	133700	A D	familial	*EXT1*	8q24.11-q24.13	Breakpoint in first intron of *EXT1*	312382	[170]
747	Neurofibromatosis type 1 (NF1)	162200	A D	familial	*NF1*	17q11.2		124432	[171]
366	Neurofibromatosis type 2 (NF2)	101000	A D	familial	*NF2*	22q12.2	Breakpoint in intron between exons 14 and 15 of *NF2*	95018	[172]

367	Neurofibromatosis type 2 (NF2)	101000	A D	familial	*NF2*	22q12.2	*NF2* gene disrupted	95018	[173]
12	Retinoblastoma	180200	A D	*de novo*	*RB1*	13q14		178211	[174]
40	Rubinstein-Taybi syndrome	180849	A D	*de novo*	*CBP*	16p13.3	Breakpoint disrupts *CREBBP* between exons 16 and 17	154142	[175]
277	Specific language impairment (SLI)	602081	A D	*de novo*	*FOXP2*	7q31	*FOXP2* gene disrupted at 7q31.2	402081	[176]
262	Trichorhino-phalangeal syndrome, type 1 (TRPS1)	190350	A D	familial	*TRPS1*	8q24.12	*TRPS1* gene disrupted	260530	[177-179]
915	Trichorhino-phalangeal syndrome, type 1 (TRPS1)	190350	A D	*de novo*	*TRPS1*	8q24.12	*TRPS1* gene disrupted	260530	[180;181]
280	Williams Beuren syndrome	194050	A D	familial	*ELN*	7q11.2	*ELN* gene disrupted in intron 5	41515	[182]
281	Williams Beuren syndrome	194050	A D	familial	*ELN*	7q11.2	*ELN* gene disrupted	41515	[183;184]
6	Alstrom syndrome	203800	A R	familial	*ALMS1*	2p13	ALMS1 gene disrupted at 2p13	224160	[185]
810	Primary microcephaly	608716	A R	familial	*ASPM*	1q31	Breakpoint in intron 17 of *ASPM*	62114	[186;187]
55	Sotos syndrome	117550	Other	*de novo*	*NSD1*	5q35	*NSD1* gene interrupted.	161835	[188;189]
81	Klippel-Trenaunay-Weber syndrome	149000	Other	*de novo*	*VG5Q*	5q13.3	Breakpoint located in promoter region of *VG5Q*. *VG5Q* transcription increased by translocation.	34803	[190;191]
87	Prader-Willi syndrome	176270	Other	*de novo*	*SNRPN*	15q12	Breakpoint between 2nd and 3rd exon of *SNRPN*.	595815	[192]
88	Prader-Willi syndrome	176270	Other	familial	*SNRPN*	15q12	Breakpoint between 2nd and 3rd exon of *SNRPN*.	595815	[193]
727	Prader-Willi syndrome	176270	Other	*de novo*	*SNRPN*	15q11.2	Breakpoint in intron 17 of *SNRPN*	595815	[194]
66	Isolated lissencephaly	607432	Unknown	*de novo*	*PAFAH1B1*	17p13.3	Breakpoint disrupts 5-prime untranslated region of *PAFAH1B1*	91952	[195]

805	Dextro-looped transposition of great arteries (DTGA), perimembranous ventricular septal defect.	608808	Unknown	*de novo*	*THRAP2*	12q24	*THRAP2* gene disrupted	318761	[196]
771	Alport syndrome	301050	X-linked	unknown	*COL4A5*	Xq22.3	Breakpoint in intron 8 of COL4A5	257922	[197]
821	Androgen insensitivity syndrome (AIS)	300068	X-linked	familial	*AR*	Xq11-q12	*AR* gene disrupted	179648	[198]
135	Choroideremia	303100	X-linked	*de novo*	*CHM*	Xq21.2		186380	[199;200]
136	Choroideremia	303100	X-linked	*de novo*	*CHM*	Xq21.2	Breakpoint between exons 3 and 4 of *CHM*	186380	[201]
155	Duchenne muscular dystrophy (DMD)	310200	X-linked	*de novo*	*DMD*	Xp21.2	Breakpoint between the first and the second exon of *DMD*	2220381	[202]
157	Duchenne muscular dystrophy (DMD)	310200	X-linked	*de novo*	*DMD*	Xp21.2	Breakpoint in intron between exons 51 and 52 of *DMD*. Normal X inactivated	2220381	[203;204]
158	Duchenne muscular dystrophy (DMD)	310200	X-linked	*de novo*	*DMD*	Xp21.2	Breakpoint in intron between exons 7 and 8 of *DMD*	2220381	[205;206]
161	Duchenne muscular dystrophy (DMD)	310200	X-linked	*de novo*	*DMD*	Xp21.2	Breakpoint between the first and the second exon of *DMD*	2220381	[207;208]
162	Duchenne muscular dystrophy (DMD)	310200	X-linked	*de novo*	*DMD*	Xp21.2	*DMD* gene interrupted	2220381	[209;210]
164	Duchenne muscular dystrophy (DMD)	310200	X-linked	*de novo*	*DMD*	Xp21.2	Breakpoint in intron between exons 7 and 8 of *DMD*	2220381	[211;212]
825	Hyper-IgM syndrome (HIGM)	308230	X-linked	*de novo*	*CD40LG*	Xq26	Breakpoint in intron 4 of *CD40LG*	12213	[213]
774	Infantile spasm syndrome (West syndrome)	308350	X-linked	*de novo*	*ARX, CDKL5 (STK9)*	Xp22, Xp22.13	Bkpt in intron between exons 10 and 11 of *STK9*	227989	[214]
775	Infantile spasm syndrome (West syndrome)	308350	X-linked	*de novo*	*ARX, CDKL5 (STK9)*	Xp22, Xp22.13	Bkpt in intron between exons 1 and 1a of *STK9*	227989	[215]

68	Lissencephaly, X-linked	300067	X-linked	*de novo*	*DCX*	Xq22.3-q23	*DCX* gene interrupted	118399	[216;217]
3	Menkes syndrome	309400	X-linked	*de novo*	*ATP7A*	Xq12-q13	*ATP7A* gene disrupted	139683	[218]
4	Menkes syndrome	309400	X-linked	*de novo*	*ATP7A*	Xq12-q13	*ATP7A* gene disrupted	139683	[219]
370	Mental retardation, X-linked 60 (MRX60)	300486	X-linked	unknown	*OPHN1*	Xq12	Breakpoint in second intron of the *OPHN1* leading to complete lack of expression	390932	[220;221]
725	Severe neonatal-onset Ornithine transcarbamylase deficiency	311250	X-linked	*de novo*	*OTC*	Xp21.1	Breakpoint between exon 1 and intron 4 of *OTC*	69251	[222]
260	Simpson-Golabi-Behmel syndrome, type 1 (SGBS1)	312870	X-linked	*de novo*	*GPC3*	Xq26	*GPC3* gene interrupted	449893	[223;224]
DBCRs in the database in which the phenotype is caused by position effect:									
137	Aniridia type II	106210	A D	familial	*PAX6*	11p13	Breakpoint 125-185 kb from 3' end of *PAX6*	21303	[225;226]
140	Aniridia type II	106210	A D	familial	*PAX6*	11p13	Breakpoint approximately 100 kb distal to *PAX6*	21303	[227]
748	Aniridia type II	106210	A D	familial	*PAX6*	11p13	Distal breakpoint 85-95 kb from 3' end of *PAX6*.	21303	[228;229]
769	Aniridia type II	106210	A D	*de novo*	*PAX6*	11p13	Breakpoint over 50 Kb from *PAX6*	21303	[230]
770	Aniridia type II	106210	A D	familial	*PAX6*	11p13	Breakpoint over 75 Kb downstream of *PAX6*	21303	[231]
21	Blepharophimosis, ptosis, and epicanthus inversus (BPES)	110100	A D	*de novo*	*FOXL2*	3q23	*MRPS22* gene interrupted. Breakpoint 171 kb from *FOXL2*.	2733	[232]
22	Blepharophimosis, ptosis, and epicanthus inversus (BPES)	110100	A D	*de novo*	*FOXL2*	3q23	*BPESC1* gene interrupted.	2733	[233-236]

24	Blepharophimosis, ptosis, and epicanthus inversus (BPES)	110100	A D	*de novo*	*FOXL2*	3q23		2733	[237]
101	Campomelic dysplasia	114290	A D	unknown	*SOX9*	17q24.3-q25.1	Breakpoint 110–140 kb upstream of *SOX9*	5400	[238]
107	Campomelic dysplasia	114290	A D	unknown	*SOX9*	17q24.3-q25.1	Breakpoint 75–350 kb upstream of *SOX9*	5400	[239;240]
767	Campomelic dysplasia	114290	A D	familial	*SOX9*	17q24.3-q25.1	Breakpoint approx. 900 Kb upstream of *SOX9*	5400	[241]
768	Acampomelic campomelic dysplasia with male to female sex reversal	114290	A D	*de novo*	*SOX9*	17q24.3-q25.1	*SDK2* gene likely to be interrupted. Breakpoint 1.3 Mb downstream of *SOX9*	5400	[242]
761	Cleidocranial dysplasia (CCD)	119600	A D	*de novo*	*CBFA1*	6p21	Breakpoint over 800 Kb from 5' end of *CBFA1*	124816	[243]
776	Familial Adenomatous Polyposis (FAP)	175100	A D	familial	*APC*	5q21		108351	[244]
761	Holoprosencephaly (HPE)	142945	A D	*de novo*	*SHH*	7q36	Breakpoint 15 Kb telomeric to 5' end of *SHH*	9410	[245]
206	Iridogoniodys-genesis, type 1 (IRID1) (glaucoma)	601631	A D	*de novo*	*FKHL7 (FOXC1)*	6p25	Breakpoint in close proximity to *FKHL7 (FOXC1)*	1661	[246]
365	Neurofibromatosis type 2(NF2)	101000	A D	*de novo*	*NF2*	22q12.2	Breakpoint 6 Mb centromeric to the *NF2* gene. *NF2* on inactivated der(X)	95018	[247]
32	Rieger syndrome	180500	A D	*de novo*	*PITX2*	4q25-q26	Breakpoint approx 76 Kb telomeric to 5' end of *PITX2*	5673	[248-250]
33	Rieger syndrome	180500	A D	familial	*PITX2*	4q25-q26	Breakpoint approx 18 Kb telomeric to 5' UTR of *PITX2*	5673	[251-253]
170	Saethre-Chotzen syndrome	101400	A D	familial	*TWIST*	7p21	Breakpoint more than 230 Kb 3' of *TWIST*	1934	[254;255]
174	Saethre-Chotzen syndrome	101400	A D	*de novo*	*TWIST*	7p21	Breakpoint approx. 5 kb 3' of *TWIST* locus	1934	[256]
772	Saethre-Chotzen syndrome	101400	A D	Unknown	*TWIST*	7p21	Breakpoint around 230 Kb 3' of *TWIST*	1934	[257]

202	Townes-Brocks syndrome (TBS)	107480	A D	unknown	*SALL1*	16q12.1	Breakpoint at least 180 kb telomeric to *SALL1*	14823	[258;259]
791	Severe brachydactyly and syndactyly, mental retardation, hypoplasia of the cerebellum, scoliosis, and ectopic anus	-	Unknown	unknown	*HOXD*	2q31	Breakpoint approximately 390 kb centromeric to *HOXD13*	2269	[260]
792	Aplasia of the ulna, shortening of the radius, finger anomalies and scoliosis	-	Unknown	unknown	*HOXD*	2q31	Breakpoint approximately 1050 kb telomeric to *HOXD13*	2269	[261]
793	Bilateral aplasia of the fibula and the radius, bilateral Hypoplasia of the ulna, unossified carpal bones and hypoplasia and dislocation of both tibiae	-	Unknown	unknown	*HOXD*	2q31	Breakpoint approximately 590 kb telomeric to *HOXD13*	2269	[262]
920	Subset of Pelizaeus-Merzbacher disease (PMD) symptoms	312080	X-linked	familial	*PLP1*	Xq22	Breakpoint approximately 70 kb from *PLP1*	15792	[263]
DBCRs in the database in which the phenotype is due to deletions causing a direct interruption or a position effect:									
175	Saethre-Chotzen syndrome	101400	A D	*de novo*	*TWIST*	7p21	>11,560 deletion on 7p including *TWIST*	1934	[264]
177	Alagille syndrome	118450	A D	familial	*JAG1*	20p12	Entire *JAG1* gene deleted	36256	[265-267]
178	Alagille syndrome	118450	A D	*de novo*	*JAG1*	20p12	Deletion >3Mb encompassing *JAG1*	36256	[268]
525	Cleidocranial dysplasia (CCD)	119600	A D	unknown	*CBFA1*	6p21	Deletion involves at least part of *CBFA1*	124816	[269;270]

311	Isolated bilateral anophthalmia		Unknown	*de novo*	*SOX2*	3q26.3-q27	Approximately 740 kb deletion situated around 60 kb centromeric to the translocation breakpoint	2499	[271;272]
63	Haemophilia B	306900	X-linked	*de novo*	*F9*	Xq27.1-q27.2	Deletion of at least part of *F9*	32722	[273]

Table 2.2. A table of DBCRs for which the molecular pathology is known

A table of cases extracted from the DBCR database in which the rearrangement has been shown to have an effect on the known causative gene, either through direct disruption, position effect or deletion, thereby causing the phenotype. Cases are ordered by inheritance and then alphabetically by disorder.

* Figures calculated from UCSC Genome Browser May 2004 assembly

2.3.6. Impact on Mendelian Disease

2.3.6.1. Phenotypic diversity

There were 501 apparently distinct phenotypes reported in the 919 DBCR cases currently in the database. 225 of these phenotypes were catalogued in OMIM of which 104 (21 % of the total number of phenotypes) were autosomal dominant, 47 (9 %) were autosomal recessive phenotypes and 30 (6 %) were X-linked. In the remaining 320 disorders, the inheritance was uncertain. These may represent new Mendelian disorders or coincidental but unrelated pathological processes.

2.3.6.2. Loci with supporting evidence for phenotypic effect

1502/2023 (74 %) of the DBCR breakpoints in the database were in areas that had not been specifically implicated in the causation of the associated phenotype. There were 459 breakpoints from 411 cases that were located in cytogenetic bands that had been previously associated with the relevant disorder through some supportive evidence. This is usually from other cytogenetic cases or from family linkage data. 191 (41 %) of these implicated breakpoints had been physically mapped to some extent.

217 of the 919 cases in the database were associated with a phenotype for which the causative gene was known (82 genes from 501 phenotypes).

2.3.6.3. X-linked disorders

X-autosome translocations have been particularly important in human genetics. Many disorders with X-linked inheritance patterns have been clinically delineated. Both male and female cases with DBCRs involving the X chromosome and an X-linked disorder are very good predictors of causative gene location. Table 2.3 lists seven X-linked disorders where the locus was first mapped using DBCRs. In six of these, at least one DBCR identified the causative gene.

There was only one X-linked disorder in the database that had breakpoints outside the band containing the causative gene, namely Rett syndrome. There were five translocations associated with this phenotype [274-279], none of which disrupted the *MECP2* gene at Xq28 or the second locus, at Xp22, which has infantile spasms as an additional feature [280].

Disorder	Inheritance	Gene	Chromosomal location	Gene OMIM Number	Type of protein/protein function	Gene size* (bases)	Ref
X-linked disorders in which DBCRs were involved in loci mapping:							
Choroideremia	X-linked	*CHM*	Xq21.2	300390	Rab escort protein	186380	[281]
Duchenne muscular dystrophy (DMD)	X-linked	*DMD*	Xp21.2	300377	Actin binding protein. May anchor cytoskeleton to plasma membrane	2220381	[60-62;282]
Ectodermal dysplasia 1, anhidrotic	X-linked	ED1	Xq12-q13.1	300451	Seems to be involved in epithelial-mesenchymal signalling during morphogenesis of ectodermal organs.	423408	[283]
Lowe Syndrome	X-linked	*OCRL*	Xq26.1	309000	Phosphatase enzyme involved in actin polymerisation	52276	[284]
Menkes syndrome	X-linked	*ATP7A*	Xq12 - q13	300011	Copper transporting ATPase	139683	[285]
Mental retardation, X-linked 60 (MRX60)	X-linked	*OPHN1*	Xq12	300127	Rho-GTPase activating protein	390932	[286]
Simpson-Golabi-Behmel syndrome	X-linked	*GPC3*	Xq26	300037	Cell surface proteoglycan. Glypican family.	449893	[287;288]
X-linked disorders in which DBCRs were involved in gene mapping:							
Chondrodysplasia punctata 1, X-linked recessive (CDPX1)	X-linked	*ARSE*	Xp22.3	300180	Belongs to the sulfatase family. May be essential for the correct composition of cartilage and bone matrix during development	29459	[289;290]
Choroideremia	X-linked	*CHM*	Xq21.2	300390	Rab escort protein	186380	[291]
Duchenne muscular dystrophy (DMD)	X-linked	*DMD*	Xp21.2	300377	Actin binding protein. May anchor cytoskeleton to plasma membrane	2220381	[292]
Ectodermal dysplasia 1, anhidrotic	X-linked	ED1	Xq12-q13.1	300451	Seems to be involved in epithelial-mesenchymal signalling during morphogenesis of ectodermal organs.	423408	[293]

X-linked lissencephaly	X-linked	*DCX*	Xq22.3 - q23	300121	Seems to be required for initial steps of neuronal dispersal and cortex lamination during cerebral cortex development	118399	[294]
Lowe Syndrome	X-linked	*OCRL*	Xq26.1	309000	Phosphatase enzyme involved in actin polymerisation	52276	[295]
Mental retardation, X-linked 60 (MRX60)	X-linked	*OPHN1*	Xq12	300127	Rho-GTPase activating protein	390932	[296]
Simpson-Golabi-Behmel syndrome	X-linked	*GPC3*	Xq26	300037	Cell surface proteoglycan. Glypican family.	449893	[297]
Disorders in the database with DBCRs occurring in, or near to, already known disease genes:							
Androgen insensitivity syndrome (AIS)	X-linked	*AR*	Xq11-q12	313700	Dihydrotestosterone receptor. Steroid receptor	179648	[298]
Haemophilia-B	X-linked	*F9*	Xq27.1-q27.2	306900	Coagulation factor	32722	[299;300]
Hyper-IgM syndrome (HIGM)	X-linked	*CD40LG*	Xq26	300386	Mediates b-cell proliferation in the absence of co- stimulus. Involved in immunoglobulin class switching	12213	[301]
Opitz-G/ GBBB syndrome	X-linked	*MID1*	Xp22	300552	May have e3 ubiquitin ligase activity which targets the catalytic subunit of protein phosphatase 2 for degradation	172294	[302]
Severe neonatal-onset Ornithine transcarbamylase deficiency	X-linked	*OTC*	Xp21.1	300461	Mitochondrial matrix enzyme	69251	[303]
Disorders in the database with DBCRs occurring outside known disease genes:							
Rett Syndrome	X-linked	*MECP2*	Xq28	300005	Methyl CpG protein	67492	[279;304-308]

Table 2.3. X-linked disorders with loci or causative gene identified via DBCRs

A table of X-linked disorders in which loci and/or causative gene were identified via DBCRs. Also included are those disorders from the database in which DBCR breakpoints have occurred within, or close to, the already known causative gene and those in which the breakpoint occurred in another region of the genome. The position and size of the gene and the type of protein encoded are also listed.

* Figures calculated from UCSC Genome Browser May 2004 assembly

2.3.6.4. Autosomal disorders

In 23 autosomal disorders (17 dominant and two recessive) the confirmed locus was first mapped by DBCRs and in 14 of these the gene was also identified using physical mapping of DBCR breakpoints. Another seven have had the genes identified from already known disease loci. All but one of these are autosomal dominant disorders, which is to be expected since loss-of-function in a haploinsufficient gene is the most obvious mutational mechanism underlying the phenotypic effect of DBCR.

In only one autosomal-recessive condition, Alstrom syndrome, has the gene been identified via a DBCR. In this case, the DBCR breakpoint interrupted one copy of the *ALMS1* gene and a point mutation was identified in other allele [309].

Disorder	Inheritance	Gene	Chromosomal location	Gene OMIM Number	Type of protein/protein function	Gene size* (bases)	Ref
Autosomal disorders in which DBCRs were involved in loci mapping:							
Aniridia type II	A-D	*PAX6*	11p13	607108	Transcription factor. Paired box/ paired homeo/ homeobox	21303	[226;310]
Blepharophimosis-ptosis-epicanthus inversus syndrome (BPES)	A-D	*FOXL2*	3q23	605597	Forkhead box protein. Probable transcriptional regulator.	2733	[311]
Campomelic dysplasia	A-D	*SOX9*	17q24.3 - q25.1	608160	Important role in normal skeletal development. Possible transcription factor/regulator. Has HMG box	5400	[312;313]
Cleidocranial dysplasia (CCD)	A-D	*CBFA1/ RUNX2*	6p21	600211	Transcription factor involved in osteoblastic differentiation and skeletal morphogenesis	124816	[314]
Cornelia de Lange syndrome	A-D	*NIPBL*	5p13.1	608667	Unknown	187314	[315]
Diamond-Blackfan anaemia (DBA)	A-D	*RPS19*	19q13	603474	Ribosomal protein	11494	[316]
Greig cephalo-polysyndactyly syndrome (GCPS)	A-D	*GLI3*	7p13	165240	Zinc finger protein, plays a role in limb/brain development	259215	[317]
Holoprosencephaly 2, HPE2	A-D	*SIX3*	2p21	603714	Homeobox protein. May be involved in visual system development.	3580	[318]
Holt-Oram syndrome	A-D	*TBX5*	12q24.1	601620	Transcriptional regulator. T-box domain.	54511	[319]
Lymphedema-distichiasis syndrome	A-D	*FOXC2*	16q24.3	602402	Forkhead box protein. May be involved in the formation of special mesenchymal tissues	1505	[320]
Multiple exostoses	A-D	*EXT1*	8q24.11 - q24.13	608177	Tumour suppressor, cell growth and maintenance	312382	[321]
Nail-Patella syndrome (NPS)	A-D	*LMX1B*	9q34.1	602575	Transcription factor. Essential for specification of dorsal limb fate	81932	[322]

Rubinstein-Taybi syndrome	A-D	*CBP/ CREBBP*	16p13.3	600140	Acetyltransferase enzyme	154142	[77;323-325]
Specific language impairment	A-D	*FOXP2*	7q31	605317	Transcriptional repressor. Forkhead.	402081	[326]
Supravalvular aortic stenosis/ William's syndrome	A-D	*ELN*	7q11.2	130160	Major structural protein of some tissues. Tropoelastin family.	41488	[327]
Townes-Brocks syndrome	A-D	*SALL1*	16q12.1	602218	Transcriptional repressor	14823	[259]
Waardenburg syndrome, type 1	A-D	*PAX3*	2q35	606597	Probable transcription factor. Paired box/ paired homeo/ homeobox	99093	[328]
Factor X deficiency	A-R	*F10*	13q34	227600	Coagulation factor	26648	[329]
Hypomagnesia with secondary hypocalcemia (HOMG)	A-R	*TRPM6*	9q22	607009	Essential ion channel and serine/threonine-protein kinase	163697	[330]
Klippel-Trenaunay-Weber syndrome	Sporadic	*VG5Q*	5q13.3	608464	Potent angiogenic factor. Contains forkhead-associated domain and G-patch domain. Promotes angiogenesis and the proliferation of endothelial cells.	34803	[331]
Sotos syndrome	Sporadic	*NSD1*	5q35	606681	Transcription factor. Enhances androgen receptor transactiavtion.	161835	[332;333]
Isolated bilateral anophthalmia	Unknown	*SOX2*	3q26.33-q27	184429	HMG box	2499	[334;335]
Isolated lissencephaly	Unknown	*PAFAH1B1*	17p13.3	601545	Platelet activating factor. Probably involved in nuclear migration during cell division	91952	[336]
Autosomal disorders in which DBCRs were involved in gene mapping:							
Cornelia de Lange syndrome	A-D	*NIPBL*	5p13.1	608667	Unknown	187314	[337]
Diamond-Blackfan anaemia (DBA)	A-D	*RPS19*	19q13	603474	Ribosomal protein	11494	[338]
Greig cephalo-polysyndactyly syndrome (GCPS)	A-D	*GLI3*	7p13	165240	Zinc finger protein, plays a role in limb/brain development	259215	[339]

Holoprosencephaly 2, HPE2	A-D	*SIX3*	2p21	603714	Homeobox protein. May be involved in visual system development.	3580	[340]
Holoprosencephaly 3 (HPE3)	A-D	*SHH*	7q36	600725	Belongs to the hedgehog family.	9409	[341]
Holt-Oram syndrome	A-D	*TBX5*	12q24.1	601620	Transcriptional regulator. T-box domain.	54511	[342]
Iridogoniodysgenesis	A-D	*FKHL7/ FOXC1*	6p25	601090	Forkhead	1661	[343]
Multiple exostoses	A-D	*EXT1*	8q24.11 - q24.13	608177	Tumour suppressor, cell growth and maintenance	312382	[344]
Papillorenal syndrome	A-D	*PAX2*	10q24.3-q25.1	167409	Paired box transcription factor	84365	[345]
Retinoblastoma	A-D	*RB1*	13q14.2	180200	Regulator of other gene, tumour suppressor	178211	[346]
Rieger syndrome, type 1	A-D	*PITX2*	4q25	601542	Homeobox. May play role in development and maintenance of anterior structures	19926	[347]
Rubinstein-Taybi syndrome	A-D	*CBP/ CREBBP*	16p13.3	600140	Acetyltransferase enzyme	154142	[348]
Specific language impairment	A-D	*FOXP2*	7q31	605317	Transcriptional repressor. Forkhead.	402081	[349]
Supravalvular aortic stenosis/ William's syndrome	A-D	*ELN*	7q11.2	130160	Major structural protein of some tissues. Tropoelastin family.	41488	[350]
Waardenburg syndrome, type 1	A-D	*PAX3*	2q35	606597	Probable transcription factor. Paired box/ paired homeo/ homeobox	99093	[351]
Alstrom Syndrome	A-R	*ALMS1*	2p13	606844	Unknown	224160	[352]
Prader-Willi syndrome	Other	*SNRPN*	15q12	182279	May be involved in tissue-specific alternative RNA processing events. Has pre-mRNA splicing factor activity	595815	[353]
Klippel-Trenaunay-Weber syndrome	Sporadic	*VG5Q*	5q13.3	608464	Potent angiogenic factor. Contains forkhead-associated domain and G-patch domain. Promotes angiogenesis and the proliferation of endothelial cells.	34803	[354]
Sotos syndrome	Sporadic	*NSD1*	5q35	606681	Transcription factor. Enhances androgen receptor transactiavtion.	161835	[355]

Isolated bilateral anophthalmia	Unknown	*SOX2*	3q26.33	184429	HMG box	2499	[356]
Isolated lissencephaly	Unknown	*PAFAH1B1*	17p13.3	601545	Platelet activating factor. Probably involved in nuclear migration during cell division	91952	[357]
Autosomal disorders in the database with DBCRs occurring In, or near to, already known disease genes:							
Beckwith-Wiedemann syndrome (BWS)	A-D	*CDKN1C*	11p15.5	600856	Cyclin dependent kinase inhibitor, negative regulator of cell proliferation	2188	[358-360]
Blepharophimosis-ptosis-epicanthus inversus syndrome (BPES)	A-D	*FOXL2*	3q23	605597	Forkhead box protein. Probable transcriptional regulator.	2733	[361-369]
CHARGE syndrome	A-D	*CHD7*	8q12.2	608892	Probable transcription regulator	188125	[370]
Cleidocranial dysplasia (CCD)	A-D	*CBFA1/ RUNX2*	6p21	600211	Transcription factor involved in osteoblastic differentiation and skeletal morphogenesis	124816	[371]
Congenital agammaglobulinemia	A-D	*LRRC8*	9q34.13	608360	Unknown	35869	[372]
Cornelia de Lange syndrome	A-D	*NIPBL*	5p13.1	608667	Unknown	187314	[373]
Dextro-looped transposition of great arteries (DTGA), perimembranous ventricular septal defect.	A-D	*THRAP2*	12q24	608771	Unknown	318761	[374]
Early onset Alzheimers	A-D	*PSEN1*	14q24.3	104311	May play a role in intracellular signalling and gene expression or in linking chromatin to the nuclear membrane. Regulates epithelial- cadherin function	69139	[375]
Ehlers-Danlos syndrome type I	A-D	*COL5A1*	9q34.2-q34.3	120215	Collagen cell precursor	201087	[376]
Familial adenomatous polyposis (FAP)	A-D	*APC*	5q21	175100	Tumour suppressor	108351	[377]

Hereditary neuropathy with liability to pressure palsies (HNPP)	A-D	*PMP22*	17p11.2	601097	May be involved in growth regulation and myelinisation in peripheral nervous system. PMP-22/ EMP/ MP20 family.	35347	[378]
Macrocephaly, multiple lipomas, and hemangiomata	A-D	*PTEN*	10q23.31	601728	Potential tumour suppressor.	102125	[379]
Neurofibromatosis type 1 (NF1)	A-D	*NF1*	17q11.2	162200	Appears to be a negative regulator of the ras signal transduction pathway.	124432	[171;380]
Neurofibromatosis type 2(NF2)	A-D	*NF2*	22q12.2	607379	Probably a membrane stabilising protein. Similar to ERM family members	95018	[381-383]
Saethre-Chotzen syndrome	A-D	*TWIST*	7p12	601622	Basic helix-loop-helix transcription factor. Implicated in cell lineage determination and differentiation	1934	[384-388]
Trichorhino-phalangeal syndrome, type 1 (TRPS1)	A-D	*TRPS1*	8q24.12	604386	Zinc finger transcription factor. Transcriptional repressor.	260529	[389;390]
Williams-Beuren syndrome (WBS)	A-D	*ELN*	7q11.2	130160	Member of the Elastin family. Major structural protein of tissues such as aorta and nuchal ligament, molecular determinant of the late arterial morphogenesis	41514	[391]
Wilms' tumour	A-D	*WT1*	11p13	607102	Zinc finger DNA-binding protein that acts as a transcriptional activator or repressor	47612	[392]
Alagille syndrome	A-R	*JAG1*	20p12	601920	Ligand for Notch receptors. Involved in cell fate decisions during haematopoiesis. Involved in mammalian cardiovascular development	36256	[393-395]
Primary microcephaly	A-R	*ASPM*	1q31	605481	Probable role in mitotic spindle regulation and coordination of mitotic processes. May have a preferential role in regulating neurogenesis	62114	[187;396]
Cataract, congenital	Unknown	*CRYBB2*	22q11.2-q12.2	123620	Encodes crystalline subunit. Crystallins are the dominant structural components of the vertebrate eye lens	10440	[397]

Situs ambiguous, asplenia and corrected transposition of the great arteries	Unknown	*ZIC3*	Xq26.2	300265	Zinc finger protein. Transcription factor	5911	[398]
Autosomal disorders in the database with DBCRs occurring outside of known disease genes:							
Beckwith-Wiedemann syndrome (BWS)	A-D	*CDKN1C*	11p15.5	600856	Cyclin dependent kinase inhibitor, negative regulator of cell proliferation	2188	[288]
Campomelic dysplasia	A-D	*SOX9*	17q24.3-q25.1	608160	Important role in normal skeletal development. Possible transcription factor/regulator. Has HMG box	5400	[399]
Cleidocranial dysplasia (CCD)	A-D	*CBFA1/ RUNX2*	6p21	600211	Transcription factor involved in osteoblastic differentiation and skeletal morphogenesis	124816	[400-402]
Cornelia de Lange syndrome	A-D	*NIPBL*	5p13.1	608667	Unknown	187314	[403-405]
Dystrophic epidermolysis bullosa (DEB).	A-D	*COL7A1*	3p21.3	120120	Stratified squamous epithelial basement membrane protein	31180	[406]
Franceschetti (Treacher Collin's syndrome)	A-D	*TCOF1*	5q32-q33.1	606847	May be involved in nucleolar-cytoplasmic transport. May play a fundamental role in early embryonic development, particularly in development of the craniofacial complex	41301	[407;408]
Hereditary cyclic neutropenia	A-D	*ELA2*	19p13.3	130130	Modifies the functions of natural killer cells, monocytes and granulocytes	3954	[409]
Holoprosencephaly 2, (HPE2)	A-D	*SIX3*	2p21	603714	Homeobox protein. May be involved in visual system development.	3580	[410]
Holoprosencephaly 3 (HPE3)	A-D	*SHH*	7q36	600725	Belongs to the hedgehog family.	9409	[411;412]
Holt-Oram syndrome	A-D	*TBX5*	12q24.1	601620	Transcriptional regulator. T-box domain.	54511	[413]

Holt-Oram syndrome with lung hypoplasia and cardiomyopathy	A-D	*TBX5*	12q24.1	601620	Transcriptional regulator. T-box domain	54511	[414]
Huntington disease (HD)	A-D	*HD*	4p16.3	143100	Huntingtin protein, may play a role in microtubule-mediated transport/ vesicle function	169244	[415]
Hypo-phosphatemic rickets, autosomal dominant (ADHR)	A-D	*FGF23*	12p13.3	605380	Fibroblast growth factor. Inhibits renal tubular phosphate transport.	11501	[416]
Macrocephaly, multiple lipomas, and hemangiomata	A-D	*PTEN*	10q23.31	601728	Potential tumour suppressor.	102125	[417]
Retinoblastoma	A-D	*RB1*	13q14	180200	Regulator of other gene, tumour suppressor	178211	[418;419]
Thanatophoric dysplasia (TD)	A-D	*FGFR3*	4p16.3	134934	Fibroblast growth factor receptor. Receptor for acidic and basic fibroblast growth factors.	14975	[420]
Trichorhino-phalangeal syndrome, type 1 (TRPS1)	A-D	*TRPS1*	8q24.12	604386	Zinc finger transcription factor. Transcriptional repressor.	260529	[421;422]
Waardenburg syndrome, type I	A-D	*PAX3*	2q35	606597	Probable transcription factor. Paired box/ paired homeo/ homeobox	99093	[423]
Wilms' tumour	A-D	*WT1*	11p13	607102	Zinc finger DNA-binding protein that acts as a transcriptional activator or repressor	47612	[424]
Alagille syndrome	A-R	*JAG1*	20p12	601920	Ligand for Notch receptors. Involved in cell fate decisions during haematopoiesis. Involved in mammalian cardiovascular development	36256	[425]
Brody Disease	A-R	*ATP2A1*	16p12	108730	Contributes to calcium sequestration involved in muscular excitation/contraction	26022	[426]

Ceroid lipofuscinosis, neuronal 3, juvenile (CLN3)	A-R	*CLN3*	16p12.1	607042	Integral membrane protein. Belongs to the battenin family	14243	[427]
Cohen syndrome	A-R	*COH1*	8q22-q23	607817	Potential transmembrane protein that may function in vesicle-mediated transport and sorting of proteins	864313	[428]
Combined methylmalonic aciduria and homocystinuria (cblC type)	A-R	*MMACHC*	1p34.1	609831	Unknown	10736	[429]
Hypomagnesia with secondary hypocalcemia (HOMG)	A-R	*TRPM6*	9q21.13	607009	Essential ion channel and serine/threonine-protein kinase. Crucial for magnesium homeostasis.	61338	[430;431]
Shwachman-Diamond syndrome	A-R	*SBDS*	7q11	607444	Belongs to the UPF0023 family. May play a role in RNA metabolism.	7898	[432;433]
Smith-Lemli-Opitz syndrome (SLOS)	A-R	*DHCR7*	11q12-3	602858	7-dehydrocholesterol reductase. ERG4/ERG24 family.	13936	[434;435]
Walker-Warburg syndrome	A-R	*POMT1*	9q34.1	607423	Unknown	20880	[436]
Combined pituitary hormone deficiency	Other	*PIT1*	3p11	173110	Pituitary-specific transcription factor of the POU family	16954	[437]
		PROP1	5q	601538	Has DNA binding and transcriptional activation activity	4007	[437]
Klippel-Trenaunay-Weber syndrome	Sporadic	*VG5Q*	5q13.3	608464	Potent angiogenic factor. Contains forkhead-associated domain and G-patch domain. Promotes angiogenesis and the proliferation of endothelial cells.	34803	[438;439]
Sotos syndrome	Sporadic	*NSD1*	5q35	606681	Transcription factor. Enhances androgen receptor transactiavtion.	161835	[440;441]

Table 2.4. Autosomal disorders with loci or causative gene identified via DBCRs

A table of autosomal disorders in which loci and/or causative gene were identified via DBCRs. Also included are those disorders in the database in which DBCR breakpoints have occurred within, or close to, the already known causative gene and those in which the breakpoint occurred in another region of the genome. The position and size of the gene and the type of protein encoded are also listed.

* Figures calculated from UCSC Genome Browser May 2004 assembly

2.3.7. Apparent False Positive DBCRs

There were 42 cases in the database, with 30 different phenotypes, for which there was a confirmed pathological gene where none of the breakpoints occurred close to a known locus i.e. the breakpoints were in distant cytogenetic bands, on the opposite arm of the chromosome or on a different chromosome altogether (tables 2.3 and 2.4). There are at least three possible explanations for this: the breakpoint may be unrelated to the disease causing mutation, there may be locus heterogeneity for the disease or the phenotype may have been clinically misclassified. These apparent false positives thus merit further analysis.

An interesting and complex example is provided by the search for the gene causing Cornelia de Lange syndrome (CdLS, OMIM 122470). Two patients with classical CdLS have been reported with t(3;17)(q26.3;q23.1) [442] and t(14;21)(q32;q11) translocations [443]. Partial phenotypic overlap between mild CdLS and duplication 3q26.3-q27 syndrome [444;445] appeared to lend credence to the 3q36.3 breakpoint. Characterisation of this breakpoint showed that a large gene, *NAALADL2,* was interrupted with no evidence of accompanying deletions or further rearrangements. The direct interruption of this gene in combination with previous supporting evidence would strongly suggest a causative event. However, the expression pattern, the relatively recent evolution of *NAALADL2* and the apparent absence of any mutations in other cytogenetically normal CdLS individuals did not make it a good candidate for the phenotype [446].

The situation was somewhat clarified by the identification of *NIPBL* at 5p13 as a major CdLS gene by two separate groups, both mapping the same t(5;13)(p13.1;q12.1) CdLS associated translocation [447;448]. This was shown to

disrupt *NIPBL* in intron 1 and mutations were then identified in 15 CdLS individuals, confirming it as the causative gene.

A subsequent report of mutational analysis in 120 unrelated CdLS individuals found that 47 % had mutations in the *NIPBL* gene [449]. One of these patients was a case with a t(14;21)(q32;q11) translocation, which was shown to have a *de novo* nonsense mutation in exon 20 of *NIPBL,* confirming that the *de novo* DBCR was unrelated to the phenotype [450].

2.3.8. Trends in Reporting DBCRs

The publication of individual DBCR cases has increased over the last 35 years (figure 2.3). As would be expected, the number of genes identified via rearrangements has also increased with the availability of whole genome resources.

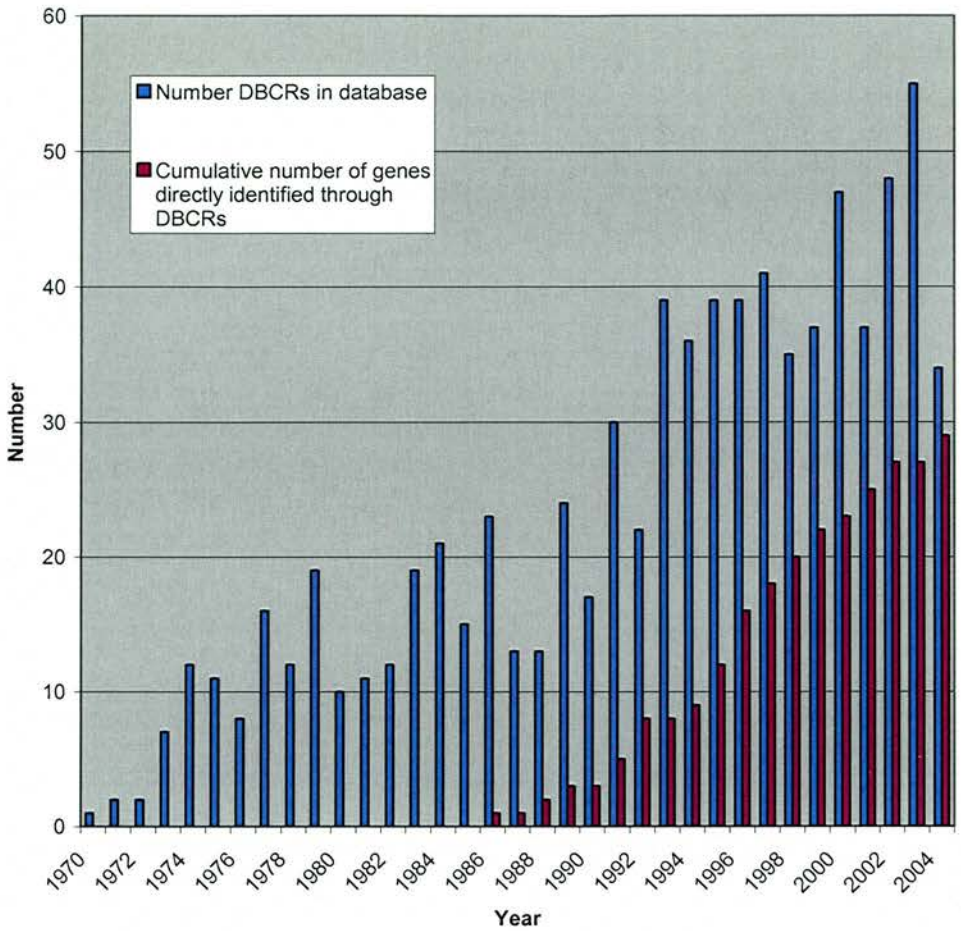

Figure 2.3. A graph showing trends in DBCR reporting

A graph showing the number of DBCR reports in the database per year (blue) and the cumulative number of genes identified through the physical mapping of DBCRs (red). The number of DBCR publications can be seen to increase over the last 35 years, as has the number of genes identified via DBCRs.

2.3.9. Conclusions

It is clear that DBCR research has contributed greatly to human genetic knowledge. The major breakthroughs have, expectedly, been in X-linked, autosomal dominant and sporadic disorders that are due to *de novo* loss of function mutations in one allele. DBCRs have so far only been involved in the identification of the causative gene for one autosomal recessive disorder, namely Alstrom syndrome, but have the potential to identify more, especially in cases with rearrangements segregating through multiple generations of a family.

In some cases, DBCR research has lead to the delineation of new and previously unrecognised Mendelian disorders. Careful delineation of the clinical phenotype is vital and a rigorous approach to syndrome diagnosis is necessary to maximise the chances of success. With regard to the molecular pathology, it is important to map all of the breakpoints in each DBCR case and a high index of suspicion should be maintained for microdeletions at and around the breakpoints.

It is hoped that DBCR research will continue to identify a number of genes for known Mendelian disorders and will also delineate new "sporadic" genetic syndromes and conditions. The existence of the DBCR database should help facilitate this important research.

2.4. Appendices

2.4.1. Search terms

2.4.1.1. Pubmed:

- De AND novo AND balanced AND translocation NOT leukaemia
- Translocation AND syndrome NOT leukaemia NOT cancer
- Translocation AND *de novo* NOT leukaemia
- Translocation AND reciprocal NOT leukaemia NOT cancer
- Translocation AND balanced NOT leukaemia NOT cancer NOT unbalanced
- (Translocation OR inversion) AND chromosom* AND human NOT (cancer OR tumour OR tumor OR leuk* OR lymphoma)

2.4.1.2. MeSH terms

- "Translocation" AND "Human" AND "Chromosomes, Human" OR "Chromosome Mapping" AND "Chromosome Aberrations" NOT "Leukemia" NOT "Neoplasms"

2.4.1.3. OMIM

- Balanced AND translocation

2.4.2. Database statistics

2.4.2.1. Cases

There are currently 919 cases entered into the DBCR database:

- Rearrangement origins:

  396 *de novo* events

  - 96 maternally inherited
  - 56 paternally inherited
  - 74 segregating through multiple generations of a family
  - 297 unknown

- Breakpoints mapped:

  - 552 only reported at the G-band level
  - 181 had one or more breakpoints mapped to some extent
  - 128 had both or all breakpoints mapped to some extent
  - 58 unknown

2.4.2.2. Breakpoints

There were 2038 breakpoints from the 919 cases:

- G-band classification:

  - 1178 breakpoints fell within Light G-bands
  - 426 breakpoints fell within dark G-bands
  - 169 fell within centromeric regions
  - 250 fell in other areas or are unknown

- Mapping resolutions:
    - 1328 not mapped below the 1 Mb level
    - 130 mapped between 250 and 500 kb
    - 95 mapped to below 250 kb
    - 225 mapped to breakpoint level
    - 245 unknown

- Previously implicated breakpoints:
    - 1502 breakpoints not previously implicated in the relevant disorder
    - 459 breakpoint had been previously implicated

2.4.2.3. Phenotypes

There were 501 apparently distinct phenotypes associated with the 919 cases:

- 225 were in the OMIM database:
    - 104 Autosomal dominant
    - 47 Autosomal recessive
    - 30 X-linked
    - 44 unknown

3: Materials and Methods

3.1. General Materials

3.1.1. Kits

Table 3.1. Kits and suppliers

Kit	Supplier
First strand cDNA synthesis kit for RT-PCR (AMV)	Roche Applied Science
Nucleon® BACC genomic DNA extraction kit	Nucleon
QIAprep® midi kits, QIAquick® gel extraction kit, QIAquick® PCR purification kit	Qiagen
Vector lab ABC kit	Vector labs

3.1.2. Bioinformatic resource URLs

Primer 3 programme: http://frodo.wi.mit.edu/cgi-bin/primer3/primer3_www.cgi

Ensembl Genome Browser: http://www.ensembl.org/index.html

UCSC Genome Bioinformatics: http://genome.ucsc.edu/

BACPAC Resources: http://bacpac.chori.org/home.htm

Wellcome Trust Sanger Institute: http://www.sanger.ac.uk/

3.2. Experimental Materials

3.2.1. Oligonucleotides

Oligonucleotides were obtained from Sigma Genosys. The primer sequences are listed in the table 3.2. Riboprobe primers were prefixed with either the T7 or T3 polymerase recognition sequence:

Forward primers were prefixed with the T7 sequence: AATACGACTCACTATAGG

Reverse primers were prefixed with the T3 sequence: ATTAACCCTCACTAAAGG

Table 3.2. Oligonucleotides

Type	Oligonucleotide	Nucleotide Sequence 5′-3′	Species
Long-Range PCR 20 kb	427E2_F	GAGAGAAGGGAGGGACAGGAAGGGAAGG	Human
	427E2_R	GCATGCACTGGGGACACCAAGTTTCTTT	Human
	C2orf22_F	CTAGGTCCCTGAGCTGGGGAAGCTGAAG	Human
	C2orf22_R	GAGACCATCCCGGCTAAAACGGTGAAAC	Human
	Cmklr1_LR1_F	GGACACAAGGAGATGAGGGGGTGTCAAG	Human
	Cmklr1_LR1_R	AGGAAGACGCTGGTGAACATGTTGTGGA	Human
	Cmklr1_LR2_F	CCACCTGCCAACTGAGTGACATGGAATC	Human
	Cmklr1_LR2_R	TGAGCTGAAAGCCATCCCAAGCAGTTCT	Human
	E2F6_F	GGCGAGGAAGTTACCCAGTCTCCTCCTG	Human
	E2F6_R	GCAGAGCTGGAGAGAGGGCAAGGTACAA	Human
	NM_182586_F	GGGCTTCTCTCCAGTGTGAAGTGGCTGT	Human
	NM_182586_R	AATCCATACCTGGCCTCATTGGGTTTGG	Human
	Q9Y4B7_LR1_F	GGAGTGAATTCATGGGGAACAGGAGCAA	Human
	Q9Y4B7_LR1_R	TTGACCTCAGGGGAGGCAAACACAATTC	Human
	Q9Y4B7_LR2_F	GCACAGAACGGACCCTAGTATCCCAGCA	Human
	Q9Y4B7_LR2_R	GCCTGGGCTTTTAAATGGTGCTCTGTCC	Human
	Q9Y4B7_LR3_F	ATGAATGGCTTTGAGGTGGCCAGAACAG	Human
	Q9Y4B7_LR3_R	TCACTGTTGGTGCCTGAGGTTCCTTGAA	Human
	Rock2_LR1_F	TTCACATTGTTGTGCAGCCATCACCACT	Human
	Rock2_LR1_R	TGACACCAGGGGTACACAAGCAAGAGGA	Human
	Rock2_LR1a_F	CCCTCCTCCCTTGTCTTCCTCCTTCCTC	Human
	Rock2_LR1a_R	TGCAGAACGGTTACCAAATGGCAAACAA	Human
	Rock2_LR2_F	ACTGCAACCTTCCCTTCCTGGGTTCAAG	Human
	Rock2_LR2_R	CCCTCTCCCTCATCCCTTCGAATCAGTC	Human
	Rock2_LR3_F	TCTTCAACCACCTGACAGAAGCGTCAGC	Human
	Rock2_LR3_R	TGGCTCATGCCTGTAATCCCAGCATTTT	Human
Long-Range PCR 10 kb	IK3_10_1a_F	GAGAAGTGGTGGGTGGGATGAGGTCACT	Human
	IK3_10_1a_R	CTTTTGCATGCCTTGTGAAAGCTGGTTG	Human
	IK3_10_1b_F	TGGAACAGAGACTTCACTGACCACACATGA	Human

IK3_10_1b_R	ATTTTAGAGTCCCCCACCTAGCCCCACA	Human
IK3_10_2a_F	AGCTTAGTGACCCAACTGCCCAAGCTGA	Human
IK3_10_2a_R	CCAGGGGACACAGGACAAAGAAGTGGAC	Human
IK3_10_2b_F	CCTTCCTCCCTCCCTCCCTCCTTTCTTT	Human
IK3_10_2b_R	ACCCACTCATTCACCGCAAGATCCATTC	Human
13G14_10_1a_F	CTGGGATTACAGGTGTGAGCCACTGTGC	Human
13G14_10_1a_R	TCAAGGAGACGCTTCCTGTGAAGCCCTA	Human
13G14_10_1b_F	CCACCAGCAAGACACAGCAGACACCATA	Human
13G14_10_1b_R	GGAAACAATCCAAATGCCCATCAACAGG	Human
131I18_10_1a_F	TCAAGCTCCACACTGACCGAGAGATTGG	Human
131I18_10_1a_R	CGTGGAGGTGCAGCTGATTCACTCATGTAT	Human
131I18_10_1b_F	GCATATGGGTAAACTGAGGCCCCAGGAG	Human
131I18_10_1b_R	ATCCAGGGGAAGCTTGCTAGGAATGCAG	Human
427E2_10_1a_F	GTGGAACTTGCGACACAGCAGAGAGGAA	Human
427E2_10_1a_R	GCCAATGCACCTGCCAAAGTGAAATACC	Human
427E2_10_1b_F	CCTGGCGTGATGTTTCTCTAAGCGTGAA	Human
427E2_10_1b_R	GCCACTGTACCTGGCCATCACCAAGTTT	Human
C2orf22_10_1a_F	GCTAGTGACAAAACCTGCTGGCCCTGAG	Human
C2orf22_10_1a_R	AGGCAGTGCCCTGTGACCACCAGTTAGT	Human
C2orf22_10_1b_F	AGACCGTGGAAAGAGAGGGAGAGGGAGA	Human
C2orf22_10_1b_R	GAGACCATCCCGGCTAAAACGGTGAAAC	Human
Cmklr1_10_1a_F	AGGTTGGTTTGGAAGGACTTGGCCTCTG	Human
Cmklr1_10_1a_R	TCTGACCACAATCAGCATCCACCCAAGT	Human
Cmklr1_10_1b_F	AGGAGCCATCACAGAGGGTTCGCAGATA	Human
Cmklr1_10_1b_R	TACAGAATGGGGTTCATGCAGCTGTTGG	Human
Cmklr1_10_2a_F	GGGGCCAGGGAAGGGGAATGAATACTAA	Human
Cmklr1_10_2a_R	AGTGAGGCCAGCAAGTCAAGGTCTCCAC	Human
Cmklr1_10_2b_F	TGCTGATGGACGTAGGCATAGAGGCTGA	Human
Cmklr1_10_2b_R	AAGCAGCCCTGAGAACTGCCAAGTTGAA	Human
LR_cmkex_1_F	ACAGTGAGGTGGGTTTCAGG	Human
LR_cmkex_1_R	ACTGCACCATCAGCTCTCCT	Human
LR_cmkex_2_F	GGGTGGGTGAGTGAGTGAGT	Human
LR_cmkex_2_R	CCATCATATCCCCTGTGACC	Human
LR_cmkex_3_F	TAGGTTACCCAGGTTGTCACCTGCATTG	Human
LR_cmkex_3_R	TAAATGCGGGAACCAGGACTTGAACGTA	Human
LR_cmkex_4_F	AGAATGGAGTGCAGTGGCACGATCTCAG	Human
LR_cmkex_4_R	CACCAGGCTATGGGCTGCATATGTGGTA	Human
E2F6_10_1a_F	GGCGAGGAAGTTACCCAGTCTCCTCCTG	Human
E2F6_10_1a_R	GCCTCATCTCACATGCTCGCCAGAACTA	Human
E2F6_10_1b_F	CCAGGCCCTTGTAGGCTGTTTCTTGCTT	Human
E2F6_10_1b_R	GCAGAGCTGGAGAGAGGGCAAGGTACAA	Human
NM_182586_10_1aF	GAACAGAACCATCAGGACAGGGGCAAAA	Human
NM_182586_10_1aR	TGAGTTCAAATGCCAGCTCTGCTGTGTG	Human
NM_182586_10_1bF	CAAGAACCCTCTCTTGGGTTGTGGATCG	Human
NM_182586_10_1bR	TTAGATGGAGCAGGGCTCCTGGAAGACA	Human
Q9Y4B7_10_1a_F	TGCACACATGGGGGAATGATGAAATTGT	Human
Q9Y4B7_10_1a_R	GAGCCTAGGAGGTCGAGGCAGTGAGCTT	Human
Q9Y4B7_10_1b_F	AACCCAGCAGCTTCAGGTGTAAGGCAGA	Human
Q9Y4B7_10_1b_R	CGACCCTGTATTTCTCTGGCCACATCGT	Human
Q9Y4B7_10_2a_F	CCGCCCCAGTTCTAACTTCTGTCCCTGT	Human
Q9Y4B7_10_2a_R	CTGAGCCAAAGCCCCATATCCTCAAAGG	Human
Q9Y4B7_10_2b_F	TTTTTCTTTCCCCTGCAGGCAGCTCTTC	Human
Q9Y4B7_10_2b_R	CACTGGAAACCAGGAGAAAGGCATGGAA	Human
Q9Y4B7_10_3a_F	GAGAAGGAGGAAGAGGAGGAGGCAGCAA	Human
Q9Y4B7_10_3a_R	CATGGACTGAGAAGTCGCCCCGTATCAT	Human
Q9Y4B7_10_3b_F	TGGAGATGCTGGATCCTGGGTGTTAAGG	Human
Q9Y4B7_10_3b_R	ACTTCAGCCTGGGTGACAGAGCAAGACC	Human

	Rock2_10_1a_F	TGGAATTGCACTTTATGAGCAGGGCAGA	Human
	Rock2_10_1a_R	CTGCCACTTAGCAGCTGCATGACTTTGG	Human
	Rock2_10_1b_F	GCACTCACCACCATGCCCAGCTAATTTT	Human
	Rock2_10_1b_R	TGTGTCTGCCTTTTGGGGCATATGGTTT	Human
	Rock2_10_2a_F	TGGGCCATATTTCCTTGTCTGTGGCCTA	Human
	Rock2_10_2a_R	TTCTGGCCTCCCTTTTCATTTCCACTGA	Human
	Rock2_10_2b_F	GCAGATTCTGAGCAACTGGCTCGTTCAA	Human
	Rock2_10_2b_R	AAGAATGATTCACAGGGCAAGGCCAGAA	Human
	Rock2_10_3a_F	CTCTGGGCACATGCAGTCCCCTCATAAT	Human
	Rock2_10_3a_R	GAGATTCCAACACTGCACTCCAGCCTGA	Human
	Rock2_10_3b_F	CAGTGGCTCACACCTGTAATCCCAGCAC	Human
	Rock2_10_3b_R	CCATCTCAATCCCAGTGGGTCTTTTCCA	Human
RT-PCR	Allc_F	ATTACCTGGTTCCCATGTCG	Mouse
	Allc_R	CCCAACCATCTGCTATGGAC	Mouse
	C2orf22_F	GCTGAGCGGTCCCTTCTC	Mouse
	C2orf22_R	GATACAGAGCAGGAGGATGACA	Mouse
	Cmklr1_F	CTGGGACTAGCACAGCATCA	Mouse
	Cmklr1_R	GATGATCACCAGACCATTGC	Mouse
	Cmklr1_2_F	AGTCACGCGCAGTAACAGAC	Mouse
	Cmklr1_2_R	CCAGGTTGACAAACCACACA	Mouse
	Colec11_F	CAGCTGAGGAAGGCTATTGG	Mouse
	Colec11_R	GTCCGAGTACACGAAAGCAC	Mouse
	E2F6_F	TGCACATAAGGAGCACCAAC	Mouse
	E2F6_R	GCCGCTACTGAGAACGAGAG	Mouse
	Esrrg_26610_F	ATGAGCCTCCTCCAGAGTGC	Mouse
	Esrrg_26610_R	GGGCCTCATGTAACACATCC	Mouse
	Esrrg_26610_2_F	GGATGAACTTGTCTATGCAGACG	Mouse
	Esrrg_26610_2_R	AGCGTCATCAGCATCTTGC	Mouse
	NM_182586_F	CTTCCCAGGTGACCAGACTC	Mouse
	NM_182586_R	TGACACAGAGTGACGGGTGT	Mouse
	Q9Y4B7_F	TTGCATGGACAGAAGGTTCC	Mouse
	Q9Y4B7_R	GGTTGAACTCAGCCATGAGG	Mouse
	Q92626_F	AGCCCTCATGGTAGAAGACC	Mouse
	Q92626_R	AACAGTCCTGCCACACTCG	Mouse
	Rarres2_F	AACCATAGGACTGAGGTGAAGC	Mouse
	Rarres2_R	ATTGTGCACTCCGGCTTTT	Mouse
	RnaseH1_F	AGGACCGGAGTCTTCCTGAG	Mouse
	RnaseH1_R	AAGAAAATGCGTCCTTGCTC	Mouse
	Rock2_F	AGTGGAGCCAGTTGGAGAAA	Mouse
	Rock2_R	CACCAACCGACTAACCCACT	Mouse
	Rps7_F	GCTTAAATCTTTCCAGAAAATCC	Mouse
	Rps7_R	TGTGTTCCACGTTGTTCTGC	Mouse
	Ush2a_F	GAAGCCCACCCTCTCTCC	Mouse
	Ush2a_R	TGGAGACAGTTGACAGAATTGG	Mouse
	56735_2_3_F	CCTGAGTCCCTTCACCACAT	Mouse
	56735_2_3_R	CATTGTATGCCACCACTTGC	Mouse
	60749_9_10_F	CAACCAAGGCAACTAAATGGA	Mouse
	60749_9_10_R	TCAGGCTCTGTCCAGGAGAT	Mouse
	Q9D178_F	GACGGTCTGGAGGAGAACAG	Mouse
	Q9D178_R	CTCCTGCACCATTGGGAAT	Mouse
	Ush2a_ex13_14_F	CAGGTTCAATTTGACGATGG	Mouse
	Ush2a_ex13_14_R	GACACTGGTGACAGCTACGC	Mouse
	Hum_Es_1_F	CAGTGACATCAAAGCCCTCA	Human
	Hum_Es_1_R	ACCAGCTGCAGGATAGCATT	Human
	Hum_Es_2_F	AGATCCCCAGACCAAGTGTG	Human
	Hum_Es_2_R	CTTTCAGCATGCCCACTTTT	Human
	Rock_seq_1F	CGAAGCCGGAGCTAGAGG	Human

	Rock_seq_1R	GACGAACCAACTGCACTTCA	Human
	Rock_seq_2F	TCCTGCTTTGAGGAAAAACAA	Human
	Rock_seq_2R	TACCATGCCTGTTTCATCCA	Human
	Rock_seq_3F	AGTTGTTCTTGCTCTGGATGC	Human
	Rock_seq_3R	TGTTATCCCAATGCCACTGA	Human
	Rock_seq_4F	TGTTTCCCTGAAGATGCAGA	Human
	Rock_seq_4R	TCCTCTTCTAGCTCCTTTGCTG	Human
	Rock_seq_5F	CAATCAAGGAAAAATGAAGTACGA	Human
	Rock_seq_5R	TCTCCAGCAGGCAGTTTTTA	Human
	Rock_seq_6F	CAACTGGATGAAACCAATGCT	Human
	Rock_seq_6R	TTTGGCTTCTTCGATGGACT	Human
	Rock_seq_7F	TCAGGAGAGATTTACTGATTTGGA	Human
	Rock_seq_7R	CTTTTCGAAGTTCAGCATTTTG	Human
	Rock_seq_8F	ACTCAGAAGCGCTGCCTTAC	Human
	Rock_seq_8R	GCATCTTTTTCCGTAAGTTCCT	Human
	Rock_seq_9F	CCCAACTGGAGATCACCTTG	Human
	Rock_seq_9R	CTTGATCATCTGCTGGGTCA	Human
	Rock_seq_10F	GGCTGAGATCATGAATCGAAA	Human
	Rock_seq_10R	TGGTCGGACATGAAATAACTTG	Human
	Rock_seq_11F	AGAAGGATGGCTTTCATTGC	Human
	Rock_seq_11R	CAGATTCTTTGCCGTTGAAA	Human
	Rock_seq_12F	CAACCAACTGTGAGGCTTGT	Human
	Rock_seq_12R	TTACAGGGAAAAGGGGAACA	Human
Sequencing	Cmk_1_F	TTGGTCTTGCTGGTATTGGTC	Human
	Cmk_1_R	TGGACAGGCTGAAGTTGTTG	Human
	Cmk_2_F	CCCCATCTCTCGTCTTCC	Human
	Cmk_2_R	AAGACATATCCTTGGGTGTCC	Human
	Cmk_A_F	GGTCTTGCTGGTATTGGTCAAC	Human
	Cmk_A_R	GGTTCTGGGACCAGACAGG	Human
	Cmk_B_F	TCCTCCCAATCCATATCACC	Human
	Cmk_B_R	CACCAGCAGAGGAAGAAGGT	Human
	Cmk_C_F	ACTGTCACCCGCTTCCTCT	Human
	Cmk_C_R	AGGTTCTTGCCTTGATCTTCAG	Human
	Cmk_450_1_F	GCTAAATAGCTGTGCCAGTCTC	Human
	Cmk_450_1_R	GCTTCCCACGCAACATTTAT	Human
	Cmk_450_2_F	CAAATTGCCTTCCCTTGAAT	Human
	Cmk_450_2_R	TGAAATTGAATCTGCATGCTAAG	Human
	ES_4_F	TCTACCTCTTTTGGTCTCTGTGC	Human
	ES_4_R	AACCCATCATGTGAGGTTGG	Human
	ES_5_F	ACATTGCCTTTGGGAAGCTA	Human
	ES_5_R	TACCTCATCTTTTTCTGGTTTCTCT	Human
	ES_6_F	TTTGTCACCTATGTGCTCTTGG	Human
	ES_6_R	CCTTGGAGTCAGTAGGGATGG	Human
	ES_7_F	TCAAAACACAAAATGCTCTAGG	Human
	ES_7_R	AATTCACCCAAATCTATATACATAACC	Human
	ES_8_F	ATGCAGAAGCCAGCTACCAT	Human
	ES_8_R	ACAAACCAGGTCTAGCAAATCC	Human
	ES_9_F	GGTTCAAGCTCAGAGAAGTTCAA	Human
	ES_9_R	CAGGAACCTATGGAGGAATCTG	Human
DOP-PCR	R710	CCGACTCGAGNNNNNNATGTGG	Human
Riboprobe	Cmklr1_F	CCGAGCCTCTACAACAGGAG	Mouse
	Cmklr1_R	GGTAACTTCCTCACCCACGA	Mouse
	Cmklr1_2_F	CAGAGGGAGGCTCTTAGGATGT	Mouse
	Cmklr1_2_R	GGCTCCTGCGACTTCAGG	Mouse
	Cmklr1_3_F	AGACCGTGAACACTGTGTGG	Mouse
	Cmklr1_3_R	ACATGTTGTGGCTGAGCAAG	Mouse
	Cmklr1_4_F	ACCACACCCTCTACCTGCTG	Mouse

	Cmklr1_4_R	GGCCACCTTGAATTTTCTGA	Mouse
	Cmklr1_5_F	CCGAGCCTCTACAACAGGAG	Mouse
	Cmklr1_5_R	GGTAACTTCCTCACCCACGA	Mouse
	Colec11_F	CATCTGAACGCCACCTTTTA	Mouse
	Colec11_R	GACCAAGACAAGAGCTTCACAG	Mouse
	Esrrg_F	GATGAGCCTCCTCCAGAGTG	Mouse
	Esrrg_R	ACCAGCTGCAGGATAGCATT	Mouse
	Q92626_F	TCTCACCCTATAGACACTGATGTG	Mouse
	Q92626_R	GCCTTACACATGTGGCTTTG	Mouse
	Rarres2_1_F	CTGTACAGCTGTGGCAGCAC	Mouse
	Rarres2_1_R	TTGGAAAGGAACAGACTCAGC	Mouse
	Rarres2_2_F	GATCCTCAGGAGTTGCAATG	Mouse
	Rarres2_2_R	TGTCTAGGGCTTATTTGGTTCTC	Mouse
	Rarres2_3_F	AACCATAGGACTGAGGTGAAGC	Mouse
	Rarres2_3_R	GCTCTGTCCACACCGATCTC	Mouse
	RnaseH1_F	CTGTGCATGGAGGACACAGT	Mouse
	RnaseH1_R	AGTCAAGGCCACCTGAGTGT	Mouse
	Ush2a_F	GAAGTGTGCTCTCTCACAGTCC	Mouse
	Ush2a_R	AATGTGACCTTCTTAGAAATAGCC	Mouse

3.2.2. Primary antibodies

All primary antibodies used are listed in the table 3.3.

Table 3.3. Primary antibodies

Antibody	Supplier	Type	Dilution
Estrogen Related Receptor gamma antibody	AbCam (ab12988)	Rabbit polyclonal to C-terminus	IHC: 1 in 500
CMKLR1 antibody	AbCam (ab13172)	Rabbit polyclonal to N-terminus extracellular	IHC: 1 in 500

3.2.3. Animals

All mice used were obtained from inbred cd1 strain crosses.

3.2.4. BACs, PACs and Fosmids

BAC and PAC clones were obtained from either BACPAC Resource Center (BPRC) at Children's Hospital Oakland Research Institute in Oakland, California or the Wellcome Trust Sanger Institute, Cambridge. Fosmids were obtained from the Wellcome Trust Sanger Institute.

3.2.5. Imaging

3.2.5.1. Colour brightfield imaging

For magnifications of less than 2.5x, imaging was performed using an imaging system comprising of a Leica MZFLIII fluorescence stereo microscope with 0.5x, 0.63x, 1x, 1.6x objectives, a 100W Hg source and Leica GFP1, GFP2, UV, B, G filters fitted with a Hamamatsu Orca AG CCD camera (Hamamatsu Photonics (UK) Ltd, Welwyn Garden City, UK) and CRI liquid crystal rgb filter (Cambridge Research & Instrumentation, Woburn, MA). Hardware control, image capture and analysis were performed using in-house scripts written for IPLab Spectrum (Scanalytics Corp, Fairfax, VA).

For magnifications of 2.5x and above, imaging was performed using a Coolsnap HQ CCD camera (Photometrics Ltd, Tucson, AZ) Zeiss Axioplan II fluorescence microscope with Plan-neofluar objectives (Carl Zeiss, Welwyn Garden City, UK) and colour additive filters (Andover Corporation, Salem, NH) installed in a motorised emission filter wheel (Prior Scientific Instruments, Cambridge, UK) were used sequentially to collect red, green and blue images, that were then superimposed to form a colour image. Image capture and analysis were performed using in-house scripts written for IPLab Spectrum (Scanalytics Corp, Fairfax, VA).

3.2.5.2. Fluorescent imaging

Imaging was performed using a Coolsnap HQ CCD camera (Photometrics Ltd, Tucson, AZ) Zeiss Axioplan II fluorescence microscope with Plan-neofluar objectives, a 100W Hg source (Carl Zeiss, Welwyn Garden City, UK) and Chroma #83000 triple band pass filter set (Chroma Technology Corp., Rockingham, VT) with the excitation filters installed in a motorised filter wheel (Prior Scientific Instruments, Cambridge, UK). Image capture and analysis were performed using in-house scripts written for IPLab Spectrum (Scanalytics Corp, Fairfax, VA).

3.2.5.3. 3D Fluorescent imaging

3D fluorescent images were captured on an imaging system comprising of a Princeton Instruments Micromax CCD camera with Kodak 1400e sensor (Universal Imaging, Maldon, UK), Zeiss Axioplan fluorescence microscope with Plan-neofluar or Plan apochromat objectives, a 100W Hg source (Carl Zeiss, Welwyn Garden City, UK) and Chroma #83000 triple band pass filter set (Chroma Technology Corp., Rockingham, VT) with the excitation filters installed in a motorised filter wheel (Ludl Electronic Products, Hawthorne, NY). A motorised stage and focus motor were employed to move the specimen in the xy and z dimensions. Hardware control, image capture and analysis were performed using in-house scripts written for IPLab Spectrum (Scanalytics Corp, Fairfax, VA).

3.3. Solutions

3.3.1. General Solutions

0.5 M EDTA pH 8.0: 186.1 g EDTA per litre. pH with NaOH

20x TBE: 216 g Tris-base, 110 g boric acid, 100 ml 0.5M EDTA, pH 8 per litre

20x SSC: 175.3 g NaCl, 88.2 g sodium citrate in 1 litre

5x Orange G loading dye: 0.06 % (w/v) Orange G, 50 % (v/v) glycerol in H_2O.

70 % Ethanol: 70% (v/v) absolute ethanol in H_2O.

TE: 10 mM Tris-HCl pH 8.0, 1 mM EDTA pH 8.0 in H_2O.

0.1M tri-Sodium citrate: 2.94g in 100ml sterile water

0.1M Citric acid: 1.92g in 100ml sterile water

10 mM citrate buffer: 41 ml 0.1 M tri-sodium citrate, 9 ml of 0.1 M citric acid, 450 ml water

0.1 M citrate buffer, PH 6: 2.1 g citric acid monohydrate in 900 ml water. pH with NaOH and make up to 1 litre.

80 % Glycerol: 80 % (v/v) glycerol with water

Heat-inactivated sheep serum: Sheep serum was heated to 60 °C for one hour before being aliquotted and stored at –20 °C.

Glutaraldehyde: 50 % (w/v) stock made up in water. Stored at 4 °C

3.3.2. Bacterial Solutions

Chloramphenicol: 10 mg/ml stock made up in ethanol. Stored at –20 °C

Kanamycin: 10 mg/ml stock in water. Stored at –20 °C

LB: 10 g tryptone, 5 g yeast extract, 10 g NaCl, 15 g agar per 1 litre

3.3.3. Tissue Culture Solutions

Trypsin: 2 g trypsin, 5 ml phenol red, 0.06 g penicillin, 0.13 g streptomycin in 1 litre PBS. pH to 7.8 with $NaHCO_3$

Versene: 0.4 g sodium EDTA, 5 ml phenol red in 1 litre PBS

Penicillin/Streptomycin: 7 g penicillin, 13 g streptomycin per litre

3.4. General Methods

3.4.1. Cell Culture

3.4.1.1. Fibroblast culture

Cells were cultured in DMEM (Life Technologies) supplemented with 10 % Foetal calf serum (FCS, Sigma) and penicillin/streptomycin. Cells were grown in a 5 % CO_2 incubator at 37 °C in 25 cm^2 or 75 cm^2 Falcon flasks. All solutions were warmed to 37 °C prior to use. The medium was removed and the cells carefully washed in PBS before incubation in 1 ml of trypsin/versene (1:1 v/v) solution at 37 °C, 5 % CO_2 for four minutes to lift cells off the surface of the flask. The flask was tapped gently to help detach the cells and the trypsin inactivated with the addition of

5 ml of fresh culture medium containing FCS. The cell suspension was pipetted up and down repeatedly to dissociate cell clumps and the cells split into clean flasks. These were then topped up with fresh medium.

3.4.1.2. Freezing cells

Cells were detached from the flask as above and the trypsin inactivated with the addition of fresh media. The suspension was transferred to a sterile 15 ml Falcon tube and spun at 1,200 rpm in a centrifuge at room temperature. The supernatant was then discarded and the pellet resuspended in 1 ml of freezing media, consisting of foetal calf serum with 10 % DMSO. This was placed into a 1.8 ml CryoTube (Nagle Nunc) and placed at –70 °C before being stored under liquid nitrogen.

3.4.1.3. Cell pellets

Cells were pelletted and stored at –40 °C until required for DNA or RNA extraction. Cells were treated as in section 3.4.1.2 but pellets washed thoroughly in PBS and then resuspended in 1 ml of sterile PBS, transferred into screw-top tubes and spun at 6,500 rpm in a microcentrifuge. The PBS was removed and the pellet frozen until ready for use.

3.4.1.4. Chromosome preparation

To enable rapid FISH screening for rearrangements, metaphase chromosome preparations were made from each of the primary fibroblast cell lines. To obtain the

maximum number of dividing cells, the fibroblasts were split (see section 3.4.1.1.) approximately 24 hours before treatment with colcemid (Gibco KaryoMAX). This was added to the culture medium to a final concentration of 0.1 μg/ml and the flask incubated at 37 °C for one hour. The medium was poured off and retained and the cells trypsinised (see section 3.4.1.1.). The trypsin was neutralised with the retained medium, the suspension transferred to 15 ml Falcon tubes and spun at 1,200 rpm for five minutes.

The supernatant was discarded and 10 ml hypotonic solution added (1:1 tri-sodium citrate: 0.56 % KCl). After incubation at 37 °C for ten minutes, the cells were once again spun and the pellet washed twice with 3:1 methanol: acetic acid fix and then resuspended in fresh fix to an appropriate concentration.

This suspension can then be stored at –20 °C indefinitely.

3.4.2. DNA Extraction and Purification

3.4.2.1. Isolation of genomic DNA from cells

DNA was isolated from cells using the Nucleon™ BACC Genomic DNA Extraction Kit, according to the manufacturer's instructions.

3.4.2.2. Isolation of genomic DNA from mouse spleen

Genomic DNA for use in PCRs was obtained from a cd1 mouse spleen. The tissue was minced, lysis buffer added (100 mM Tris pH 8, 5 mM EDTA pH 8, 0.2 % SDS, 200 mM NaCl, 4 mg proteinase K) and the mixture incubated overnight at 50-

55 °C. The tube was spun and the supernatant transferred to a new tube. Isopropanol (1 volume) was added and the precipitated DNA spooled. The DNA was washed thoroughly in 70 % ethanol, dried and resuspended in TE buffer. The DNA was then stored at 4 °C.

If required, a phenol: chloroform purification step can be included (see section 3.4.2.4.)

3.4.2.3. Preparation of BAC/PAC/Fosmid DNA

BAC, PAC and fosmid clones were grown in 5 ml Luria-Bertani broth (LB) containing 20 µg/ml chloramphenicol (BACs and fosmids) or 25 µg/ml kanamycin (PACs). Cultures were derived from either stabs or glycerol stocks and were incubated overnight at 37 °C in a shaking incubator. DNA extraction was performed by alkaline lysis, in accordance with the BACPAC resources protocol (http://bacpac.chori.org/bacpacmini.htm).

Glycerol stocks were prepared for every clone used. 800 µl sterile 80 % glycerol (v/v) was added to 200 µl of the relevant LB culture in a CryoTube (Nagle Nunc). This was mixed thoroughly and stored at –80 °C.

3.4.2.4. Extraction of DNA from paraffin embedded tissue

Paraffin blocks were cut and sections placed into screw top tubes. The paraffin wax was removed through three, five minute washes in xylene and the sections rehydrated though an ethanol series (two, five minute washes in 100 % ethanol and two minute washes in 80 %, 50 %, 30 % and distilled water). Once

rehydrated, the water was replaced with 500 µl proteinase K solution (400 µg/ml in 5 mM Tris-HCl, pH 7.5, 1 mM $CaCl_2$) and the tube incubated overnight in a 37 °C waterbath.

To deproteinise and purify the DNA, one volume of phenol:chloroform:isoamyl alcohol (25:24:1) was added and the tube contents mixed by vortexing. After being spun at 13,000 rpm in a microcentrifuge for ten minutes, the top layer containing the insoluble DNA was removed to a fresh tube and the DNA precipitated by adding one volume of isopropanol and storing at –20 °C for two hours to overnight. The tubes were then spun at 13,000 rpm for 30 minutes at 4 °C, the supernatant removed and the pellet rinsed with 70 % (v/v) ethanol. Once completely dry, the DNA was resuspended in Tris/EDTA (TE) buffer, pH 8, or ultra-pure water (Invitrogen).

3.4.3. Agarose Gel Electrophoresis

DNA molecules were separated according to size by agarose gel electrophoresis. Gel solutions of 0.8 to 2 % (w/v) were created by combining agarose with 0.5xTBE and microwaving until fully dissolved. Once the solution had cooled to below 50 °C, ethidium bromide was added to a final concentration of 200 ng/ml, and the gel was cast. DNA samples were mixed with 1x loading dye and run alongside either a 100 bp or 1 kb DNA ladder (approximately 300-600 ng).

Gels were electrophoresed for lengths of time varying from 30 minutes to two hours at between 50 and 100 volts. Gels were visualised using a UV transilluminator.

3.4.4. RNA Methods

3.4.4.1. RNA isolation

RNA was isolated from various tissues and cells using Trizol (Invitrogen) reagent and Phase-lock heavy gel tubes (Eppendorf), according to the manufacturer's protocols.

3.4.4.2. cDNA synthesis

cDNA was synthesised using the first strand cDNA synthesis kit for RT-PCR (AMV) (Roche Applied Science) according to the manufacturer's protocol.

3.4.5. Mouse Embryo Methods

3.4.5.1. Embryo dissection and fixation

Wild-type embryos were obtained from cd1 mouse crosses. The embryos were dissected from the uterus, under RNase free conditions, in ultra-pure PBS and fixed in 4 % PFA (w/v) in PBS for 2 hours at room temperature or overnight at 4 °C. The embryos were then washed twice (for five minutes each) in PTW (PBS with 0.1 % Tween-20), once in 50 % PTW: methanol and twice in 100 % methanol. At this stage the embryos could be stored in methanol at –20 °C indefinitely.

3.4.5.2. Paraffin embedding and sectioning

Embryos aged 11.5 dpc or over were processed using a TissueTek VIP processor. Younger embryos and dissected kidneys were dehydrated through an ethanol series, washed twice, for 15 minutes each, in 100 % ethanol, once in xylene at room temperature, once in xylene at 60 °C and then taken through three, 30 minute washes in paraffin wax (60 °C). Embryos were then embedded in clean paraffin wax and placed on ice or at 4 °C to harden.

4-6 μm sections were cut from the paraffin blocks using a microtome and floated onto superfrost plus slides (BDH). The slides were air-dried and then baked at 50 °C for 2 hours to overnight.

3.4.5.3. Wholemount *in-situ* hybridisations

See section 3.4.11.2.

3.4.6. Immunohistochemistry

3.4.6.1. Immunohistochemistry on paraffin sections

The paraffin wax on the slides was removed through three, five minute washes in xylene and the slides rehydrated though an ethanol series (two, five minute washes in 100 % ethanol and two minute washes in 80 %, 50 %, 30 % and distilled water).

Antigen retrieval was performed to unmask the antigen sites. Boiling 10 mM citrate buffer was poured into a glass coplin jar and the rehydrated slides added.

These were microwaved on full power for 30 seconds, left to stand for one minute and then microwaved for a further 30 seconds. The slides were then left to cool in the buffer for 20 minutes, washed twice in PBS, for five minutes each, and rinsed in distilled water.

In order to minimise the amount of antibody required for the sections, and to allow multiple antibodies to be applied to different sections on a single slide, a PAP pen (Sigma) was used. This is a wax-based pen that forms a hydrophobic barrier around the sections. The excess water was drained from the slide and the pen applied. The relevant liquid could then be applied almost immediately.

After antigen retrieval, a blocking buffer (PBS with 10 % heat-inactivated sheep serum) was applied to the sections to reduce non-specific binding. This was incubated at room temperature, in a humidified chamber, for at least one hour. After this time, the slides were washed twice in PBS and once in PTW (PBS with 0.1 % Tween-20) (for five minutes each). The primary antibody could then be applied at the relevant dilution, in blocking buffer and the slides incubated in a humidified chamber overnight at 4 °C.

After incubation with the primary antibody, the slides were again washed twice with PBS and once with PTW. The secondary antibody was then applied at the relevant dilution in blocking buffer and incubated at room temperature for one hour. The secondary antibody was washed off with PBS and PTW as before. If fluorescent secondary antibodies were used, the slides were mounted at this point in Vectashield mounting medium (Vector Labs), with or without the addition of 1 ng/ml DAPI (Sigma).

If the Vector lab ABC kit was being used, the ABC reagent was made up 30 minutes before use and left at room temperature. The reagent was applied for 30-60 minutes, after the secondary antibody had been washed off and the slides were washed as before. The colour on the slides was produced with the application of NBT and BCIP (3.3 µl and 3.5 µl per 1 ml respectively), which was applied in NTMT (100 mM Tris-HCl, pH 9.5, 100 mM NaCl, 50 mM $MgCl_2$). Once the colour had developed, the slides are washed with distilled water, counterstained with eosin (1 part 1 % eosin solution to 3 parts 70 % ethanol. Acetic acid added to 0.05 %) and dehydrated through three, two minute ethanol washes. The PAP pen was removed through three, five minute changes of Histoclear (National Diagnostics) and the slides were mounted in Histomount (National Diagnostics).

NBT/BCIP stained sections were imaged as in section 3.2.5.1. Sections for which a fluorescent secondary antibody was used were imaged as in section 3.2.5.2.

3.4.6.2. Immunohistochemistry on cells

In order to determine the cellular localisation of proteins, immunohistochemistry (IHC) was performed on cell lines. Approximately $5x10^4$ cells were seeded onto 12 mm diameter glass coverslips in 24-well plates and grown overnight at 37 °C.

The next day, the cells were rinsed in PBS and then fixed in 4 % paraformaldehyde (PFA) in PBS for 30 minutes at room temperature. This was washed off with five changes of PBS and the cells permeabilised for 30 minutes in PBS with 0.5 % Triton X-100 (Sigma). This was again removed through five changes of PBS. To prevent non-specific antibody staining, the cells were treated

with blocking buffer (2 % BSA in PBS) for two hours before the primary antibody was applied, diluted in the same blocking buffer, and incubated overnight at 4 °C.

The primary antibody was removed by washing the cells in PBS with 0.05 % Tween-20 (Sigma) and a fluorescent secondary antibody applied in blocking buffer. After one hour, the cells were again washed with PBS+0.05 % Tween and then post-fixed in 4 % PFA in PBS for 15 minutes at room temperature. This was rinsed off and the coverslips mounted on glass slides using Vectashield mounting medium (Vector Labs) with 1 ng/ml DAPI. The edges of the coverslips were sealed with clear nail varnish to prevent drying out.

Imaging was performed as in section 3.2.5.2.

3.4.7. Polymerase Chain Reaction (PCR)

3.4.7.1. Oligonucleotide Primers

All primers were designed using the Whitehead Institute for Biomedical Research Primer 3 programme (http://frodo.wi.mit.edu/cgi-bin/primer3/primer3_www.cgi). All, apart from those for riboprobe synthesis, were resuspended to 1 mM using TE buffer, pH 8. These were diluted 1 in 100 to create working stocks.

Riboprobe primers were diluted to 1 ng/µl and 1 µl of each primer diluted with 18 µl Ultra-Pure water to create a working stock.

For primer sequences, see table 3.2.

3.4.7.2. Standard PCR

Standard PCR reactions were performed in 50 µl volumes using 1 unit Amplitaq (Roche) with 200 µM dNTPs, 1xAmplitaq buffer, 1.25 mM $MgCl_2$ and 1 µM each primer. The amount of template DNA varied from 10-100 ng. All reactions were carried out in thick walled 0.5 ml tubes and amplifications carried out in MJ Research Peltier thermal cyclers.

The annealing temperature varied depending on the primers used but generally fell with the 58 °C to 62 °C range. PCRs were thermal cycled on the following touch-down programme:

TD55:
1) 95 °C for 5 minutes
2) 94 °C for 15 seconds
3) 69 °C for 30 seconds
-1 °C each cycle
4) 72 °C for 30 seconds
5) Repeat step 2 to 4 for 13 cycles
6) 94 °C for 15 seconds
7) 55 °C for 30 seconds
8) 72 °C for 30 seconds
9) Repeat steps 6 to 8 for 34 cycles
10) 72 °C for 2 minutes

3.4.7.3. Reverse-Transcriptase PCR (RT-PCR)

RT-PCR reactions were performed in 25 µl volumes as in section 3.4.7.2, using between 10 and 100 ng of cDNA (see section 3.4.4.2). In order to prevent any false positives, the number of cycles in the PCR programme was reduced.

RT_TD55: 1) 95 °C for 5 minutes
2) 94 °C for 15 seconds
3) 62 °C for 30 seconds
-1 °C each cycle
4) 72 °C for 30 seconds
5) Repeat steps 2 to 4 for 8 cycles
6) 94 °C for 15 seconds
7) 55 °C for 30 seconds
8) 72 °C for 30 seconds
9) Repeat steps 6 to 8 for 25 cycles
10) 72 °C for 2 minutes

3.4.7.4. Long-Range PCR

Long Range PCR reactions were performed using the Expand Long Template PCR system (Roche), according to the manufacturer's protocol. The following programme was used for all amplifications:

LR: 1) 92 °C for 2 minutes
2) 92 °C for 10 seconds
3) 65 °C for 30 seconds
4) 68 °C for 8 minutes
5) Repeat steps 2 to 4 for 10 cycles
6) 92 °C for 15 seconds
7) 65 °C for 30 seconds
8) 68 °C for 8 minutes
+20 seconds per cycle for 20 cycles
9) 68 °C for 7 minutes
10) 15 °C forever

3.4.7.5. Sequencing PCRs

Sequencing reactions were performed as in section 3.4.7.2 but using AmpliTaq gold (Roche) combined with Native PFU DNA polymerase (Stratagene). The PFU has proof reading activity and therefore reduces the chance of PCR induced errors. They were combined in a ratio of nine units AmpliTaq gold with one unit of PFU.

Sequencing PCRs were purified using either Qiagen gel purification kit or Qiagen PCR purification kit.

3.4.7.6. Degenerate Oligonucleotide Primed PCR (DOP-PCR)

Chromosome arm specific paint primary DOP products were kindly provided by Dr J. Trent. Primary DOP-PCR products were amplified through two rounds of DOP-PCR. 3 µl of the primary or secondary DOP product was added to a 47 µl standard PCR reaction mix (see section 3.4.7.2) containing 200 ng R710 primer (see table 3.2).

DOP-PCRs were run on the following programme:

DOP_P:
1) 92 °C for 2 minutes
2) 92 °C for 30 seconds
3) 56 °C for 30 seconds
4) 72 °C for 2 minutes
+3 seconds per cycle for 30 cycles

10 µl of the tertiary DOP-PCR products were ethanol precipitated by adding $1/10^{th}$ reaction volume 3M NaOAc, 2x volume ethanol and stored at –20 °C for two

hours to overnight. Tubes were then spun at 13,000 rpm for 20 minutes in a 4 °C microcentrifuge, the pellet washed with 70 % ethanol, re-spun, air-dried and each reaction resuspended in 40 µl TE buffer. These were then labelled by nick translation (see section 3.4.10.2).

3.4.7.7. Riboprobe synthesis PCR

Riboprobe synthesis PCRs were performed as in section 3.4.7.2, with the addition of 1 µl 1 in 50 dilution of mouse genomic DNA. PCRs were run on one of the following programmes and purified using Qiagen PCR purification kit. Elution was performed in ultra-pure water.

TD55: See section 3.4.7.2.

RIBO:
1) 94°C for 5 mins
2) 94°C for 1 min
3) 49°C for 1 min
4) 60°C for 1 min
5) Repeat steps 2 to 4 for 35 cycles
6) 60°C for 15 mins

TD62:

1) 95°C for 5 mins
2) 94°C for 15 secs
3) 72°C for 30 secs
   -1°C each cycle
4) 72°C for 30 secs
5) Repeat steps 2 to 4 for 10 cycles
6) 94°C for 15 secs
7) 62°C for 30 secs
8) 72°C for 30 secs
9) Repeat steps 6 to 8 for 34 cycles
10) 72°C for 2 mins

3.4.8. Sequencing of PCR Products

Sequencing reactions were set up using Big-Dye terminator version 3 (Applied Biosystems). 4 µl Big-Dye, diluted 1:1 with water was added to 5 µl PCR product and 1 µl of the relevant primer (diluted 1 in 1000 from the main stock). These were then run on the BD55 programme.

BD55:

1) 96 °C for 2 minutes
2) 96 °C for 30 seconds
3) 55 °C for 15 seconds
4) 69 °C for 4 minutes
5) Repeat steps 2 to 4 for 24 cycles

The reactions were purified by adding 50 µl ethanol, 2 µl 3M sodium acetate and 0.5 µl NF co-precipitant pellet paint (VWR International). The tubes were incubated in the dark, at room temperature, for 30 minutes and then spun at 13,000

rpm for 30 minutes. The pellets were washed in 70 % ethanol and dried in a 95 °C hot-block for 2 minutes.

Samples were then run on a ABI Prism 3100 Genetic Analayser (Applied Biosystems) and analysed using Sequencher software (GeneCodes Corporation).

3.4.9. Dissociation of Nuclei from Paraffin Embedded Tissue Sections

Sections (10-20 μm) were cut from paraffin blocks using a microtome and the appropriate number of sections (normally two or three) placed into an eppendorf tube containing Histoclear (National Diagnostics). The wax was removed through three, ten minute washes in histoclear and the tissue rinsed in ethanol before being rehydrated through an ethanol series (five minute washes in 100 %, 80 %, 70 %) and rinsed twice with distilled water. Between steps, the tissue was sedimented through centrifugation (9,000 rpm in a microcentrifuge).

To dissociate the nuclei within the tissue, the water was replaced with a pepsin solution (4 mg/ml in 10 mM HCl) and the tube incubated at 37 °C for four hours, vortexing thoroughly every 30 minutes. The cells were then passed through a 40 μm cell strainer (Falcon) and rinsed through with PBS. Centrifugation at 1,000 rpm for eight minutes in a bench-top centrifuge produced a pellet that was rinsed twice in PBS and once in 3:1 methanol: acetic acid fix. Fresh fix was added and the suspension was stored at –20 °C.

3.4.10. Fluorescent *In-Situ* Hybridisation (FISH)

3.4.10.1. FISH locus specific probe preparation

DNA from BACs, PACs, fosmids and long-range PCR products were labelled for FISH by nick translation, incorporating either digoxigenin 11-dUTP or biotin16-dUTP (both from Roche). Approximately 1 μg DNA was added to 5 μl 10x nick translation salts (500 mM Tris-HCl, pH 7.5, 50 mM $MgCl_2$, 100 mM □-mercaptoethanol, 100 μg/ml BSA), 5 μl 10x dNTPs (0.5 mM aATP, 0.5 mM dGTP, 0.5 mM dCTP and 0.3 mM dTTP) and 5 μl 0.2 mM biotin or digoxigenin dUTP. 1 μl 1:300 dilution of DNase I in water (10 units/μl, Roche) was added, along with 1 μl DNA polymerase I (10 units/μl, Sigma or Invitrogen). The total volume of the mixture was made up to 50 μl with water, the reaction mixed and incubated at 16 °C for 90 minutes.

The size of the nick translation products were checked by running 5 μl of the reaction on a 1 % agarose gel with ethidium bromide and a 100 bp ladder (see section 3.4.3.). The required size range of the products was 200-600 bp. If the products were too large, another 1 μl 1:300 DNase I was added and the mixture incubated at 16 °C for an extra 15 minutes.

The reaction was stopped using EDTA and unincorporated deoxynucleotides removed by ethanol precipitation. For each 50 μl reaction, 5 μl 0.5 M EDTA and 5 μl 3 M NaOAc, pH 5, were added to each reaction, along with 100 μl ethanol. Tubes were incubated at –20 °C for a minimum of one hour, generally overnight. Tubes were then spun in a 4 °C microcentrifuge at 13,000 rpm for 30 minutes, the pellet rinsed in 70 % (v/v) ethanol, air-dried and resuspended in 50 μl TE buffer.

3.4.10.2. Chromosome arm specific paint preparation

10 µl of the tertiary DOP-PCR products (see section 3.4.7.6) were labelled by nick translation as in section (3.4.10.1).

3.4.10.3. FISH on fixed cell suspensions

Cell suspensions (see section 3.4.1.4.) were diluted to an appropriate cell density with 3:1 methanol: acetic acid fix and dropped onto clean glass microscope slides. These were air-dried and then baked at 68 °C for 30 minutes. Once remove from the oven and cooled, slides were placed into pre-warmed 2xSSC at 37 °C for 30 minutes before being dehydrated through an ethanol series (70 %, 80 % and 100 % for two minutes each) and air-dried. Slides were denatured for two minutes in pre-warmed 70 % formamide/2xSSC (v/v), pH 7.5, at 72 °C and then dehydrated through an ethanol series as before, beginning with ice-cold 70 % ethanol.

Approximately 100 ng of the labelled probe (see section 3.4.10.1) was mixed with 1 µl salmon sperm DNA (Sigma; 10 mg/ml, sonicated to ~500 bp in size), 1.5 µl human cot-1 DNA per probe (1 mg/ml; Life Tech) and 2 volumes of ethanol. The mixture was dried in a vacuum drier and the resultant pellet resuspended in 3 µl hybridisation mix (50 % formamide, 10 % dextran sulphate, 2xSSC) at 37 °C for 30 minutes. The probes were denatured in a 72 °C waterbath for five minutes and then pre-annealed for 15 minutes at 37 °C. The probe could then be applied to the denatured slide on a 11x11 mm coverslip, which was sealed and the slide incubated for a minimum of 16 hours in a humidified chamber at 37 °C.

Post-hybridisation washes consisted of two, seven minute washes in 50 % formamide/ 2xSSC at 45 °C and two seven minute washes in .01xSSC at 60 °C. Blocking buffer (4xSSC/ 3 % BSA/ 0.1 % Tween-20) was applied and the slide incubated at 37 °C for five minutes and then the detection antibodies were applied (see table 3.4) in 4xSSC/ 1 % BSA/ 0.1 % Tween-20 and the slide once again incubated at 37 °C in a humidified chamber for at least 30 minutes. To remove the excess antibody, the slides were washed twice, for seven minutes each, in 4xSSC, 0.1 % Tween-20 at 37 °C. Slides were mounted with Vectashield mounting medium (Vector Labs) with 1 ng/ml DAPI.

Imaging was performed as in section 3.2.5.2.

Antibody	Species raised in	Source	Stock concentration (mg/ml)	Dilution
Fluorescein (FITC) avidin	Goat	Vecor	2	1:500
Rhodamine anti-digoxigenin	Sheep	Roche	0.2	1:100

Table 3.4. Detection antibodies used for FISH

3.4.10.4. FISH on paraffin embedded tissue sections

Sections on superfrost-plus slides (BDH) were heated to 60 °C for 20 minutes to melt the paraffin, which was then removed through four, ten minute washes in xylene. The slides were rehydrated through an ethanol series (ten minutes in each) into water. Sections were microwaved in 0.1 M citrate buffer for ten to 15 minutes and allowed to cool in the buffer for a further 20 minutes. The buffer was removed through several washes in water.

Slides were rinsed in 2xSSC and then placed into 2xSSC at 75 °C for two minutes, followed by denaturation in 70 % formamide/2XSSC for 3 minutes. Dehydration was performed through three minute washes in 70 %, 80 % and 100 % ethanol. The slides were then air-dried and FISH continued in the standard method (see section 3.4.10.3).

3.4.10.5. FISH on nuclei dissociated from paraffin embedded tissue

FISH on nuclei dissociated from paraffin embedded tissue was performed using a modified version of the method described in section 3.4.10.3.

Slides were made from fixed cell suspensions, baked at 68 °C for 30 minutes and then cooled. Pre-warmed proteinase K solution (5 mg/ml in 50 mM Tris, 1 mM $CaCl_2$ pH 7.5) was applied and the slides incubated for a relevant length of time at 37 °C. The proteinase K was removed through two five minute washes in PBS and the same in water, before being dehydrated through an alcohol series. Denaturation was performed in 70 % formamide/2xSSC at 72 °C for 15 minutes and the slides once again dehydrated.

Probes were prepared and applied and post hybridisation washes performed according as in section 3.4.10.3. Imaging was performed as in section 3.2.5.2 or 3.2.5.3.

3.4.11. RNA *In-Situ* Hybridisations

3.4.11.1. Riboprobe synthesis

Riboprobes were synthesised in 20 µl reactions, as below.

2 µl	Transcription buffer (Roche)
1 µl	RNase Inhibitor (Roche)
2 µl	Dig RNA labelling mix (Roche)
x µl	Purified PCR product (100-200 ng) (maximum 14 µl)
2 µl	RNA polymerase (T7 or T3) (Roche)
y µl	Ultra-pure water
20 µl	TOTAL

Reactions were incubated at 37 °C for two hours. 1 µl of the product was then run out on a 1 % agarose gel with ethidium bromide to check the quality of the reaction. DNase treatment was performed by adding 1 µl DNase in 80 µl ultra-pure water to the reaction and incubating at 37 °C for 10 minutes. The probe was then ethanol precipitated (10 µl 3 M NaOAc and 250 µl ethanol to each) at –20 °C overnight.

Reactions were spun at 13,000 rpm in a 4 °C microcentrifuge for 30 minutes, rinsed in 70 % ethanol, air-dried and resuspended in 49 µl ultra-pure water and 1 µl RNase inhibitor (Roche).

Aliquots of the probe were stored at –80°C.

3.4.11.2. Wholemount RNA *in-situ* hybridisations

RNA *in-situ* hybridisations were performed on wholemount mouse embryos under RNase free conditions and all solutions were made using ultra-pure water.

Hybridisation mix:

50 %	Ultra-pure formamide (Invitrogen)
5x	SSC
5 mM	0.5 M EDTA
100 µg/ml	Yeast RNA (Sigma, 50 mg/ml in 100 mM NaOAc, pH 5)
0.2 %	Tween-20
0.5 %	10 % CHAPS (w/v in water, Sigma)
100 µg/ml	Heparin (50 mg/ml in 1xSSC, Sigma)

Pre-treatment and hybridisation:

Embryos (see section 3.4.5.1.) were rehydrated through a methanol: PTW (PBS with 0.1 % Tween-20) series (75 %, 50 %, 25 %, PTW), letting the embryos sink in each solution. Once rehydrated, the embryos were washed twice in PTW and treated with 10 µg/ml proteinase K in PTW at 37 °C. The amount of time in proteinase K depended on the age of the embryos: five minutes for embryos aged 6.5 to 7.5 dpc and an additional five minutes for each extra day of development. After the relevant time, the proteinase K solution was very carefully removed and the embryos rinsed in PTW and then post-fixed for 20 minutes at room temperature in 4 % PFA with 0.1 % glutaraldehyde. Embryos were then washed in PTW, 1:1 PTW: hybridisation mix and then hybridisation mix, with embryos being allowed to sink in each solution.

Fresh hybridisation mix was added and the embryos incubated at 65 °C for three hours or overnight. Embryos could be stored indefinitely in this hybridisation mix, either before or after the 65 °C incubation step, at –20 °C.

For hybridisation, approximately 1 μg/ml of the heat-shocked labelled RNA probe (85 °C for five minutes) was added to pre-warmed hybridisation mix. The embryos were incubated in this solution overnight at 65 °C.

Post-hybridisation washes:

Embryos were rinsed twice in pre-warmed (65 °C) hybridisation mix then washed twice (30 minutes each) in pre-warmed hybridisation mix at 65 °C and once in pre-warmed 1:1 hybridisation mix: TBST (0.1 M Tris pH 7.5, 0.4 M NaCl) for ten minutes. Embryos were allowed to cool in this solution.

Once cool, the embryos were transferred to glass vials and washed in TBST overnight (or longer) at room temperature on an orbital shaker, with the solution being changed frequently.

Blocking and antibody application:

Embryos were incubated in blocking buffer (TBST with 3 % BSA and 20 % heat-inactivated sheep serum) at room temperature for a minimum of three hours on an orbital shaker. The alkaline-phosphatase anti-digoxigenin antibody (Roche) was applied at 1 in 2000 in fresh blocking buffer and the embryos incubated overnight at 4 °C.

Post-Antibody washes and signal detection:

Embryos were washed in large volumes of TBST to remove the antibody. Washes were performed in glass vials at room temperature on an orbital shaker and the solution was changed frequently (every 30 minutes for the first few hours and then as often as possible). Washes were performed at least overnight to help reduce background staining.

Signal detection was performed using NBT/BCIP. Embryos were washed twice, for ten minutes each, in NTMT (100 mM Tris-HCl, pH 9.5, 100 mM NaCl, 50 mM $MgCl_2$) and then placed into fresh NTMT with NBT/BCIP (3.3 µl and 3.5 µl per 1 ml respectively) in the dark. Colour development was checked every ten minutes and once colour had developed, the embryos were washed at least twice (five minutes each) in PTW pH 4.5 with 1 mM EDTA. This enhances the colour reaction and helps to reduce the background. Embryos are kept in this, in the dark, at least overnight before being washed in PBS, fixed in 4 % PFA with 0.1 % glutaraldehyde overnight at 4 °C and then washed in PTW. Embryos were stored in the dark in either PTW or PBS at 4 °C.

Imaging:

Embryos were imaged as in section 3.2.5.1

4: Strategy and Validation of Fluorescent *in-situ* hybridisation (FISH) Mapping of Chromosome Rearrangement Breakpoints in Interphase Nuclei

4.1. Introduction

Most molecular cytogenetic mapping of balanced chromosomal rearrangement breakpoints is performed on fixed cell suspensions made from peripheral blood leukocyte culture or established cell lines. Cases that do not have these available are generally considered impossible to study. This can be extremely disadvantageous as it leads to a subset of cases being overlooked, many of which may be associated with interesting phenotypes and could potentially lead to the identification of disease-causing genes.

To redress this balance, a method was developed to allow chromosomal rearrangements to be mapped using interphase nuclei from paraffin embedded tissue samples to a similar resolution to standard metaphase FISH approaches. The purpose of this chapter is to introduce the general approach that will be used to map the breakpoints in the cases described in chapters 5 and 6. This chapter will also demonstrate the broader utility of the interphase FISH mapping approach by confirming mosaicism for a balanced translocation in uncultured cells from child with Hypomelanosis of Ito.

4.2. Interphase FISH Breakpoint Mapping

Each structural chromosome anomaly studied was initially identified as an apparently balanced chromosomal rearrangement by conventional G-banded cytogenetic analysis (performed by the Lothian Regional clinical cytogenetic laboratory) and the breakpoints assigned to specific chromosome bands. Written consent was obtained from all families for use of the samples for research purposes.

Cytogenetic analyses of the cases described in chapters 5 and 6 were performed on metaphase preparations but these were no longer available as fixed cell suspensions had been discarded and the fibroblast cell-lines failed to recover from storage under liquid nitrogen. The chromosomal abnormalities in these cases could not, therefore, be studied any further using standard approaches. In the third case presented in this chapter, the interphase FISH mapping approach was used to confirm the presence of a mosaic balanced chromosomal rearrangement in uncultured cells.

4.2.1. Probe Testing

Before initiating interphase FISH mapping, each probe was tested on metaphase preparations from normal, control cell lines to confirm that they mapped solely to the expected chromosomal location. This is essential to the interpretation of the interphase mapping results and only probes showing single copy hybridisation signals at the expected loci were used.

The initial probes used for breakpoint mapping were BACs obtained from a set spaced at approximately 1 Mb intervals throughout the genome (from Dr Nigel Carter of the Sanger Centre, Cambridge). Clones were chosen from within the

cytogenetic band in which the breakpoint was reported, and from the bands on either side.

4.2.2. General Mapping Strategy

The general strategy of the interphase FISH mapping was to allow the position of a locus-specific probe to be unambiguously determined in relation to the translocation breakpoint. A crucial component of this approach was the availability of arm specific chromosome paints (a kind gift from Dr Jeff Trent [451]). In normal interphase nuclei, these paints will display two discrete domains, representing each homologous chromosome arm [452]. In the majority of reciprocal translocations, three domains will be detected representing the normal chromosome arm and the two derivative chromosomes, the identity of which can be determined by co-hybridising with either centromere or telomere-specific probes (see figure 4.1). In some cases the difference in the size of the domains is sufficient to distinguish between the two derivative chromosomes. Co-localisation of locus-specific probes with arm specific paints can be used to unambiguously map translocation breakpoints and has been used to successfully map a translocation associated with anophthalmia in peripheral blood leukocytes [453]. However, such an approach had not previously been applied to either paraffin-embedded tissue sections or uncultured cells.

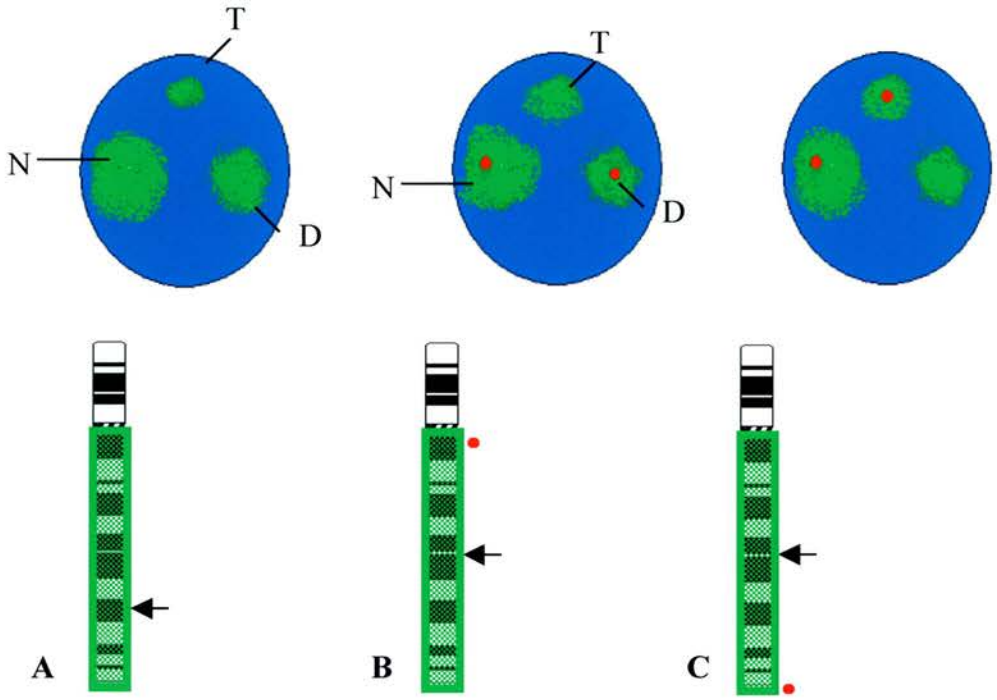

Figure 4.1. Interphase FISH with chromosome arm-specific paints

Blue circles indicate the nuclei, green domains, the chromosome-arm specific paints and red spots, the locus-specific clones. Arrows indicate the position of the breakpoints, N the normal paint domain, D the derived chromosome and T the translocated region. A) The breakpoint is at a position on the chromosome that produces paint domains of different sizes, allowing the two derived chromosomes to be distinguished. The largest domain is the normal chromosome. In this example, the medium sized is the derived chromosome and the smallest is the translocated region. B and C) The breakpoints are located near to the centre of the chromosome long arm. The paint therefore produces one large domain (the normal chromosome) and two similarly sized domains that can be distinguished by co-hybridising either a centromere probe (B) or telomere probe (C).

4.2.3. Mapping of Two DBCR Cases

Interphase FISH mapping was used to map the breakpoints in two translocation cases, which will be discussed in more detail in chapters 5 and 6. The mapping strategy had to be adapted slightly for some of the breakpoints, due to their location at the end of the chromosome arm, near to the telomere. The translocated region of the chromosome in these cases was too small to be detected with the chromosome arm specific paint, meaning that only two paint domains were visible instead of the expected three. The strategies used are outlined below.

4.2.3.1. Breakpoint mapping using arm-specific chromosome paints

The translocations in the two cases studied were reported as a t(1;2)(q32;p25) and a t(2;12)(p25.1;q24.1). The breakpoints on chromosomes 1 and 12 resulted in three domains on the application of the relevant arm specific chromosome paint. These domains were different sizes and could easily be distinguished, meaning that the location of co-hybridised locus-specific probes was easy to determine (see figure 4.2).

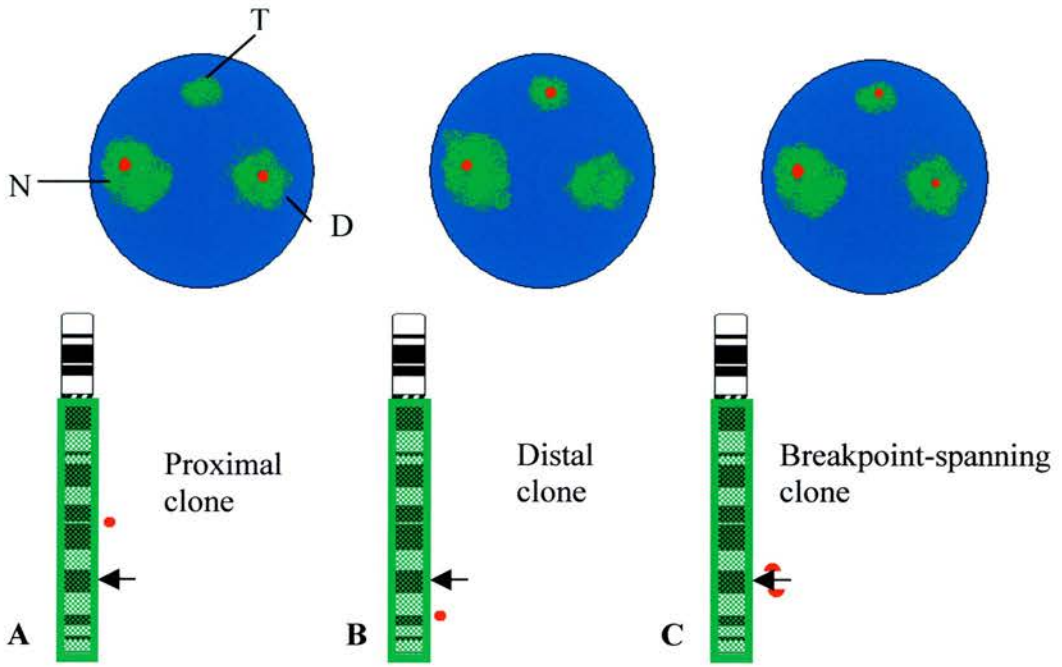

Figure 4.2. Chromosome 1 or 12 mapping using arm specific chromosome paints.

Blue circles indicate the nuclei, green domains, the chromosome-arm specific paints and red spots, the locus-specific clones. Arrows indicate the position of the breakpoints, N the normal paint domain, D the derived chromosome and T the translocated region. There are three sizes of paint domain: the largest representing the normal chromosome, the slightly smaller domain the derived chromosome 1 or 12 and the smallest, the translocated region. Proximal clones (A) can be seen to co-localise with the largest and slightly smaller paint domains, whereas a distal clones (B) will co-localise with the largest domain and the smallest domain. A breakpoint-spanning clone (C) will show three signals, one in each domain, indicating hybridisation to the normal and both derived chromosomes.

However, a complication arose when examining both chromosome 2 breakpoints, as these were located very close to the telomere of the chromosome. The translocated region was therefore too small to be detected using the 2p specific paint, a situation that would also arise if breaks were close to the centromere of the chromosomes. The result was two paint domains of apparently equal size, namely the normal 2p arm and the remaining part of 2p on the der(2) chromosome. In this circumstance, BAC clones that do not localise to either paint domain will co-localise with either a centromere or a telomere probe.

Therefore, for both cases, probes that were distal to the translocation breakpoint on chromosome 2p would only co-localise with one paint domain (the normal 2p) and, conversely, those that were proximal, would co-localise with both. Breakpoint spanning probes would have smaller signals both inside and outside the paint domain and also a signal in the normal domain (see figure 4.2). In both cases, there should always be one co-localising signal, representing the probe on the normal copy of the chromosome. In these cases, care has to be taken to ensure that probes are obtained that are both proximal and distal to the breakpoints to exclude the presence of deletions in the area undetectable by the chromosome paint.

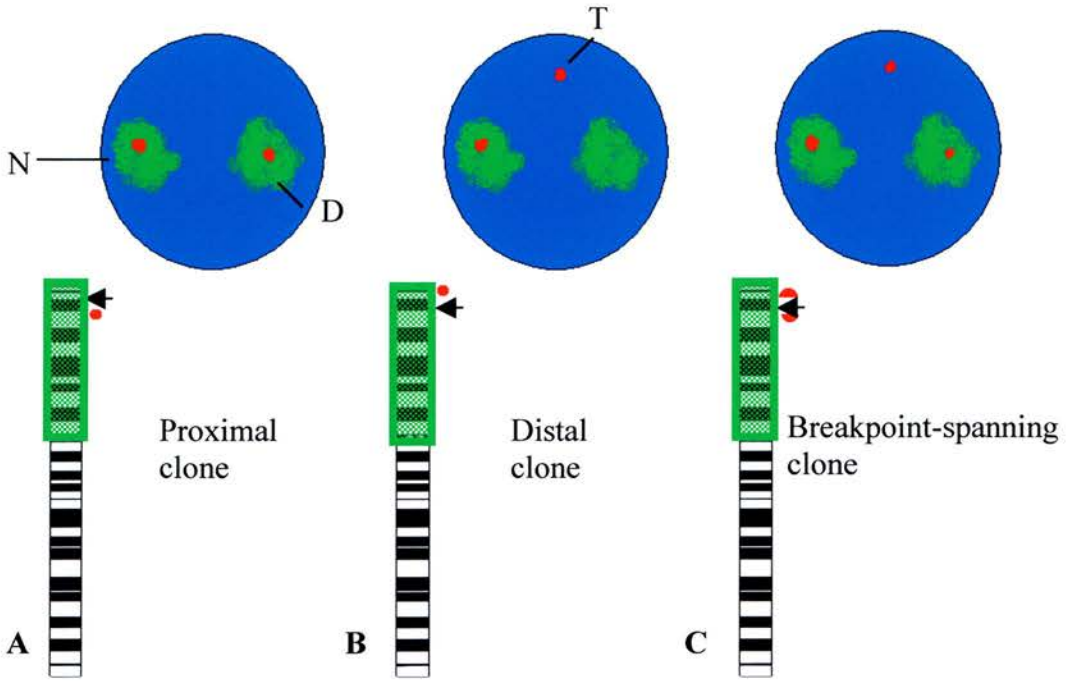

Figure 4.3. Chromosome 2 mapping using arm specific chromosome paints.

Blue circles indicate the nuclei, green domains, the chromosome-arm specific paints and red spots, the locus-specific clones. Arrows indicate the position of the breakpoints, N the normal paint domain, D the derived chromosome and T the translocated region. Proximal clones (A) can be seen to co-localise with both paint domains, whereas a distal clone (B) will co-localise with one domain (the normal chromosome 2) and appear outside the other domain, on the translocated region of the chromosome. A breakpoint-spanning clone (C) will show three signals, one in the normal chromosome 2 paint domain and two smaller signals; one in the other paint domain and one outside, indicating that the clone hybridises to both derived chromosomes.

4.2.3.2. Breakpoint mapping using pairs of probes

Nuclei extracted from archival paraffin embedded tissue sections are of poor quality for molecular cytogenetics. Although locus-specific probe signals may be clearly visible, the chromosome paint domains are sometimes very diffuse and hard to elucidate. To overcome this problem, it was decided to perform the high-resolution mapping of some breakpoints using BACs (or fosmids) applied in pairs, so that one can act as a reference for the other. Probes that have been localised using the chromosome paint strategy can be hybridised along with another probe, which has a different fluorescent label. The position of the probe can then be determined by examining whether the two signals co-localise.

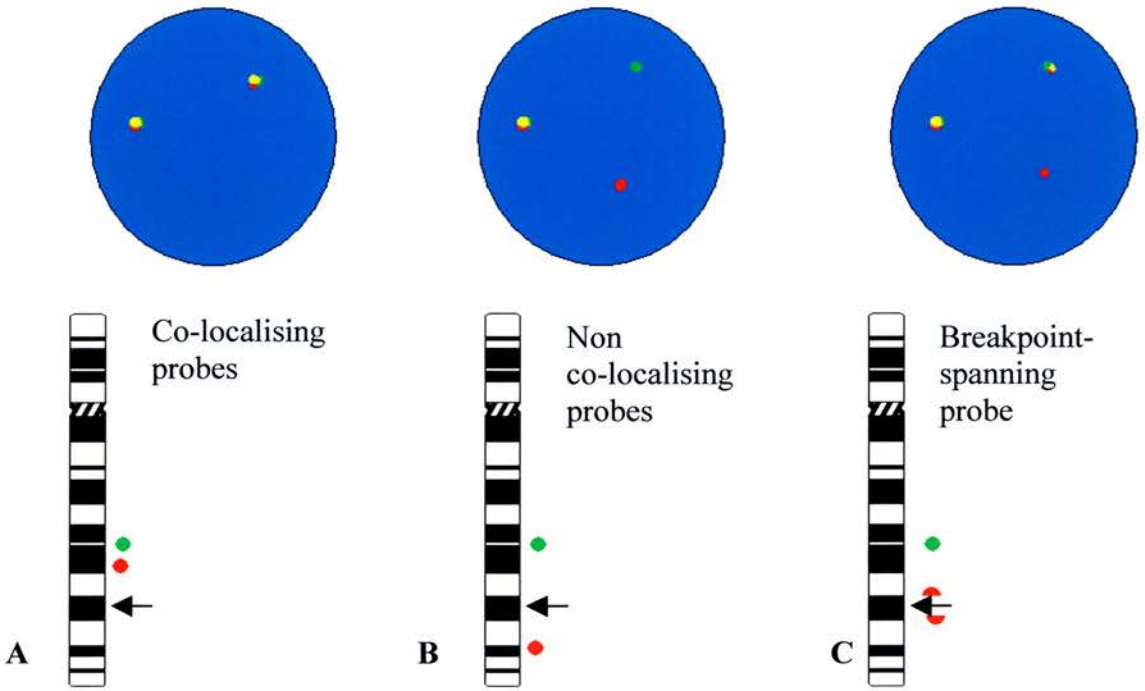

Figure 4.4. Breakpoint mapping using pairs of differently labelled probes.

The blue circles indicate the nuclei, the green and red dots, the differently labelled probes and the arrows, the position of the breakpoints. In this example, the reference probe (green) has been previously determined to be proximal to the breakpoint. If the test probe (red) co-localises with both green signals, the probe is also proximal (A). If only one signal co-localises (B), the test probe is distal, with one red signal being on the normal chromosome, and hence co-localising, and the other being on the translocated region. A breakpoint-spanning clone will produce three red signals, two of which co-localise with the green signals and one that does not, indicating hybridisation to the normal chromosome and both derived chromosomes.

4.2.4. Methods

For a description of the methods used, see sections 3.4.9 and 3.4.10.5.

4.2.5. Results and Discussion

4.2.5.1. FISH on tissue sections

The initial attempts at mapping were performed on paraffin embedded tissue sections from control cases that were mounted on glass microscope slides before FISH was performed. Although some signals were visible, the analysis of the co-hybridising signals was difficult, predominantly due to the thickness of the sections and the level of tissue autofluorescence (see figure 4.5). The samples from the cases featured in chapter 5 and 6 were received as 20 μm sections and the layers of overlapping nuclei made it impossible to determine any signals, in spite of optimisation of the proteinase K digestion times.

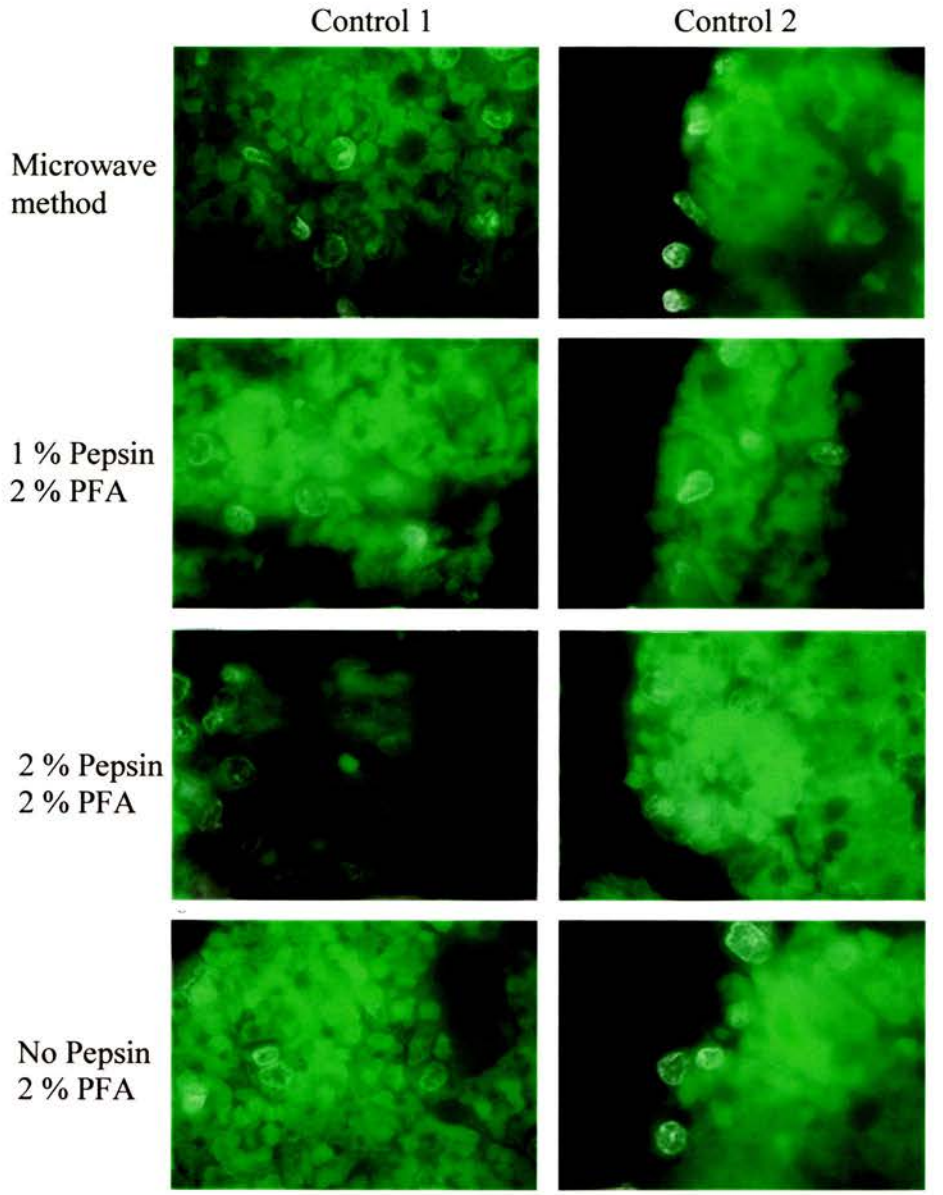

Figure 4.5. FISH on paraffin embedded sections

FISH on paraffin embedded tissue sections using arm specific chromosome paints labelled with biotin and detected with FITC (green). The paint signals cannot be distinguished from the high level of background caused by both autofluorescence and detection of biotin within the tissue. Two different controls were used and pepsin treatment and fixation were altered in an attempt to decrease the background staining and increase the permeability of the DAPI stained nuclei (grey). No signals were discernable in any of the sections.

4.2.5.2. FISH on nuclei dissociated from tissue sections

In order to overcome the problems encountered when performing FISH on tissue sections, nuclei were isolated from control tissue sections using a technique adapted from Liehr *et al* [454]. This involved de-waxing and rehydrating the sections, then dissociating the nuclei by treating the sections with pepsin and vortexing regularly. The solution was filtered through a cell strainer to remove any clumps of cells or debris to produce a single cell suspension. The cells were pelletted, washed, fixed in 3:1 methanol: acetic acid fix and then dropped onto slides.

As these nuclei had been formalin fixed prior to embedding in paraffin, using a standard clinical pathology protocol optimised for tissue histology, the nuclear membrane proved difficult to penetrate for the purposes of hybridisation of fluorescently labelled DNA probes. To improve penetration, the slides were treated with proteinase K for varying lengths of time, depending on the age and fixation of the sample. The length of time for denaturation of the samples was also increased as compared to that for normal fixed cell suspensions.

Overall, this method has proved to be very successful for performing FISH on nuclei from paraffin embedded tissue samples (see figure 4.5). Each sample required very careful titration of the incubation time in proteinase K. In general, the older samples required longer in proteinase K but this was not always the case as fixation methods of the samples may differ. The required incubation times were elucidated by performing a simple time-course experiment and times generally fell within the 10-20 minute range (see table 4.1).

This method has provided an easy, efficient way to study those previously difficult or impossible cases in which there are no fixed cell suspensions or viable material available.

	PK digestion (minutes)						
	5	10	12	15	17	20	25
Control 1	+++	+	-	-	-	-	-
Control 2	-	-	-	++	+++	++	+
t(2;12)	-	-	+	++	+++	-	-
t(1;2)	-	-	++	+++	+++	++	-

Table 4.1. Proteinase K treatment times

A table showing the optimum proteinase K (PK) digestion times (in minutes) for each case. +++ indicates very good signals, ++ good signals, + average signals and – indicates no or very poor quality signals. t(2;12) and t(1;2) are the translocation cases described in chapters 5 and 6 respectively.

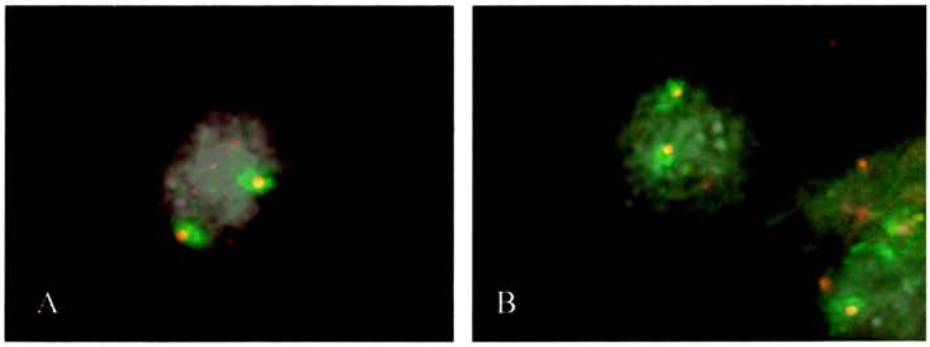

Figure 4.6. FISH on nuclei dissociated from paraffin embedded tissue

FISH using biotin labelled arm specific chromosome paints detected with FITC (green) and co-localising rhodamine detected BACs (red) on DAPI stained nuclei dissociated from control paraffin embedded tissue sections. BAC signals are clear and can be seen within the distinct chromosome paint domains.

4.2.5.3. Advantages and disadvantages of FISH on dissociated nuclei

As with all methods, FISH on nuclei dissociated from paraffin embedded tissue sections has both advantages and disadvantages.

The disadvantages of this method depend upon the samples available. The lack of dividing cells, and therefore metaphases, does not compromise the ability to map chromosomal rearrangements but the quality of the nuclei dissociated from the tissue sections, can. As many samples are obtained from formalin fixed archival patient material, the nuclei can be hard to penetrate with the FISH probes or, conversely, the nuclei may be extremely fragile and degraded. The intensity of the signals from locus specific probes is also not as good as that on fresh fixed cell suspensions, meaning that breakpoint spanning clones or small locus-specific probes may not be discerned. The method itself, however, is fairly robust, only requiring slight optimisation for each new sample.

The disadvantages are far outweighed by the advantages of this method. The main advantage is that it allows the study of a previously impossible subset of cases, namely those with only paraffin embedded material available. This utilisation is vital for researchers wishing to study chromosomal rearrangements as cell lines often do not survive retrieval from liquid nitrogen and fixed cell suspensions are often only stored for a short time. The ability to map chromosomal rearrangements using nuclei dissociated from archival patient material, or any other interphase nuclei, is a valuable asset and can be utilised in all manner of ways using many different cell

types. One case demonstrating the broad applicability of this method is outlined below.

4.3. FISH on Buccal Cells

Described below is a case that aptly demonstrates the broad applicability of interphase FISH analysis and which proved to be very useful to the clinical interpretation of the cytogenetic results. In this case, interphase FISH using arm-specific chromosome paints on uncultured buccal cells was used to confirm a finding of mosaicism in a young boy.

4.3.1. Case Report

The male child was diagnosed as having Hypomelanosis of Ito on the basis of macrocephaly, developmental delay and pigmentary mosaicism Hypomelanosis of Ito, is a rare sporadic disorder characterised by unilateral or bilateral macular (i.e. spotty) hypopigmented whorls or streaks. A significant proportion of cases are associated with chromosomal mosaicism. Routine cytogenetic analysis on peripheral blood leukocytes showed a normal 46,XY karyotype.

Analysis of fibroblasts grown from a skin biopsy from this boy was found to have a t(1;9)(q21-23;q22) translocation in 4 out of 50 metaphases. However, these cells had grown very poorly in culture and in view of the normal blood cytogenetics in 50 metaphases examined, the rearrangement was suspected to be a cultural artefact. To test this hypothesis, FISH was performed on buccal cells from the patient.

FISH on these cells has many advantages, the main one being that the cells do not require culturing, meaning that FISH can be performed directly on the sample, enabling a quick result and eliminating the risk of further abnormalities developing in culture. They are also particularly useful for mosaicism studies as large numbers of cells can be obtained non-invasively using either mouthwash or cytobrushes, allowing an accurate elucidation of the proportion of translocation carrying cells.

The initial protocol was obtained from the Nina T. Holland superfund protocol library (http://ehs.sph.berkeley.edu/holland/ProtocolLibrary.html) but results obtained using this were unsatisfactory. The method was adapted, mainly by changing the fixation methods of the cells, to enable long-term storage of samples and to increase the permeability of the cells to the FISH probes.

4.3.2. Methods

The FISH method for buccal cells was adapted from that obtained from the Nina T. Holland superfund protocol library (http://ehs.sph.berkeley.edu/holland/ProtocolLibrary.html).

Buccal cells were obtained by intraoral scraping using a soft nylon cytology brush. The brush was agitated vigorously in 0.01 M Tris HCI, 0.1 M EDTA and 0.02 M NaCl at pH 7.0 to release the cells, which were washed twice in the same buffer and once in 3:1 methanol: acetic acid fix, then stored in fresh fix at –20 °C. The resulting cell suspension was dropped onto glass slides, baked at 68 °C for 30 minutes and treated with pepsin (300 μg/ml in 10 mM HCl at 37 °C for 30 minutes). The slides were post-fixed in 4 % PFA in PBS for 20 minutes on ice, then washed in

water, followed by PBS and baked for a further 20 minutes at 68 °C. FISH was performed using standard methods (see Section 3.4.10.5), with the following modifications: denaturation time in 70 % formamide/2xSSC was increased to four minutes, post-hybridisation washes consisted of two, seven minute washes in 50 % formamide/2xSSC at 45 °C, then seven minutes in 2xSSC at 45 °C, followed by seven minutes in 2xSSC at room temperature. The arm-specific chromosome paint (a kind gift from Dr Trent [455]) for 1q was labelled in biotin and detected with FITC and the paint for 9q was labelled in digoxigenin and detected with Rhodamine.

4.3.3. Results

Buccal cells were collected and FISH performed using arm-specific chromosome paints for 1q (labelled in biotin and detected with FITC) and 9q (labelled in digoxigenin and detected with Rhodamine). Three signals were identified using the chromosome 1q paint, indicating the normal chromosome, the derived chromosome 1 and the derived chromosome 9. The chromosome 9q paint only showed two signals, which corresponded to the normal chromosome 9 and the derived chromosome 1 (see figure 4.6). The der (9) was not visible because the heterochromatin dominating this region did not stain well with the 9q chromosome paint due to the competitive hybridisation with COT1 DNA in the hybridisation mix. Using FISH, the translocation was detected in 5 % of the 200 buccal cells examined. Two domains were seen for each chromosome paint in 100 control buccal cells scored.

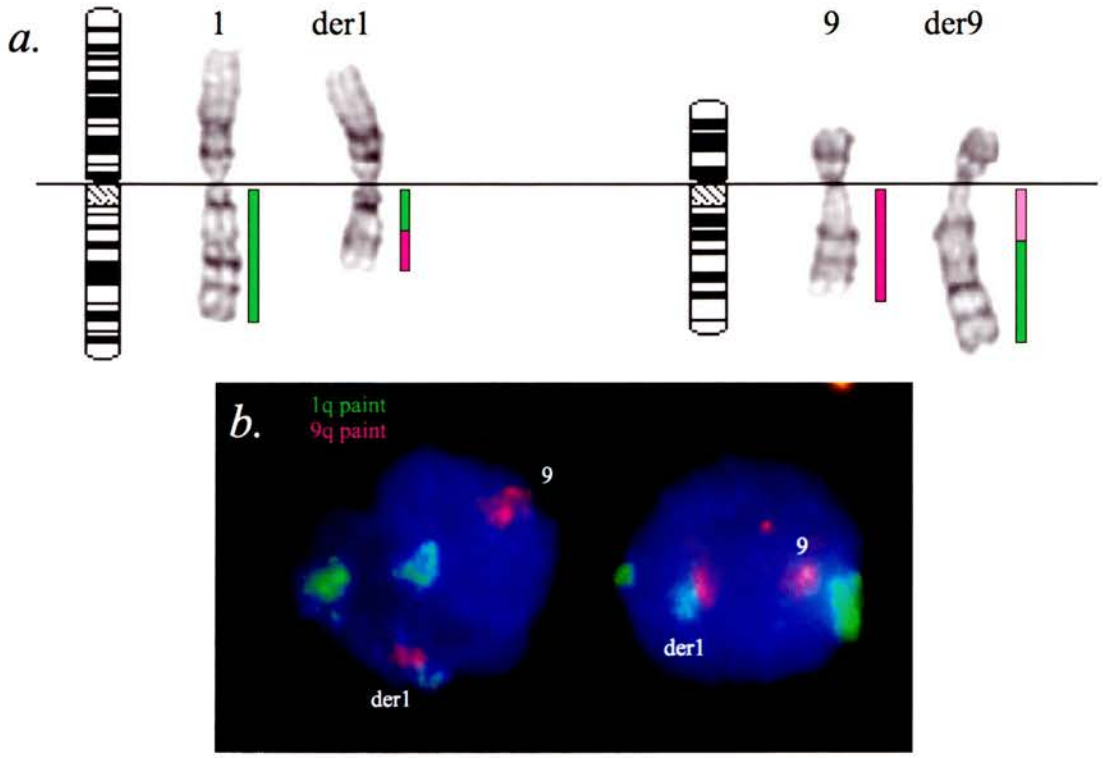

Figure 4.7. Cytogenetic and FISH analysis of t(1;9)(q21 or q23;q22).

A partial ideogram and a partial karyotype showing the normal and derived chromosomes 1 and 9 (a). The coloured bars represent the expected signals from the arm-specific chromosome paints. The der (9) is not visible using the 9q paint as the heterochromatin dominating (pink bar) does not stain due to competitive hybridisation with COT1 DNA in the hybridisation mix. (b) Two uncultured buccal cell nuclei following FISH with arm-specific chromosome paints for 1q (labelled in biotin and detected with FITC) and 9q (labelled in digoxigenin and detected with Rhodamine). Three green signals were identified with the 1q paint, indicating the normal chromosome, the derived chromosome 1 and the derived chromosome 9. The chromosome 9q paint only showed two signals, which corresponded to the normal chromosome 9 and the derived chromosome 1 (labelled).

4.3.4. Discussion

Buccal cells from the t(1;9) patient were FISHed with chromosome paints specific for the long arms of chromosome 1 and 9 (1q and 9q) and scored for the presence of the rearrangement. 10 of 200 nuclei scored (5 %) appeared to have the translocation, a similar proportion to that found by cytogenetics. This was determined by the presence of three domains for the 1q chromosome paint. Although it was clear which cells contained the rearrangement by looking at the number of domains for the chromosome 1 paint, the results were not as expected for that of chromosome 9. As this was a balanced translocation, there should have been three signals visible for each of the chromosome paint probes. However, there were only ever two seen with the 9q paint, even in cells with three domains for 1q. This is due to a lack of hybridisation of the 9q paint to the heterochromatic region on the derivative chromosome 9. Therefore, instead of three signals, cells with the translocation showed a large signal for the normal chromosome 9 and a smaller signal for the region translocated to the derivate chromosome 1. This can be seen as directly adjacent to a region of chromosome 1 paint.

Although the translocation was obvious and FISH on these buccal cells was successful, it was decided not to map the breakpoints in this case any further due to the low proportion of cells that contain the translocation. Interphase FISH on uncultured buccal cells has already proved useful in confirming mosaic structural and numerical chromosomal abnormalities [456;457] but we believe this is the first time this approach has been used for balanced chromosomal rearrangements.

5: Mapping of a t(2;12) Translocation leads to the Identification of a Candidate Gene for Symmetrical Peromelia and Phocomelia

5.1. Abstract

DBCR breakpoints of a *de novo* t(2;12)(p25.1;q23.3) associated with upper limb peromelia and lower limb phocomelia were mapped using interphase FISH on nuclei extracted from archive paraffin embedded tissue sections. The breakpoint at 2p25.1 interrupted the *ROCK2* gene, which encodes a Rho-associated, coiled-coil containing protein kinase. Mice homozygous for disruptions in this gene often die before birth due to placental thrombosis but survivors are small with no major malformations. This gene was therefore not a good candidate for the predicted heterozygous loss-of function genetic mechanism with a major and specific effect in the developing limb bud. The 12q23.3 breakpoint mapped between 0-25 kb 5' (telomeric) of *CMKLR1,* which encodes chemokine-like receptor 1. Using RT-PCR and immunocytochemical localisation with polyclonal antisera raised against CMKLR1, we show developmentally dynamic expression of the orthologous gene in mouse embryos in migratory myoblasts from 9.5 days *post coitum* (dpc), prior to their entry into the limb bud. This expression is maintained in embryonic skeletal muscle. This receptor has only one known ligand, a retinoic acid receptor response gene named *RARRES2*. By RT-PCR this gene was co-expressed with *Cmklr1* in the early limb bud. *CMKLR1* appears to be a good causative candidate for the phenotype

of the proband. Our finding support recent data suggesting that myoblasts may be required for normal limb outgrowth. One case with a similar phenotype was available for study but no gene deletion or point mutations in *CMKLR1* or a candidate regulatory region could be identified. A mouse model is being created to further elucidate the novel developmental role of this signaling system.

5.2. Introduction

Peromelia and phocomelia are two types of limb reduction defects. Peromelia results in the formation of a stump (asymmetrical), or stumps (symmetrical), with the absence or malformation of the extremities, whereas in phocomelia, there is a deficiency of the long bones of the limb but the relative preservation of the hands or feet.

Most cases of peromelia are sporadic and affect only one side of the body (unilateral). Symmetrical peromelia can be associated with many syndromes, including, amongst others, aglossia-adactylia (OMIM 103300), acheiropody (OMIM 200500) and Poland syndrome (OMIM 173800). It may also have a vascular aetiology as some limb reduction abnormalities, such as peromelia, have been suggested to be linked to chorionic villus sampling, with the severity of the phenotype being linked to the time of the sampling [458].

Symmetrical phocomelia is often associated with teratogens, such as thalidomide, and can also be associated with syndromes, such as Roberts SC syndrome (OMIM 268300). This syndrome is associated with cleft lip/palate and chromosome analysis in these individuals shows characteristic puffing around the centromere regions or premature centromere separation [459].

The phenotype in this case consists of both symmetrical peromelia of the upper limbs and symmetrical lower limb phocomelia with no cleft lip/palate or other gross abnormalities.

5.2.1. Clinical Case Report

This case was originally published by Murray *et al* [460]. The clinical details are summarised below.

The foetus was the result of the third pregnancy of a healthy couple. An ultrasound examination at 15 weeks showed pronounced limb shortening and am amniocentesis was performed. Chromosome analysis of the foetal cells showed an apparently balanced translocation between chromosomes 2 and 12, t(2;12)(p25.1;q24.1). The parental chromosomes were normal, indicating that the rearrangement was a *de novo* event. The pregnancy was electively terminated at 20 weeks. Written consent was obtained from the family to use the clinical photographs, case details and tissue samples for research purposes.

Post-mortem examination showed a female foetus with severe, symmetrical shortening of all four limbs. The upper limbs had what appeared to be a rudimentary digit and the both feet were abnormal, with cutaneous syndactyly giving the appearance of only two digits. There were minor craniofacial abnormalities, poorly developed external genitalia and long, narrow but histologically normal kidneys. All other internal organs appeared normal. The brain was not examined.

X-ray analysis of the foetus showed that there was no calcification of the femora, both tibiae were bowed and the feet were flipper-like. There was pointing of the distal humeri in the upper limbs and an absence of any limb distal to this.

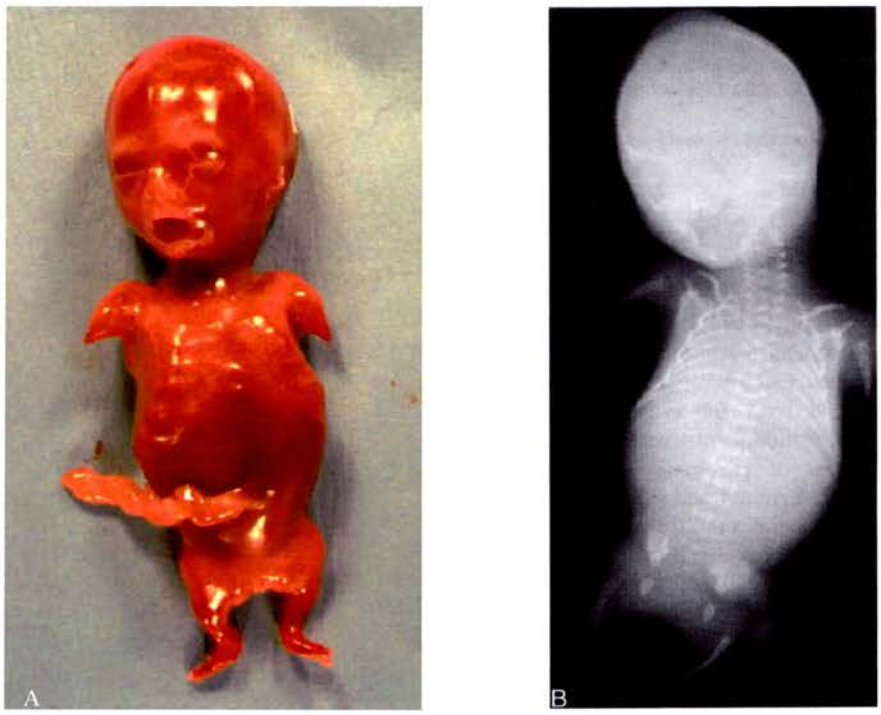

Figure 5.1. Images of the proband foetus

A clinical photograph (A) and X-ray (B) of the proband foetus showing the symmetrical limb abnormalities.

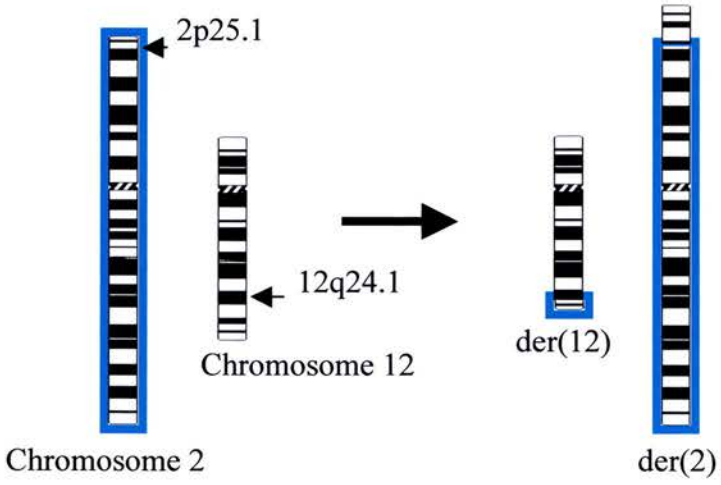

Figure 5.2. Partial ideogram of chromosome 2 and 12.

A partial ideogram showing the normal and derived chromosomes 2 and 12. The breakpoints are indicated by arrows. Chromosome 2 is outlined for clarity.

5.2.2. The Chromosome 12 Breakpoint has been Previously Implicated in Limb Development

The presence of a *de novo* translocation and a rare malformation phenotype suggests the interruption of a vital gene, or genes, at the rearrangement breakpoints. In this case the breakpoints are on the short arm of chromosome 2 and the long arm of chromosome 12. There do not appear to be any previous reports of rearrangements in the chromosome 2 region resulting in a limb phenotype and there are no immediately obvious candidate genes in this area. The chromosome 12 breakpoint, however, has some supporting evidence as the *TBX3* and *TBX5* genes are located in band 12q24.1 and these are both known to have a role in limb development.

TBX3 and *TBX5* are members of the T-box family of transcription factors. Mutations in *TBX3* have been shown to cause ulnar-mammary syndrome (UMS) (OMIM 181450) [461], an autosomal dominant condition, characterised by upper limb abnormalities, mammary hypoplasia, dental abnormalities and urogenital abnormalities. Bamshad *et al* [462] found a 1 bp deletion in members of a family affected by UMS that resulted in a frameshift and premature termination and they also found a splice site mutation in another family. They hypothesised that both mutations perturbed DNA binding and that the phenotype was caused by haploinsufficiency of *TBX3*.

Mutations in *TBX5* have also been shown to cause a phenotype, namely Holt-Oram syndrome (HOS, OMIM 142900). This is a rare autosomal dominant disorder, with a birth incidence of approximately 1 in 100,000 [463]. The condition was described in 1960 by Holt and Oram, who reported atrial septal defects and abnormalities of the thumbs segregating through four generations of a family [464].

Since then, many other cases have been described with the limb abnormalities varying from abnormal or absent thumbs, to phocomelia [465]. Linkage studies had mapped the gene to chromosome 12q and in 1997, Li *et al* [466] mapped the chromosome 12 breakpoint in a patient with HOS and isolated three exons that had similarity to both *TBX3* and *TBX5*. They subsequently found mutations in *TBX5* in both familial and sporadic cases of HOS. Further *TBX5* mutations were found in affected members of two other families at around the same time [467].

However, although both of these genes have obvious roles in limb development, they seem to be specific for the upper limbs. Misexpression studies in the chick have shown that ectopic expression of *TBX5* in the leg bud induced wing-like morphological changes, suggesting it plays a role in forelimb identity [468]. Both *TBX3* and *TBX5* are expressed in the developing forelimbs of embryos and seem to play an important role in their development. However, although *TBX3* is also expressed in the hind limbs, loss of function mutations do not seem to have an effect as individuals with ulnar-mammary syndrome generally have normal lower limbs. This indicates that although disruption of *TBX3* and/or *TBX5* may result in the peromelia present in the t(2;12) translocation case, it would not appear to be responsible for the lower limb phocomelia.

This suggests that there may be another, as yet unknown, limb development gene in the 12q24.1 region of chromosome 12, that the causative gene may be on chromosome 2, or that the phenotype is the result of both breakpoints having a combined effect.

5.2.3. Phenotypically Similar Cases

Although the symmetrical peromelia and phocomelia phenotype seen in the translocation case is rare, a literature search did locate a very similar case [469] and we had access to another case, which although slightly different, still showed some striking similarities. The report from Witters *et al* [470] was of a male foetus with shortened humeri with distal hypoplasia and an absence of the forearms and hands. The lower limbs showed an only one bone was present in the right leg, thought to be the tibia, and the right food was malformed. There were no bones visible in the left leg. There was no cleft lip or palate. Chromosome analysis showed a normal male 46,XY karyotype with none of the premature centromere separation characteristic of Roberts-SC syndrome.

This phenotype in this case is practically identical to that of the t(2;12) translocation case but unfortunately, there was no material of any type available, making further studies impossible.

The second case was a male foetus of 14 weeks gestation with absent upper limbs, absent femora and fibula and bowed tibiae. The feet were also abnormal (see figure 5.3). Once again, the karyotype was 46,XY, that of a normal male and there was no evidence of centromere puffing or premature centromere separation. Paraffin embedded tissue sections and a fibroblast cell line (named T01-2856) were available for this case.

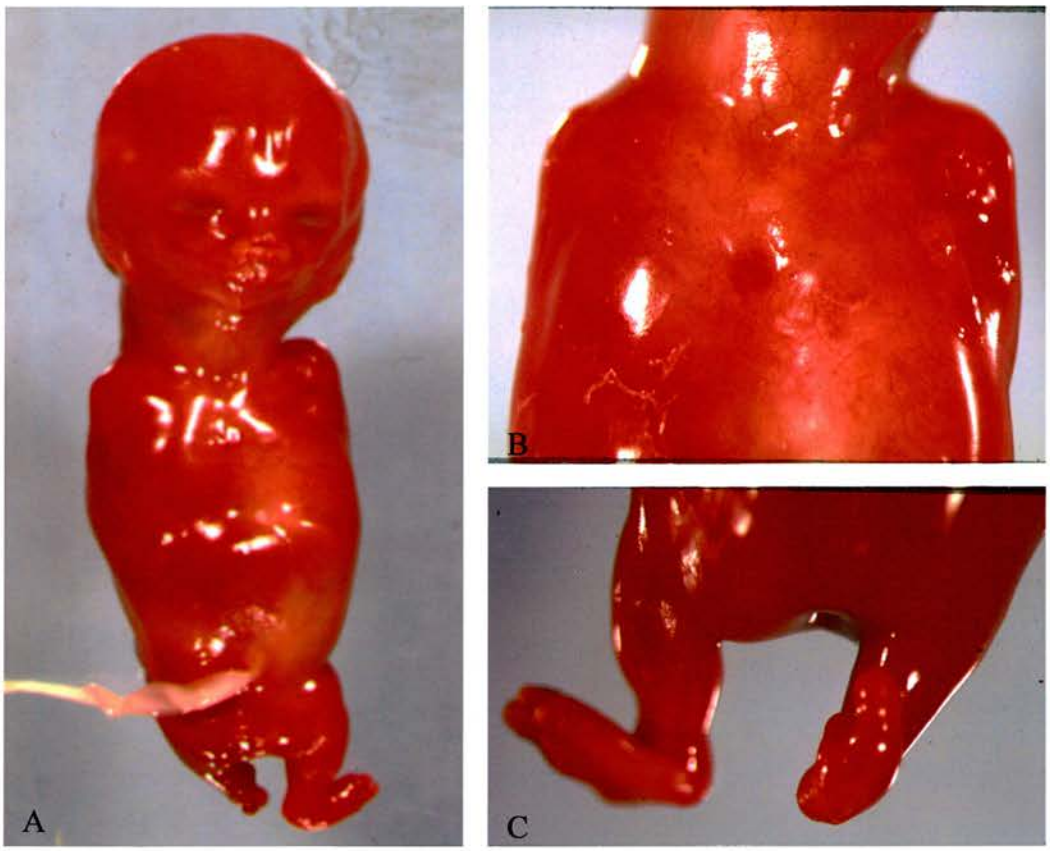

Figure 5.3. Clinical photographs of a phenotypically similar case

Clinical photographs of case T01-2856 showing a similar phenotype to the proband. This foetus has a lack of upper limbs (A), absent femora and fibula and bowed tibiae (A and C). The feet are also abnormal (C).

5.2.4. A brief overview of Limb Development

5.2.4.1. The origin and development of the limb buds

Limb development is first apparent as limb buds in neurula stage embryos (approximately 9.5 dpc in mice and 26 dpc in human). The dorsal (preaxial) mesoderm separates into somites, which subsequently give rise to the cells that form, amongst other things, the skeleton and skeletal muscles of the back, body wall and limbs. The cells of the ventral part of the somite become the sclerotome, which will

give rise to cartilage and subsequently the axial skeleton. Cells from the lateral portion of the somite will become the dermomyotome. This is double-layered, the dorsal part being the dermatome, which gives rise to the dermis, and the inner layer of cells being the myotome, which gives rise to the skeletal muscles of the back. The cells that form the muscles in the limb migrate away from the lateral portion of the dermomyotome, down towards the prospective limbs.

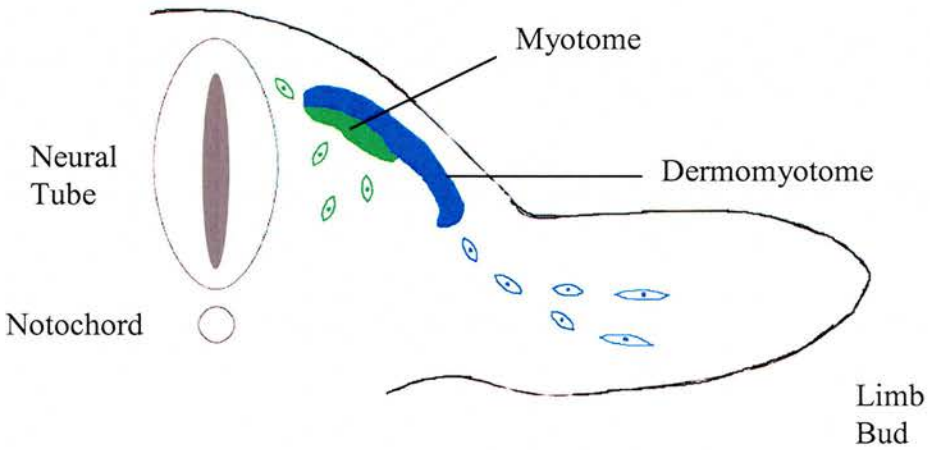

Figure 5.4. The origin of skeletal muscle

A schematic diagram showing the origin of skeletal muscle. Cells migrate out from the myotome (green) to form the skeletal muscles of the back, whilst at the limb bud level, cells migrating from the dermomyotome (blue) form the skeletal muscles of the limb.

The limb bud is formed from the accumulation of muscle and skeletal precursor cells forming a bulge under the epidermal tissue of the embryo. These mesenchyme cells proliferate and induce the overlying ectoderm to form the apical ectodermal ridge (AER). The interaction of the AER with the underlying

mesenchyme, known as the progress zone (PZ) is essential for sustained limb outgrowth and development [471;472].

The rapid proliferation of the mesenchyme results in the elongation of the limb bud and the length of time that cells have spent in the PZ is thought to determine their proximodistal (PD) identity [473;474]. Cells that have spent a long time in the PZ and have undergone a large number of divisions become proximal structures, such as the radius and ulna in the arm, and those that have undergone fewer divisions become more distal structures [475]. This is shown by experiments in which removal of the AER at an early stage results in only the humerus being formed [476;477], whereas with later removal, the humerus, elbow and parts of the radius and ulna develop.

The mesenchyme in the posterior region of the limb bud, known as the zone of polarising activity (ZPA), specifies the pattern of the limb along the anterioposterior axis. Transplantation experiments have shown that transferral of this area to the anterior margin of a chick wing-bud results in mirror-image duplication of the digits [478]. The dorsoventral limb pattern is specified via signals from the dorsal ectoderm [479].

5.2.4.2. A timetable of limb development in humans

Limb development in humans is first apparent in the fourth week of gestation, with the appearance of the arm limb buds at around day 26-28. The leg buds appear at around day 30 and the all buds undergo rapid proliferation and outgrowth. By day 33, the AER will have reached its maximum thickness and the arm buds will be paddle shaped. Histodifferentiation will be apparent at this point as a core of

chondrogenic cells appears in the centre of the bud, surrounded by the mesenchyme that will form the future muscle and dermis. During the sixth week, the AER will subside as the limbs lengthen and finger-rays become apparent. Further differentiation and outgrowth are accompanied by limb rotation and joint formation in the seventh week and muscle contraction in week eight. Ossification of the bones begins in week 12.

5.2.4.3. Timing of the limb defects in the translocation case

The severity of the limb defects in the translocation case and the phenotypically similar case suggests that the causative event occurred very early on in limb development. The limbs are very short but have begun to form, indicating that the limb buds were present. However, the outgrowth and subsequent development of the limbs, including the patterning, appears to have been dramatically disrupted.

5.3. Results

5.3.1. Chromosome 2 FISH Mapping

In order to identify the precise location of the chromosome 2 breakpoint, FISH was performed using a range of probes from around the suspected breakpoint region. The results of the FISH mapping can be seen in table 5.1. The location of the chromosome 2 breakpoint is within band 2p25.1, between BAC clones RP11-295J19 and RP11-427E2 (see figure 5.6).

Chromosome Band	Library name	Clone name	Mb*	Result
2ptel	GS1	8L3	0.33	Distal to breakpoint
2p25.3	RP11	352J11	2.23	Distal to breakpoint
	RP11	168K7	2.83	Distal to breakpoint
2p25.2	RP11	350H23	5.63	Distal to breakpoint
	RP11	485O17	6.51	Distal to breakpoint
2p25.1	RP11	16D24	7.57	Distal to breakpoint
	RP11	542B5	7.9	Distal to breakpoint
	RP11	69D8	8.43	Distal to breakpoint
	RP11	687B11	8.54	Distal to breakpoint
	RP11	217D23	8.57	Distal to breakpoint
	RP11	434B12	8.71	Distal to breakpoint
	RP11	327F6	8.89	Distal to breakpoint
	RP11	734K21	9.24	Distal to breakpoint
	RP11	385J23	9.43	Distal to breakpoint
	RP11	214N9	9.45	Distal to breakpoint
	RP11	295J19	11.31	Distal to breakpoint
	RP11	427E2	11.49	Proximal to breakpoint
	RP13	912N19	11.8	Proximal to breakpoint
	RP11	484O9	11.88	Proximal to breakpoint
	RP11	489A14	12.06	Proximal to breakpoint
	RP11	375P12	12.36	Proximal to breakpoint
	RP11	168G24	12.65	Proximal to breakpoint
2p24.3	RP11	333O1	12.57	Proximal to breakpoint

Table 5.1. A list of BAC clones used to map the 2p breakpoint

A list of BACs used to map the 2p breakpoint, their position within the genome and their position relative to the breakpoint as determined by FISH. The clones highlighted in blue are those that flank the chromosome 2p breakpoint, located within band 2p25.1.

*Figures from Ensembl NCBI 35, July 2004 assembly

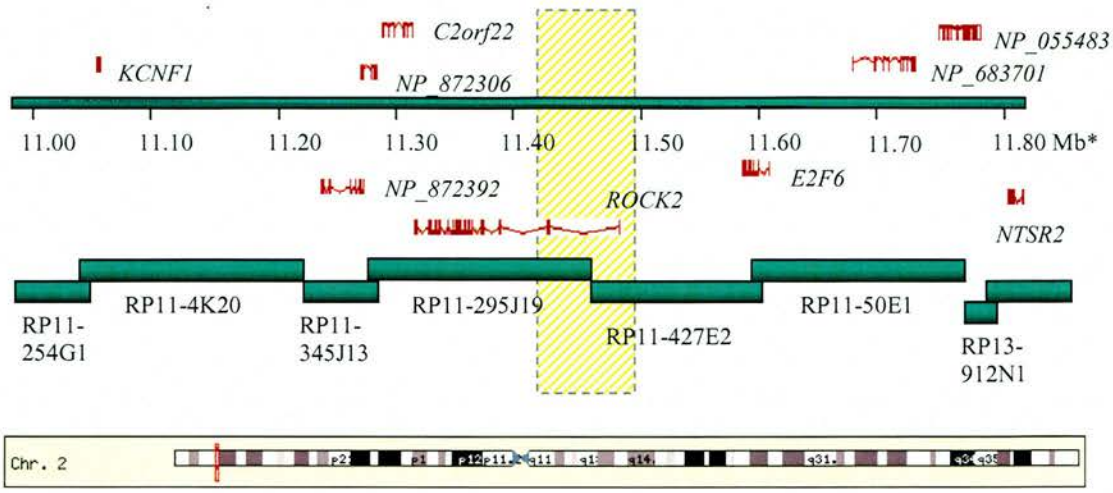

Figure 5.5. Diagram of the area around the 2p25.1 breakpoint.

A diagram of the area around the chromosome 2p breakpoint in the t(2;12) translocation case. Green rectangles represent the BAC clones used for FISH mapping. The position of the genes relative to the BACs can be seen. The breakpoint falls within the shaded region between BACs RP11-295J19 (distal) and RP11-427E2 (proximal) and may disrupt the *ROCK2* gene.

*Figures from Ensembl NCBI 35, July 2004 assembly

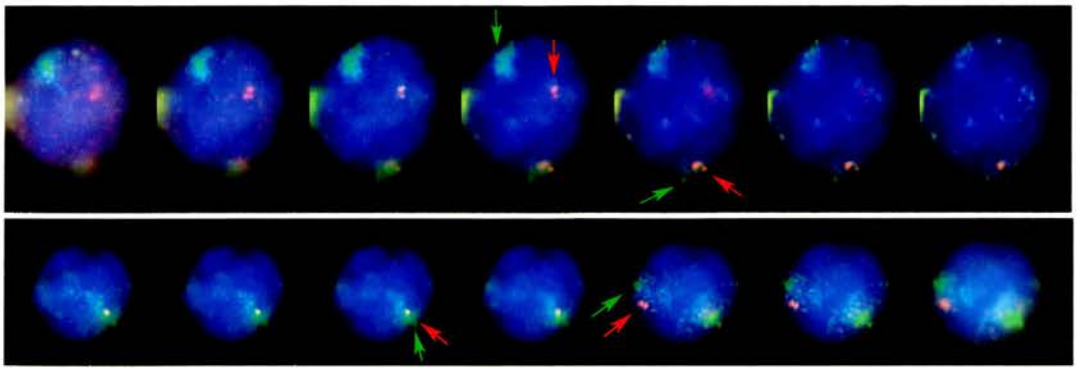

Figure 5.6. FISH with distal and proximal BAC clones and 2p paint

FISH with BACs RP11-295J19 (top panel) and RP11-427E2 (bottom) with a chromosome 2p specific paint (green). The panels show selected sections taken every 0.5 μM through a DAPI stained nucleus for each experiment. The arrows indicate the paint domains (green) and BAC signals (red). The top panel shows that the BAC only localises with one chromosome paint domain, indicating that the BAC is distal to the breakpoint, on the translocated part of the chromosome. In the bottom panel, both BAC signals co-localise with the paint domains, indicating that the BAC is proximal. Arrows indicate the position of the signals.

5.3.2. Chromosome 12 FISH Mapping

5.3.2.1. Mapping with BACs

In order to identify the precise location of the chromosome 12 breakpoint, FISH was performed using a range of probes from around the suspected breakpoint region. The results from the BAC mapping can be seen in table 5.2. The breakpoints in this case lie within band 12q23.3, between BACs RP11-1K3 and RP11-13G14. The clone between these two BACs (RP11-131I18) cross-hybridised to another chromosome, meaning that it could not be used for mapping purposes.

The *TBX3* and *TBX5* genes, known to be involved in upper limb development, are located over 6 Mb from the translocation breakpoint and are therefore not directly disrupted.

Chromosome Band	Library name	Clone name	Mb*		Result
12q23.3	RP11	1C11	106.39		Proximal to breakpoint
	RP11	1K3	107.02		Proximal to breakpoint
	RP11	131I18	107.19		Cross hybridises to chr 2
	RP11	13G14	107.26		Distal to breakpoint
	RP11	951I11	107.35		Distal to breakpoint
12q24.11	RP11	689B22	107.52		Distal to breakpoint
	RP11	423G4	107.63		Distal to breakpoint
	RP11	117B7	107.89		Distal to breakpoint
	RP11	443D10	107.99		Distal to breakpoint
	RP11	256L11	108.76		Distal to breakpoint
12q24.12	RP11	162P23	111.01		Maps to chr 10
12q24.13	RP11	303O9	112.6		Distal to breakpoint
12q24.21	RP11	435A10	113.65	TBX5	Distal to breakpoint
	RP11	162N7	113.85	TBX3	Distal to breakpoint
	RP11	110L15	115.04		Distal to breakpoint
12q24.33	CTC	221K18	131.84		Distal to breakpoint

Table 5.2. A list of BAC clones used to map the 12q breakpoint

A list of BACs used to map the 12q breakpoint, their position within the genome and their position relative to the breakpoint as determined by FISH. The clones highlighted in blue are those that flank the breakpoint, located in band 12q23.3. The clone between these two cross-hybridised to chromosome 2 and was therefore excluded. The position of the *TBX5* and *TBX3* genes is also included for reference. These are located over 6 Mb from the translocation breakpoint.

*Figures from Ensembl NCBI 35, July 2004 assembly

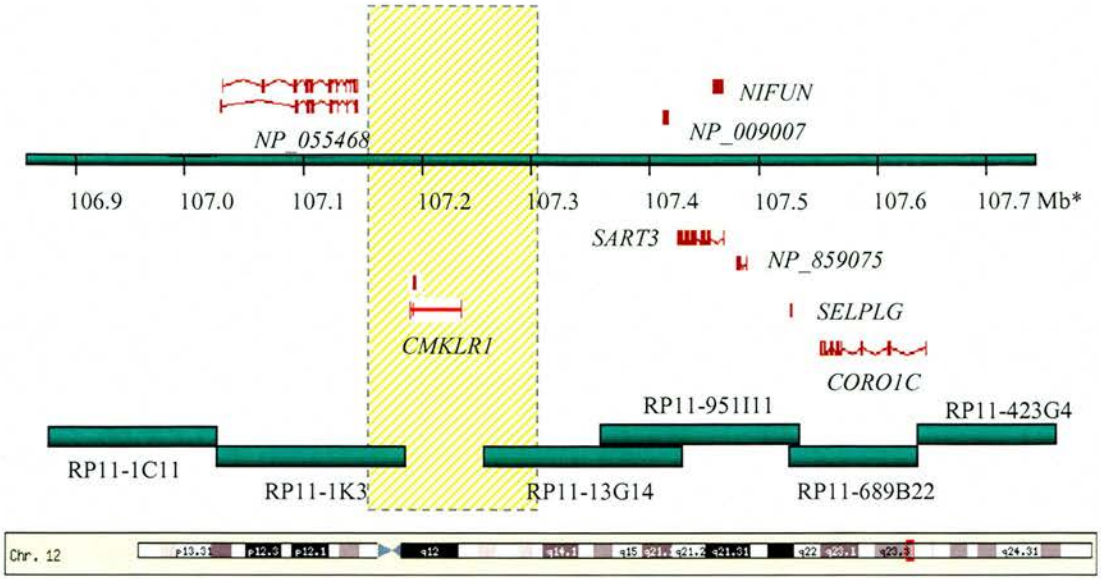

Figure 5.7. Diagram of the area around the 12p23.3 breakpoint.

A diagram of the area around the chromosome 12 breakpoint in the t(2;12) translocation case. Green rectangles represent the BAC clones used for FISH mapping. The position of the genes relative to the BACs can be seen. The breakpoint falls within the shaded region between BACs RP11-1K3 (proximal) and RP11-13G14 (distal). The only gene in this region is *CMKLR1*.

*Figures from Ensembl NCBI 35, July 2004 assembly

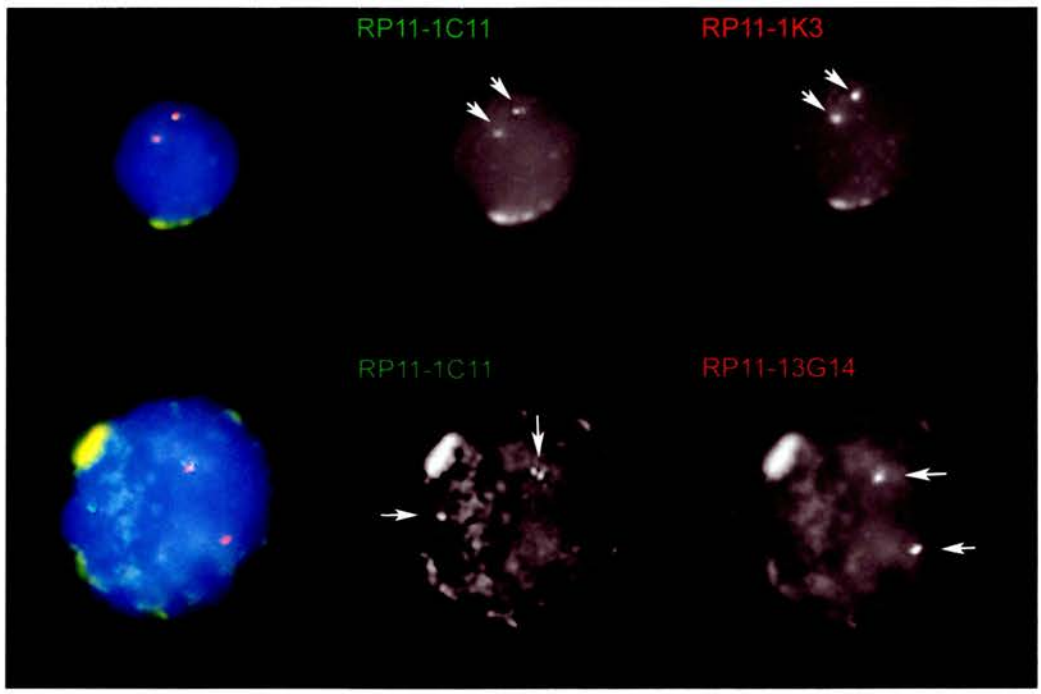

Figure 5.8. FISH showing proximal and distal 12q BACs

FISH on DAPI stained nuclei using proximal 12q BAC RP11-1C11 (green) along with BAC RP11-1K3 (top panel) and RP11-13G14 (bottom panel). The arrows indicate the position of the signals. Co-localising signals in the top panel indicate that BAC RP11-1K3 is proximal to the breakpoint, whereas BAC RP11-13G14 has only one co-localising signal, indicating that the BAC is distal to the breakpoint, on the translocated part of the chromosome.

5.3.2.2. Long-Range PCR probe mapping

The BAC mapping put the breakpoint within the region of the *CMKLR1* gene. To try to narrow the breakpoint further, long-range PCR products were designed for the gene itself and for the distal part of the BAC RP11-1K3 (see figure 5.9). These were labelled and used as FISH probes, named 1K3_1, CMKLR1_1 and CMKLR1_2. All three probes were found to be proximal to the breakpoint on the derived chromosome 12. This puts the breakpoint either within, or distal, to the 5′ end of the *CMKLR1* gene.

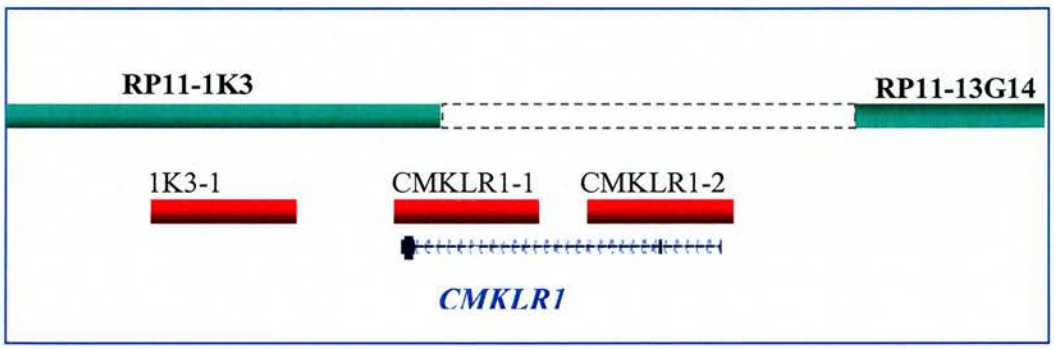

Figure 5.9. Long-Range PCR FISH probes

A diagram showing the location of the long-range PCR probes used for FISH mapping around the *CMKLR1* gene. The green rectangles represent the BACs previously used for breakpoint mapping and found to flank the breakpoint. FISH with all three long-range PCR probes showed that they were proximal to the translocation breakpoint, meaning that the breakpoint was located either within, or distal to, the 5′ end of the *CMKLR1* gene.

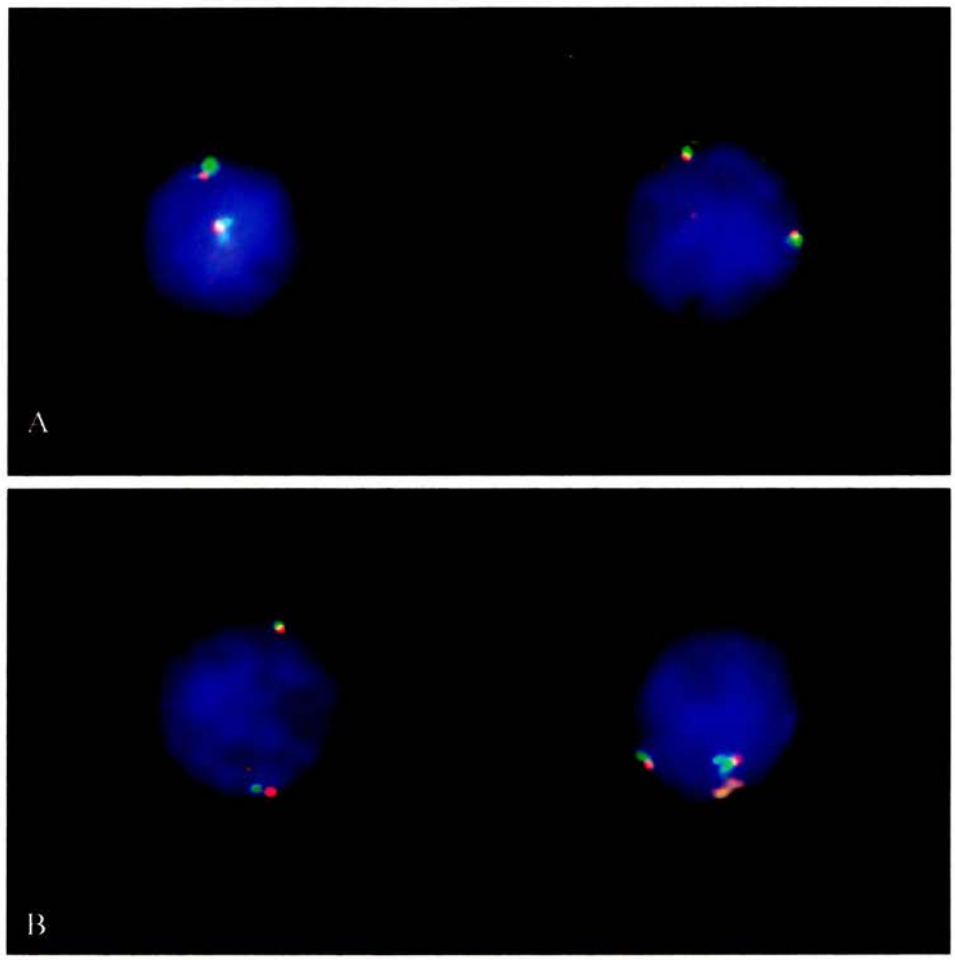

Figure 5.10. *CMKLR1* PCR probes co-localise with proximal BACs

FISH with long-range PCR probes *CMKLR1*_1 (A) and *CMKLR1*_2 (B) (red signals) applied with BACs that map proximal to the chromosome12q breakpoint (green signals). Both BACs show two signals that co-localise with the proximal BAC, indicating all probes are proximal to the t(2;12) translocation breakpoint.

5.3.2.3. Mapping with fosmids

To attempt to map the chromosome 12 breakpoint to a higher resolution, fosmids were ordered that formed a contig across the region. Fosmids G248P89648H8 and G248P88875G1 were found to be proximal and distal to the breakpoint, respectively.

Fosmid Name	Mapping result
G248P86973A10	Proximal to breakpoint
G248P82022F11	Proximal to breakpoint
G248P83714D2	Proximal to breakpoint
G248P81173A11	Proximal to breakpoint
G248P89648H8	Proximal to breakpoint
G248P88875G1	Distal to breakpoint
G248P85171H8	Distal to breakpoint

Table 5.3. List of fosmid clones used to map the chromosome 12 breakpoint

A list of the fosmid clones used to map the t(2;12) breakpoint and the results obtained from FISH. The clones highlighted in blue are those that were found to flank the translocation breakpoint.

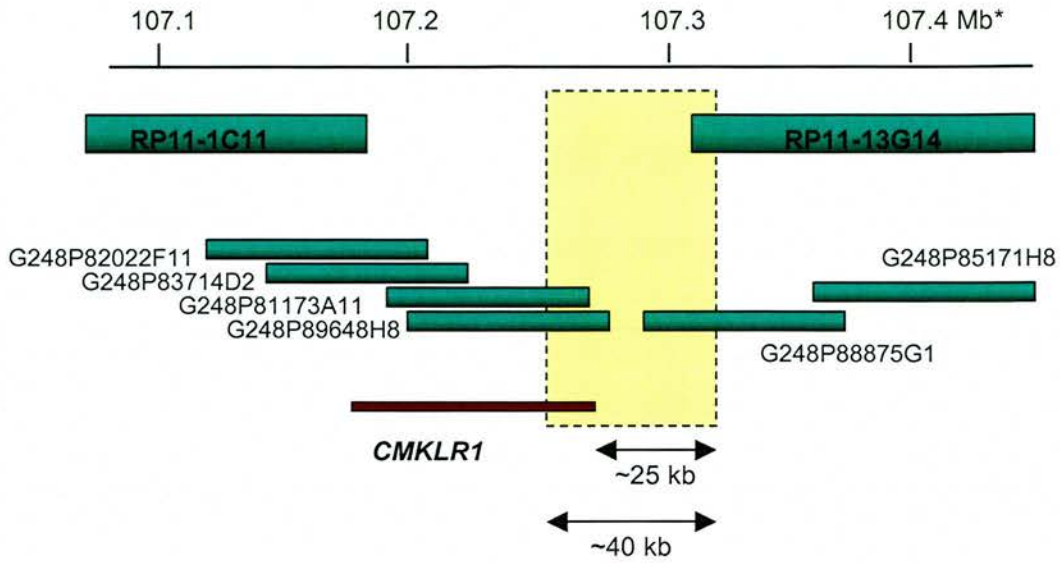

Figure 5.11. Location of the fosmids around the 12q23.3 Breakpoint

The green rectangles represent the fosmid clones used for FISH mapping. The breakpoint falls within the approximately 40 kb area shaded yellow. This puts the breakpoint within the 5′ end of *CMKLR1* or less than 25 kb from that end of the gene.

*Figures obtained from UCSC gemone browser, NCBI build 25, May 2004

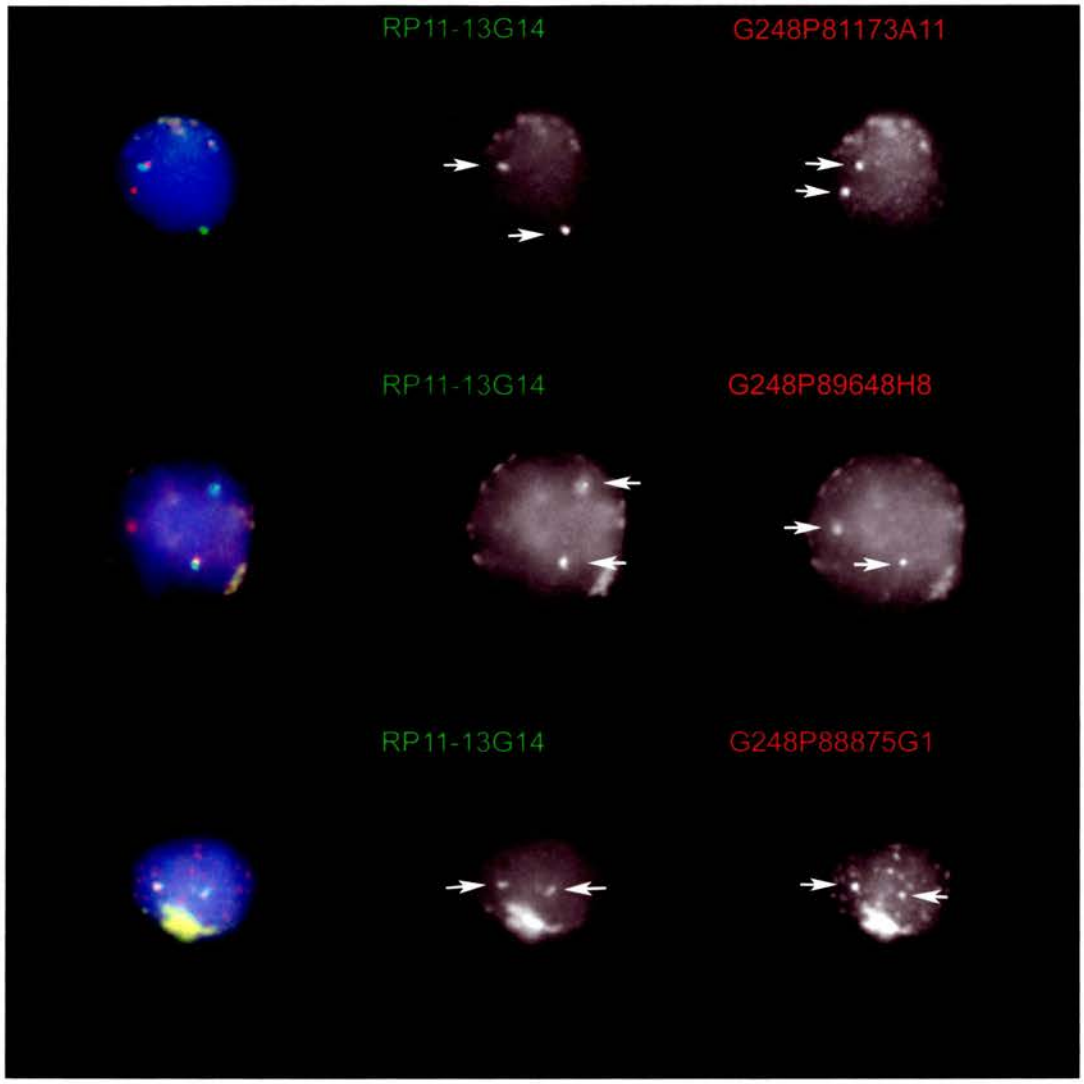

Figure 5.12. FISH with 12q23.3 fosmids

FISH experiments with a BAC that maps distal to the translocation breakpoint in green (RP11-13G14) and a selection of 12q23.3 fosmids (red). Fosmids G248P81173A11 (top) and G248P89648H8 (middle) show only one signal that co-localises with the BAC (these co-localising signals represent the normal chromosome 12) and one signal that does not co-localise. These fosmids are therefore proximal to the breakpoint. Fosmid G248P88875G1 (bottom) shows two signals co-localising with the distal BAC signals and is therefore also distal. Arrows indicate the position of the signals.

5.3.3. RT-PCR

In order to determine the expression of Cmklr1 and Rarres2 in the developing mouse limb, RT-PCR was performed on dissected limb buds from 10.5 dpc to 13.5 dpc mouse embryos. A band of the expected size was seen for all stages of limb bud tested. Extra bands of approximately 500 bp were seen in the Rarres2 reactions, possibly indicating the presence of multiple isoforms. The negative control, containing no RT template, showed no bands other than primer dimer. The results show that both Cmklr1 and Rarres2 are expressed in all stages of limb bud tested.

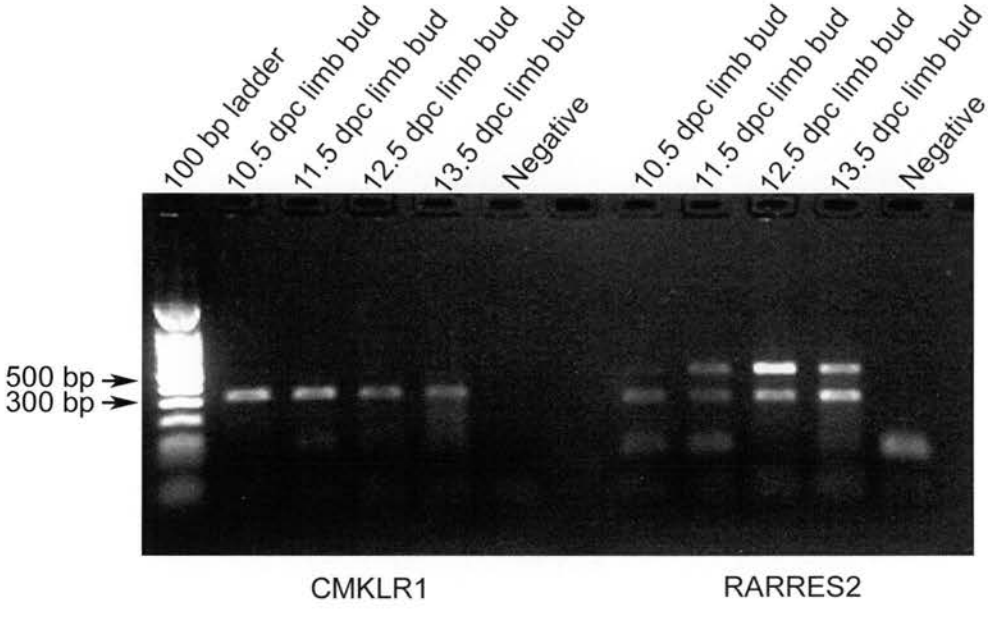

Figure 5.13. Cmklr1 and Rarres2 RT-PCR results on mouse embryonic limb buds

RT-PCR on limb buds from 10.5 to 13.5 dpc mouse embryos. Expression of both Cmklr1 and Rarres2 can be seen in all stages of limb bud tested. The double bands for Rarres2 may indicate the presence of multiple isoforms. The lowest bands (under 100 bp) represent primer dimer.

5.3.4. Wholemount RNA *In-Situ* Hybridisation

To attempt to elucidate the expression pattern of Cmklr1 throughout development, wholemount RNA *in-situ* hybridisations were performed on mouse embryos from a number of different developmental stages. However, the expression pattern could not be determined due to a high level of background staining on the embryos. Due to time constraints, these experiments were not repeated.

5.3.5. Antibody Staining on Embryonic Mouse Sections

In order to elucidate the expression pattern of the Cmklr1 protein throughout embryonic mouse development, antibody staining was performed on paraffin embedded sections from mouse embryos from 9.5 to 14.5 dpc. All negative controls, in which no primary Cmklr1 antibody was added, were clear of any staining on addition of the detection agents, indicating that the Cmklr1 signal was specific.

5.3.5.1. Cmklr1 expression through mouse embryogenesis

The expression of Cmklr1 was seen to alter dynamically during embryonic development. The expression is summarised in table 5.4. Examples of the staining can be seen in figure 5.14.

	9.5 dpc	10.5 dpc	11.5 dpc	12.5 dpc	14.5 dpc
Limb bud					
Neural Tube					?
Heart					?
Liver			?	?	
Brain					
Lung			?		
Eye					
Gonad					
Kidney					
Muscle/ muscle precursors					
Bone/cartilage precursors					

Table 5.4. Expression of Cmklr1 through mouse embryogenesis

A table showing the expression of Cmklr1 in mouse embryos as determined by antibody staining. Blue boxes indicate expression, grey boxes indicate a lack of expression and question marks indicate that expression could not be determined in the sections available. Hashed boxes indicate organs that could not be identified in the developmental stage or the sections available.

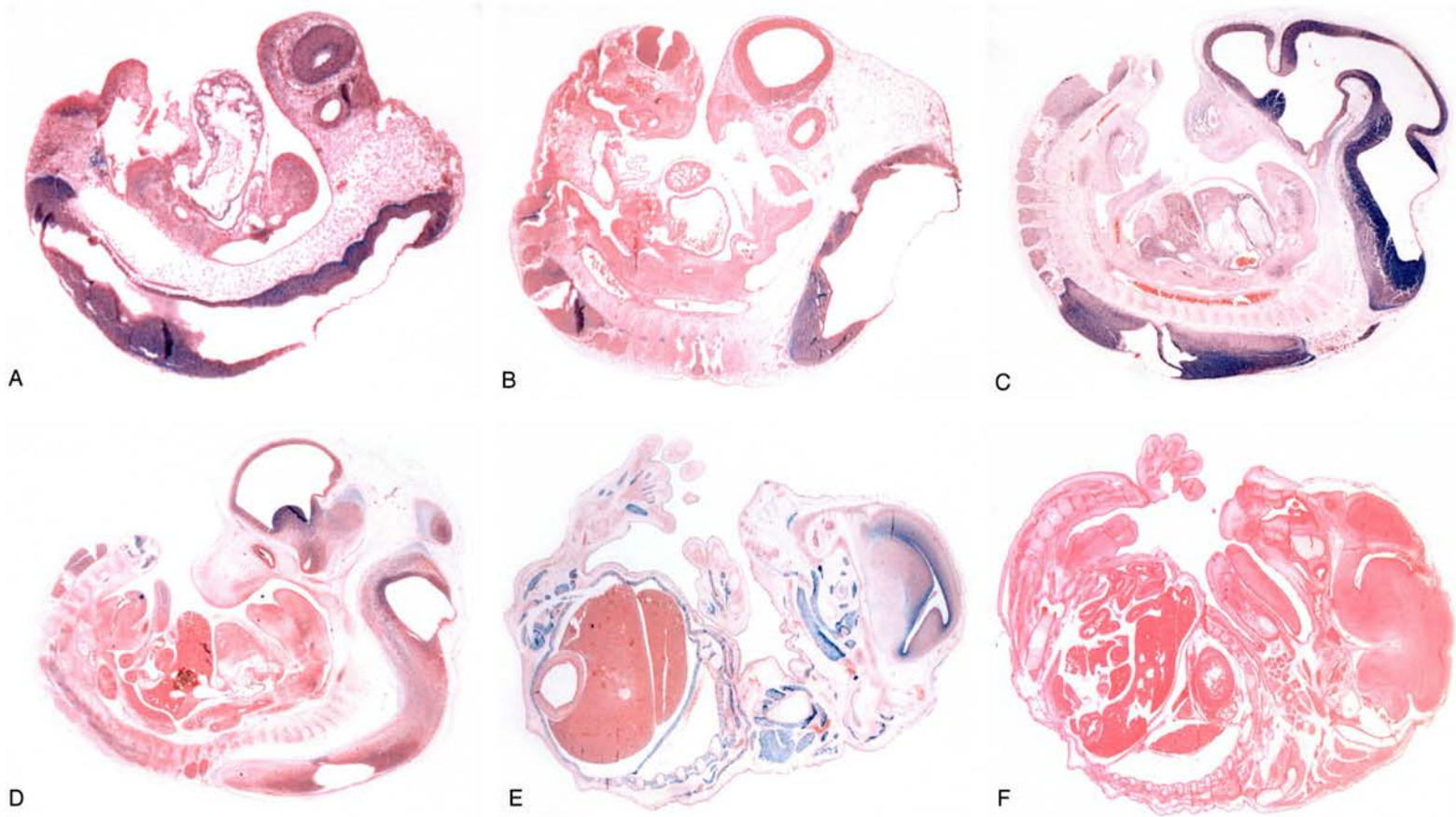

Figure 5.14. Cmklr1 expression in the mouse embryo

Examples of Cmklr1 antibody staining in mouse embryo sections aged 9.5 (A), 10.5 (B), 11.5 (C), 12.5 (D) and 14.5 dpc (E). The negative control shows no blue staining indicating that the signal is specific to the Cmklr1 antibody (F). Sections are counterstained with eosin (pink) and signal is detected with NBT/BCIP (blue/purple). Full expression details can be seen in table 5.4.

5.3.5.2. Cmklr1 expression in the developing mouse limbs

Cmklr1 expression was observed in the mesenchyme of the limb buds of mouse embryos aged 9.5 dpc (figure 5.15 A) and also in the myotome (figure 5.15 B). Embryos aged 10.5 dpc showed Cmklr1 staining in a subset of cells in the limb bud that appear to have migrated from the myotome (figure 5.15 C and D), although this cannot be confirmed in fixed tissue. These cells are thought to be the muscle precursor cells, the myoblasts.

At 11.5 dpc, the expression in the limb can be seen to be located around the area where the bone will form (figure 5.16 A and B), a pattern that is maintained at 12.5 dpc (figure 5.15 C) and 14.5 dpc (figure 5.15 D to F). By 14.5 dpc the expression is restricted to the muscle of the limb and the developing bone remains negative.

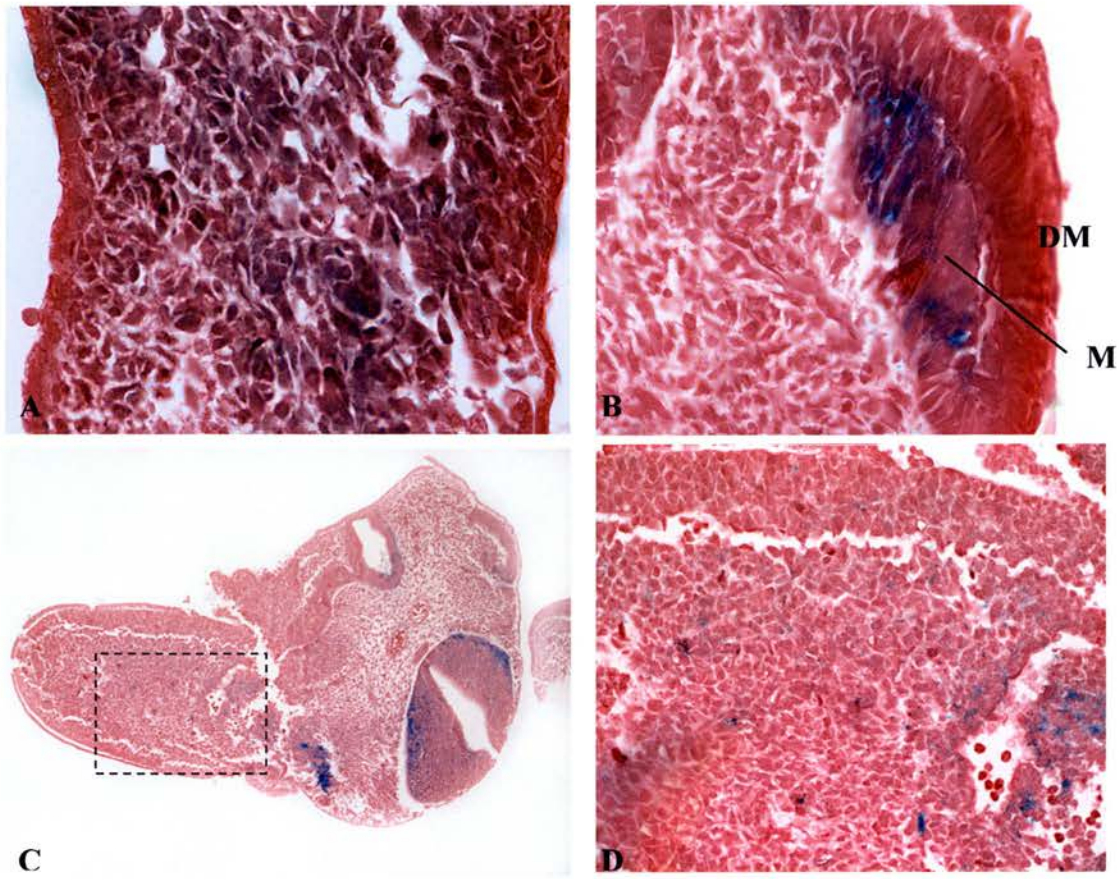

Figure 5.15. Cmklr1 expression in the mouse limb bud

Cmklr1 antibody staining on mouse embryo sections. Sections are counterstained with eosin (pink) and signal is detected with NBT/BCIP (blue/purple). The dashed box shows the enlarged region in D. Expression can be seen in (A) the mesenchyme of the limb bud and (B) in the myotome (M) but not the dermamyotome (DM) of 9.5 dpc embryos. At 10.5 dpc, Cmklr1 positive cells have appeared in the limb bud, possibly having migrated from the myotome (C and enlarged in D).

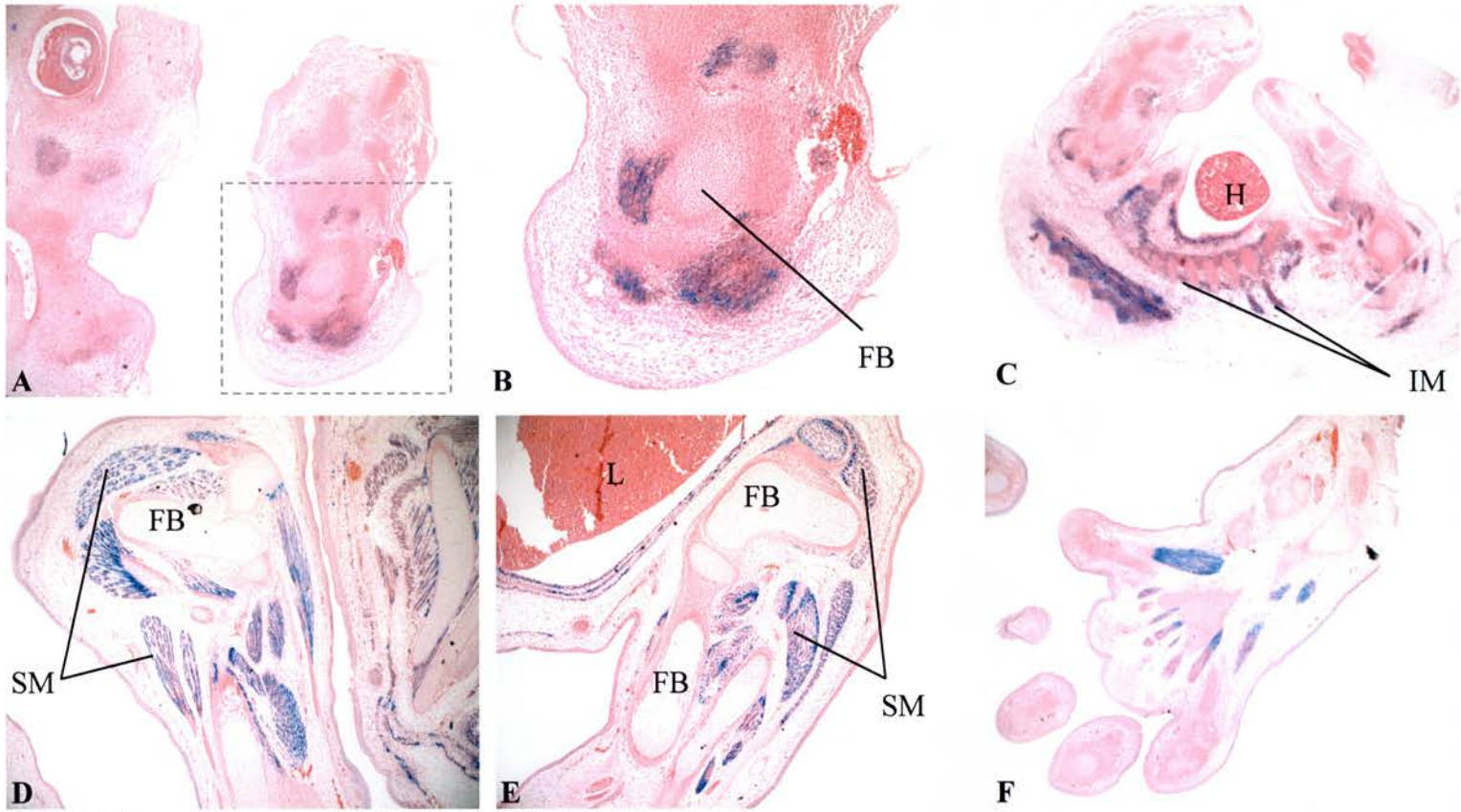

Figure 5.16. Cmklr1 expression in the developing limb

Cmklr1 antibody staining on sections from mouse embryos aged 11.5 (A and B), 12.5 (C) and 14.5 dpc (D-F). Sections are counterstained with eosin (pink) and signal is detected with NBT/BCIP (blue/purple). The dashed boxed indicated the enlarged region in B. Expression is restricted to the developing muscle of the limb. FB, forming bone, H, heart, IM, intercostals muscles and SM, skeletal muscle.

5.3.6. Case T01-2856

5.3.6.1. FISH

FISH using the clones that were found to flank the breakpoints in the t(2;12) case were applied to this case and found to be present on both copies of the chromosome, in apparently the correct position (see figure 5.17).

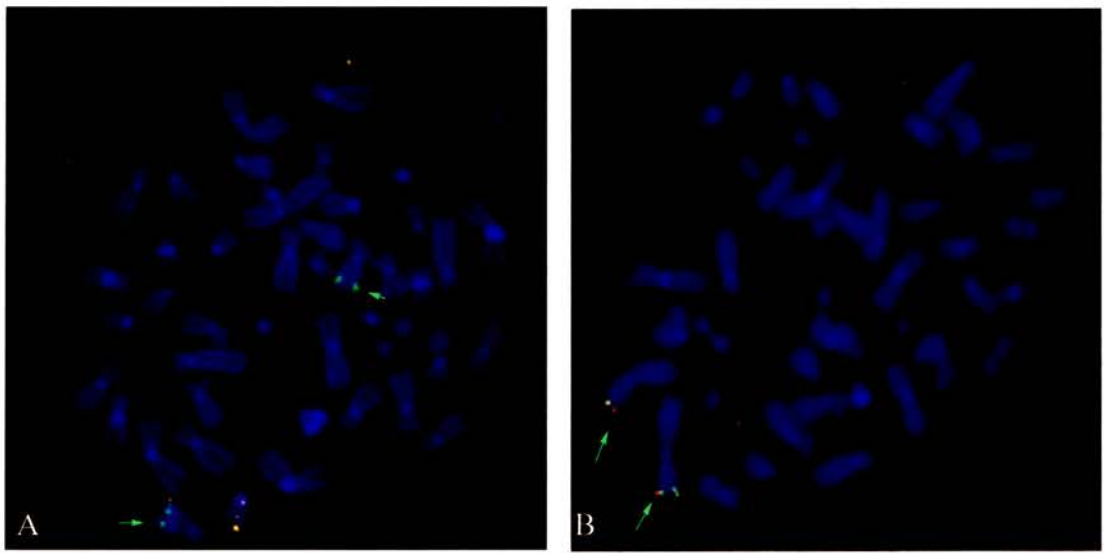

Figure 5.17. FISH on T01-2856 metaphases

FISH on case T01-2856 using breakpoint flanking BACs from the t(2;12) case. Chromosomes are counterstained with DAPI (blue) and arrows indicate the location of the signals. A) BACs RP11-1K3 (green) and RP11-13G14 (red) co-localise and both appear on the expected region of both chromosome 12s. B) BACs RP11-427E2 (green) and RP11-295J19 (red) co-localise and both appear on the expected region of both chromosome 2s.

Long-range PCR probes described in section 5.3.2.2 were also applied and found to be present and in the expected location on chromosome 12 (see figure 5.18).

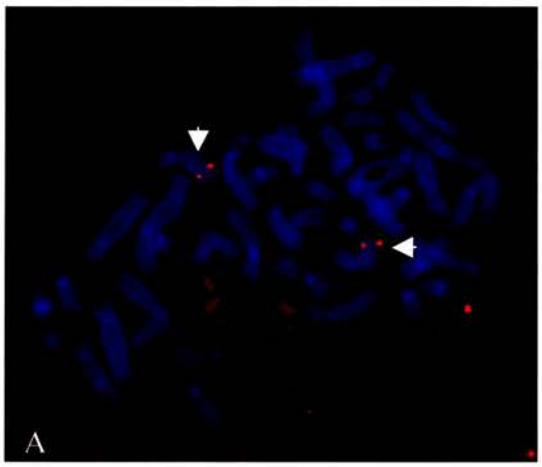

Figure 5.18. *CMKLR1* PCR probes on T01-2856 metaphases

Chromosomes are counterstained with DAPI (blue). Red signals are the PCR probes A) 1K3_1, B) CMKLR1_1, C) CMKLR1_2. All show two normal signals on the chromosome 12s (arrowed).

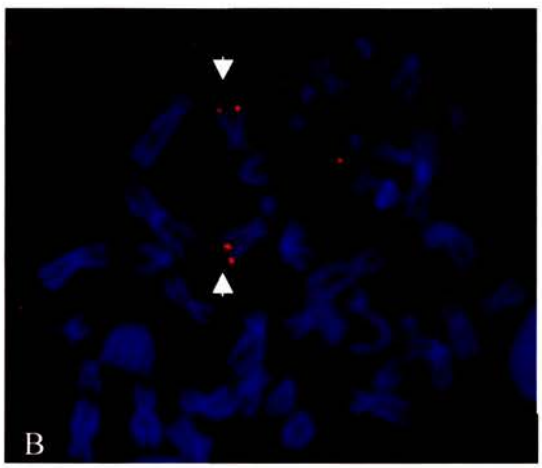

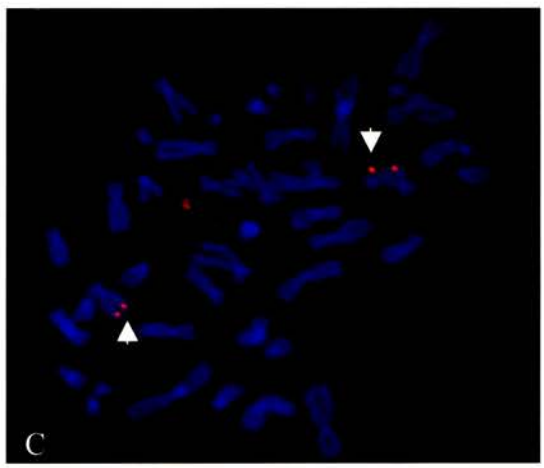

5.3.6.2. *CMKLR1* Sequencing

To check for mutations in *CMKLR1* in this cytogenetically normal case, sequencing of genomic DNA, extracted from the fibroblast cell line, was performed. Primers were positioned to ensure that all of the coding sequence and splice sites of this one exon gene were obtained and to accommodate the poor quality sequence obtained at the beginning and end of every reaction. As the exon is large, 1,119 bp, overlapping primer sets were used. These were organised so that there was a minimum of 100 bp of overlapping sequence to ensure that good quality sequence was obtained for every nucleotide. Sequence was obtained via Ensembl (NCBI 35 assembly, June 2004) and the untranslated regions (UTR) were not sequenced.

No changes in the nucleotide sequence of *CMKLR1* were discovered. One fibroblast cell line from a phenotypically and cytogenetically normal individual was also sequenced as a control.

5.3.6.3. Sequencing of a possible *CMKLR1* regulatory element

Genome alignment performed using the DCODE's evolutionary conserved region (ECR) browser (http://ecrbrowser.dcode.org/), led to the identification of a conserved region, approximately 500 bp in size in human. This was located approximately 145 kb from the 5′ end of *CMKLR1*, in an area with no other genes and had over 70 % conservation between human and mouse, rat, chick or xenopus (see figure 5.19). The conservation and situation of this region suggested that it may have a possible role in the regulation of the *CMKLR1* gene. To rule out any mutations in this potential element, the region was sequenced but no nucleotide

changes could be identified in relation to the reference sequence. The region was also sequenced in one fibroblast cell line from a phenotypically and cytogenetically normal individual as a control.

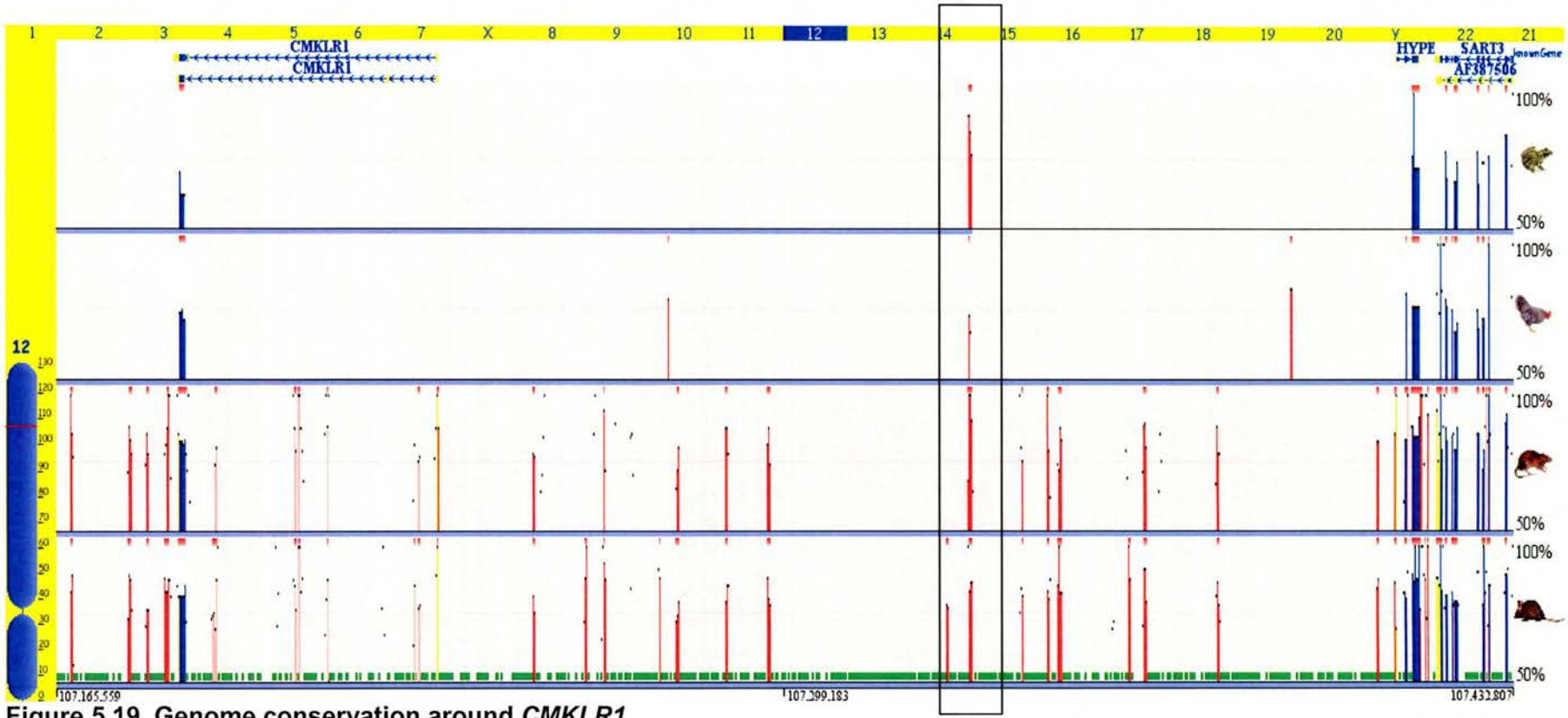

Figure 5.19. Genome conservation around *CMKLR1*

An ECR browser plot showing genomic conservation of the area around *CMKLR1* through, from top to bottom, frog, chicken, rat and mouse. Coding exons are coloured blue, untranslated regions yellow, introns pink and intergenic elements red. Synteny is represented by the pale blue bar under each track and synteny can be seen to stop at the putative element (boxed).

5.3.6.4. ROCK2 cDNA sequencing

As the *ROCK2* gene comprises a large number of exons, it was decided to attempt to sequence the mRNA transcript of the gene as opposed to the nucleotide sequence. This, however, proved to be unsuccessful and the cell line had subsequently become unviable, meaning that the experiment could not be repeated.

5.4. Discussion

5.4.1. The Chromosome 2 Breakpoint Appears to Disrupt the *ROCK2* Gene

The breakpoint on chromosome 2 is between BACs RP11-295J19 and RP11-427E2, suggesting that the *ROCK2* gene is disrupted. *ROCK2* is an isoform of *ROCK*, a Rho-associated kinase involved in signalling from the small GTPase Rho to the actin cytoskeleton. The involvement of *ROCK2* in the cytoskeleton initially suggested this as a promising candidate gene for the limb abnormality phenotype. However, evidence from a mouse with a targeted disruption of *ROCK2* [480] was not consistent with this gene being a causative candidate.

Thumkeo *et al* [481] found that approximately 90 % of the homozygote *ROCK*-/- mice died *in utero* after 13.5 days *post coitum* (dpc) and those that did survive were born runts but then apparently developed normally. The only limb abnormality observed was a slight abnormality of the toes in some of the mice, most likely caused by haemorrhages that occur in the hind limb buds at 13.5 dpc. This bleeding was caused by the blood vessels in the bud dilating and rupturing at 12.5 dpc and the bleeding generally resolved within a few days after birth. The rest of the limbs appeared to be normal in the homozygote mice.

This suggests that although *ROCK2* may be disrupted in the t(2;12) translocation case, the disruption of the gene does not seem sufficient to cause the phenotype. Although mice do not always represent accurate models of human disorders, it would be expected that a homozygote loss in the mouse would present a

similar phenotype to the human, especially as in it would appear that only one copy of the *ROCK2* gene had been disrupted by the translocation.

The other genes in the vicinity of the chromosome 2 breakpoint are summarised in table 5.4. None of these were considered to be good candidates for the peromelia/phocomelia phenotype based on their functional annotation, although no genes can be definitely excluded at this point.

Gene	Conservation (nucleotide)	Description/ Function	Protein type/ family
KCNF1	Dog – 94 % Rat – 89 % Mouse – 89 %	Putative voltage-gated potassium channel.	Potassium channel
C2orf22	Chimp – 100 % Dog – 84 % Mouse – 83 %	Hypothetical protein	Unknown
NP_872306	Unknown	Hypothetical protein	Unknown
NP_055483/ GREB 1 isoform a	Mouse – 85 % Zebrafish – 76 % Chicken – 73 %	Gene regulated by estrogen in breast cancer	Unknown
NP_683701/ GREB 1 isoform c	Mouse – 85 % Zebrafish – 76 % Chicken – 73 %	Gene regulated by estrogen in breast cancer	Unknown
NP_872392	Unknown	Unknown	Unknown
ROCK 2	Chimp – 98 % Mouse – 91 % Rat – 90 %	Rho-associated protein kinase 2 Essential in proliferation of yeast cells Regulates cytokinesis, smooth muscle contraction, formation of actin stress fibres and local adhesions	Ser/Thr protein kinase
E2F6	Chimp – 100 % Rat – 84 % Mouse – 83 %	Inhibition of E2F dependent transcription	E2F transcription factor
NTSR2	Dog – 80 % Mouse – 79 %	Neurotensin receptor type 2	G-protein coupled receptor 1

Table 5.5. A summary of the genes around the chromosome 2 breakpoint

A table summarising the genes around the chromosome 2p breakpoint and the proteins they encode. The conservation column lists the three species with the highest conservation at the nucleotide level.

5.4.2. The Chromosome 12 Breakpoint Lies Close to the *CMKLR1* Gene

The breakpoint on chromosome 12 was found to lie between 0 and 25 kb 5′ (telomeric) to the *CMKLR1* gene. No other genes in the region of the breakpoint were considered to be good candidates for the peromelia/phocomelia phenotype based on their functional annotation, although none of the genes can definitely be excluded at this point. A list of these genes and the properties of the proteins they encode can be seen in table 5.6.

Gene	Conservation (nucleotide)	Description/ Function	Protein type/ family
NP_055468	Chimp – 99 % Dog – 90 % Rat – 80 %	No description	Unknown
NIFUN	Chimp – 100 % Dog – 95 % Rat – 88 %	NifU-like N-terminal domain containing protein	Nif
NP_009007	Chimp – 99 % Dog – 89 % Mouse – 88 %	Huntingtin interacting protein E Mutations cause hyper-IgM syndrome	TPR/ Fic
CMKLR1	Dog – 87 % Mouse – 82 % Rat – 81 %	Could be a chemotactic peptide receptor. May have a function in bone metabolism. Acts as co-receptor for several SIV strains and a primary HIV-1 strain	G-protein coupled receptor 1
SART3	Chimp – 99 % Dog – 89 % Mouse – 83 %	Squamous cell carcinoma antigen recognized by T cells 3	Rnp/ Elav family
NP_859075	Rat – 77 % Mouse – 75 % Chicken – 62 %	Hypothetical protein	Unknown
SELPLG	Chimp – 97 % Mouse – 66 % Rat – 66 %	P-selectin glycoprotein ligand 1 precursor Binds to P-, E- and L-selectins	Unknown
CORO1C	Dog – 94 % Mouse – 89 % Chicken – 81 %	Coronin 1C May be involved in cytokinesis, motility, and signal transduction	WD repeat family

Table 5.6. A summary of the genes around the chromosome 12 breakpoint

A table summarising the genes around the chromosome 12q breakpoint and the proteins they encode. The conservation column lists the three species with the highest conservation at the nucleotide level.

5.4.2.1. *CMKLR1*

The *CMKLR1* gene was first described in 1996 as encoding the chemokine-like receptor 1, a functionally unknown protein with notable sequence and structural homology to the seven transmembrane G-protein coupled chemokine receptors [482]. These receptors are involved in cellular migration in response to ligand binding. One example can be seen during inflammation, where the activation of these receptors contributes to the recruitment of leukocytes and the defence against microbes or antigens [483]. *CMKLR1* is expressed in dendritic cells and macrophages and acts as a co-receptor for entry of human and simian immunodeficiency viruses (HIV-1 and SIV respectively) into CD4+ cells.

The endogenous ligand for *CMKLR1* is the retinoic acid receptor responder protein, RARRES2, otherwise known as chemerin or Tazarotene induced gene 2 (TIG2) [484]. Analogues of retinoic acid, known as retinoids, bind the retinoic acid receptors and alter the expression of retinoic acid responsive genes, such as *RARRES2*.

RARRES2 and *CMKLR1* have been implicated in many physiological roles, including bone development, immune and inflammatory responses and the maintenance of the skin [485-487]. Much of the evidence from this has come from analysis of their expression patterns.

5.4.2.2. *Cmklr1* expression in the mouse

The mouse orthologue of *CMKLR1* was described under the name *Dez* [488] and *in situ* hybridisation in mouse embryos and adult mouse tissues showed the

receptor to be differentially regulated. Methner *et al* [489] stated that expression was seen in the caudal part of the tongue and the umbilical cord at 11 dpc and that expression in the forming bone and cartilage regions was seen to increase from 11 to 14.5 dpc, where abundant expression was present in all areas of osteogenesis and chondrification. The signal was noted to subsequently diminish. No signal was noted in neural tissue, even though Methner *et al* had originally isolated the DEZ clone form a neuroblastoma cell line and had observed expression in cells with neuronal characteristics.

The adult tissues showed a different pattern of expression. The expression in the tongue remained and expression was seen in the parenchyme of the parathyroid gland, the lung mesenchyme and in the walls of some blood vessels. Patchy expression was noted in the medulla of the thymus and no expression was seen in the liver, heart or skeletal muscle.

The expression seen by Methner *et al* [490] only partly correlates with the results seen from the antibody staining of embryonic mouse sections. High levels of expression were seen in the tongue and expression was also seen in the brain. The most striking expression, especially in the older embryos, was that in the skeletal muscle. Signal was seen in all of the muscles of the limbs, as well as those of the body wall, intercostal muscles, diaphragm and facial muscles. In the early embryos, the signal was seen to be myotome specific and could be seen to correlate with the migration of the myoblast precursor cells. No expression was observed in any of the developing bones.

Ideally, co-localisation studies with positive control antibodies for the relevant tissues would have been performed in order to confirm the localisation of the Cmklr1 signal. However, due to time constraints, these were not possible.

5.4.2.3. Retinoic acid in limb development

The endogenous ligand for CMKLR1 is the retinoic acid responsive protein RARRES2. Retinoic acid (RA) is a transcriptional regulator that has long been implicated in the development of the limb. The application of RA to the anterior region of a limb bud will mimic the activity of a ZPA and result in duplication of the limb along the anteroposterior axis [491]. RA has also been implicated in proximodistal limb patterning with experiments in both axolotl and chick showing that RA exposure increases proximalisation in the limb [492-495] and induces the expression of proximal genes [496].

The level of active retinoic acid is determined by its synthesis from retinol (vitamin A) by retinaldehyde dehydrogenases (RALDH) and its degradation by cytochrome P450s (CYP26) enzymes. Mice with targeted disruptions of *Raldh2*, which is responsible for the majority of RA synthesis in early mouse embryogenesis, die at 9.5 to 10 dpc due to severe cardiac defects and show no evidence of limb bud formation [497]. Survival of the *Raldh2*$^{-/-}$ mice could be prolonged via maternal RA supplementation and surviving embryos exhibited highly reduced forelimb bud outgrowth, the severity of which was dependent on the dose and stage to which RA was provided, and apparently normal hindlimbs. The mutant forelimbs varied from markedly hypoplastic with no anteroposterior patterning and a single rudimentary digit, to near wild-type size but with variant anteroposterior patterning abnormalities

[498]. Examination of the phenotype of the rescued and unrescued mice led Mic *et al* [499] to determine that RA is required at two distinct time points during early limb development; primarily, it is required for the initiation of forelimb budding and later it is required for the expansion of the AER and, therefore, the maintenance of limb outgrowth [500].

There were three possible explanations proposed by Neiderreither *et al* [501] for the lack of any detectable abnormalities in the hindlimbs of the *Raldh2*$^{-/-}$ embryos: The maternal supplementation of RA fully rescues hindlimb development; there is another RA synthesising enzyme that provides RA to the hindlimb; hindlimb development may be predominantly controlled by other growth or inducing factors. They do, however, state that hindlimb development is not likely to be RA independent [502].

The lack of the CYP26B1 protein in mice also results in limb abnormalities. CYP26B1 is one of the three mouse cytochrome p450 enzymes that metabolise retinoic acid to inactive, or less active forms. These isozymes show different expression patterns in the embryo, with CYP26B1 being expressed in restricted regions of the developing limb [503;504] particularly in the distal regions and the AER [505]. *Cyp26b1*$^{-/-}$ mice have severe limb abnormalities affecting both fore and hindlimbs.

5.4.2.4. Retinoic acid and *CMKLR1*

Mice with targeted disruptions of *Raldh2* or *Cyp26b1* [506;507] both show limb abnormalities, reiterating the role of RA in limb development. The endogenous ligand of CMKLR1 is circulating RARRES2, a retinoic acid inducible protein. The

disruption of *CMKLR1* by the chromosomal translocation in the peromelia/phocomelia case would be expected to have an effect on the downstream RA reactions. The chemoattractant nature of CMKLR1 and its expression in the migratory myoblasts suggests that the disruption would interrupt a signalling cascade or chemotactic event that is crucial to the outgrowth, development and patterning of the limb. There is evidence to show that myoblasts may be required for normal limb outgrowth. Chicken ovalbumin upstream promoter transcription factor II (COUP-TFII) is a nuclear orphan receptor that is expressed in the myotome and muscle precursor cells. Experiments using mice harbouring a conditional knockout of *COUP-TFII* showed that loss of the receptor led to hypoplastic skeletal muscle and shorter limbs [508]. This suggests that migration of the muscle precursor cells is required for the maintenance of normal limb bud outgrowth. Disruption of the proper migration of the myoblasts, and their subsequent signalling events, may contribute to the phocomelia/peromelia phenotype.

5.4.2.5. Creation of a *Cmklr1* mutant mouse model

In order to help elucidate the role of *Cmklr1* in development, a mutant mouse is currently under development by Dr. Robert Hill (MRC Human Genetics Unit). This will involve the targeted disruption of the *Cmklr1* gene using a construct that will result in deletion of the coding exon of the gene. This construct will place human placental alkaline phosphatase (HP-AP) under the control of *Cmklr1* regulatory elements and allow the expression of the protein to be elucidated during developmental processes. The phenotype in the translocation case is thought to be caused by the disruption, by the translocation, of just one allele, although it was not

possible to sequence the other allele to check for mutations due to a lack of suitable material. It is therefore possible that a phenotype will also be observed in the heterozygous mouse. Although mouse models do not always accurately represent the situation seen in humans, it is hoped that, if *Cmklr1* is the causative gene, some phenotypic similarities will be observed in either the heterozygous or homozygous mouse. The mutant mouse should help determine whether the disruption of *Cmklr1* is sufficient to cause the peromelia/phocomelia phenotype seen in the translocation case.

5.4.2.6. *CMKLR1* is a good candidate gene for the peromelia/ phocomelia phenotype

The chromosome 12 breakpoint in the peromelia/phocomelia case lies between 0 and 25 kb from the 5′ end of the *CMKLR1* gene. The breakpoint may, therefore, directly disrupt the gene or separate the gene from *cis*-regulatory elements, such as the putative element located approximately 145 kb from the 5′ end. The expression and functional annotation of *CMKLR1* make it a good candidate for the severe limb phenotype irrespective of the fact that no mutations were found in one similar case. There have been a number of limitations in this study: the material available excluded the possibility of sequence analysis of the proband case or studies to check for *CMKLR1* mis-regulation or mis-expression. The rarity of the phenotype was also disadvantageous as there was only one other case available, which did not have an identical phenotype. However, *CMKLR1* has been identified as a good candidate gene for the symmetrical upper limb peromelia and lower limb phocomelia

phenotype and the development of a mouse model should help elucidate the function and expression of the gene throughout development and determine whether disruption of *CMKLR1* is sufficient to cause the phenotype seen in the translocation case.

6: Mapping of a t(1;2) Translocation Leads to the Identification of a Candidate Gene for Bilateral Renal Adysplasia

6.1. Abstract

The breakpoints of a *de novo* t(1;2)(q41;p25.3) with bilateral renal adysplasia were mapped using interphase FISH on nuclei extracted from archive paraffin embedded tissue sections. The human deletion map had previously predicted the existence of a dosage sensitive gene critical to normal human kidney development in the 1q region. The 1q41 breakpoint mapped within the *USH2A* gene, which encodes a large basement membrane-associated protein. Homozygous loss of function mutations in this gene cause Usher syndrome type 2A, associated with retinal degeneration and hearing loss. No renal phenotype has been reported with *USH2A* mutations and this was not, therefore, considered to be a good candidate for the bilateral renal adysplasia. The 1q breakpoint lies in a 1.5 Mb region containing only *USH2A* and *ESRRG*, the latter of which encodes an orphan nuclear steroid hormone receptor, estrogen-related receptor gamma. This genomic organization is conserved down to *fugu* (*Takifugu rubripes*). Expression analysis of Esrrg in the mouse embryo shows site and stage specific expression in the developing metanephric kidney. Initially expressed in the mesenchyme or stroma surrounding the ureteric bud at 12.5 dpc, the expression becomes duct specific at later stages of embryogenesis. This, combined with expression in the developing liver and lung, suggest a possible role in duct formation or branching. Comprehensive mutation analysis in six cases of lethal renal adysplasia and four families with dominant renal adysplasia did not identify

any mutations. This gene remains a very good candidate for the renal agenesis locus on 1q. Efforts to produce a mouse deficient in this gene are currently underway. The 2p25.3 breakpoint was shown to lie in a gap in the reference sequence in a gene-poor region, 3.1 Mb from the p arm telomere. The closest transcribed genes were a small cluster consisting of *RNASEH*, *RPS7*, *COLEC11*, *ALLC* and two novel genes of unknown function. None were obvious candidate on the basis of their functional annotation or developmental expression as determined by RT-PCR analysis.

6.2. Introduction

Renal adysplasia is defined as abnormal metanephric differentiation and can affect one or both of the kidneys (unilateral or bilateral respectively). It is generally a sporadic condition but can also occur in several syndromes, such as Walker-Warburg (OMIM 236670), Smith-Lemli-Opitz (OMIM 270400) or Townes-Brocks syndrome (OMIM 107480).

The severity of the adysplasia phenotype is extremely variable. If only one kidney is affected, renal function is usually unimpaired and no phenotype is observed. In bilateral disease, both kidneys may be affected to the point of total dysfunction, leading to a characteristic phenotype known as Potter sequence [509;510]. The lack of functional kidneys leads to a loss of urine output and, therefore, a severe reduction in amniotic fluid during the pregnancy (oligohydramnios). This causes compression of the foetus by the mother's uterus and results in many physical deformities, including abnormal facies and positioning of the hands and feet. Babies with bilateral renal adysplasia usually die very early in life due to respiratory insufficiency, as lungs require amniotic fluid for normal development.

6.2.1. Case Report/Clinical Data

This case was originally reported by Joss *et al*, 2003 [511]. The clinical data is summarised here.

This was the first child of a healthy couple who were non-consanguineous. At 29 weeks, an ultrasound revealed the apparent absence, bilaterally, of renal tissue and

oligohydramnios. At 32 weeks, the foetal lungs were found to be hypoplastic and the parents opted to have labour induced. The baby died an hour after birth.

The baby was male and had features of Potter sequence, including a flattened nose, large squashed ears, rocker bottom feet and marked skin laxity over the trunk and limbs. Post-mortem analysis revealed haemorrhagic masses with no recognisable renal structuring in the place of kidneys. Histology revealed undifferentiated mesenchyme with foci of cartilage, indicating bilateral renal adysplasia.

Cytogenetic analysis revealed the presence of a translocation between chromosomes 1 and 2, namely t(1;2)(q32;p25). The parents' chromosomes were normal, indicating a *de novo* event. Written consent was obtained from the family to use clinical photographs, case details and tissue samples for research purposes.

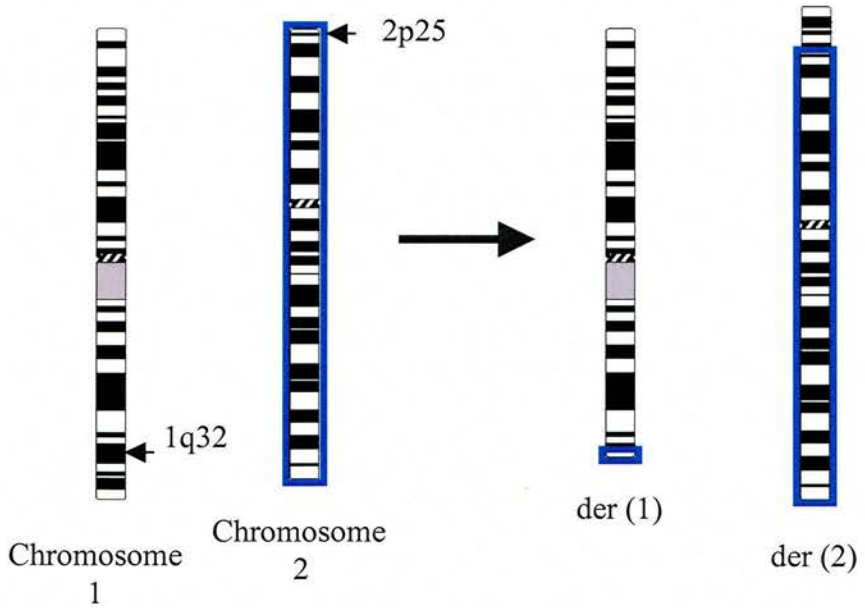

Figure 6.1. Partial ideogram of chromosomes 1 and 2

A partial ideogram showing the normal chromosomes 1 and 2 and the derived chromosomes resulting from the t(1;2)(q32;p25) translocation. Chromosome 2 is outlined for clarity.

6.2.2.Chromosome 1q has been Previously Implicated in Kidney Disorders

Chromosome abnormalities have previously been associated with bilateral renal adysplasia or Potter sequence but these are generally not recurrent and often include other phenotypes. Chromosomes abnormalities include trisomy 7 [512-514], chromosome 22q11 deletion [515], ring chromosome 4 [516], chromosome 4p deletion [517] and chromosome 15q22-q24 deletion [518].

Brewer *et al.* [519], looked at deletions associated with human malformations and found highly significant association between renal agenesis and chromosome band 1q31, a band just proximal to the breakpoint in the translocation case. Deletions of 1q31-q32 have also been observed in two cases of unilateral renal agenesis and multiple congenital abnormalities [520]. These deletions suggest the presence of a gene, or genes, involved in kidney development in the 1q31-q32 region. The breakpoint in the translocation case was reported to be in band 1q32 and it was hypothesised that disruption of a gene in this region would be responsible for the kidney phenotype.

There is no human genetic evidence linking any renal anomalies with the 2p25 locus.

6.2.3. Other Renal Adysplasia Cases

Renal adysplasia can occur in many different forms that vary in severity from unilateral cysts to bilateral lethal renal adysplasia. A number of cell lines were

available from individuals with either sporadic or familial adysplasia. The phenotypes of these individuals are outlined below.

6.2.3.1. Lethal renal adysplasia cases

Cell lines T96-2020, T96-2338, T97-1060, T97-1759, T98-2209 and T05-0100 were from lethal renal adysplasia cases.

6.2.3.2. REWKI

This cell line was from a boy with unilateral cystic adysplasia of the kidney born to a mother who a normal ultrasound renal scan but went on to have a bilateral cystic adysplasia child by a different father. The result of a third pregnancy was unknown to us, although an ultrasound scan at 22 weeks showed no abnormalities.

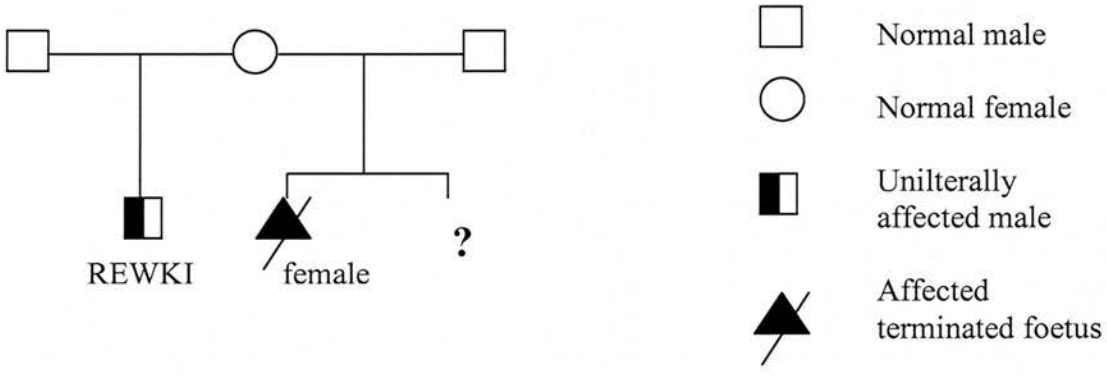

Figure 6.2. A pedigree of the cell line REWKI

A partial pedigree showing the immediate family of cell line REWKI. REWKI had unilateral cystic adysplasia and his normal mother subsequently had a female foetus, by a different father, with bilateral cystic adysplasia, which was electively terminated. The result of the third pregnancy was unknown to us.

6.2.3.3. RUFUL

This is the cell line from a woman with a bifid ureter who had one child with bilateral renal agenesis and further normal children by the same father. The result of a fourth pregnancy, by another man, was unknown to us although an ultrasound scan at 20 weeks showed the presence of at least one, and probably both, kidneys and normal amniotic fluid content.

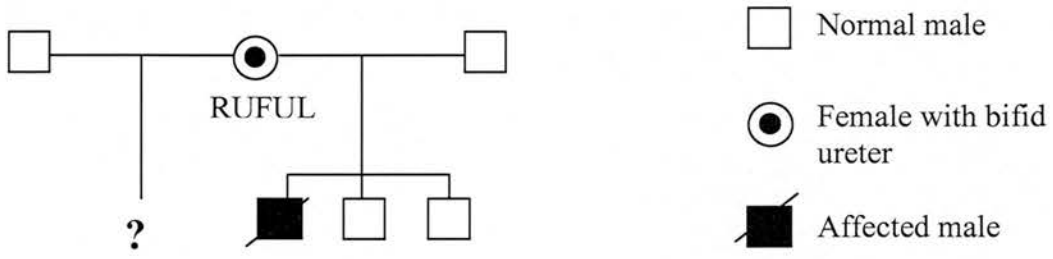

Figure 6.3. A pedigree of the cell line RUFUL

A partial pedigree showing the immediate family of cell line RUFUL. RUFUL had a bifid ureter and had a child with bilateral renal agenesis. She subsequently went on to have two normal children with the same father and a fourth pregnancy by another man. The result of this fourth pregnancy was unknown to us.

6.2.3.4. EDPOR

This cell line is from a boy with multicystic kidneys, born to an apparently normal mother. His mother's cousin had unilateral renal agenesis and had lost two children with cystic adysplasia before having a normal child.

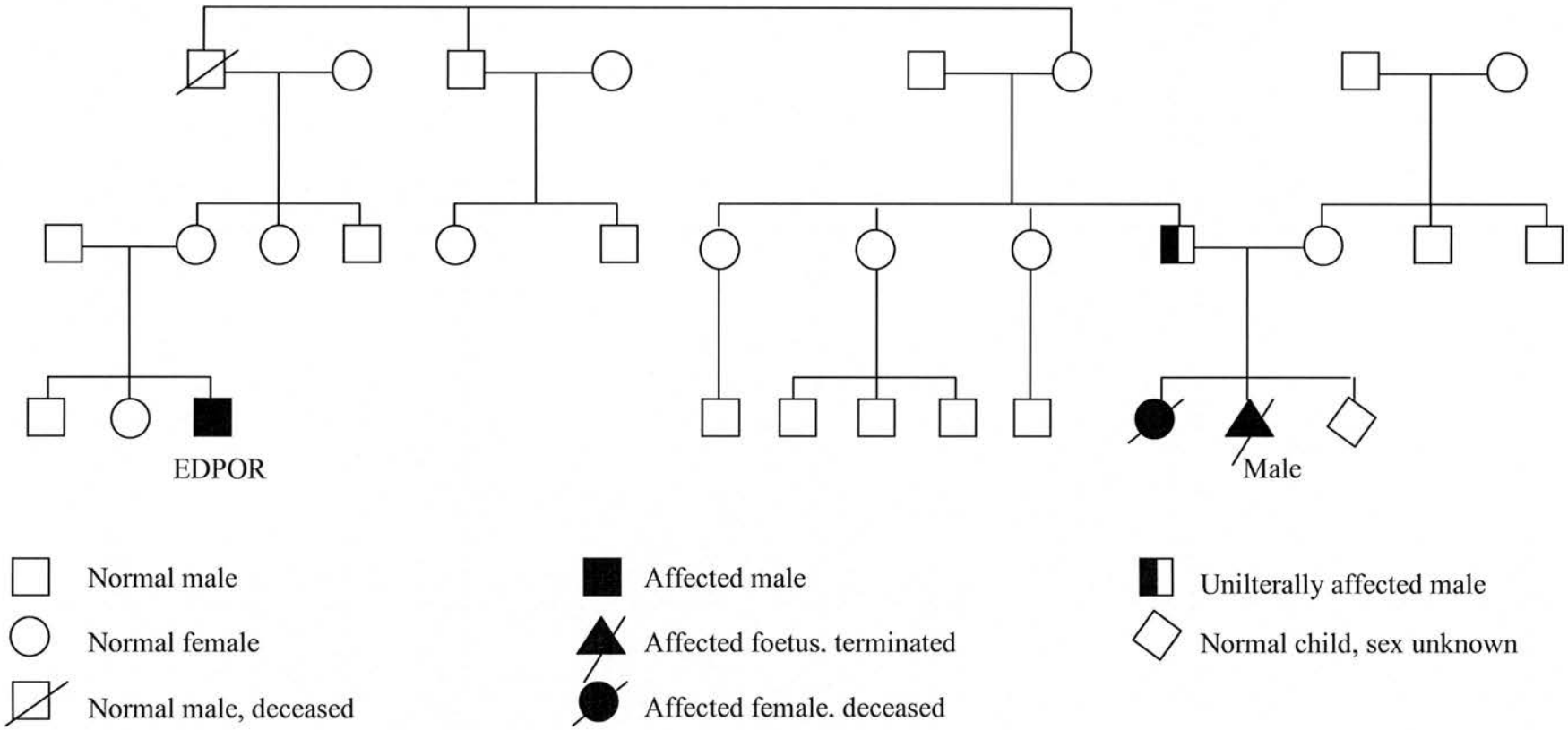

Figure 6.4. A pedigree of the cell line EDPOR

A pedigree for cell line EDPOR, a boy with multicystic kidneys born to a normal mother. The mother's cousin had unilateral renal agenesis and had two children with bilateral renal agenesis before having a normal child.

6.2.3.5. CRAST

This is the cell line from a woman who was examined at 7 years of age and found to have a very small, rudimentary kidney on the right hand side, with an ectopic ureter opening into the urethra. These were subsequently removed. Her mother had an absence of the right kidney.

The daughter later married and produced two foetuses, both of which had bilateral renal agenesis. The father of the foetuses had a normal renal ultrasound scan.

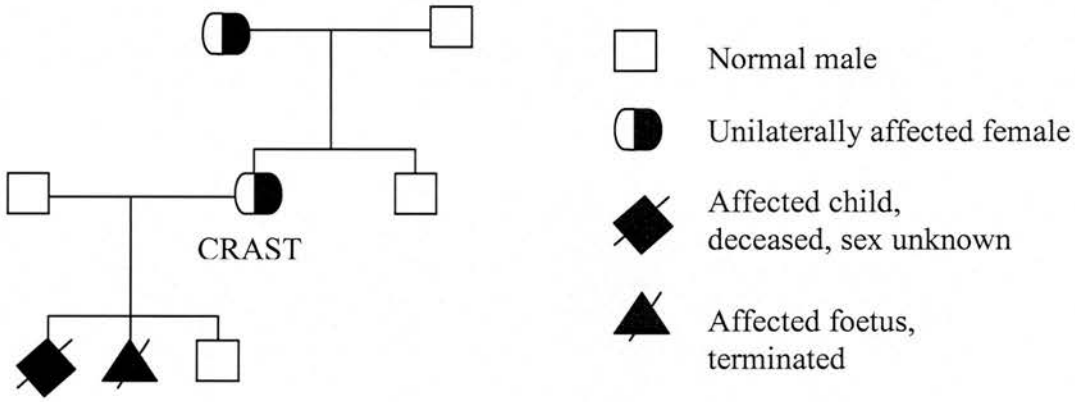

Figure 6.5. A pedigree of the cell line CRAST

A pedigree of cell line CRAST, a female with a small rudimentary kidney born to a mother with unilateral renal agenesis. CRAST went on to have two foetuses, both with bilateral renal agenesis and a normal child.

6.2.4. A Brief Overview of Metanephric Kidney Development

Metanephric kidney development is very complex and involves many different cell and genetic interactions. A brief outline of the development is given here.

The metanephric kidney is the only kidney that persists into adult life in mammals, reptiles and birds. Development of the metanephric kidney begins at around day 11 dpc in the mouse (around day 30 in humans) with the aggregation of mesenchymal cells near to the pelvic aorta. The ureteric bud, a finger-like projection formed from the nephric duct, then invades the aggregated cells, known as the metanephric mesenchyme. Reciprocal interactions occur between the mesenchyme and the invading bud: The mesenchyme induces the bud to grow and branch to form the collecting duct system and the ureters and the bud induces the mesenchyme to proliferate and differentiate into nephrons. The first six to eight ureteric bud branches go on to form the ureter, renal pelvis and parts of the bladder. The collecting duct system is formed from subsequent branching events [521]. As the ureteric bud continues to branch, it induces more and more cells to undergo nephrogenesis. This branching is critical to normal renal development as it determines the number of nephrons formed in the kidney.

The foetal kidney exhibits a gradient of development with regions inside the kidney being more mature than those towards the outer cortex.

6.3. Results

6.3.1. FISH Mapping

FISH mapping was performed to determine the exact location of the translocation breakpoints. The mapping strategy utilised is described in section 4.1.

6.3.1.1. Chromosome 1 breakpoint

The breakpoint on 1q was found to be within band 1q41, between BACs RP4-723P6 and RP11-239I22. The *USH2A* gene is directly interrupted. The only other gene in the region is the orphan nuclear hormone receptor, *ESRRG*.

Chromosome Band	Library name	Clone name	Mb*	Result
1q24.2	RP11	277C14	168.4	Proximal to breakpoint
	RP11	480I12	199.17	Proximal to breakpoint
	RP11	739N20	200.68	Proximal to breakpoint
	RP11	534L20	203.28	Proximal to breakpoint
1q41	RP11	323K10	211.6	Proximal to breakpoint
	RP11	438G15	212.68	Proximal to breakpoint
	RP11	415H9	212.99	Proximal to breakpoint
	RP5	861H2	213.14	Proximal to breakpoint
	RP11	22M7	213.16	Proximal to breakpoint
	RP4	723P6	213.32	Proximal to breakpoint
	RP11	239I22	213.5	Distal to breakpoint
	RP11	152K20	213.59	Distal to breakpoint
	RP11	23B9	213.74	Distal to breakpoint
	RP11	426K17	213.8	Distal to breakpoint
	RP11	66M7	214.2	Distal to breakpoint
	RP11	224O19	215.52	Distal to breakpoint
	RP11	392O17	216.47	Distal to breakpoint
	RP11	332J14	217.69	Distal to breakpoint
	RP11	528D17	218.2	Distal to breakpoint
	RP11	239E10	220.3	Distal to breakpoint
1q42.2	RP11	99J16	227.9	Distal to breakpoint
1q44	**CTB**	160H23	245	Distal to breakpoint

Table 6.1. A list of BAC clones used to map the 1q breakpoint

A list of BACs used to map the 1q breakpoint, their position within the genome and their position relative to the breakpoint as determined by FISH. The clones highlighted in blue are those that flank the breakpoint. The clones highlighted in blue are those that flank the breakpoint, which is located within band 1q41.

*Figures from Ensembl NCBI 35, July 2004 assembly

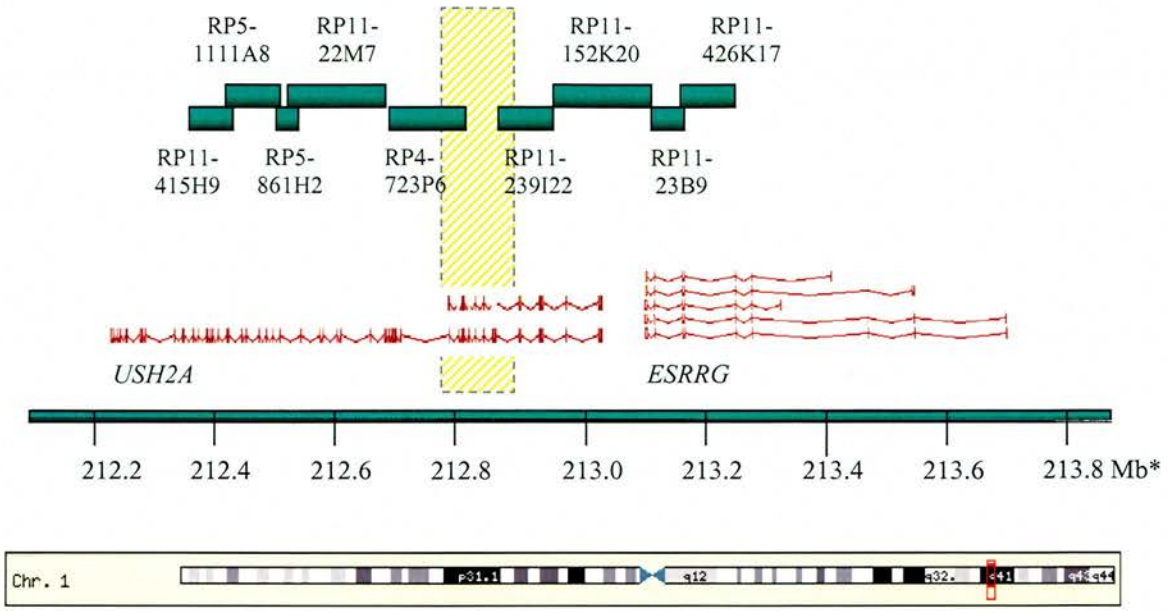

Figure 6.6. Diagram of the area around the 1q breakpoint

Green rectangles represent the BAC clones used for FISH mapping. The position of the genes relative to the BACs can be seen. The breakpoint falls within the shaded region between BACs RP4-723P6 (proximal) and RP11-239I22 (distal) and disrupts the *USH2A* gene.

*Figures from Ensembl NCBI 35, July 2004 assembly

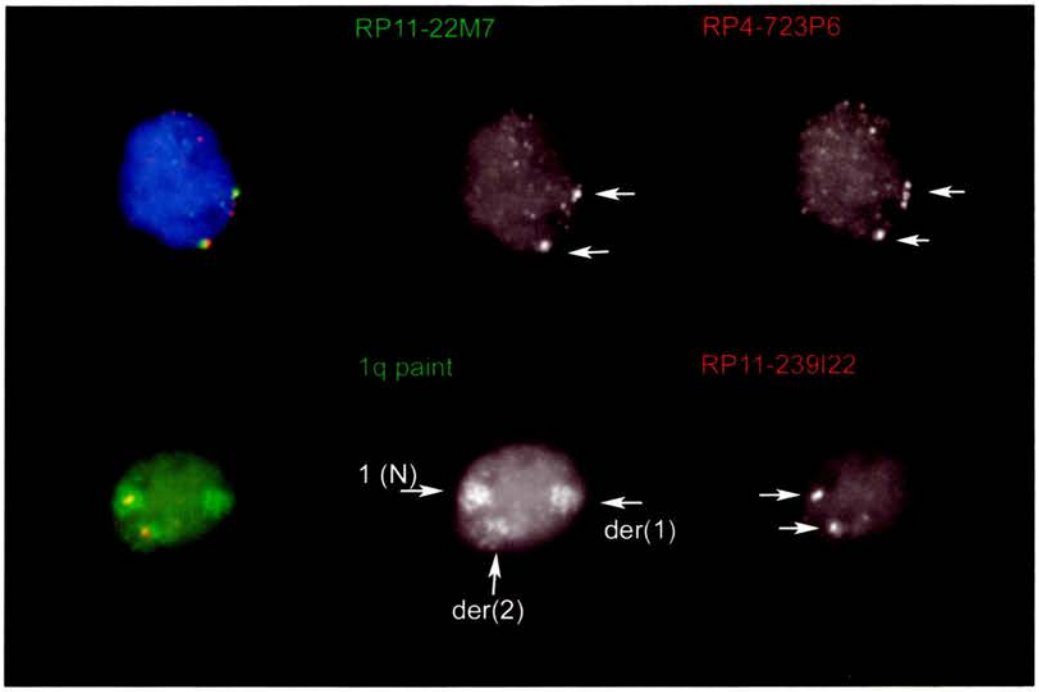

Figure 6.7. FISH with proximal and distal 1q41 BACs

FISH experiments with BACs around the 1q41 breakpoint. In the top panel, BAC RP11-723P6 (red) is applied with a BAC that is proximal to the breakpoint (RP11-22M7 in green). The co-localisation of the signals indicated that RP4-723P6 is also proximal to the breakpoint. Note, the 3 signals indicated by the top arrow in the RP4-723P6 image were not present in every cell. However, many nuclei were difficult to capture and the above nuclei showed the clearest probe signals after capturing and was therefore included. In the bottom panel, BAC RP11-239I22 (red) is applied with a chromosome 1q arm specific paint (green). The BAC co-localises with the small paint domain, indicating that it is on the translocated part of chromosome 1 (on the der(2)) and is therefore distal to the breakpoint. 1(N) indicates the domain of the normal chromosome 1 and the arrows indicate the positions of the signals.

6.3.1.2. Chromosome 2 breakpoint

The breakpoint on chromosome 2 was found to lie in a gap in the contig in band 2p25.3. The flanking clones were BACs RP11-410L9 and RP11-568H24. Hybridisations with the BAC between these two clones, RP13-512J5, failed in numerous FISH experiments and these were not repeated due to a lack of material.

Chromosome Band	Library name	Clone name	Mb*	Result
2ptel	GS1	8L3	0.33	Distal to breakpoint
2p25.3	RP11	168K7	2.83	Distal to breakpoint
	RP11	352J11	2.23	Distal to breakpoint
	RP11	744D24	2.37	Distal to breakpoint
	RP11	141G5		Distal to breakpoint
	RP11	163G21	2.73	Distal to breakpoint
	RP11	410L9	2.88	Distal to breakpoint
	RP13	512J5		FAIL
	RP11	568H24	3.2	Proximal to breakpoint
	RP11	327H5	3.51	Proximal to breakpoint
2p25.2	RP13	868N24	5.2	Proximal to breakpoint
	RP11	350H23	5.63	Proximal to breakpoint
	RP11	485O17	6.51	Proximal to breakpoint
2p25.1	RP11	214N9	9.45	Proximal to breakpoint
2p24.3	RP11	333O1	12.57	Proximal to breakpoint

Table 6.2. A list of BAC clones used to map the 2p breakpoint

A list of the BAC clones used for mapping the 2p translocation breakpoint, their position within the genome and their position relative to the breakpoint as determined by FISH. The clones highlighted in blue indicate those that flank the breakpoint, which is located within band 2p25.3. The clone in between these failed repeatedly in FISH experiments and was therefore excluded.

*Figures from Ensembl NCBI 35, July 2004 assembly

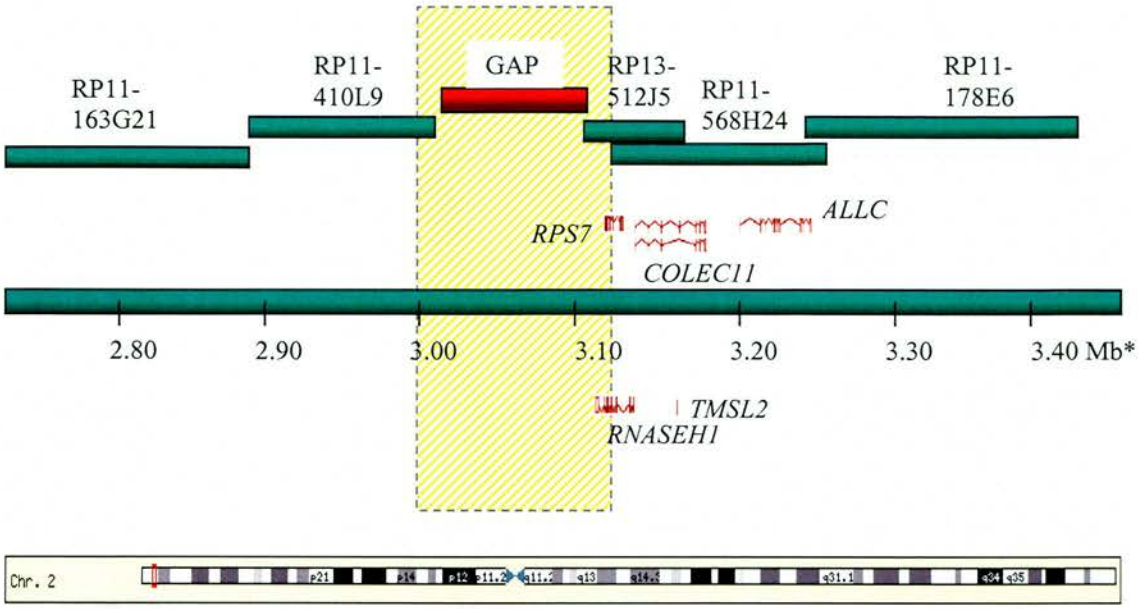

Figure 6.8. Diagram of the area around the 2p breakpoint

Green rectangles represent the BAC clones used for FISH mapping. The position of the genes relative to the BACs can be seen. The breakpoint falls within the shaded region between BACs RP11-410L9 (distal) and RP11-568H24 (proximal). The breakpoint could not be narrowed further due to the presence of a gap in the reference sequence in this area, represented by the red rectangle in the diagram.

*Figures from Ensembl NCBI 35, July 2004 assembly

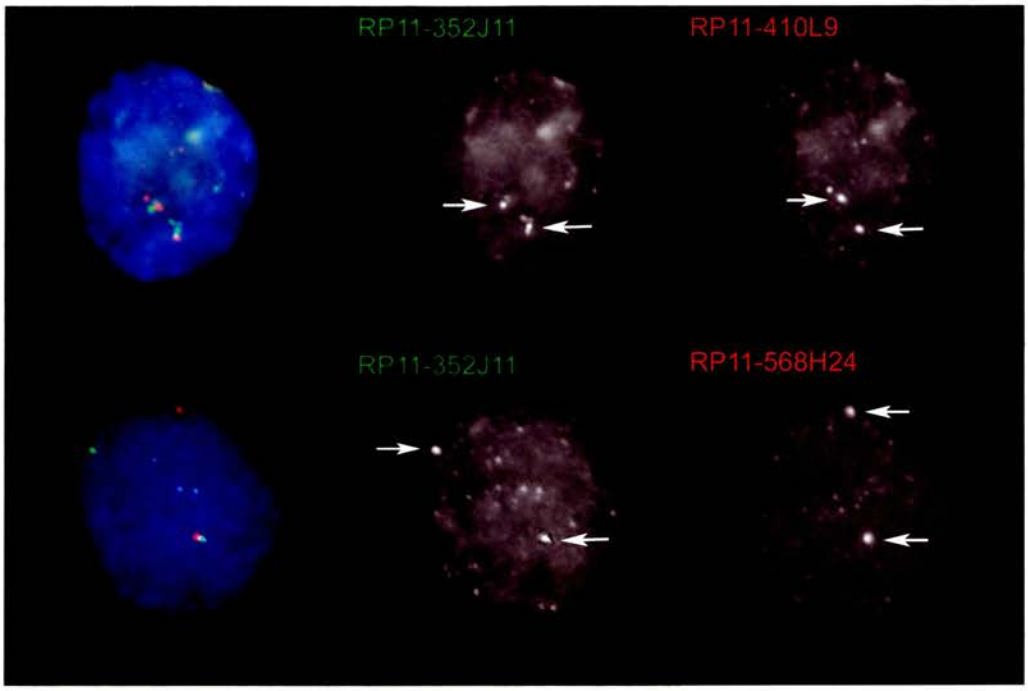

Figure 6.9. FISH with proximal and distal 2p BACs

FISH on DAPI stained nuclei using distal 2p BAC RP11-352J11 (green) along with BACs RP11-410L9 (top panel) and RP11-568H24 (bottom panel). The arrows indicate the position of the signals. Co-localising signals in the top panel indicate that BAC RP11-410L9 is distal to the translocation breakpoint, whereas BAC RP11-568H24 only has one co-localising signal, indicating that the BAC is proximal. Arrows indicate the position of the signals.

6.3.2. RT-PCR

In order to determine whether *Ush2a* and *Esrrg* were expressed in the developing mouse kidney, RT-PCR was performed on dissected kidneys from mouse embryos aged 13.5 dpc, 14.5 dpc and adult mouse kidneys. Bands of the expected size were seen in all stages of kidney tested. The negative reaction, containing no RT template, showed no bands other than primer dimer. The results show that both Ush2a and Esrrg are expressed at all stages of kidney development tested. However, Ush2a is present only at low levels and probably has multiple transcripts.

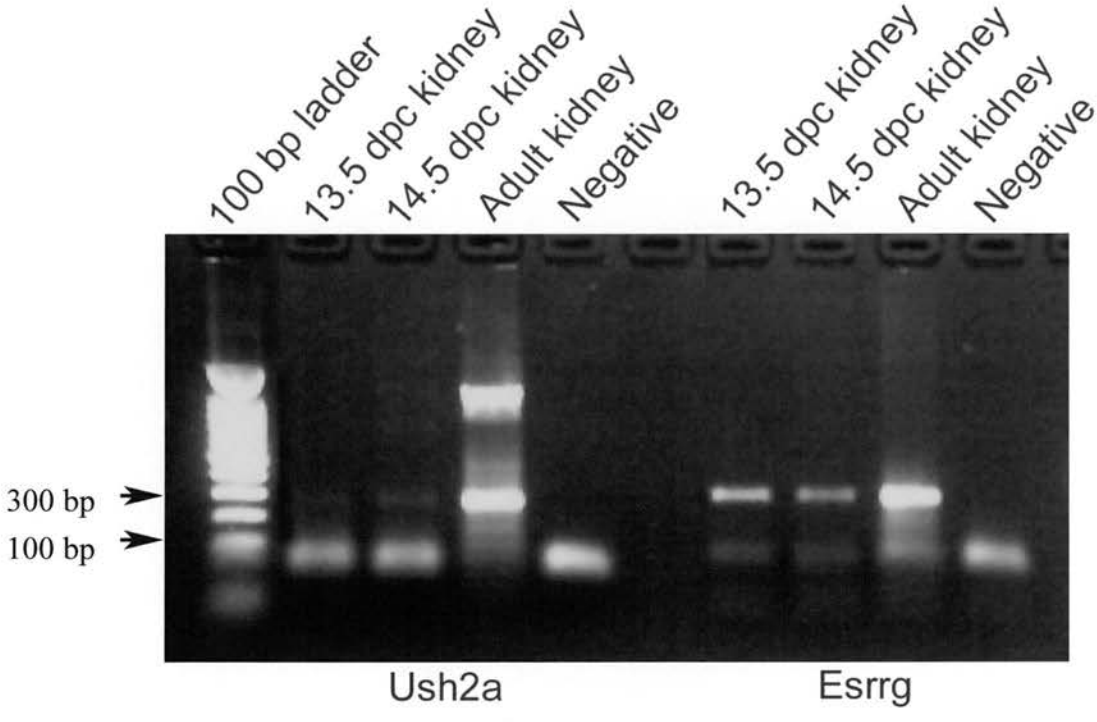

Figure 6.10. Esrrg and Ush2a RT-PCR on mouse embryonic and adult kidneys

RT-PCR on dissected kidneys from mouse embryos aged 13.5 and 14.5 dpc and adult mice. Expression of Ush2a can be seen in the adult kidney and faintly in the embryonic kidneys. The multiple bands indicate multiple isoforms. Esrrg expression can be clearly seen in both embryonic kidney stages and in the adult kidney. The bands under 100 bp represent primer dimer.

6.3.3. Wholemount RNA *In-Situ* Hybridisation

To attempt to elucidate the expression pattern of Esrrg throughout development, wholemount RNA *in-situ* hybridisations were performed on mouse embryos from a number of different developmental stages. However, the expression pattern could not be determined due to a high level of background staining on the embryos. Due to time constraints, these experiments were not repeated.

6.3.4. Esrrg Antibody Staining

In order to elucidate the expression pattern of the Esrrg protein throughout embryonic mouse development, antibody staining was performed on paraffin embedded sections from mouse embryos from 9.5 to 14.5 dpc. All negative controls, in which no primary Esrrg antibody was added, were clear of any staining on addition of the detection agents, indicating that the Esrrg signal was specific.

6.3.4.1. Antibody staining on embryonic mouse sections

The expression of Esrrg was seen to alter dynamically during embryonic development. The expression is summarised in table 6.3. Examples of the staining can be seen in figure 6.11.

	9.5 dpc	10.5 dpc	11.5 dpc	12.5 dpc	14.5 dpc
Limb bud					
Neural Tube					
Heart					
Liver					
Brain					
Lung					
Eye					
Gonad					
Kidney			?		
Muscle/ muscle precursors					
Bone/cartilage precursors					
Stomach					

Table 6.3. Expression of Esrrg through mouse embryogenesis

Esrrg expression as determined by antibody staining. Blue boxes indicate expression, grey boxes a lack of expression and question marks indicate that expression could not be determined. Hashed boxes indicate organs that could not be identified in the developmental stage or the sections available.

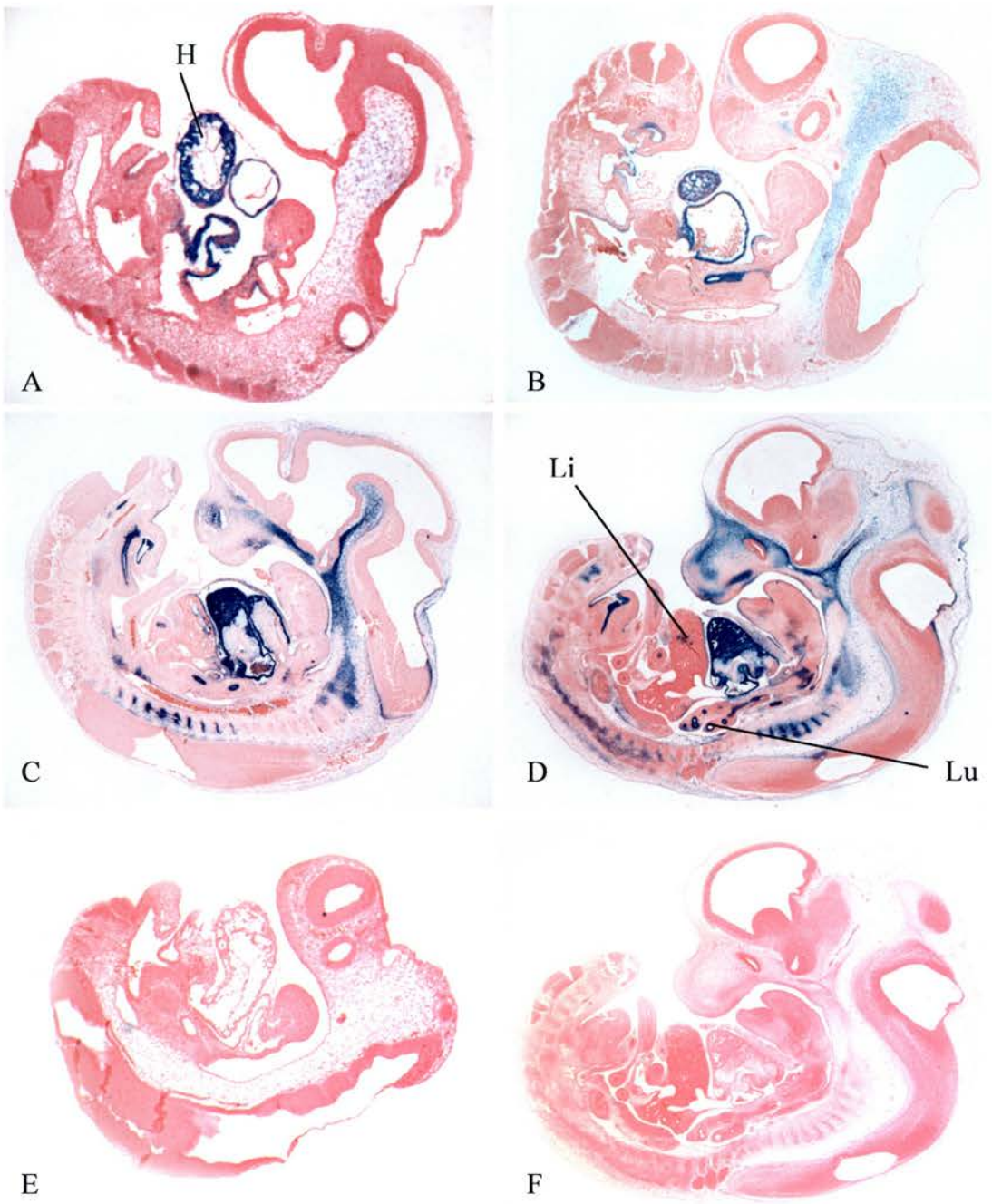

Figure 6.11. Esrrg staining on mouse embryo sections

Examples of Esrrg staining on sections from mouse embryos aged 9.5 (A), 10.5 (B), 11.5 (C) and 12.5 dpc (D). Sections are counterstained with eosin (pink) and signal detected with NBT/BCIP (blue). Expression can be seen in the heart (H), liver (Li) and the developing lung (Lu). Full details of expression can be seen in table 6.3. Negative controls (9.5 dpc, E and 12.5 dpc, F) show no blue signal, indicating that the staining is specific to the Cmklr1 antibody.

6.3.4.2. Esrrg antibody staining on embryonic and neonatal mouse kidneys

Antibody staining of embryonic kidneys from 12.5 to 18.5 dpc showed dynamic developmental expression. At 12.5 dpc, expression appears to be in the metanephric mesenchyme or the stroma towards the outer edge of the developing kidney, towards where the capsule will form. As the kidney becomes more developed, expression can be seen in the capsule (and the adrenal gland) and in the collecting ducts, formed by branching of the ureteric bud. This expression in and around the collecting duct continues throughout development and is still visible in the neonate kidney, with the signal appearing strongest in and around the most mature collecting ducts located in the pelvis (centre) of the kidney. The collecting ducts in this region are surrounded by stroma, whereas younger ducts located towards the outer cortex are not.

The forming nephrons appear negative for Esrrg staining.

6.3.4.3. Esrrg antibody staining on adult mouse kidneys

No expression could be seen in the adult mouse kidney sections examined. Due to time constraints, this experiment was not repeated.

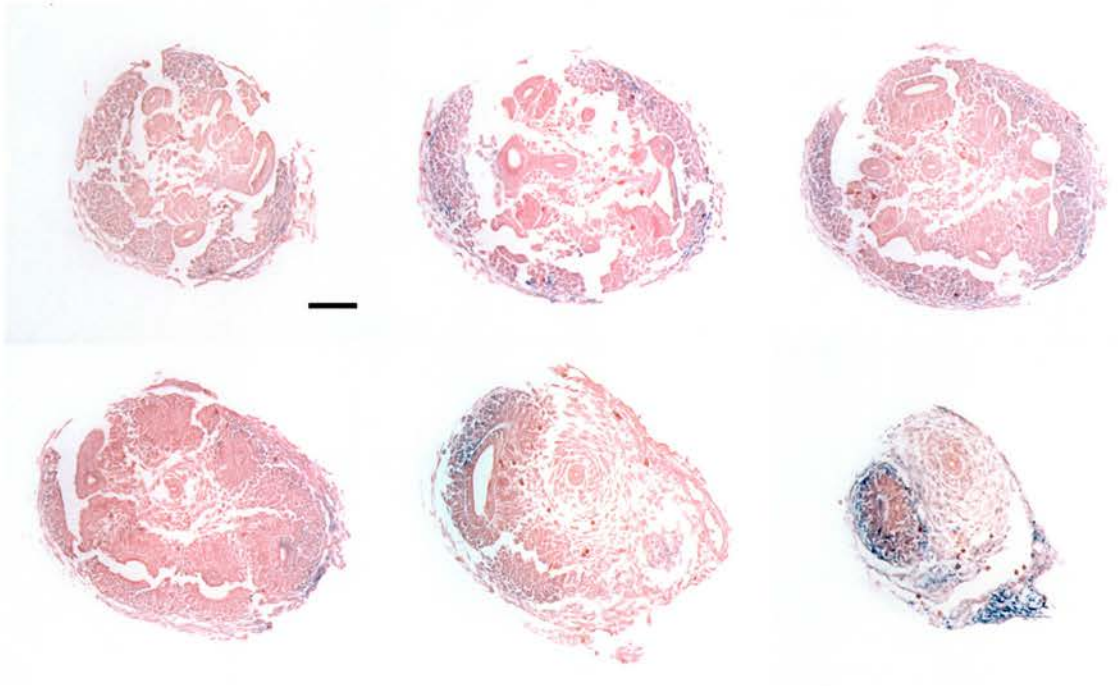

Figure 6.12. Esrrg antibody staining on 12.5 dpc mouse kidney sections

Kidney sections are counterstained with eosin (pink) and Esrrg is detected with NBT/BCIP (blue). Signal can be seen in the metanephric mesenchyme or the stroma towards the outer edge of the forming kidney, where the capsule will form. The black bar represents 100 µm.

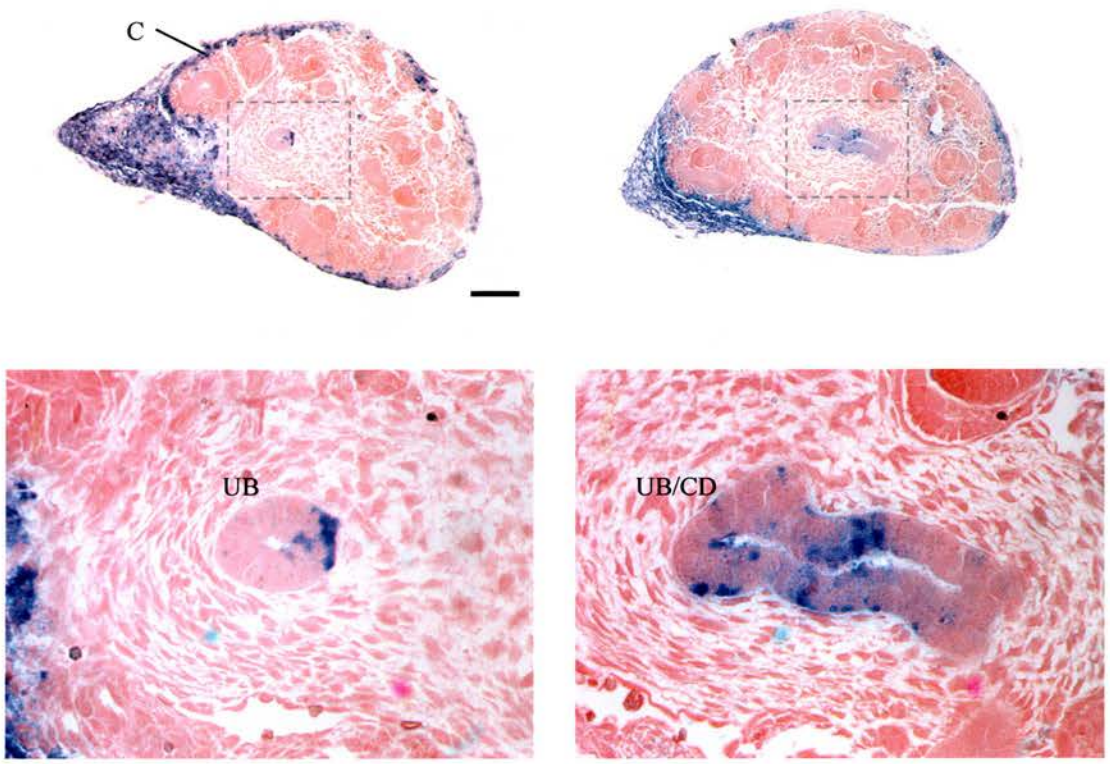

Figure 6.13. Esrrg antibody staining on 13.5 dpc mouse kidney sections

Sections are counterstained with eosin (pink) and Esrrg is detected with NBT/BCIP (blue). Signal can be seen in the branching ureteric bud (UB) that subsequently forms the collecting ducts (CD). Expression can also be seen in the capsule (C) surrounding the kidney. The black bar represents 100 μm and the hashed boxes indicate the area enlarged in the images below.

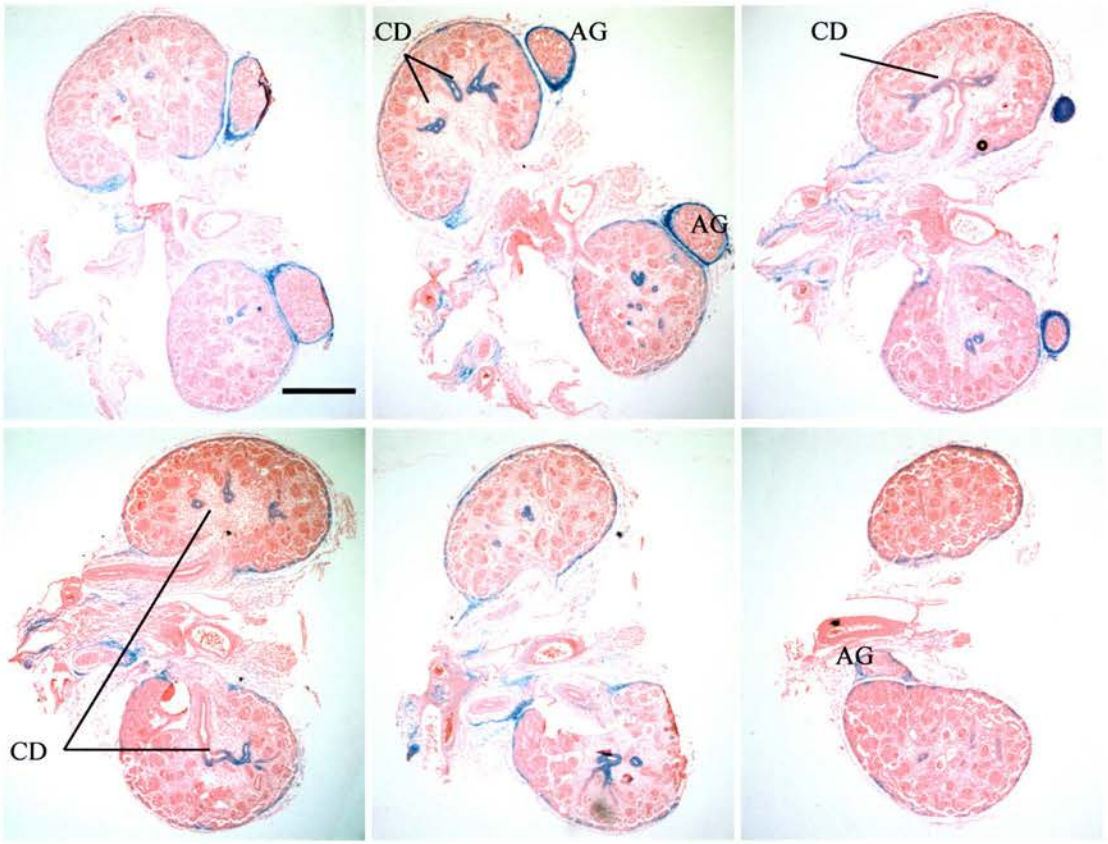

Figure 6.14. Esrrg antibody staining on 14.5 dpc mouse kidney sections

Sections are counterstained with eosin (pink) and Esrrg is detected with NBT/BCIP (blue). Signal can be seen in the collecting ducts (CD) formed from the branching ureteric bud and expression is still visible in the capsule (C) surrounding the kidneys and the adrenal glands (AG). The black bar represents 500 µm.

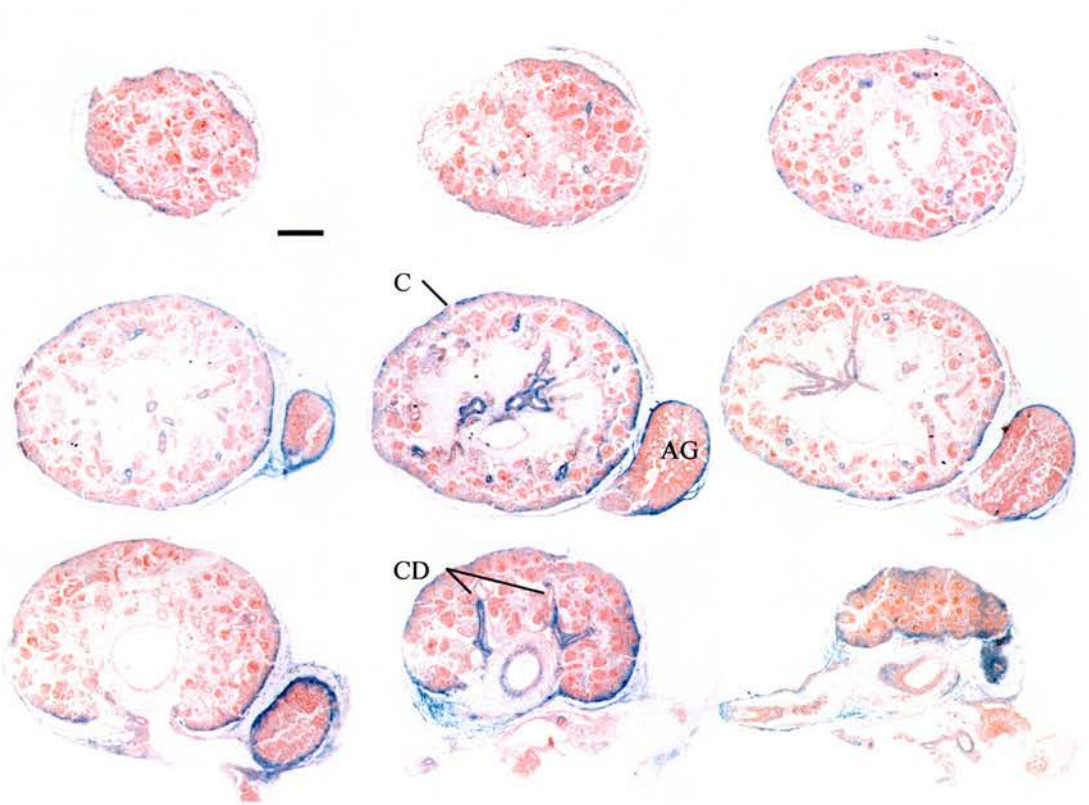

Figure 6.15. Esrrg antibody staining on 15.5 dpc mouse kidney sections

Sections are counterstained with eosin (pink) and Esrrg is detected with NBT/BCIP (blue). Signal can still be seen in the collecting duct system (CD) and the capsule (C) surrounding the kidney and adrenal gland (AG). The black line represents 200 μm.

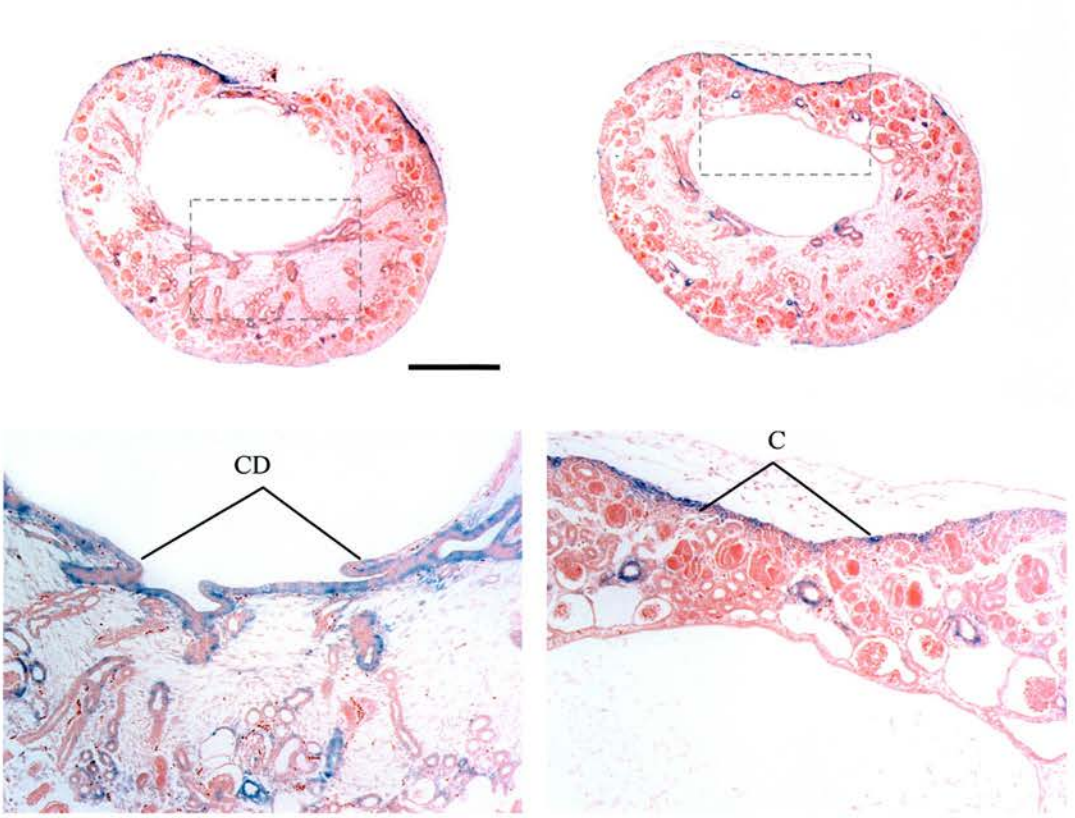

Figure 6.16. Esrrg antibody staining on 16.5 dpc mouse kidney sections

Sections are counterstained with eosin (pink) and Esrrg is detected with NBT/BCIP (blue). Esrrg expression can be seen in the collecting ducts (CD) and the capsule (C) of the kidney. Dashed boxes indicate the enlarged regions seen in the images below. The black bar represents 500 μm.

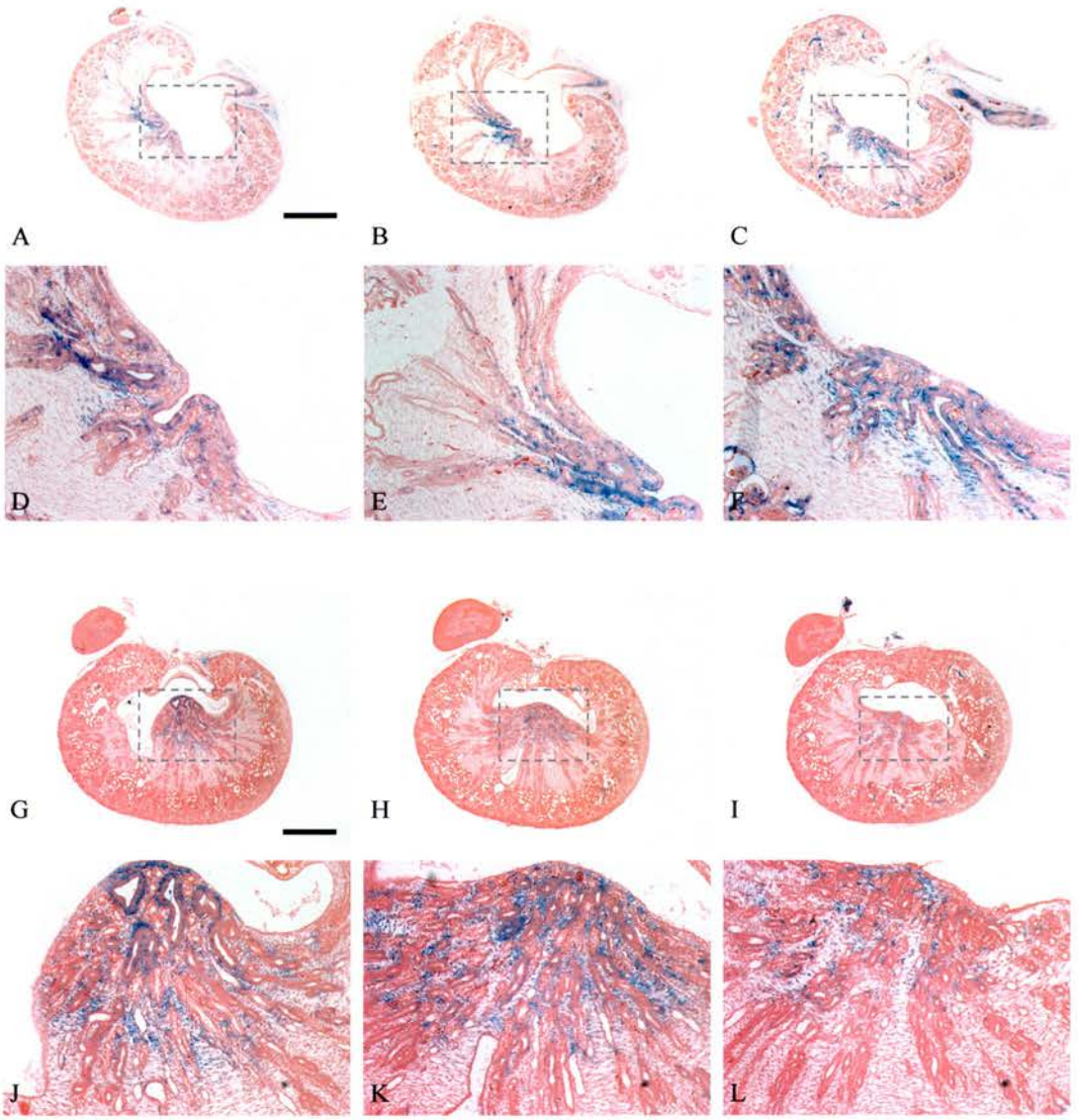

Figure 6.17. Esrrg expression in 17.5 and 18.5 dpc mouse kidney sections

Esrrg antibody straining in 17.5 dpc (A-F) and 18.5 dpc (G-L) mouse kidney sections. Sections are counterstained with eosin (pink) and the Esrrg antibody is detected with NBT/BCIP (blue). Dashed boxes indicate the enlarged region, showing signal in and around the more mature collecting ducts located within the pelvis (centre) of the kidney. The black bars represent 500 μm.

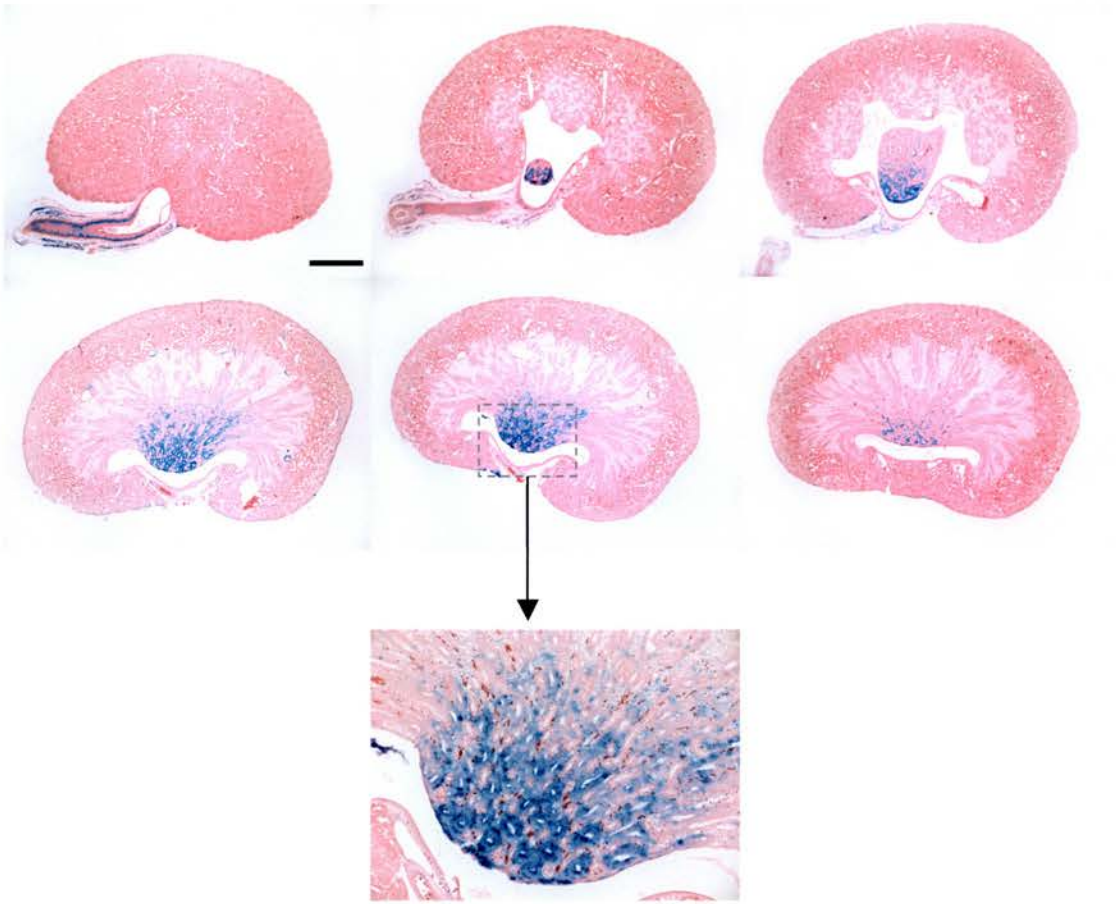

Figure 6.18. Esrrg staining on neonate (day 0) mouse kidney sections

Sections are counterstained with eosin (pink) and Esrrg is detected with NBT/BCIP (blue). The dashed box shows the enlarged region. Esrrg expression can clearly be seen in and around the more mature collecting ducts located in the pelvis (centre) of the kidney. The black bar represents 500 μm.

6.3.4.4. ESRRG antibody staining on control cell lines

In order to determine whether ESRRG was expressed in fibroblasts and, if so, the subcellular localisation of the protein, antibody staining was performed on control human fibroblasts. ESRRG was expressed and appeared cytoplasmic and punctate. The nucleus appeared negative and the negative control, which had no ESRRG antibody added, was also negative, indicating that staining was specific.

The punctate cytoplasmic staining suggested that the protein may be inside, or on the membrane of, the peroxisomes. To attempt to confirm this, the ESRRG antibody was applied in combination with an antibody for catalase, a peroxisome specific protein. The expression patterns co-localised, indicating that ESRRG was associated with the peroxisomes (figure 6.19).

To determine whether ESRRG was expressed in other cell lines and if the expression pattern was the same between types, the experiment was repeated on human HeLa cells and also on M15 cells, a mouse embryonic kidney cell line derived from the mesonephros. Both cell types showed a similar punctate staining pattern (figure 6.20). The expression in both cell types did appear to vary from cell to cell, with some staining appearing much brighter than others (see table 6.4). The reason for this is unknown but it is possibly cell cycle related.

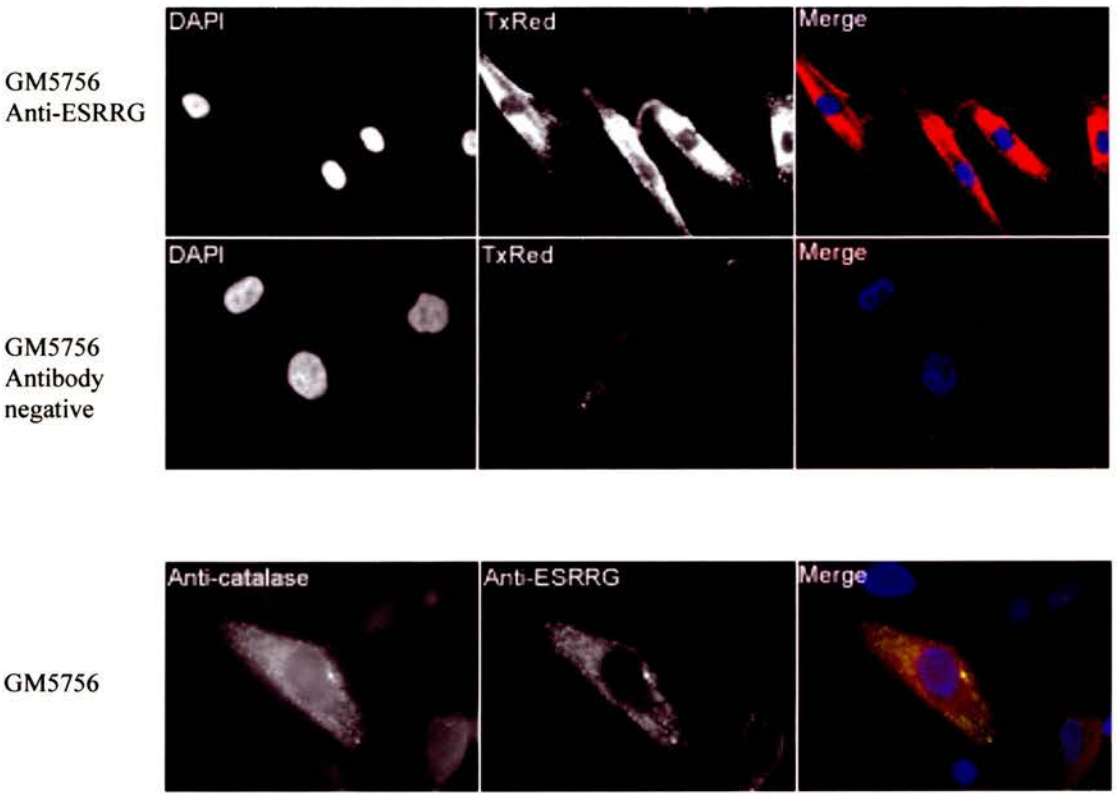

Figure 6.19. ESRRG and catalase antibody staining on a control fibroblast cell line

ESRRG antibody staining on control fibroblast cell line GM5756. Nuclei are counterstained with DAPI (blue) and the ESRRG signal detected with an Alexa-594 antibody (red). The top panel shows that ESRRG is expressed in the cytoplasm of the cells. The panel below shows the negative experiment in which the ESRRG antibody was not added, indicating that the expression is specific. The bottom panel shows staining of the same cell line with both anti-ESRRG and anti-catalase antibodies. Catalase is a peroxisome specific protein and the co-localisation of the two signals suggests that ESRRG is located in, or on the membrane of, the peroxisomes.

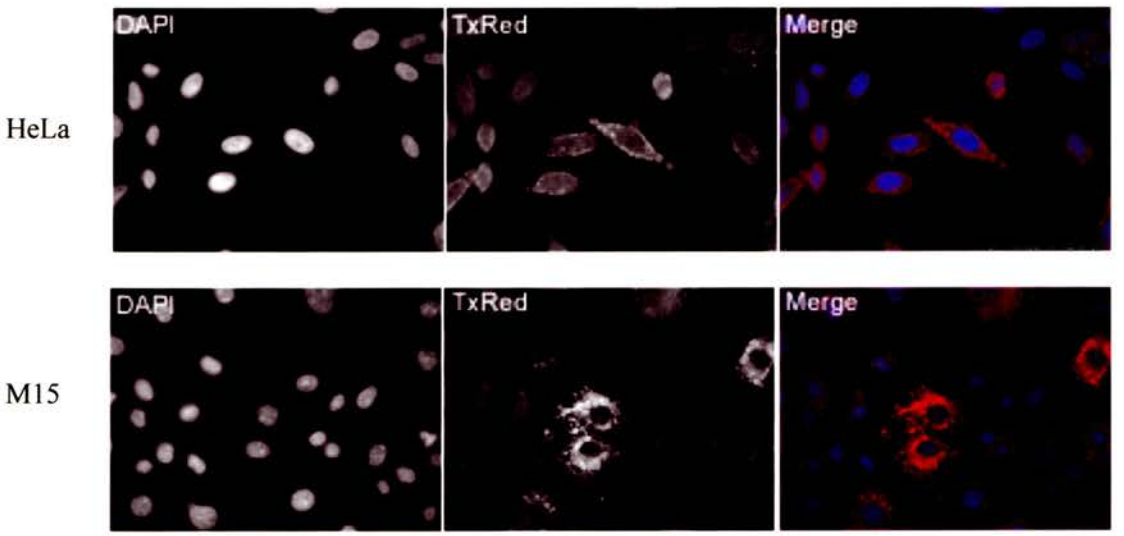

Figure 6.20. ESRRG antibody staining in HeLa and mouse M15 cells.

ESRRG antibody staining in the human HeLa and mouse embryonic kidney (M15) cell lines. Nuclei are counterstained with DAPI (blue) and ESRRG is detected with an Alexa-594 anti-rabbit antibody (red). Both cell lines show expression of ESRRG and show a similar pattern of punctate cytoplasmic staining as the control fibroblast cell line. The staining intensity appears to vary dramatically between cells (see table 6.4).

	Approximate proportion of cells (%)		
	Very bright staining	Bright Staining	Weak Staining
HeLa	6	12	82
M15	10	3	87

Table 6.4. ESRRG staining intensities in HeLa and M15 cells

A table showing the relative intensity of ESRRG antibody staining in HeLa and mouse M15 cells. The proportion of cells with each intensity is shown. As can be seen, the majority show weak staining, with only a small proportion showing bright or very bright staining.

6.3.4.5. ESRRG antibody staining on lethal renal adysgenesis cell lines

In order to determine whether ESRRG is expressed in the lethal renal adysgenesis and whether the expression pattern is the same as in the control fibroblast cell lines, antibody staining was performed on five of the six cell lines. The results showed that there was expression in every cell line tested and that there was no apparent protein mis-localisation (figure 6.21).

The intensity of the antibody staining was variable from cell to cell (see table 6.5) as in the HeLa and M15 cells.

	Approximate proportion of cells (%)		
	Very bright staining	Bright Staining	Weak Staining
T96-2020	5	15	80
T96-2338	8	8	84
T97-1060	7	14	79
T98-2209	10	5	85
T05-0100	8	8	84

Table 6.5. ESRRG staining intensities in lethal adysgenesis cell lines

A table showing the relative intensity of ESRRG antibody staining in the lethal renal adysgenesis cell lines. The proportion of cells with each intensity is shown. As can be seen, the majority show weak staining, with only a small proportion showing bright or very bright staining. This is a similar pattern than seen in the HeLa and M15 cell lines.

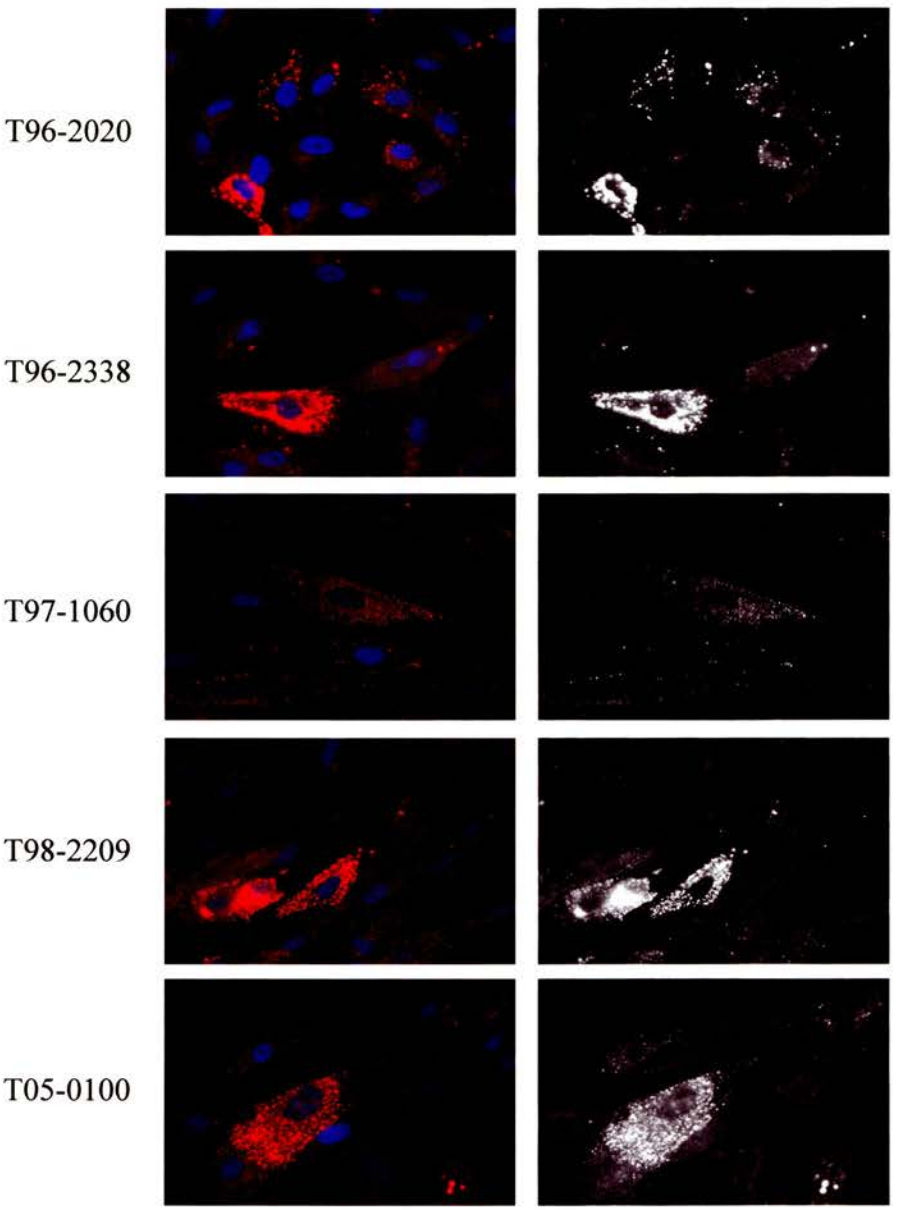

Figure 6.21. ESRRG antibody staining in five lethal renal adysgenesis cases.

Nuclei are counterstained with DAPI (blue) and ESRRG is detected with an Alexa-594 anti-rabbit antibody (red). All cell lines show a similar expression pattern that is comparable to that of the control cell lines, with the majority of cells showing a weak punctate staining pattern, and others showing bright or very bright staining. There is no evidence of any protein mis-localisation.

6.3.4.6. Punctate Esrrg staining on embryo sections

In order to confirm that the antibody staining on the paraffin embedded mouse embryo sections matched the of the cell lines with regards to subcellular localisation, high magnification images were taken of cells from different regions of the embryos. Punctate cytoplasmic staining was observed. The expression did alter between cell types but there was no evidence of nuclear staining observed.

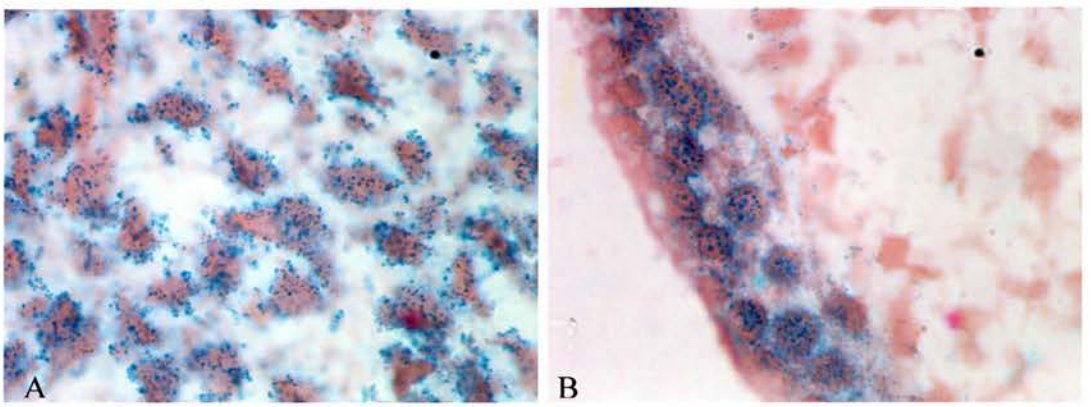

Figure 6.22. Esrrg in paraffin sections at high magnification

Esrrg antibody staining in 12.5 dpc mouse embryo sections at high magnification. Sections are counterstained with eosin (pink) and signal detected with NBT/BCIP (blue). Esrrg appears cytoplasmic and punctate, as in the cell lines, in A) mesenchymal cells from the head/face area and B) cells from the dermis.

6.3.5. Patient Cohort *ESRRG* Mutation Screening

6.3.5.1. Cell line FISH analysis

Chromosome preparations from five of the six (cells from T97-1759 were unavailable) lethal renal adysplasia fibroblast cell lines were screened for rearrangements by FISH, using BACs which cover the *ESRRG* gene and also the breakpoint flanking BACs from chromosome 2p, found in the t(1;2) case. All cell lines showed two copies of the BACs in apparently the correct positions on the chromosomes.

Chromosome preparations were unavailable for the familial cell lines.

6.3.5.2. Cell line *ESRRG* sequencing

Genomic DNA from all fibroblast cell lines and a normal fibroblast control were screened for mutations in the *ESRRG* gene by sequencing. Primers were designed with a minimum of 50 bp of intronic sequence before and after the exon to ensure that all of the coding region and the splice sites were included and to accommodate for any poor sequence at the beginning and end of each reaction. Sequence was obtained via Ensembl (NCBI 35 assembly, June 2004) and all coding exons were sequenced (exons 4 to 8 and part of exon 9). Introns and the untranslated regions (UTR) that make up exons 1-3 and the last part of exon 9 were not examined. No mutations were discovered although two different synonymous single nucleotide polymorphisms (SNPs) were found in some individuals (see table 6.6.).

All of the individuals carrying SNP rs11572766, an intronic SNP, were heterozygous for the nucleotide change. All other individuals had the most common

G/G genotype. All but one of the patients were heterozygous for the SNP in exon 8, rs945453, with only one individual having the ancestral C/C genotype, whilst the control cell line (GM5756) was T/T.

	Exon 4 (416 bp)	Exon 5 (117 bp)	Exon 6 (111 bp)	Exon 7 (162 bp)	Exon 8 (270 bp)	Exon 9 (245 bp without UTR)
T96-2020	Wild-type	Wild-type	Wild-type (G/G)	Wild-type	SNP rs945453 (C/T)	Wild-type
T96-2338	Wild-type	Wild-type	SNP rs11572766 (A/G)	Wild-type	SNP rs945453 (C/C)	Wild-type
T97-1060	Wild-type	Wild-type	SNP rs11572766 (A/G)	Wild-type	SNP rs945453 (C/T)	Wild-type
T97-1759	Wild-type	Wild-type	Wild-type (G/G)	Wild-type	SNP rs945453 (C/T)	Wild-type
T98-2209	Wild-type	Wild-type	SNP rs11572766 (A/G)	Wild-type	SNP rs945453 (C/T)	Wild-type
T05-0100	Wild-type	Wild-type	Wild-type (G/G)	Wild-type	SNP rs945453 (C/T)	Wild-type
CRAST	Wild-type	Wild-type	Wild-type (G/G)	Wild-type	SNP rs945453 (C/T)	Wild-type
EDPOR	Wild-type	Wild-type	SNP rs11572766 (A/G)	Wild-type	SNP rs945453 (C/T)	Wild-type
REWKI	Wild-type	Wild-type	Wild-type (G/G)	Wild-type	SNP rs945453 (C/T)	Wild-type
RUFUL	Wild-type	Wild-type	SNP rs11572766 (A/G)	Wild-type	SNP rs945453 (C/T)	Wild-type
GM5756 (control)	Wild-type	Wild-type	Wild-type (G/G)	Wild-type	Wild-type (T/T)	Wild-type

Table 6.6. Cell line *ESRRG* sequencing results

A table showing the results obtained from *ESRRG* sequencing of lethal renal adysgenesis cell lines, familial renal adysgenesis cell lines and a phenotypically and karyotypically normal control cell line (GM5756). The top row shows the exons and their sizes. Two different synonymous SNPs were found in exons 6 and 8 in a number of individuals (one intronic and one coding respectively). The nucleotides seen at these positions are noted in the table. As can be seen, all but one of the SNP carriers are heterozygous. Case T96-2338 is homozygous for the SNP in exon 8 (rs945453). No other nucleotide changes were observed.

SNP rs11572766:

T96-2020:

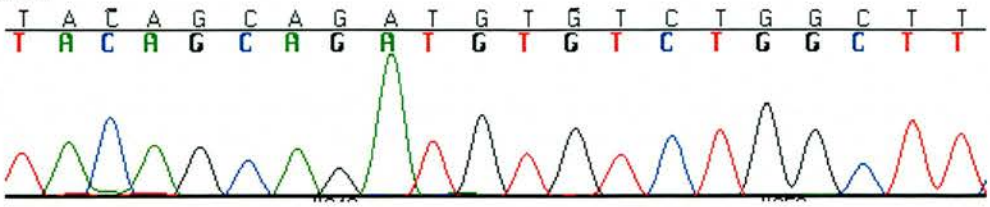

T96-2338:

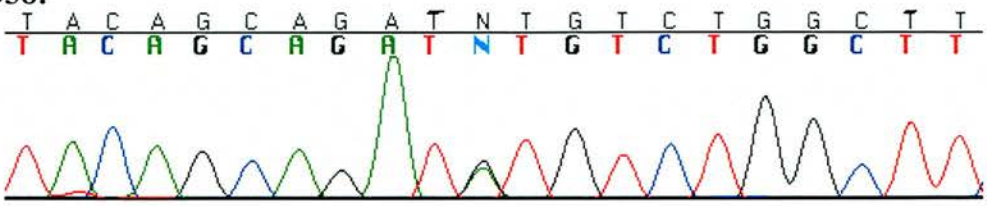

T97-1060:

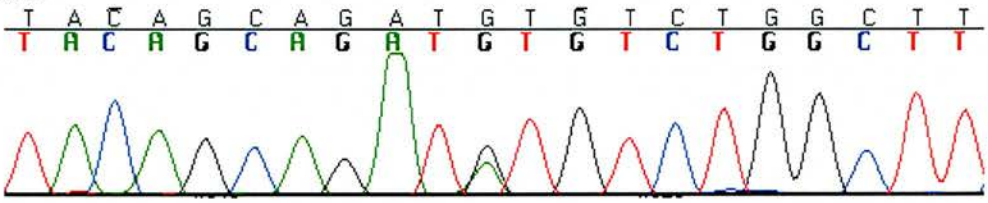

T97-1759:

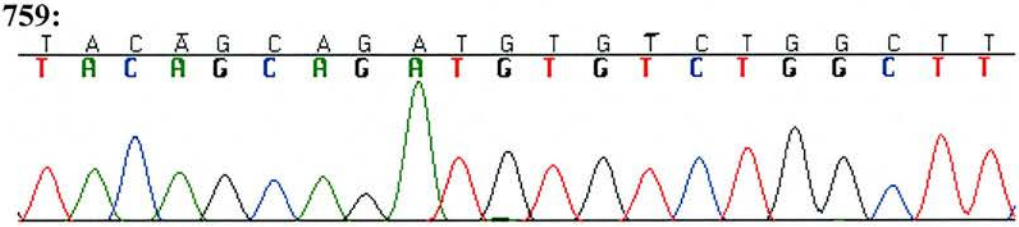

T98-2209:

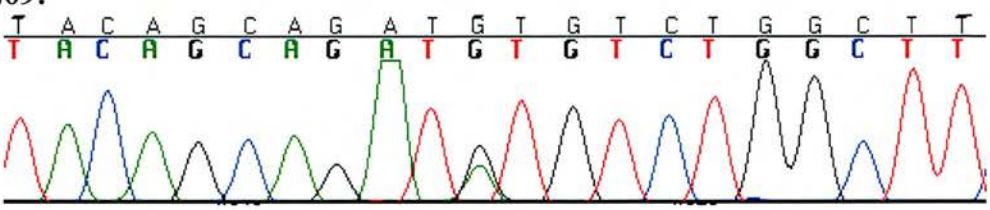

T05-0100:

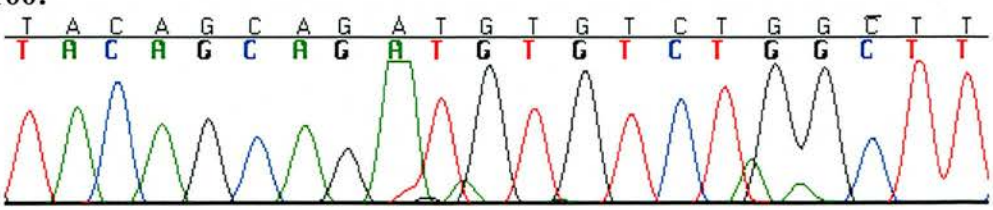

CRAST:

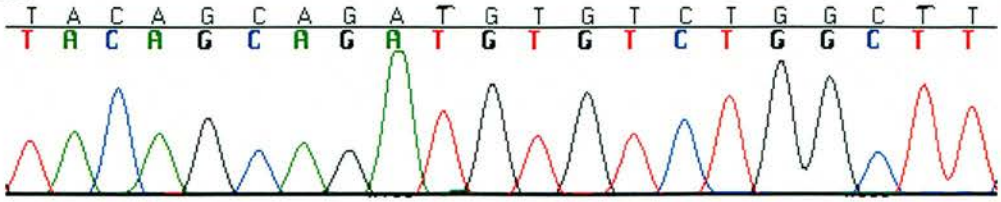

EDPOR:

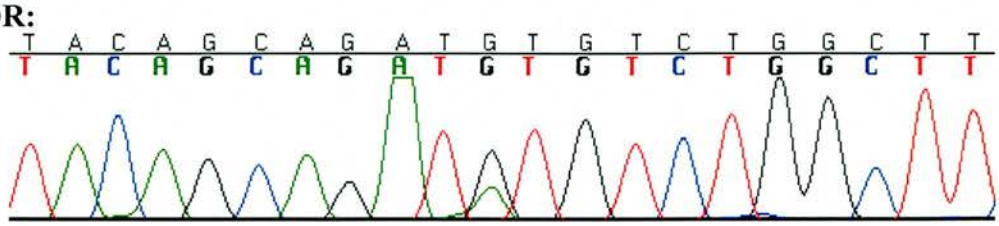

REWKI:

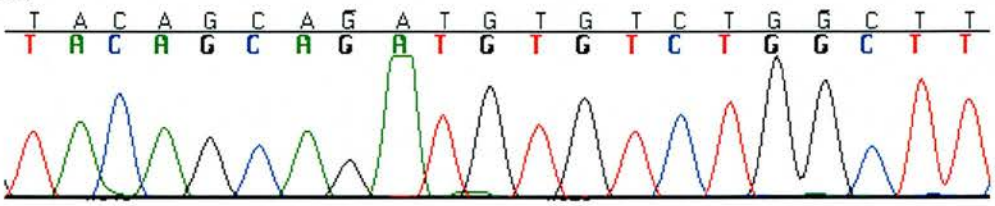

RUFUL:

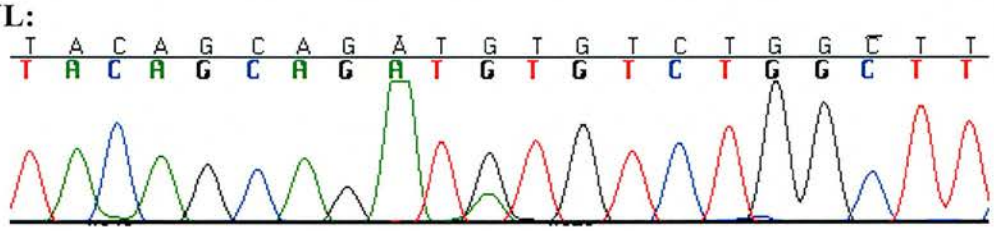

GM5756 (control):

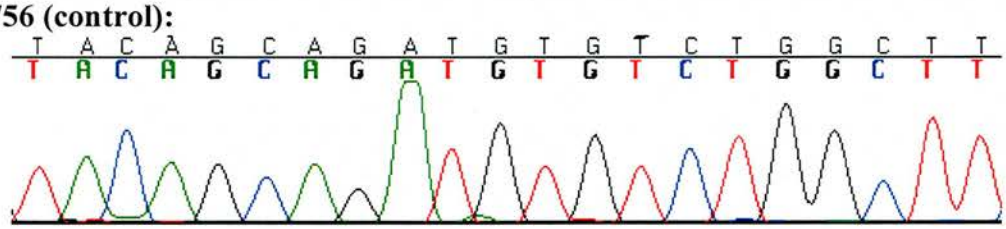

Figure 6.23. Chromatograms of SNP rs11572766

Chromatograms showing the sequence data in the region of SNP rs11572766 in all 10 renal adysplasia cell lines and one control. The SNP (in the centre of the sequence) can be seen to be heterozygous (A/G) in five of the cell lines and wild-type (G/G) in the remaining five and in the control.

SNP rs945453:

T96-2020:

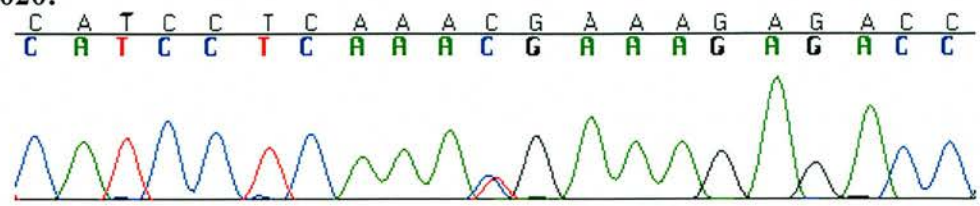

T96-2338:

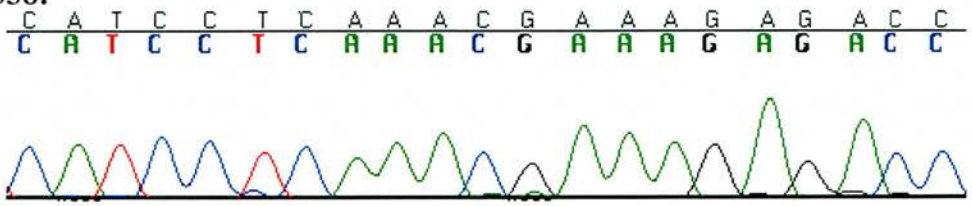

T97-1060:

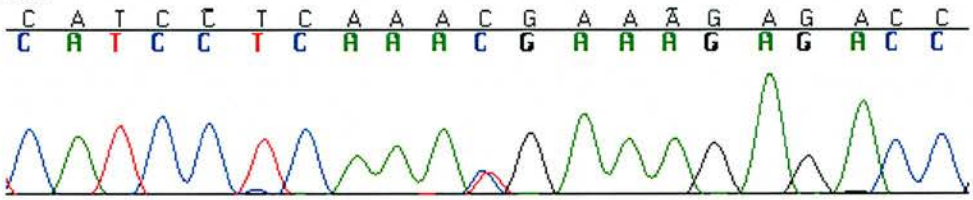

T97-1759:

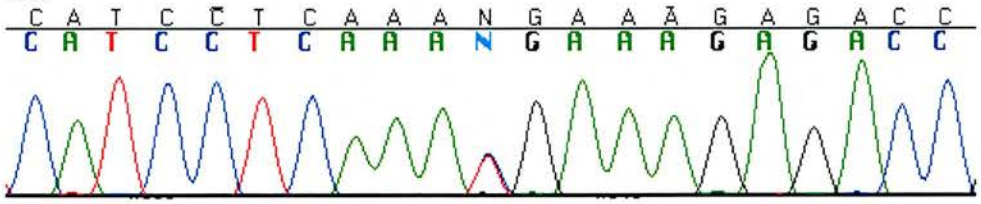

T98-2209:

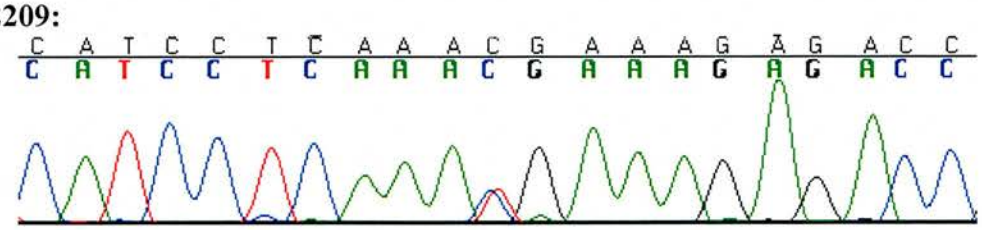

T05-0100:

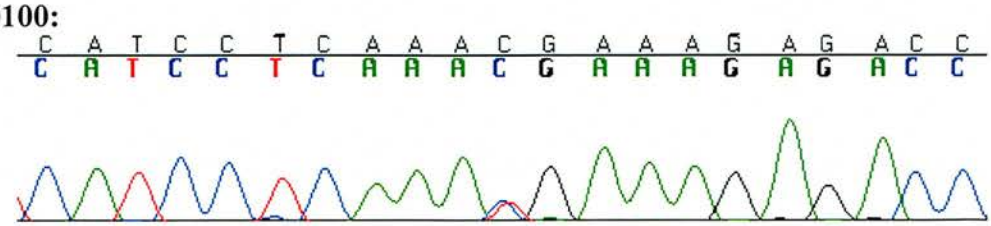

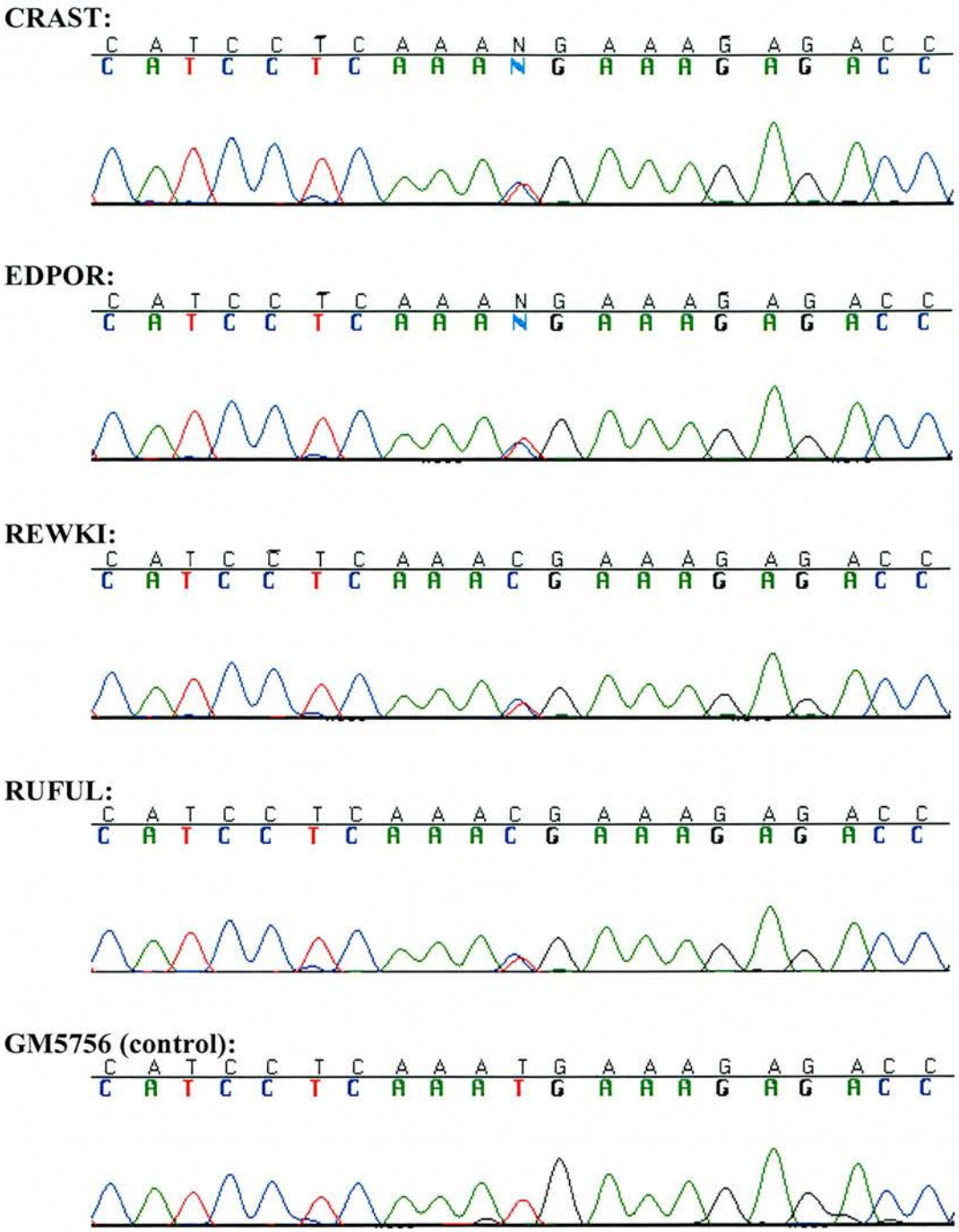

Figure 6.24. Chromatograms of SNP rs945453

Chromatograms showing the sequence data in the region of SNP rs945453 in all 10 renal adysplasia cell lines and one control. The SNP (in the centre of the sequence) can be seen to be heterozygous (C/T) in nine of the cell lines, homozygous (C/C) in one and wild-type (T/T) in the control.

6.3.5.3. dHPLC screening of *ESRRG*

Denaturing high performance liquid chromatography (dHPLC) was performed by Dr Kathy Williamson (MRC Human Genetics Unit) on DNA from all 10 renal adysplasia cell lines The SNPs found via sequencing were confirmed and no further nucleotide changes were found in *ESRRG* (data not shown).

6.3.5.4. Tissue section *ESRRG* sequencing

DNA was extracted from the tissue sections with the intention of sequencing the *ESRRG* gene. However, the DNA appeared degraded and the PCR products required for sequencing would not amplify.

6.4. Discussion

6.4.1. The Chromosome 2 Breakpoint Lies Within a Gap in the Contig

The translocation breakpoint on chromosome 2 appears to lie within a gap in the contig in a relatively gene poor area. There is a small cluster of genes to one side of the breakpoint but none appear to be directly interrupted and, on the basis of their functional annotation, none were considered to be good candidates for the kidney phenotype. A list of these genes is available in table 6.7.

Gene	Conservation (nucleotide)	Description/ Function	Protein type/ family
RNASEH1	Rat - 82 % Mouse - 81 % Xenopus - 76 %	Endonuclease that degrades RNA of RNA-DNA hybrids specifically	RNaseH family
RPS7	Mouse – 90 % Rat – 88 % Xenopus – 83 %	Encodes ribosomal protein that is a component of the 40s subunit	S7E family of ribosomal proteins
COLEC11	Mouse – 84 % Rat – 83 % Xenopus – 75 %	Phosphate transport Sugar binding	Collagen superfamily
TMSL2	Unknown	May be involved in cytoskeletal organisation and biogenesis	Unknown
ALLC	Rat – 82 % Mouse – 81 % Xenopus – 74 %	Not thought to be active in mammals. Part of uricolytic pathway enzyme in fish and amphibians	Allantoicase

Table 6.7. A summary of the genes around the chromosome 2 breakpoint

A table summarising the genes around the chromosome 2p breakpoint and the proteins they encode.

6.4.2. The Chromosome 1 Breakpoint Directly Interrupts the *USH2A* Gene

The breakpoint on chromosome 1 lies in band 1q41 and falls between BACs RP4-723P6 and RP11-239I22 and therefore directly interrupts the *USH2A* gene. *USH2A* is the gene responsible for Usher syndrome type 2A (OMIM 276901), an autosomal recessive disorder characterised by adolescent onset retinitis pigmentosa and moderate to severe congenital deafness.

USH2A was not considered to be a good candidate gene for the bilateral renal adysplasia phenotype on the basis of mutations causing a known Mendelian disorder, Usher syndrome type 2A, and the previous finding that Ush2a is not expressed in the mouse or human kidney [522;523], although expression in the adult kidney was seen via RT-PCR. The most convincing evidence against the gene comes from a knockout mouse that has recently been created. This results in fully viable mice that have progressive blindness but no other detectable abnormalities by two years of age (Dr. Dominic Cosgrave, Personal communication). It is possible there could be yet unknown *USH2A* isoform-specific effects or alternative promoters that may be vital for renal development in spite of the apparently contradictory null phenotype. However, there is no evidence for this in mice or humans and it was decided to concentrate on *ESRRG*, given the expression data. The entire *USH2A* gene will be sequenced in the future.

6.4.3. *ESRRG* Lies close to the Chromosome 1 Breakpoint

The only other gene in the region of the chromosome 1 breakpoint is the orphan nuclear steroid hormone receptor, estrogen-related receptor gamma (*ESRRG*). The 1.5 Mb region only contains these two functional genes and is conserved down to *fugu* (*Takifugu rubripes*).

Gene	Conservation (nucleotide)	Description/ Function	Protein type/ family
USH2A	Rat – 79 % Mouse – 79 %	May be important in homeostasis of inner ear and retina. Mutations in *USH2A* cause Usher syndrome type 2A	Unknown
ESRRG	Rat – 91 % Mouse – 92 %	Orphan receptor. Binds to estrogen response elements and regulates reporter genes controlled by them	Nuclear hormone receptor family

Table 6.8. A summary of the genes around the chromosome 1 breakpoint

A table summarising the genes around the chromosome 1q breakpoint and the proteins they encode.

6.4.3.1. *ESRRG* encodes an orphan nuclear receptor

ESRRG, also known as *ERRγ* or *ERR3*, was molecularly cloned on the basis of sequence similarity to other nuclear receptors and was found to be expressed in a number of adult and foetal tissues, including heart, kidney, brain and skeletal muscle [524]. *ESRRG* encodes a nuclear receptor for which no endogenous ligand is known (an orphan receptor), although there is evidence to show that the transcriptional

activity of the receptor does not require ligand binding [525]. ESRRG binds, via the DNA binding domain, to estrogen response elements (EREs) and estrogen related receptor response elements (ERREs) and regulates the expression of genes driven by these [526].

6.4.3.2. Esrrg is expressed throughout mouse embryonic kidney development

Esrrg is expressed through the embryonic development of the mouse kidney. This expression begins in the metanephric mesenchyme or stroma that surrounds the invading ureteric bud and that which will go on to form the capsule of the kidney. The expression is dynamic and becomes more collecting duct specific as development continues, with expression in the capsule appearing to diminish by 17.5 dpc. As the kidney matures, the expression appears to be stronger in and around the more mature collecting ducts, located in the kidney pelvis. The collecting ducts in this region are surrounded by stroma, whereas younger ducts located towards the outer cortex are not. Expression is also seen in the ureter.

Ideally, co-localisation studies with positive control antibodies for the relevant tissues would have been performed in order to confirm the localisation of the Esrrg signal. However, due to time constraints, these were not possible.

No expression was observed in antibody stained adult kidney sections although strong expression was seen in the adult tissue via RT-PCR. As expression appears to be restricted to the kidney pelvis in the neonate kidneys, it is possible that

all expression sites in the adult tissue were excluded in the tissue sections examined. The staining experiment was not repeated due to time constraints.

6.4.3.3. ESRRG may play a role in branching or ductogenesis

The expression of Esrrg in the ureteric bud and, subsequently, the collecting ducts and the stroma suggests that ESRRG may play a role in branching of the bud or in the maturation of the collecting ducts. This hypothesis is strengthened by the expression of Esrrg in the liver and the lung (figure 6.7), which employ branching mechanisms similar to that of the kidney. Expression was also seen in the stomach and the skin, both of which contain branched exocrine glands, namely the acid producing gastric glands and the sebaceous and sweat glands of the skin. For normal branching to occur in the kidney, the ureteric bud requires interactions with both the metanephric mesenchyme and the stroma. It is thought that the stroma situated around the collecting ducts, the medullary stroma, releases growth, differentiation and transcription factors such as Foxd1 (or BF-2) [527] and Fibroblast growth factor 7 (FGF-7 or KGF) [528], required for proper branching morphogenesis. The presence of Esrrg in the stroma and the ducts themselves suggests that it may also be involved in this process.

6.4.3.4. Mutation screening did not reveal any *ESRRG* mutations

Comprehensive mutation screening in six lethal and four familial dominant renal adysplasia cases did not reveal any mutations in the *ESRRG* coding region.

Two synonymous SNPs, one intronic and one coding, were found in the patients screened for *ESRRG* mutations. SNP rs11572766 is intronic and approximately 24 % of the population are thought to be heterozygous, with 75 % having the G/G genotype and 1 % having A/A. SNP rs 945453 is located within exon 8 of *ESRRG* and approximately 42 % of individuals are heterozygous, with 40 % having the T/T phenotype and 18 % having C/C, although these figures vary greatly between populations. Within European populations tested, the proportion of C/C can be as high as 37 % with C/T being around 58 %. The ancestral allele at this location is C (all SNP information from NCBI dbSNP, build 125, 2005, http://www.ncbi.nlm.nih.gov/SNP).

All of the individuals carrying SNP rs11572766, the intronic SNP, were heterozygous for the nucleotide change. All other individuals had the most common G/G genotype. All but one of the patients were heterozygous for the SNP in exon 8, rs945453, with only one individual having the ancestral C/C genotype, whilst the control cell line (GM5756) was T/T. There does appear to be an over-representation of heterozygous individuals for both SNPs, but especially the coding SNP in exon 8. However, as only one control cell line was sequenced, no conclusions can be drawn from this.

Although these SNPs do not result in an amino acid change, it cannot be confirmed that they have no effect as synonymous SNPs have been shown to affect mRNA stability and folding [529;530] and could also have an effect on splicing. The possible role of these SNPs in the phenotype is not investigated further here.

The lack of any mutations in the patients screened is perhaps not surprising due to the small number of cases sampled. It is hoped that screening of further cases

will result in mutations being discovered and this will be done as soon as cases become available. The nucleotides present at the SNP positions will also be noted in these cases and further normal cases will be sequenced to determine whether the over-representation of heterozygotes in the affected individuals is a real finding.

6.4.3.5. ESRRG appears to be peroxisome specific

Antibody staining using anti-ESRRG and anti-catalase (a peroxisomal protein) in fibroblasts produced co-localising signals, suggesting that ESRRG is located in, or on the membrane of, the peroxisomes. Peroxisomes are involved in lipid metabolism and hydrogen peroxide detoxification but also play a role in development [531]. Signaling lipids released by the peroxisomes bind and activate nuclear receptors such as retinoic acid receptors and peroxisome proliferator-activated receptors (PPARs) [532], both of which are nuclear hormone receptors, as is ESRRG. It is therefore entirely plausible that the endogenous ligand of ESRRG is a product of peroxisomal metabolism and that the location of the protein on, or in, the peroxisomes, reflects this.

The association of ESRRG with the peroxisomes is also interesting as patients with Zellweger syndrome (OMIM 214100), a peroxisome biogenesis disorder, have renal cysts, suggesting that disruption of *ESRRG* may also play a role in cyst formation. Due to time constraints, further investigations into this could not be performed but experiments to determine whether *ESRRG* has a role in renal cyst formation, by knocking down the RNA in cultured mouse kidneys, are in the process of development (Prof. Nicholas Hastie's group, MRC Human Genetics Unit).

6.4.3.6. Creation of an *ESRRG* mutant mouse model

In order to help elucidate the role of *ESRRG* in kidney development, a mutant mouse model is currently in the process of being created (Prof. Nicholas Hastie's group, MRC Human Genetics Unit). This should allow determination of the role and expression of ESRRG throughout development and help determine whether disruption of the gene would be sufficient to cause the severe kidney phenotype seen in the translocation case.

6.4.3.7. *ESRRG* is a good candidate for the bilateral renal adysplasia phenotype

The location of the *ESRRG* gene in relation to the translocation breakpoint and the expression pattern in the developing mouse kidney make *ESRRG* a very good candidate for the bilateral renal adysplasia phenotype seen in the translocation case. The presence of haemorrhagic masses and undifferentiated mesenchyme in place of kidneys suggests that the causative event occurred very early in kidney development. *ESRRG* is expressed in the metanephric mesenchyme or stroma and the ureteric bud and disruption of this expression, and therefore any subsequent pathways, could be supposed to be the cause of the severe kidney phenotype. The mutant mouse model and further mutation screening should help to elucidate this and screening of further bilateral renal adysgenesis cases will hopefully reveal causative mutations.

7: Conclusions

7.1. DBCRs are an Important Tool in the Identification of Disease Genes

Disease-associated balanced chromosomal rearrangements, predominantly inversions or translocations, have proved to be very important in disease gene and loci identification and are continuing to prove their worth. They have been instrumental in the identification of causative genes for many disorders, predominantly those with dominant or X-linked inheritance but also, more recently, for an autosomal recessive disorder.

The process of mapping DBCRs with the aim of identifying disease genes or loci does, however, have its disadvantages. The hypothesis that the rearrangement directly interrupts a dosage sensitive gene, thereby causing the phenotype, does not always prove correct. The breakpoint may occur some distance from the causative gene, causing a position effect, or may interrupt one gene yet have an effect on another, thereby implicating the wrong gene in the disorder. The rearrangement may also have no discernable effect, with the individual having a causative mutation in another gene or genes, totally unrelated to the DBCR.

In spite of these disadvantages, the presence of a DBCR in combination with a phenotype can provide vital clues to disease loci and the potential to identify the causative gene or genes. The presence of more than one DBCR with the same phenotype and one or more similar breakpoints, increases the chances of the DBCR being a causative, rather than a coincidental, event. This is also true for DBCRs in

which there is other evidence, such as linkage studies or deletion map data, that implicate one of the rearrangement breakpoints.

The mapping of DBCRs remains, therefore, an effective method for the identification of disease loci and phenotype causing genes, especially when used in combination with other evidence sources and DBCRs should continue to benefit human genetic research.

7.2. The DBCR Database - an Invaluable Tool for the Study of DBCRs

A major disadvantage to anyone wishing to study DBCRs is the fact that only a small number of DBCRs are actually reported in the literature. Only those that are considered to be interesting cases are published, meaning that many cases are inaccessible in individual laboratory archives. Even those that have been published can be difficult to identify, involving numerous, time consuming searches. Databases, such as the Mendelian Cytogenetics Network database (MDNdb, http://www.mcndb.org/), have attempted to increase the ascertainment of cases. However, at the time of initiating the DBCR database, the MCNdb had been offline for some time with no indication of becoming re-accessible.

Therefore, to help redress the problem, a DBCR database was created. This easily accessible, regularly updated, central resource allows easy searching for similar cases, for example in phenotype or chromosomal abnormality. The data contained covers the phenotype, the rearrangement and each breakpoint individually

and in detail. Each case is also hyperlinked to the original data and to OMIM, where applicable, so that references and phenotypic data can be easily obtained.

The database contains a large number of cases (919 at the time of writing) and is continually being updated as new cases are identified. It is currently in the process of being converted to a web-based format to allow open access to the data and should shortly be available through the research pages of Dr. David FitzPatrick, via the MRC Human Genetics Unit website (http://www.hgu.mrc.ac.uk/Research/Fitzpatrick). Although the initial compilation of the database was time consuming, the maintenance, involving the identification of new cases and their subsequent entry, is quick and simple. Automatic literature searches have been set up through the PubCrawler web service (http://pubcrawler.gen.tcd.ie/about.html) and there are generally only a few new DBCR cases appearing in the literature each week. The maintenance of the database is being jointly undertaken by Louise Harewood and Dr. David FitzPatrick (MRC Human Genetics Unit).

The DBCR database should prove to be an essential tool for anybody wishing to identify or study DBCRs and will become more so as it continues to expand and be updated.

7.3. FISH on Nuclei from Paraffin Embedded Tissue allows the Study of Previously Impossible Cases

Ascertainment of an individual DBCR case does not necessarily mean that it will be available for study. Many cases, especially those more than a few years old, do not have viable cell-lines available, fixed cell suspensions are often only kept for a short time, especially in diagnostic labs, and cell lines are not always viable after recovery from liquid nitrogen or deep freezing. This leads to a subset of potentially interesting cases being unavailable for study. This thesis presents a technique that will enable the mapping of rearrangement breakpoints in cases with only archival paraffin embedded patient material available.

The adaptation of an existing fluorescent *in-situ* hybridisation (FISH) protocol allowed the mapping of these cases to a similar resolution to that on fixed cell suspensions. This adaptation involved the addition of only a few steps, which do not add considerably to the overall protocol time, allowing cases to be studied in a similar timescale to those on other materials. Although some optimisation is required for each sample, the protocol has proved to be robust on many ages of tissue, from a few years old to over 15 years old, and on many different tissue types. The protocol has since been given, or taught, to scientists from other laboratories and has proved to be successful for numerous different types of home-grown and commercial FISH probes, from chromosome specific paints, to BACs, to probes derived from 10 kb PCR products.

The method of FISH on nuclei dissociated from archival paraffin embedded tissue sections provides the ability to study a much larger number of DBCR cases

than previously possible and should result in the identification of many more disease genes or loci. It has already been utilised, in this thesis, to map the breakpoints in two translocation cases and has resulted in the identification of good candidate genes for each phenotype.

7.4. The Study of Two DBCR Cases Identifies Good Candidate Genes for each Phenotype

The cases studied using the adapted FISH method had very different phenotypes, namely upper limb peromelia and lower limb phocomelia with a t(2;12)(p25.1;q24.1) and bilateral renal adysplasia with a t(1;2)(q41;p25.3). Both cases had supporting evidence for one of the breakpoints with genes involved in limb development being located at 12q24 and a locus for kidney development being found on 1q via the human deletion map. However, the cases could not be mapped past the original Giemsa-banded cytogenetic level due to the fact that neither had fixed cell suspensions or viable material available. FISH on nuclei dissociated from paraffin embedded tissue sections allowed the previously impossible mapping of the breakpoints in these cases.

One of the breakpoints in the renal adysplasia case was found to directly disrupt a large gene, *USH2A*, mutations in which have been shown to cause Usher syndrome type 2A, a disorder characterised by retinal degradation and hearing loss and not associated with kidney abnormalities. Although this gene was directly interrupted, it was not thought to be a good candidate for the kidney phenotype on the basis of mutations causing a known Mendelian disorder and from a mouse

knockout model, which had apparently normal kidneys. Although it cannot be totally excluded, it does not seem a likely candidate.

Similarly, in the limb abnormality case, the chromosome 2 breakpoint may possibly interrupt the *ROCK2* gene. A mouse with a homozygous targeted disruption of this gene showed only very minor toe abnormalities and not the dramatic limb abnormalities that we would expect if disruption of *ROCK2* was responsible for the phenotype in the peromelia/phocomelia case. Again, this gene could not be totally excluded but seemed an unlikely candidate.

Although all of the genes in the region of the translocation breakpoints have to be considered as candidates due to their location, analysis of their functional annotation can allow the formation of a hierarchy of candidacy.

The genes identified as the most likely candidates for the two phenotypes were located in the region of the translocation breakpoints and although one (*CMKLR1*) may have been disrupted, the other, *ESRRG*, definitely was not. These genes were considered to be good candidates on their position, their functional annotation and the expression of the RNA and protein in, amongst others, the relevant locations: namely Esrrg expression in the developing kidneys and Cmklr1 expression in the limb buds.

However, mutation screening of a small number of phenotypically similar individuals failed to reveal any mutations in these genes and due to the nature of the material available in the proband cases, expression analysis was not possible. It is hoped that further mutation screening and the production of mouse models will provide some insight as to whether disruption of these genes are in fact responsible for the phenotypes observed.

At the very least, the identification of *CMKLR1* and *ESRRG* as candidate genes for peromelia/phocomelia and bilateral renal adysplasia (respectively) and the subsequent expression analysis has led to the study of new developmental pathways involved in both limb and kidney development. Further studies into the developmental roles of these genes has the potential to confirm or redefine the processes involved in the formation of these organs.

7.5. The Study of Two DBCRs has Initiated the Study of New Developmental Pathways

FISH on nuclei dissociated from paraffin embedded tissue sections has allowed the study of two previously impossible cases and identified two good candidate genes for very different phenotypes. The identification of these genes has opened up the study of new, previously unexplored developmental pathways and provided new insights into both limb and kidney development.

Of particular interest is the role of *CMKLR1* in limb development and the potential requirement of the muscle precursor cells in the development of not only the muscle, but also the bones and digits of the limb. The identification of *CMKLR1* as a candidate gene for phocomelia/peromelia has implicated this subset of cells, and the associated signalling events, in the outgrowth and patterning of the developing limb. Should this theory prove correct, this represents the identification of a novel mechanism for limb formation.

Although the role of *CMKLR1* in limb development may be of interest to developmental biologists, the identification of a candidate gene for the

phocomelia/peromelia phenotype is perhaps not as important as the identification of one for bilateral renal adysplasia. The limb phenotype seen in the test case is extremely rare and not necessarily fatal, whereas bilateral renal adysplasia is much more common, whether as a sole abnormality or as a part of a syndrome, and is always lethal. The identification of the causative gene and investigation into the processes and mechanisms in which it is involved, may also help to identify other genes involved in these mechanisms, which are mutated in similar phenotypes. Ultimately, the understanding of the disorder could potentially result in a treatment, or prevention, being found.

Therefore, although the postulation of *CMKLR1* and *ESRRG* as candidate genes for the two phenotypes studied in this thesis are of interest in the development field, they could also have much more of an impact in human genetics if they do prove to be the causative genes.

Studies to further understand the role of these genes in development and to attempt to prove their causality on the phenotypes are currently underway, or are planned for the near future. Some of the ongoing/future work is outlined below.

7.5.1. Mouse Models are Under Construction

Mice that are deficient for the candidate genes identified via DBCR mapping are currently under development. Although animal models do not always accurately represent the situation seen in humans, the phenotypes caused by the disruption of one copy of the gene in these cases are so severe that some effect is almost certain to be seen in any mouse model created, assuming that they are viable to an appropriate stage. The disadvantage of mouse models is that they are very time consuming and

laborious to produce and there is always the chance that the loss of the gene will prove to be lethal at an early embryonic, or post-implantation, stage, or that the heterozygous mice will be infertile and will not show a phenotype.

However, if successful, the mouse models should answer a large number of questions about the roles of these genes in development and elucidate whether the disruption of one copy of the gene is sufficient to cause the phenotypes seen in the translocation cases.

7.5.2. RNAi on Cultured Tissue

Another method that can be used to determine the effect of gene disruption is to knock down the RNA, and therefore protein levels in cultures of the relevant tissue. Kidneys or torsos, complete with limb buds, can be dissected from mouse embryos and cultured with the appropriate RNAi constructs. By comparing these cultures with controls, the effect on growth and differentiation of the tissue should be apparent. RNAi against Esrrg in kidney cultures would hopefully result in a lack of differentiation of the metanephric mesenchyme and an absence of ureteric bud branching. Renal cysts may also be apparent in later kidneys, as in patients with Zellweger syndrome. RNAi against Cmklr11 in limb bud cultures would be hoped to result in significantly shorter limbs due to errors in limb bud outgrowth, possibly due to disruption of the AER. Patterning of the limb may also be affected.

RNAi does, however, have disadvantages. Dissected tissues can prove difficult to culture or may differentiate differently than they would *in vivo*. The tissue can also prove difficult to penetrate, meaning that only the exterior structures of the organ are affected, which can be problematic if there is expression in interior regions.

This method could be potentially very interesting and quick but may require a considerable amount of optimisation.

7.5.3. Embryonic Stem Cell Studies

The creation of mice deficient for candidate genes can be very time consuming and many problems can be encountered along the way. After the deletion construct is made, it is injected into embryonic stem (ES) cells, which are subsequently used to generate the mice. These ES cells can also be used to determine the effect of the loss of the candidate gene by examining their differentiation properties. As ES cells are pluripotent, they can differentiate into any cell type, including kidney and muscle cells, on stimulation by the relevant signal. By attempting to differentiate the *Esrrg* deficient cells along kidney associated lineages and the *Cmklr1* deficient cells down limb associated lineages, the effect of the loss of the gene should become apparent. Ideally, differentiation into the relevant cell types will be impaired, proving the role of the gene in that pathway.

This method could provide quick, easy answers about the developmental role of the two candidate genes and provide a good indication of their function in different cell lineages.

7.5.4. Further Mutation Screening

Although good candidate genes have been identified for each phenotype studied, these genes cannot be unambiguously proven to cause the phenotypes in the study cases, as expression studies cannot be performed on the material available.

Although animal models may shed some light on the developmental role of these genes and the effect of their disruption, the most compelling evidence will come from the identification of mutations in phenotypically similar individuals. This will be problematic in the case of *CMKLR1* as the phocomelia/peromelia phenotype is extremely rare and no further samples may become available. Bilateral renal adysplasia on the other hand is relatively common and it is hoped that further samples will soon become available for mutation screening.

8: References

[1] Rasmussen SA, Wong LY, Yang Q, May KM, Friedman JM. Population-based analyses of mortality in trisomy 13 and trisomy 18. Pediatrics 2003; 111(4 Pt 1):777-784.

[2] Nagaishi M, Yamamoto T, Iinuma K, Shimomura K, Berend SA, Knops J. Chromosome abnormalities identified in 347 spontaneous abortions collected in Japan. J Obstet Gynaecol Res 2004; 30(3):237-241.

[3] Robinson W. Trisomy accounted for 41% of miscarriages: chromosomal abnormalities linked to age seen in most miscarriages. Ob/Gyn News . 1-9-2004.
Ref Type: Abstract

[4] Kuzminov A. Single-strand interruptions in replicating chromosomes cause double-strand breaks. Proc Natl Acad Sci U S A 2001; 98(15):8241-8246.

[5] Vilenchik MM, Knudson AG. Endogenous DNA double-strand breaks: production, fidelity of repair, and induction of cancer. Proc Natl Acad Sci U S A 2003; 100(22):12871-12876.

[6] van Gent DC, Hoeijmakers JH, Kanaar R. Chromosomal stability and the DNA double-stranded break connection. Nat Rev Genet 2001; 2(3):196-206.

[7] Davis L, Smith GR. Meiotic recombination and chromosome segregation in Schizosaccharomyces pombe. Proc Natl Acad Sci U S A 2001; 98(15):8395-8402.

[8] Davis L, Smith GR. Meiotic recombination and chromosome segregation in Schizosaccharomyces pombe. Proc Natl Acad Sci U S A 2001; 98(15):8395-8402.

[9] Davis L, Smith GR. Meiotic recombination and chromosome segregation in Schizosaccharomyces pombe. Proc Natl Acad Sci U S A 2001; 98(15):8395-8402.

[10] Richardson C, Horikoshi N, Pandita TK. The role of the DNA double-strand break response network in meiosis. DNA Repair (Amst) 2004; 3(8-9):1149-1164.

[11] Valencia M, Bentele M, Vaze MB, Herrmann G, Kraus E, Lee SE, Schar P, Haber JE. NEJ1 controls non-homologous end joining in Saccharomyces cerevisiae. Nature 2001; 414(6864):666-669.

[12] Schwacha A, Kleckner N. Interhomolog bias during meiotic recombination: meiotic functions promote a highly differentiated interhomolog-only pathway. Cell 1997; 90(6):1123-1135.

[13] Haber JE. Partners and pathwaysrepairing a double-strand break. Trends Genet 2000; 16(6):259-264.

[14] Richardson C, Jasin M. Frequent chromosomal translocations induced by DNA double-strand breaks. Nature 2000; 405(6787):697-700.

[15] Lewis LK, Resnick MA. Tying up loose ends: nonhomologous end-joining in Saccharomyces cerevisiae. Mutat Res 2000; 451(1-2):71-89.

[16] Lewis LK, Resnick MA. Tying up loose ends: nonhomologous end-joining in Saccharomyces cerevisiae. Mutat Res 2000; 451(1-2):71-89.

[17] Shaikh TH, Kurahashi H, Saitta SC, O'Hare AM, Hu P, Roe BA, Driscoll DA, McDonald-McGinn DM, Zackai EH, Budarf ML, Emanuel BS. Chromosome 22-specific low copy repeats and the 22q11.2 deletion syndrome: genomic organization and deletion endpoint analysis. Hum Mol Genet 2000; 9(4):489-501.

[18] Zackai EH, Emanuel BS. Site-specific reciprocal translocation, t(11;22) (q23;q11), in several unrelated families with 3:1 meiotic disjunction. Am J Med Genet 1980; 7(4):507-521.

[19] Kurahashi H, Shaikh TH, Hu P, Roe BA, Emanuel BS, Budarf ML. Regions of genomic instability on 22q11 and 11q23 as the etiology for the recurrent constitutional t(11;22). Hum Mol Genet 2000; 9(11):1665-1670.

[20] Kurahashi H, Shaikh TH, Zackai EH, Celle L, Driscoll DA, Budarf ML, Emanuel BS. Tightly clustered 11q23 and 22q11 breakpoints permit PCR-based detection of the recurrent constitutional t(11;22). Am J Hum Genet 2000; 67(3):763-768.

[21] Kurahashi H, Inagaki H, Yamada K, Ohye T, Taniguchi M, Emanuel BS, Toda T. Cruciform DNA structure underlies the etiology for palindrome-mediated human chromosomal translocations. J Biol Chem 2004; 279(34):35377-35383.

[22] Kurahashi H, Emanuel BS. Long AT-rich palindromes and the constitutional t(11;22) breakpoint. Hum Mol Genet 2001; 10(23):2605-2617.

[23] Yu X, Gabriel A. Reciprocal translocations in Saccharomyces cerevisiae formed by nonhomologous end joining. Genetics 2004; 166(2):741-751.

[24] Gotter AL, Shaikh TH, Budarf ML, Rhodes CH, Emanuel BS. A palindrome-mediated mechanism distinguishes translocations involving LCR-B of chromosome 22q11.2. Hum Mol Genet 2004; 13(1):103-115.

[25] Nimmakayalu MA, Gotter AL, Shaikh TH, Emanuel BS. A novel sequence-based approach to localize translocation breakpoints identifies the molecular basis of a t(4;22). Hum Mol Genet 2003; 12(21):2817-2825.

[26] Gotter AL, Shaikh TH, Budarf ML, Rhodes CH, Emanuel BS. A palindrome-mediated mechanism distinguishes translocations involving LCR-B of chromosome 22q11.2. Hum Mol Genet 2004; 13(1):103-115.

[27] Dunham I, Shimizu N, Roe BA, Chissoe S, Hunt AR, Collins JE, Bruskiewich R, Beare DM, Clamp M, Smink LJ, Ainscough R, Almeida JP, Babbage A, Bagguley C, Bailey J, Barlow K, Bates KN, Beasley O, Bird CP, Blakey S, Bridgeman AM, Buck D, Burgess J, Burrill WD, O'Brien KP, . The DNA sequence of human chromosome 22. Nature 1999; 402(6761):489-495.

[28] Shaikh TH, Kurahashi H, Saitta SC, O'Hare AM, Hu P, Roe BA, Driscoll DA, McDonald-McGinn DM, Zackai EH, Budarf ML, Emanuel BS. Chromosome 22-specific low copy repeats and the 22q11.2 deletion syndrome: genomic organization and deletion endpoint analysis. Hum Mol Genet 2000; 9(4):489-501.

[29] Bailey JA, Yavor AM, Massa HF, Trask BJ, Eichler EE. Segmental duplications: organization and impact within the current human genome project assembly. Genome Res 2001; 11(6):1005-1017.

[30] Stankiewicz P, Lupski JR. Genome architecture, rearrangements and genomic disorders. Trends Genet 2002; 18(2):74-82.

[31] Stankiewicz P, Lupski JR. Molecular-evolutionary mechanisms for genomic disorders. Curr Opin Genet Dev 2002; 12(3):312-319.

[32] Shaw CJ, Lupski JR. Implications of human genome architecture for rearrangement-based disorders: the genomic basis of disease. Hum Mol Genet 2004; 13 Spec No 1:R57-R64.

[33] Stankiewicz P, Lupski JR. Genome architecture, rearrangements and genomic disorders. Trends Genet 2002; 18(2):74-82.

[34] Milunsky JM, Huang XL. Unmasking Kabuki syndrome: chromosome 8p22-8p23.1 duplication revealed by comparative genomic hybridization and BAC-FISH. Clin Genet 2003; 64(6):509-516.

[35] Cheung J, Estivill X, Khaja R, MacDonald JR, Lau K, Tsui LC, Scherer SW. Genome-wide detection of segmental duplications and potential assembly errors in the human genome sequence. Genome Biol 2003; 4(4):R25.

[36] Kurotaki N, Harada N, Shimokawa O, Miyake N, Kawame H, Uetake K, Makita Y, Kondoh T, Ogata T, Hasegawa T, Nagai T, Ozaki T, Touyama M, Shenhav R, Ohashi H, Medne L, Shiihara T, Ohtsu S, Kato Z, Okamoto N, Nishimoto J, Lev D, Miyoshi Y, Ishikiriyama S, Sonoda T, Sakazume S, Fukushima Y, Kurosawa K, Cheng JF, Yoshiura K, Ohta T, Kishino T, Niikawa N, Matsumoto N. Fifty microdeletions among 112 cases of Sotos syndrome: low copy repeats possibly mediate the common deletion. Hum Mutat 2003; 22(5):378-387.

[37] de Mollerat XJ, Gurrieri F, Morgan CT, Sangiorgi E, Everman DB, Gaspari P, Amiel J, Bamshad MJ, Lyle R, Blouin JL, Allanson JE, Le Marec B, Wilson M, Braverman NE, Radhakrishna U, Delozier-Blanchet C, Abbott A, Elghouzzi V, Antonarakis S, Stevenson RE, Munnich A, Neri G, Schwartz CE. A genomic rearrangement resulting in a tandem duplication is associated with split hand-split foot malformation 3 (SHFM3) at 10q24. Hum Mol Genet 2003; 12(16):1959-1971.

[38] Stankiewicz P, Lupski JR. Genome architecture, rearrangements and genomic disorders. Trends Genet 2002; 18(2):74-82.

[39] Stankiewicz P, Shaw CJ, Dapper JD, Wakui K, Shaffer LG, Withers M, Elizondo L, Park SS, Lupski JR. Genome architecture catalyzes nonrecurrent chromosomal rearrangements. Am J Hum Genet 2003; 72(5):1101-1116.

[40] Potocki L, Chen KS, Park SS, Osterholm DE, Withers MA, Kimonis V, Summers AM, Meschino WS, Anyane-Yeboa K, Kashork CD, Shaffer LG, Lupski JR. Molecular mechanism for duplication 17p11.2- the homologous recombination reciprocal of the Smith-Magenis microdeletion. Nat Genet 2000; 24(1):84-87.

[41] Stankiewicz P, Shaw CJ, Dapper JD, Wakui K, Shaffer LG, Withers M, Elizondo L, Park SS, Lupski JR. Genome architecture catalyzes nonrecurrent chromosomal rearrangements. Am J Hum Genet 2003; 72(5):1101-1116.

[42] Stankiewicz P, Lupski JR. Molecular-evolutionary mechanisms for genomic disorders. Curr Opin Genet Dev 2002; 12(3):312-319.

[43] Shaw CJ, Lupski JR. Implications of human genome architecture for rearrangement-based disorders: the genomic basis of disease. Hum Mol Genet 2004; 13 Spec No 1:R57-R64.

[44] Spiteri E, Babcock M, Kashork CD, Wakui K, Gogineni S, Lewis DA, Williams KM, Minoshima S, Sasaki T, Shimizu N, Potocki L, Pulijaal V, Shanske A, Shaffer LG, Morrow BE. Frequent translocations occur between low copy repeats on chromosome 22q11.2 (LCR22s) and telomeric bands of partner chromosomes. Hum Mol Genet 2003; 12(15):1823-1837.

[45] Spiteri E, Babcock M, Kashork CD, Wakui K, Gogineni S, Lewis DA, Williams KM, Minoshima S, Sasaki T, Shimizu N, Potocki L, Pulijaal V, Shanske A, Shaffer LG, Morrow BE. Frequent translocations occur between low copy repeats on chromosome 22q11.2 (LCR22s) and telomeric bands of partner chromosomes. Hum Mol Genet 2003; 12(15):1823-1837.

[46] Moore CM, Leland MM, Brzyski RG, McKeand J, Witte SM, Rogers J. A baboon (Papio hamadryas) with an isochromosome for the long arm of the X. Cytogenet Cell Genet 1998; 82(1-2):80-82.

[47] Wolff DJ, Miller AP, Van Dyke DL, Schwartz S, Willard HF. Molecular definition of breakpoints associated with human Xq isochromosomes: implications for mechanisms of formation. Am J Hum Genet 1996; 58(1):154-160.

[48] Niebuhr E. The Cri du Chat syndrome: epidemiology, cytogenetics, and clinical features. Hum Genet 1978; 44(3):227-275.

[49] Zhang A, Zheng C, Hou M, Lindvall C, Li KJ, Erlandsson F, Bjorkholm M, Gruber A, Blennow E, Xu D. Deletion of the telomerase reverse transcriptase gene and haploinsufficiency of telomere maintenance in Cri du chat syndrome. Am J Hum Genet 2003; 72(4):940-948.

[50] Mainardi PC, Perfumo C, Cali A, Coucourde G, Pastore G, Cavani S, Zara F, Overhauser J, Pierluigi M, Bricarelli FD. Clinical and molecular characterisation of 80 patients with 5p deletion: genotype-phenotype correlation. J Med Genet 2001; 38(3):151-158.

[51] Overhauser J, McMahon J, Oberlender S, Carlin ME, Niebuhr E, Wasmuth JJ, Lee-Chen J. Parental origin of chromosome 5 deletions in the cri-du-chat syndrome. Am J Med Genet 1990; 37(1):83-86.

[52] Mainardi PC, Perfumo C, Cali A, Coucourde G, Pastore G, Cavani S, Zara F, Overhauser J, Pierluigi M, Bricarelli FD. Clinical and molecular characterisation of 80 patients with 5p deletion: genotype-phenotype correlation. J Med Genet 2001; 38(3):151-158.

[53] Overhauser J, Huang X, Gersh M, Wilson W, McMahon J, Bengtsson U, Rojas K, Meyer M, Wasmuth JJ. Molecular and phenotypic mapping of the short arm of chromosome 5: sublocalization of the critical region for the cri-du-chat syndrome. Hum Mol Genet 1994; 3(2):247-252.

[54] Marinescu RC, Johnson EI, Dykens EM, Hodapp RM, Overhauser J. No relationship between the size of the deletion and the level of developmental delay in cri-du-chat syndrome. Am J Med Genet 1999; 86(1):66-70.

[55] Ogilvie CM, Braude P, Scriven PN. Successful pregnancy outcomes after preimplantation genetic diagnosis (PGD) for carriers of chromosome translocations. Hum Fertil (Camb) 2001; 4(3):168-171.

[56] Warburton D. De novo balanced chromosome rearrangements and extra marker chromosomes identified at prenatal diagnosis: clinical significance and distribution of breakpoints. Am J Hum Genet 1991; 49(5):995-1013.

[57] Lindenbaum RH, Clarke G, Patel C, Moncrieff M, Hughes JT. Muscular dystrophy in an X; 1 translocation female suggests that Duchenne locus is on X chromosome short arm. J Med Genet 1979; 16(5):389-392.

[58] Morton NE, Chung CS. Formal genetics of muscular dystrophy. Am J Hum Genet 1959; 11:360-379.

[59] Wulfsberg EA, Skoglund RR. Duchenne muscular dystrophy in a 46 XY female. Clin Pediatr (Phila) 1986; 25(5):276-278.

[60] Greenstein RM, Reardon MP, Chan TS. An X-autosome translocation in a girl with Duchenne muscular dystrophy (DMD): evidence for DMD gene localization. Pediat.Res. 11, 457. 1977.
Ref Type: Abstract

[61] Verellen C, Markovic V, DeMeyer R, Freund M, Laterre C, Worton RG. Expression of an X-linked recessive disease in a female due to non-random inactivation of the X chromosome. Am.J.Hum.Genet 30, 97A. 1978.
Ref Type: Abstract

[62] Canki N, Dutrillaux B, Tivadar I. Dystrophie musculaire de Duchenne chez une petite fille porteuse d'une translocation t(X;3) (p21;q13) de novo. Ann Genet 1979; 22:35 or 435-39.

[63] Jacobs PA, Hunt PA, Mayer M, Bart RD. Duchenne muscular dystrophy (DMD) in a female with an X/autosome translocation: further evidence that the DMD locus is at Xp21. Am J Hum Genet 1981; 33(4):513-518.

[64] Zatz M, Vianna-Morgante AM, Campos P, Diament AJ. Translocation (X;6) in a female with Duchenne muscular dystrophy: implications for the localisation of the DMD locus. J Med Genet 1981; 18(6):442-447.

[65] Bjerglund NL, Nielsen IM. Turner's syndrome and Duchenne muscular dystrophy in a girl with an X; autosome translocation. Ann Genet 1984; 27(3):173-177.

[66] Verellen-Dumoulin C, Freund M, De Meyer R, Laterre C, Frederic J, Thompson MW, Markovic VD, Worton RG. Expression of an X-linked muscular dystrophy in a female due to translocation involving Xp21 and non-random inactivation of the normal X chromosome. Hum Genet 1984; 67(1):115-119.

[67] Worton RG, Duff C, Sylvester JE, Schmickel RD, Willard HF. Duchenne muscular dystrophy involving translocation of the dmd gene next to ribosomal RNA genes. Science 1984; 224(4656):1447-1449.

[68] Ray PN, Belfall B, Duff C, Logan C, Kean V, Thompson MW, Sylvester JE, Gorski JL, Schmickel RD, Worton RG. Cloning of the breakpoint of an X;21 translocation associated with Duchenne muscular dystrophy. Nature 1985; 318(6047):672-675.

[69] Passos-Bueno MR, Bakker E, Kneppers AL, Takata RI, Rapaport D, den Dunnen JT, Zatz M, van Ommen GJ. Different mosaicism frequencies for proximal and distal Duchenne muscular dystrophy (DMD) mutations indicate difference in etiology and recurrence risk. Am J Hum Genet 1992; 51(5):1150-1155.

[70] Cremers FP, van de Pol DJ, van Kerkhoff LP, Wieringa B, Ropers HH. Cloning of a gene that is rearranged in patients with choroideraemia. Nature 1990; 347(6294):674-677.

[71] Attree O, Olivos IM, Okabe I, Bailey LC, Nelson DL, Lewis RA, McInnes RR, Nussbaum RL. The Lowe's oculocerebrorenal syndrome gene encodes a protein highly homologous to inositol polyphosphate-5-phosphatase. Nature 1992; 358(6383):239-242.

[72] Gleeson JG, Allen KM, Fox JW, Lamperti ED, Berkovic S, Scheffer I, Cooper EC, Dobyns WB, Minnerath SR, Ross ME, Walsh CA. Doublecortin, a brain-specific gene mutated in human X-linked lissencephaly and double cortex syndrome, encodes a putative signaling protein. Cell 1998; 92(1):63-72.

[73] RUBINSTEIN JH, TAYBI H. Broad thumbs and toes and facial abnormalities. A possible mental retardation syndrome. Am J Dis Child 1963; 105:588-608.

[74] Imaizumi K, Kuroki Y. Rubinstein-Taybi syndrome with de novo reciprocal translocation t(2;16)(p13.3;p13.3). Am J Med Genet 1991; 38(4):636-639.

[75] Bazacliu E, Tonceanu S, Ghisoiu V, Carp G, Rosca GH, Rosca S. Rubinstein-Taybi syndrome with karyotype changes and recurring pneumopathy (original in Hungarian). Ftziologia 22, 645-650. 1979.
Ref Type: Abstract

[76] Tommerup N, van der Hagen CB, Heiberg A. Tentative assignment of a locus for Rubinstein-Taybi syndrome to 16p13.3 by a de novo reciprocal translocation, t(7;16)(q34;p13.3). Am J Med Genet 1992; 44(2):237-241.

[77] Tommerup N, van der Hagen CB, Heiberg A. Tentative assignment of a locus for Rubinstein-Taybi syndrome to 16p13.3 by a de novo reciprocal translocation, t(7;16)(q34;p13.3). (Abstract). Cytogenet.Cell Genet 58, 2002-2003. 1991.
Ref Type: Abstract

[78] Lacombe D, Saura R, Taine L, Battin J. Confirmation of assignment of a locus for Rubinstein-Taybi syndrome gene to 16p13.3. Am J Med Genet 1992; 44(1):126-128.

[79] Petrij F, Giles RH, Dauwerse HG, Saris JJ, Hennekam RC, Masuno M, Tommerup N, van Ommen GJ, Goodman RH, Peters DJ, . Rubinstein-Taybi syndrome caused by mutations in the transcriptional co-activator CBP. Nature 1995; 376(6538):348-351.

[80] Petrij F, Dorsman JC, Dauwerse HG, Giles RH, Peeters T, Hennekam RC, Breuning MH, Peters DJ. Rubinstein-Taybi syndrome caused by a De Novo reciprocal translocation t(2;16)(q36.3;p13.3). Am J Med Genet 2000; 92(1):47-52.

[81] Ogle RF, Dalzell P, Turner G, Wass D, Yip MY. Multiple exostoses in a patient with t(8;11)(q24.11;p15.5). J Med Genet 1991; 28(12):881-883.

[82] Yoshiura K, Inazawa J, Koyama K, Nakamura Y, Niikawa N. Mapping of the 8q23 translocation breakpoint of t(8;13) observed in a patient with multiple exostoses. Genes Chromosomes Cancer 1994; 9(1):57-61.

[83] Ahn J, Ludecke HJ, Lindow S, Horton WA, Lee B, Wagner MJ, Horsthemke B, Wells DE. Cloning of the putative tumour suppressor gene for hereditary multiple exostoses (EXT1). Nat Genet 1995; 11(2):137-143.

[84] Collin GB, Marshall JD, Cardon LR, Nishina PM. Homozygosity mapping at Alstrom syndrome to chromosome 2p. Hum Mol Genet 1997; 6(2):213-219.

[85] Macari F, Lautier C, Girardet A, Dadoun F, Darmon P, Dutour A, Renard E, Bouvagnet P, Claustres M, Oliver C, Grigorescu F. Refinement of genetic localization of the Alstrom syndrome on chromosome 2p12-13 by linkage analysis in a North African family. Hum Genet 1998; 103(6):658-661.

[86] Collin GB, Marshall JD, Ikeda A, So WV, Russell-Eggitt I, Maffei P, Beck S, Boerkoel CF, Sicolo N, Martin M, Nishina PM, Naggert JK. Mutations in

ALMS1 cause obesity, type 2 diabetes and neurosensory degeneration in Alstrom syndrome. Nat Genet 2002; 31(1):74-78.

[87] Hearn T, Renforth GL, Spalluto C, Hanley NA, Piper K, Brickwood S, White C, Connolly V, Taylor JF, Russell-Eggitt I, Bonneau D, Walker M, Wilson DI. Mutation of ALMS1, a large gene with a tandem repeat encoding 47 amino acids, causes Alstrom syndrome. Nat Genet 2002; 31(1):79-83.

[88] Collin GB, Marshall JD, Cardon LR, Nishina PM. Homozygosity mapping at Alstrom syndrome to chromosome 2p. Hum Mol Genet 1997; 6(2):213-219.

[89] Hearn T, Renforth GL, Spalluto C, Hanley NA, Piper K, Brickwood S, White C, Connolly V, Taylor JF, Russell-Eggitt I, Bonneau D, Walker M, Wilson DI. Mutation of ALMS1, a large gene with a tandem repeat encoding 47 amino acids, causes Alstrom syndrome. Nat Genet 2002; 31(1):79-83.

[90] Collin GB, Marshall JD, Ikeda A, So WV, Russell-Eggitt I, Maffei P, Beck S, Boerkoel CF, Sicolo N, Martin M, Nishina PM, Naggert JK. Mutations in ALMS1 cause obesity, type 2 diabetes and neurosensory degeneration in Alstrom syndrome. Nat Genet 2002; 31(1):74-78.

[91] Ledbetter SA, Kuwano A, Dobyns WB, Ledbetter DH. Microdeletions of chromosome 17p13 as a cause of isolated lissencephaly. Am J Hum Genet 1992; 50(1):182-189.

[92] Reiner O, Carrozzo R, Shen Y, Wehnert M, Faustinella F, Dobyns WB, Caskey CT, Ledbetter DH. Isolation of a Miller-Dieker lissencephaly gene containing G protein beta-subunit-like repeats. Nature 1993; 364(6439):717-721.

[93] Kurahashi H, Sakamoto M, Ono J, Honda A, Okada S, Nakamura Y. Molecular cloning of the chromosomal breakpoint in the LIS1 gene of a patient with isolated lissencephaly and balanced t(8;17). Hum Genet 1998; 103(2):189-192.

[94] Basson CT, Huang T, Lin RC, Bachinsky DR, Weremowicz S, Vaglio A, Bruzzone R, Quadrelli R, Lerone M, Romeo G, Silengo M, Pereira A, Krieger J, Mesquita SF, Kamisago M, Morton CC, Pierpont ME, Muller CW, Seidman JG, Seidman CE. Different TBX5 interactions in heart and limb defined by Holt-Oram syndrome mutations. Proc Natl Acad Sci U S A 1999; 96(6):2919-2924.

[95] Li QY, Newbury-Ecob RA, Terrett JA, Wilson DI, Curtis AR, Yi CH, Gebuhr T, Bullen PJ, Robson SC, Strachan T, Bonnet D, Lyonnet S, Young ID, Raeburn JA, Buckler AJ, Law DJ, Brook JD. Holt-Oram syndrome is caused by mutations in TBX5, a member of the Brachyury (T) gene family. Nat Genet 1997; 15(1):21-29.

[96] Basson CT, Huang T, Lin RC, Bachinsky DR, Weremowicz S, Vaglio A, Bruzzone R, Quadrelli R, Lerone M, Romeo G, Silengo M, Pereira A, Krieger J, Mesquita SF, Kamisago M, Morton CC, Pierpont ME, Muller CW, Seidman JG, Seidman CE. Different TBX5 interactions in heart and limb defined by Holt-Oram syndrome mutations. Proc Natl Acad Sci U S A 1999; 96(6):2919-2924.

[97] Petrij F, Dorsman JC, Dauwerse HG, Giles RH, Peeters T, Hennekam RC, Breuning MH, Peters DJ. Rubinstein-Taybi syndrome caused by a De Novo reciprocal translocation t(2;16)(q36.3;p13.3). Am J Med Genet 2000; 92(1):47-52.

[98] Kumar A, Becker LA, Depinet TW, Haren JM, Kurtz CL, Robin NH, Cassidy SB, Wolff DJ, Schwartz S. Molecular characterization and delineation of subtle deletions in de novo "balanced" chromosomal rearrangements. Hum Genet 1998; 103(2):173-178.

[99] Astbury C, Christ LA, Aughton DJ, Cassidy SB, Kumar A, Eichler EE, Schwartz S. Detection of deletions in de novo "balanced" chromosome rearrangements: further evidence for their role in phenotypic abnormalities. Genet Med 2004; 6(2):81-89.

[100] Astbury C, Christ LA, Aughton DJ, Cassidy SB, Kumar A, Eichler EE, Schwartz S. Detection of deletions in de novo "balanced" chromosome rearrangements: further evidence for their role in phenotypic abnormalities. Genet Med 2004; 6(2):81-89.

[101] Fantes J, Ragge NK, Lynch SA, McGill NI, Collin JR, Howard-Peebles PN, Hayward C, Vivian AJ, Williamson K, van Heyningen V, FitzPatrick DR. Mutations in SOX2 cause anophthalmia. Nat Genet 2003; 33(4):461-463.

[102] Gribble SM, Prigmore E, Burford DC, Porter KM, Ng BL, Douglas EJ, Fiegler H, Carr P, Kalaitzopoulos D, Clegg S, Sandstrom R, Temple IK, Youings SA, Thomas NS, Dennis NR, Jacobs PA, Crolla JA, Carter NP. The complex nature of constitutional de novo apparently balanced translocations in patients presenting with abnormal phenotypes. J Med Genet 2005; 42(1):8-16.

[103] Baptista J, Prigmore E, Gribble SM, Jacobs PA, Carter NP, Crolla JA. Molecular cytogenetic analyses of breakpoints in apparently balanced reciprocal translocations carried by phenotypically normal individuals. Eur J Hum Genet 2005.

[104] Gribble SM, Prigmore E, Burford DC, Porter KM, Ng BL, Douglas EJ, Fiegler H, Carr P, Kalaitzopoulos D, Clegg S, Sandstrom R, Temple IK, Youings SA, Thomas NS, Dennis NR, Jacobs PA, Crolla JA, Carter NP. The complex nature of constitutional de novo apparently balanced translocations in patients presenting with abnormal phenotypes. J Med Genet 2005; 42(1):8-16.

[105] Shaw-Smith C, Redon R, Rickman L, Rio M, Willatt L, Fiegler H, Firth H, Sanlaville D, Winter R, Colleaux L, Bobrow M, Carter NP. Microarray based comparative genomic hybridisation (array-CGH) detects submicroscopic chromosomal deletions and duplications in patients with learning disability/mental retardation and dysmorphic features. J Med Genet 2004; 41(4):241-248.

[106] Vissers LE, de Vries BB, Osoegawa K, Janssen IM, Feuth T, Choy CO, Straatman H, Van der Vliet, Huys EH, van Rijk A, Smeets D, Ravenswaaij-Arts CM, Knoers NV, van der Burgt I, de Jong PJ, Brunner HG, van Kessel

AG, Schoenmakers EF, Veltman JA. Array-based comparative genomic hybridization for the genomewide detection of submicroscopic chromosomal abnormalities. Am J Hum Genet 2003; 73(6):1261-1270.

[107] Kleinjan DJ, van Heyningen V. Position effect in human genetic disease. Hum Mol Genet 1998; 7(10):1611-1618.

[108] Kleinjan DA, van Heyningen V. Long-range control of gene expression: emerging mechanisms and disruption in disease. Am J Hum Genet 2005; 76(1):8-32.

[109] Fantes J, Redeker B, Breen M, Boyle S, Brown J, Fletcher J, Jones S, Bickmore W, Fukushima Y, Mannens M, . Aniridia-associated cytogenetic rearrangements suggest that a position effect may cause the mutant phenotype. Hum Mol Genet 1995; 4(3):415-422.

[110] Kleinjan DA, Seawright A, Elgar G, van Heyningen V. Characterization of a novel gene adjacent to PAX6, revealing synteny conservation with functional significance. Mamm Genome 2002; 13(2):102-107.

[111] Kleinjan DA, Seawright A, Schedl A, Quinlan RA, Danes S, van Heyningen V. Aniridia-associated translocations, DNase hypersensitivity, sequence comparison and transgenic analysis redefine the functional domain of PAX6. Hum Mol Genet 2001; 10(19):2049-2059.

[112] Davis A, Cowell JK. Mutations in the PAX6 gene in patients with hereditary aniridia. Hum Mol Genet 1993; 2(12):2093-2097.

[113] Gessler M, Simola KO, Bruns GA. Cloning of breakpoints of a chromosome translocation identifies the AN2 locus. Science 1989; 244(4912):1575-1578.

[114] Kleinjan DA, Seawright A, Elgar G, van Heyningen V. Characterization of a novel gene adjacent to PAX6, revealing synteny conservation with functional significance. Mamm Genome 2002; 13(2):102-107.

[115] Lauderdale JD, Wilensky JS, Oliver ER, Walton DS, Glaser T. 3' deletions cause aniridia by preventing PAX6 gene expression. Proc Natl Acad Sci U S A 2000; 97(25):13755-13759.

[116] Lettice LA, Horikoshi T, Heaney SJ, van Baren MJ, van der Linde HC, Breedveld GJ, Joosse M, Akarsu N, Oostra BA, Endo N, Shibata M, Suzuki M, Takahashi E, Shinka T, Nakahori Y, Ayusawa D, Nakabayashi K, Scherer SW, Heutink P, Hill RE, Noji S. Disruption of a long-range cis-acting regulator for Shh causes preaxial polydactyly. Proc Natl Acad Sci U S A 2002; 99(11):7548-7553.

[117] Sharpe J, Lettice L, Hecksher-Sorensen J, Fox M, Hill R, Krumlauf R. Identification of sonic hedgehog as a candidate gene responsible for the polydactylous mouse mutant Sasquatch. Curr Biol 1999; 9(2):97-100.

[118] Sharpe J, Lettice L, Hecksher-Sorensen J, Fox M, Hill R, Krumlauf R. Identification of sonic hedgehog as a candidate gene responsible for the polydactylous mouse mutant Sasquatch. Curr Biol 1999; 9(2):97-100.

[119] Hill RE, Heaney SJ, Lettice LA. Sonic hedgehog: restricted expression and limb dysmorphologies. J Anat 2003; 202(1):13-20.

[120] Lettice LA, Horikoshi T, Heaney SJ, van Baren MJ, van der Linde HC, Breedveld GJ, Joosse M, Akarsu N, Oostra BA, Endo N, Shibata M, Suzuki M, Takahashi E, Shinka T, Nakahori Y, Ayusawa D, Nakabayashi K, Scherer SW, Heutink P, Hill RE, Noji S. Disruption of a long-range cis-acting regulator for Shh causes preaxial polydactyly. Proc Natl Acad Sci U S A 2002; 99(11):7548-7553.

[121] Lettice LA, Horikoshi T, Heaney SJ, van Baren MJ, van der Linde HC, Breedveld GJ, Joosse M, Akarsu N, Oostra BA, Endo N, Shibata M, Suzuki M, Takahashi E, Shinka T, Nakahori Y, Ayusawa D, Nakabayashi K, Scherer SW, Heutink P, Hill RE, Noji S. Disruption of a long-range cis-acting regulator for Shh causes preaxial polydactyly. Proc Natl Acad Sci U S A 2002; 99(11):7548-7553.

[122] Lettice LA, Horikoshi T, Heaney SJ, van Baren MJ, van der Linde HC, Breedveld GJ, Joosse M, Akarsu N, Oostra BA, Endo N, Shibata M, Suzuki M, Takahashi E, Shinka T, Nakahori Y, Ayusawa D, Nakabayashi K, Scherer SW, Heutink P, Hill RE, Noji S. Disruption of a long-range cis-acting regulator for Shh causes preaxial polydactyly. Proc Natl Acad Sci U S A 2002; 99(11):7548-7553.

[123] Escamilla MA, DeMille MC, Benavides E, Roche E, Almasy L, Pittman S, Hauser J, Lew DF, Freimer NB, Whittle MR. A minimalist approach to gene mapping: locating the gene for acheiropodia, by homozygosity analysis. Am J Hum Genet 2000; 66(6):1995-2000.

[124] Ianakiev P, van Baren MJ, Daly MJ, Toledo SP, Cavalcanti MG, Neto JC, Silveira EL, Freire-Maia A, Heutink P, Kilpatrick MW, Tsipouras P. Acheiropodia is caused by a genomic deletion in C7orf2, the human orthologue of the Lmbr1 gene. Am J Hum Genet 2001; 68(1):38-45.

[125] Lettice LA, Heaney SJ, Purdie LA, Li L, de Beer P, Oostra BA, Goode D, Elgar G, Hill RE, de Graaff E. A long-range Shh enhancer regulates expression in the developing limb and fin and is associated with preaxial polydactyly. Hum Mol Genet 2003; 12(14):1725-1735.

[126] Kleinjan DA, Seawright A, Schedl A, Quinlan RA, Danes S, van Heyningen V. Aniridia-associated translocations, DNase hypersensitivity, sequence comparison and transgenic analysis redefine the functional domain of PAX6. Hum Mol Genet 2001; 10(19):2049-2059.

[127] Crisponi L, Uda M, Deiana M, Loi A, Nagaraja R, Chiappe F, Schlessinger D, Cao A, Pilia G. FOXL2 inactivation by a translocation 171 kb away: analysis of 500 kb of chromosome 3 for candidate long-range regulatory sequences. Genomics 2004; 83(5):757-764.

[128] Bagheri-Fam S, Ferraz C, Demaille J, Scherer G, Pfeifer D. Comparative genomics of the SOX9 region in human and Fugu rubripes: conservation of short regulatory sequence elements within large intergenic regions. Genomics 2001; 78(1-2):73-82.

[129] Pop R, Conz C, Lindenberg KS, Blesson S, Schmalenberger B, Briault S, Pfeifer D, Scherer G. Screening of the 1 Mb SOX9 5' control region by array CGH identifies a large deletion in a case of campomelic dysplasia with XY sex reversal. J Med Genet 2004; 41(4):e47.

[130] Jamieson RV, Perveen R, Kerr B, Carette M, Yardley J, Heon E, Wirth MG, van Heyningen V, Donnai D, Munier F, Black GC. Domain disruption and mutation of the bZIP transcription factor, MAF, associated with cataract, ocular anterior segment dysgenesis and coloboma. Hum Mol Genet 2002; 11(1):33-42.

[131] Fernandez B, Siegel-Bartelt J, Herbrick JA, Teshima I, Scherer S. Holoprosencephaly and cleidocranial dysplasia in a patient due to two position-effect mutations: case report and review of the literature. Clin Genet 2005; 68(4):349-359.

[132] Gabellini D, Green MR, Tupler R. Inappropriate gene activation in FSHD: a repressor complex binds a chromosomal repeat deleted in dystrophic muscle. Cell 2002; 110(3):339-348.

[133] Jiang G, Yang F, van Overveld PG, Vedanarayanan V, van der Maarel S., Ehrlich M. Testing the position-effect variegation hypothesis for facioscapulohumeral muscular dystrophy by analysis of histone modification and gene expression in subtelomeric 4q. Hum Mol Genet 2003; 12(22):2909-2921.

[134] Masny PS, Bengtsson U, Chung SA, Martin JH, van Engelen B, van der Maarel SM, Winokur ST. Localization of 4q35.2 to the nuclear periphery: is FSHD a nuclear envelope disease? Hum Mol Genet 2004; 13(17):1857-1871.

[135] de Chadarevian JP, Dunn S, Malatack JJ, Ganguly A, Blecker U, Punnett HH. Chromosome rearrangement with no apparent gene mutation in familial adenomatous polyposis and hepatocellular neoplasia. Pediatr Dev Pathol 2002; 5(1):69-75.

[136] Davies AF, Mirza G, Flinter F, Ragoussis J. An interstitial deletion of 6p24-p25 proximal to the FKHL7 locus and including AP-2alpha that affects anterior eye chamber development. J Med Genet 1999; 36(9):708-710.

[137] Wild A, Kalff-Suske M, Vortkamp A, Bornholdt D, Konig R, Grzeschik KH. Point mutations in human GLI3 cause Greig syndrome. Hum Mol Genet 1997; 6(11):1979-1984.

[138] Di Paola J, Goldman T, Qian Q, Patil SR, Schutte BC. Breakpoint of a balanced translocation (X:14) (q27.1;q32.3) in a girl with severe hemophilia B maps proximal to the factor IX gene. J Thromb Haemost 2004; 2(3):437-440.

[139] Wallis DE, Roessler E, Hehr U, Nanni L, Wiltshire T, Richieri-Costa A, Gillessen-Kaesbach G, Zackai EH, Rommens J, Muenke M. Mutations in the homeodomain of the human SIX3 gene cause holoprosencephaly. Nat Genet 1999; 22(2):196-198.

[140] Roessler E, Ward DE, Gaudenz K, Belloni E, Scherer SW, Donnai D, Siegel-Bartelt J, Tsui LC, Muenke M. Cytogenetic rearrangements involving the loss of the Sonic Hedgehog gene at 7q36 cause holoprosencephaly. Hum Genet 1997; 100(2):172-181.

[141] Li QY, Newbury-Ecob RA, Terrett JA, Wilson DI, Curtis AR, Yi CH, Gebuhr T, Bullen PJ, Robson SC, Strachan T, Bonnet D, Lyonnet S, Young ID, Raeburn JA, Buckler AJ, Law DJ, Brook JD. Holt-Oram syndrome is caused by mutations in TBX5, a member of the Brachyury (T) gene family. Nat Genet 1997; 15(1):21-29.

[142] Enattah NS, Sahi T, Savilahti E, Terwilliger JD, Peltonen L, Jarvela I. Identification of a variant associated with adult-type hypolactasia. Nat Genet 2002; 30(2):233-237.

[143] Fang J, Dagenais SL, Erickson RP, Arlt MF, Glynn MW, Gorski JL, Seaver LH, Glover TW. Mutations in FOXC2 (MFH-1), a forkhead family transcription factor, are responsible for the hereditary lymphedema-distichiasis syndrome. Am J Hum Genet 2000; 67(6):1382-1388.

[144] Spitz F, Montavon T, Monso-Hinard C, Morris M, Ventruto ML, Antonarakis S, Ventruto V, Duboule D. A t(2;8) balanced translocation with breakpoints near the human HOXD complex causes mesomelic dysplasia and vertebral defects. Genomics 2002; 79(4):493-498.

[145] Lettice LA, Heaney SJ, Purdie LA, Li L, de Beer P, Oostra BA, Goode D, Elgar G, Hill RE, de Graaff E. A long-range Shh enhancer regulates expression in the developing limb and fin and is associated with preaxial polydactyly. Hum Mol Genet 2003; 12(14):1725-1735.

[146] Trembath DG, Semina EV, Jones DH, Patil SR, Qian Q, Amendt BA, Russo AF, Murray JC. Analysis of two translocation breakpoints and identification of a negative regulatory element in patients with Rieger's syndrome. Birth Defects Res A Clin Mol Teratol 2004; 70(2):82-91.

[147] Cai J, Goodman BK, Patel AS, Mulliken JB, Van Maldergem L, Hoganson GE, Paznekas WA, Ben Neriah Z, Sheffer R, Cunningham ML, Daentl DL, Jabs EW. Increased risk for developmental delay in Saethre-Chotzen syndrome is associated with TWIST deletions: an improved strategy for TWIST mutation screening. Hum Genet 2003; 114(1):68-76.

[148] McElreavy K, Vilain E, Abbas N, Costa JM, Souleyreau N, Kucheria K, Boucekkine C, Thibaud E, Brauner R, Flamant F, . XY sex reversal associated with a deletion 5' to the SRY "HMG box" in the testis-determining region. Proc Natl Acad Sci U S A 1992; 89(22):11016-11020.

[149] Scherer SW, Cheung J, MacDonald JR, Osborne LR, Nakabayashi K, Herbrick JA, Carson AR, Parker-Katiraee L, Skaug J, Khaja R, Zhang J, Hudek AK, Li M, Haddad M, Duggan GE, Fernandez BA, Kanematsu E, Gentles S, Christopoulos CC, Choufani S, Kwasnicka D, Zheng XH, Lai Z, Nusskern D, Zhang Q, Gu Z, Lu F, Zeesman S, Nowaczyk MJ, Teshima I, Chitayat D, Shuman C, Weksberg R, Zackai EH, Grebe TA, Cox SR, Kirkpatrick SJ, Rahman N, Friedman JM, Heng HH, Pelicci PG, Lo-Coco F,

Belloni E, Shaffer LG, Pober B, Morton CC, Gusella JF, Bruns GA, Korf BR, Quade BJ, Ligon AH, Ferguson H, Higgins AW, Leach NT, Herrick SR, Lemyre E, Farra CG, Kim HG, Summers AM, Gripp KW, Roberts W, Szatmari P, Winsor EJ, Grzeschik KH, Teebi A, Minassian BA, Kere J, Armengol L, Pujana MA, Estivill X, Wilson MD, Koop BF, Tosi S, Moore GE, Boright AP, Zlotorynski E, Kerem B, Kroisel PM, Petek E, Oscier DG, Mould SJ, Dohner H, Dohner K, Rommens JM, Vincent JB, Venter JC, Li PW, Mural RJ, Adams MD, Tsui LC. Human chromosome 7: DNA sequence and biology. Science 2003; 300(5620):767-772.

[150] Crackower MA, Scherer SW, Rommens JM, Hui CC, Poorkaj P, Soder S, Cobben JM, Hudgins L, Evans JP, Tsui LC. Characterization of the split hand/split foot malformation locus SHFM1 at 7q21.3-q22.1 and analysis of a candidate gene for its expression during limb development. Hum Mol Genet 1996; 5(5):571-579.

[151] Tufarelli C, Stanley JA, Garrick D, Sharpe JA, Ayyub H, Wood WG, Higgs DR. Transcription of antisense RNA leading to gene silencing and methylation as a novel cause of human genetic disease. Nat Genet 2003; 34(2):157-165.

[152] Kioussis D, Vanin E, deLange T, Flavell RA, Grosveld FG. Beta-globin gene inactivation by DNA translocation in gamma beta-thalassaemia. Nature 1983; 306(5944):662-666.

[153] Balemans W, Patel N, Ebeling M, Van Hul E, Wuyts W, Lacza C, Dioszegi M, Dikkers FG, Hildering P, Willems PJ, Verheij JB, Lindpaintner K, Vickery B, Foernzler D, Van Hul W. Identification of a 52 kb deletion downstream of the SOST gene in patients with van Buchem disease. J Med Genet 2002; 39(2):91-97.

[154] de Kok YJ, Vossenaar ER, Cremers CW, Dahl N, Laporte J, Hu LJ, Lacombe D, Fischel-Ghodsian N, Friedman RA, Parnes LS, Thorpe P, Bitner-Glindzicz M, Pander HJ, Heilbronner H, Graveline J, den Dunnen JT, Brunner HG, Ropers HH, Cremers FP. Identification of a hot spot for microdeletions in patients with X-linked deafness type 3 (DFN3) 900 kb proximal to the DFN3 gene POU3F4. Hum Mol Genet 1996; 5(9):1229-1235.

[155] Brewer C, Holloway S, Zawalnyski P, Schinzel A, FitzPatrick D. A chromosomal deletion map of human malformations. Am J Hum Genet 1998; 63(4):1153-1159.

[156] Bugge M, Bruun-Petersen G, Brondum-Nielsen K, Friedrich U, Hansen J, Jensen G, Jensen PK, Kristoffersson U, Lundsteen C, Niebuhr E, Rasmussen KR, Rasmussen K, Tommerup N. Disease associated balanced chromosome rearrangements: a resource for large scale genotype-phenotype delineation in man. J Med Genet 2000; 37(11):858-865.

[157] Astbury C, Christ LA, Aughton DJ, Cassidy SB, Kumar A, Eichler EE, Schwartz S. Detection of deletions in de novo "balanced" chromosome rearrangements: further evidence for their role in phenotypic abnormalities. Genet Med 2004; 6(2):81-89.

[158] Fantes J, Ragge NK, Lynch SA, McGill NI, Collin JR, Howard-Peebles PN, Hayward C, Vivian AJ, Williamson K, van Heyningen V, FitzPatrick DR. Mutations in SOX2 cause anophthalmia. Nat Genet 2003; 33(4):461-463.

[159] Johnson DS, Morrison N, Grant L, Turner T, Fantes J, Connor JM, Murday VA. Confirmation of CHD7 as a cause of CHARGE association identified by mapping a balanced chromosome translocation in affected monozygotic twins. J Med Genet 2005.

[160] Sawada A, Takihara Y, Kim JY, Matsuda-Hashii Y, Tokimasa S, Fujisaki H, Kubota K, Endo H, Onodera T, Ohta H, Ozono K, Hara J. A congenital mutation of the novel gene LRRC8 causes agammaglobulinemia in humans. J Clin Invest 2003; 112(11):1707-1713.

[161] Krantz ID, McCallum J, DeScipio C, Kaur M, Gillis LA, Yaeger D, Jukofsky L, Wasserman N, Bottani A, Morris CA, Nowaczyk MJ, Toriello H, Bamshad MJ, Carey JC, Rappaport E, Kawauchi S, Lander AD, Calof AL, Li HH, Devoto M, Jackson LG. Cornelia de Lange syndrome is caused by mutations in NIPBL, the human homolog of Drosophila melanogaster Nipped-B. Nat Genet 2004; 36(6):631-635.

[162] Tonkin ET, Smith M, Eichhorn P, Jones S, Imamwerdi B, Lindsay S, Jackson M, Wang TJ, Ireland M, Burn J, Krantz ID, Carr P, Strachan T. A giant novel gene undergoing extensive alternative splicing is severed by a Cornelia de Lange-associated translocation breakpoint at 3q26.3. Hum Genet 2004; 115(2):139-148.

[163] Draptchinskaia N, Gustavsson P, Andersson B, Pettersson M, Willig TN, Dianzani I, Ball S, Tchernia G, Klar J, Matsson H, Tentler D, Mohandas N, Carlsson B, Dahl N. The gene encoding ribosomal protein S19 is mutated in Diamond-Blackfan anaemia. Nat Genet 1999; 21(2):169-175.

[164] Gustavsson P, Skeppner G, Johansson B, Berg T, Gordon L, Kreuger A, Dahl N. Diamond-Blackfan anaemia in a girl with a de novo balanced reciprocal X;19 translocation. J Med Genet 1997; 34(9):779-782.

[165] Willig TN, Draptchinskaia N, Dianzani I, Ball S, Niemeyer C, Ramenghi U, Orfali K, Gustavsson P, Garelli E, Brusco A, Tiemann C, Perignon JL, Bouchier C, Cicchiello L, Dahl N, Mohandas N, Tchernia G. Mutations in ribosomal protein S19 gene and diamond blackfan anemia: wide variations in phenotypic expression. Blood 1999; 94(12):4294-4306.

[166] Toriello HV, Glover TW, Takahara K, Byers PH, Miller DE, Higgins JV, Greenspan DS. A translocation interrupts the COL5A1 gene in a patient with Ehlers-Danlos syndrome and hypomelanosis of Ito. Nat Genet 1996; 13(3):361-365.

[167] van der Luijt RB, Tops CM, Khan PM, van der Klift HM, Breukel C, Leeuwen-Cornelisse IS, Dauwerse HG, Beverstock GC, van Noort E, Snel P, . Molecular, cytogenetic, and phenotypic studies of a constitutional reciprocal translocation t(5;10)(q22;q25) responsible for familial adenomatous polyposis in a Dutch pedigree. Genes Chromosomes Cancer 1995; 13(3):192-202.

[168] Nadal M, Valiente A, Domenech A, Pritchard M, Estivill X, Ramos-Arroyo MA. Hereditary neuropathy with liability to pressure palsies: two cases with a reciprocal translocation t(16;17)(q12;11.2) interrupting the PMP22 gene. J Med Genet 2000; 37(5):396-398.

[169] Basson CT, Huang T, Lin RC, Bachinsky DR, Weremowicz S, Vaglio A, Bruzzone R, Quadrelli R, Lerone M, Romeo G, Silengo M, Pereira A, Krieger J, Mesquita SF, Kamisago M, Morton CC, Pierpont ME, Muller CW, Seidman JG, Seidman CE. Different TBX5 interactions in heart and limb defined by Holt-Oram syndrome mutations. Proc Natl Acad Sci U S A 1999; 96(6):2919-2924.

[170] Pramparo T, Gregato G, De Gregori M, Friso A, Clementi M, Ardenghi P, Rocchi M, Zuffardi O, Tenconi R. Reciprocal translocation associated with multiple exostoses in seven members of a three generation family and discovered through an infertile male. Am J Med Genet A 2003; 123(1):79-83.

[171] Messiaen LM, Callens T, Mortier G, Beysen D, Vandenbroucke I, Van Roy N, Speleman F, Paepe AD. Exhaustive mutation analysis of the NF1 gene allows identification of 95% of mutations and reveals a high frequency of unusual splicing defects. Hum Mutat 2000; 15(6):541-555.

[172] Arai E, Ikeuchi T, Karasawa S, Tamura A, Yamamoto K, Kida M, Ichimura K, Yuasa Y, Tonomura A. Constitutional translocation t(4;22) (q12;q12.2) associated with neurofibromatosis type 2. Am J Med Genet 1992; 44(2):163-167.

[173] Tsilchorozidou T, Menko FH, Lalloo F, Kidd A, De Silva R, Thomas H, Smith P, Malcolmson A, Dore J, Madan K, Brown A, Yovos JG, Tsaligopoulos M, Vogiatzis N, Baser M, Wallace AJ, Evans DG. Constitutional rearrangements of chromosome 22 as a cause of neurofibromatosis 2. J Med Genet 2004; 41(7):529-534.

[174] Trivino E, Guitart M, Egozcue J, Coll MD. Characterization by FISH of a t(5;13) in a patient with bilateral retinoblastoma. Cancer Genet Cytogenet 1997; 96(1):23-25.

[175] Petrij F, Dorsman JC, Dauwerse HG, Giles RH, Peeters T, Hennekam RC, Breuning MH, Peters DJ. Rubinstein-Taybi syndrome caused by a De Novo reciprocal translocation t(2;16)(q36.3;p13.3). Am J Med Genet 2000; 92(1):47-52.

[176] Lai CS, Fisher SE, Hurst JA, Vargha-Khadem F, Monaco AP. A forkhead-domain gene is mutated in a severe speech and language disorder. Nature 2001; 413(6855):519-523.

[177] Ludecke HJ, Schmidt O, Nardmann J, von Holtum D, Meinecke P, Muenke M, Horsthemke B. Genes and chromosomal breakpoints in the Langer-Giedion syndrome region on human chromosome 8. Hum Genet 1999; 105(6):619-628.

[178] Momeni P, Glockner G, Schmidt O, von Holtum D, Albrecht B, Gillessen-Kaesbach G, Hennekam R, Meinecke P, Zabel B, Rosenthal A, Horsthemke

B, Ludecke HJ. Mutations in a new gene, encoding a zinc-finger protein, cause tricho-rhino-phalangeal syndrome type I. Nat Genet 2000; 24(1):71-74.

[179] Marchau FE, Van Roy BC, Parizel PM, Lambert JR, De Canck I, Leroy JG, Gevaert CM, Willems PJ, Dumon JE. Tricho-rhino-phalangeal syndrome type I (TRP I) due to an apparently balanced translocation involving 8q24. Am J Med Genet 1993; 45(4):450-455.

[180] Ludecke HJ, Schmidt O, Nardmann J, von Holtum D, Meinecke P, Muenke M, Horsthemke B. Genes and chromosomal breakpoints in the Langer-Giedion syndrome region on human chromosome 8. Hum Genet 1999; 105(6):619-628.

[181] Momeni P, Glockner G, Schmidt O, von Holtum D, Albrecht B, Gillessen-Kaesbach G, Hennekam R, Meinecke P, Zabel B, Rosenthal A, Horsthemke B, Ludecke HJ. Mutations in a new gene, encoding a zinc-finger protein, cause tricho-rhino-phalangeal syndrome type I. Nat Genet 2000; 24(1):71-74.

[182] Duba HC, Doll A, Neyer M, Erdel M, Mann C, Hammerer I, Utermann G, Grzeschik KH. The elastin gene is disrupted in a family with a balanced translocation t(7;16)(q11.23;q13) associated with a variable expression of the Williams-Beuren syndrome. Eur J Hum Genet 2002; 10(6):351-361.

[183] Curran ME, Atkinson DL, Ewart AK, Morris CA, Leppert MF, Keating MT. The elastin gene is disrupted by a translocation associated with supravalvular aortic stenosis. Cell 1993; 73(1):159-168.

[184] Morris CA, Loker J, Ensing G, Stock AD. Supravalvular aortic stenosis cosegregates with a familial 6; 7 translocation which disrupts the elastin gene. Am J Med Genet 1993; 46(6):737-744.

[185] Hearn T, Renforth GL, Spalluto C, Hanley NA, Piper K, Brickwood S, White C, Connolly V, Taylor JF, Russell-Eggitt I, Bonneau D, Walker M, Wilson DI. Mutation of ALMS1, a large gene with a tandem repeat encoding 47 amino acids, causes Alstrom syndrome. Nat Genet 2002; 31(1):79-83.

[186] Pichon B, Vankerckhove S, Bourrouillou G, Duprez L, Abramowicz MJ. A translocation breakpoint disrupts the ASPM gene in a patient with primary microcephaly. Eur J Hum Genet 2004; 12(5):419-421.

[187] Perez-Castillo A, Martin-Lucas MA, Abrisqueta JA. Is a gene for microcephaly located on chromosome 1? Hum Genet 1984; 67(2):230-232.

[188] Kurotaki N, Imaizumi K, Harada N, Masuno M, Kondoh T, Nagai T, Ohashi H, Naritomi K, Tsukahara M, Makita Y, Sugimoto T, Sonoda T, Hasegawa T, Chinen Y, Tomita Ha HA, Kinoshita A, Mizuguchi T, Yoshiura KK, Ohta T, Kishino T, Fukushima Y, Niikawa N, Matsumoto N. Haploinsufficiency of NSD1 causes Sotos syndrome. Nat Genet 2002; 30(4):365-366.

[189] Imaizumi K, Kimura J, Matsuo M, Kurosawa K, Masuno M, Niikawa N, Kuroki Y. Sotos syndrome associated with a de novo balanced reciprocal translocation t(5;8)(q35;q24.1). Am J Med Genet 2002; 107(1):58-60.

[190] Tian XL, Kadaba R, You SA, Liu M, Timur AA, Yang L, Chen Q, Szafranski P, Rao S, Wu L, Housman DE, DiCorleto PE, Driscoll DJ, Borrow J, Wang Q. Identification of an angiogenic factor that when mutated causes susceptibility to Klippel-Trenaunay syndrome. Nature 2004; 427(6975):640-645.

[191] Whelan AJ, Watson MS, Porter FD, Steiner RD. Klippel-Trenaunay-Weber syndrome associated with a 5:11 balanced translocation. Am J Med Genet 1995; 59(4):492-494.

[192] Sun Y, Nicholls RD, Butler MG, Saitoh S, Hainline BE, Palmer CG. Breakage in the SNRPN locus in a balanced 46,XY,t(15;19) Prader-Willi syndrome patient. Hum Mol Genet 1996; 5(4):517-524.

[193] Kuslich CD, Kobori JA, Mohapatra G, Gregorio-King C, Donlon TA. Prader-Willi syndrome is caused by disruption of the SNRPN gene. Am J Hum Genet 1999; 64(1):70-76.

[194] Schule B, Albalwi M, Northrop E, Francis DI, Rowell M, Slater HR, Gardner RJ, Francke U. Molecular breakpoint cloning and gene expression studies of a novel translocation t(4;15)(q27;q11.2) associated with Prader-Willi syndrome. BMC Med Genet 2005; 6(1):18.

[195] Kurahashi H, Sakamoto M, Ono J, Honda A, Okada S, Nakamura Y. Molecular cloning of the chromosomal breakpoint in the LIS1 gene of a patient with isolated lissencephaly and balanced t(8;17). Hum Genet 1998; 103(2):189-192.

[196] Muncke N, Jung C, Rudiger H, Ulmer H, Roeth R, Hubert A, Goldmuntz E, Driscoll D, Goodship J, Schon K, Rappold G. Missense mutations and gene interruption in PROSIT240, a novel TRAP240-like gene, in patients with congenital heart defect (transposition of the great arteries). Circulation 2003; 108(23):2843-2850.

[197] Hertz JM, Persson U, Juncker I, Segelmark M. Alport syndrome caused by inversion of a 21 Mb fragment of the long arm of the X-chromosome comprising exon 9 through 51 of the COL4A5 gene. Hum Genet 2005;1-6.

[198] Xu W, Robert C, Thornton PS, Spinner NB. Complete androgen insensitivity syndrome due to X chromosome inversion: a clinical report. Am J Med Genet A 2003; 120(3):434-436.

[199] Merry DE, Lesko JG, Siu V, Flintoff WF, Collins F, Lewis RA, Nussbaum RL. DXS165 detects a translocation breakpoint in a woman with choroideremia and a de novo X; 13 translocation. Genomics 1990; 6(4):609-615.

[200] Siu VM, Gonder JR, Jung JH, Sergovich FR, Flintoff WF. Choroideremia associated with an X-autosomal translocation. Hum Genet 1990; 84(5):459-464.

[201] van Bokhoven H, Schwartz M, Andreasson S, van den Hurk JA, Bogerd L, Jay M, Ruther K, Jay B, Pawlowitzki IH, Sankila EM, . Mutation spectrum in the CHM gene of Danish and Swedish choroideremia patients. Hum Mol Genet 1994; 3(7):1047-1051.

[202] Bodrug SE, Burghes AH, Ray PM, Worton RG. Mapping of four translocation breakpoints within the Duchenne muscular dystrophy gene. Genomics 1989; 4(1):101-104.

[203] van B, I, Holt S, Craig I, Boyd Y. Sequence analysis of the breakpoint regions of an X;5 translocation in a female with Duchenne muscular dystrophy. Am J Hum Genet 1995; 57(2):329-336.

[204] Nevin NC, Hughes AE, Calwell M, Lim JH. Duchenne muscular dystrophy in a female with a translocation involving Xp21. J Med Genet 1986; 23(2):171-173.

[205] Bodrug SE, Burghes AH, Ray PM, Worton RG. Mapping of four translocation breakpoints within the Duchenne muscular dystrophy gene. Genomics 1989; 4(1):101-104.

[206] Bodrug SE, Ray PN, Gonzalez IL, Schmickel RD, Sylvester JE, Worton RG. Molecular analysis of a constitutional X-autosome translocation in a female with muscular dystrophy. Science 1987; 237(4822):1620-1624.

[207] Bodrug SE, Burghes AH, Ray PM, Worton RG. Mapping of four translocation breakpoints within the Duchenne muscular dystrophy gene. Genomics 1989; 4(1):101-104.

[208] Jacobs PA, Hunt PA, Mayer M, Bart RD. Duchenne muscular dystrophy (DMD) in a female with an X/autosome translocation: further evidence that the DMD locus is at Xp21. Am J Hum Genet 1981; 33(4):513-518.

[209] Astbury C, Christ LA, Aughton DJ, Cassidy SB, Kumar A, Eichler EE, Schwartz S. Detection of deletions in de novo "balanced" chromosome rearrangements: further evidence for their role in phenotypic abnormalities. Genet Med 2004; 6(2):81-89.

[210] Emanuel BS, Zackai EH, Tucker SH. Further evidence for Xp21 location of Duchenne muscular dystrophy (DMD) locus: X;9 translocation in a female with DMD. J Med Genet 1983; 20(6):461-463.

[211] Bodrug SE, Burghes AH, Ray PM, Worton RG. Mapping of four translocation breakpoints within the Duchenne muscular dystrophy gene. Genomics 1989; 4(1):101-104.

[212] Lindenbaum RH, Clarke G, Patel C, Moncrieff M, Hughes JT. Muscular dystrophy in an X; 1 translocation female suggests that Duchenne locus is on X chromosome short arm. J Med Genet 1979; 16(5):389-392.

[213] Imai K, Shimadzu M, Kubota T, Morio T, Matsunaga T, Park YD, Yoshioka A, Nonoyama S. Female hyper IgM syndrome type 1 with a chromosomal

translocation disrupting CD40LG. Biochim Biophys Acta 2006; 1762(3):335-340.

[214] Kalscheuer VM, Tao J, Donnelly A, Hollway G, Schwinger E, Kubart S, Menzel C, Hoeltzenbein M, Tommerup N, Eyre H, Harbord M, Haan E, Sutherland GR, Ropers HH, Gecz J. Disruption of the serine/threonine kinase 9 gene causes severe X-linked infantile spasms and mental retardation. Am J Hum Genet 2003; 72(6):1401-1411.

[215] Kalscheuer VM, Tao J, Donnelly A, Hollway G, Schwinger E, Kubart S, Menzel C, Hoeltzenbein M, Tommerup N, Eyre H, Harbord M, Haan E, Sutherland GR, Ropers HH, Gecz J. Disruption of the serine/threonine kinase 9 gene causes severe X-linked infantile spasms and mental retardation. Am J Hum Genet 2003; 72(6):1401-1411.

[216] Matsumoto N, Pilz DT, Fantes JA, Kittikamron K, Ledbetter DH. Isolation of BAC clones spanning the Xq22.3 translocation breakpoint in a lissencephaly patient with a de novo X;2 translocation. J Med Genet 1998; 35(10):829-832.

[217] Gleeson JG, Allen KM, Fox JW, Lamperti ED, Berkovic S, Scheffer I, Cooper EC, Dobyns WB, Minnerath SR, Ross ME, Walsh CA. Doublecortin, a brain-specific gene mutated in human X-linked lissencephaly and double cortex syndrome, encodes a putative signaling protein. Cell 1998; 92(1):63-72.

[218] Sugio Y, Sugio Y, Kuwano A, Miyoshi O, Yamada K, Niikawa N, Tsukahara M. Translocation t(X;21)(q13.3; p11.1) in a girl with Menkes disease. Am J Med Genet 1998; 79(3):191-194.

[219] Abusaad I, Mohammed SN, Ogilvie CM, Ritchie J, Pohl KR, Docherty Z. Clinical expression of Menkes disease in a girl with X;13 translocation. Am J Med Genet 1999; 87(4):354-359.

[220] Billuart P, Bienvenu T, Ronce N, des Portes V, Vinet MC, Zemni R, Roest CH, Carrie A, Fauchereau F, Cherry M, Briault S, Hamel B, Fryns JP, Beldjord C, Kahn A, Moraine C, Chelly J. Oligophrenin-1 encodes a rhoGAP protein involved in X-linked mental retardation. Nature 1998; 392(6679):923-926.

[221] Bienvenu T, Der-Sarkissian H, Billuart P, Tissot M, des Portes V, Bruls T, Chabrolle JP, Chauveau P, Cherry M, Kahn A, Cohen D, Beldjord C, Chelly J, Cherif D. Mapping of the X-breakpoint involved in a balanced X;12 translocation in a female with mild mental retardation. Eur J Hum Genet 1997; 5(2):105-109.

[222] Zenker M, Wermuth B, Trautmann U, Knerr I, Kraus C, Rauch A, Reis A. Severe, neonatal-onset OTC deficiency in twin sisters with a de novo balanced reciprocal translocation t(X;5)(p21.1;q11). Am J Med Genet 2004.

[223] Pilia G, Hughes-Benzie RM, MacKenzie A, Baybayan P, Chen EY, Huber R, Neri G, Cao A, Forabosco A, Schlessinger D. Mutations in GPC3, a glypican gene, cause the Simpson-Golabi-Behmel overgrowth syndrome. Nat Genet 1996; 12(3):241-247.

[224] Punnett HH. Simpson-Golabi-Behmel syndrome (SGBS) in a female with an X-autosome translocation. Am J Med Genet 1994; 50(4):391-393.

[225] Fantes J, Redeker B, Breen M, Boyle S, Brown J, Fletcher J, Jones S, Bickmore W, Fukushima Y, Mannens M, . Aniridia-associated cytogenetic rearrangements suggest that a position effect may cause the mutant phenotype. Hum Mol Genet 1995; 4(3):415-422.

[226] Simola KO, Knuutila S, Kaitila I, Pirkola A, Pohja P. Familial aniridia and translocation t(4;11)(q22;p13) without Wilms' tumor. Hum Genet 1983; 63(2):158-161.

[227] Crolla JA, Cross I, Atkey N, Wright M, Oley CA. FISH studies in a patient with sporadic aniridia and t(7;11) (q31.2;p13). J Med Genet 1996; 33(1):66-68.

[228] Fantes J, Redeker B, Breen M, Boyle S, Brown J, Fletcher J, Jones S, Bickmore W, Fukushima Y, Mannens M, . Aniridia-associated cytogenetic rearrangements suggest that a position effect may cause the mutant phenotype. Hum Mol Genet 1995; 4(3):415-422.

[229] Fukushima Y, Hoovers J, Mannens M, Wakui K, Ohashi H, Ohno T, Ueoka Y, Niikawa N. Detection of a cryptic paracentric inversion within band 11p13 in familial aniridia by fluorescence in situ hybridization. Hum Genet 1993; 91(3):205-209.

[230] Crolla JA, van Heyningen V. Frequent chromosome aberrations revealed by molecular cytogenetic studies in patients with aniridia. Am J Hum Genet 2002; 71(5):1138-1149.

[231] Crolla JA, van Heyningen V. Frequent chromosome aberrations revealed by molecular cytogenetic studies in patients with aniridia. Am J Hum Genet 2002; 71(5):1138-1149.

[232] Boccone L, Meloni A, Falchi AM, Usai V, Cao A. Blepharophimosis, ptosis, epicanthus inversus syndrome, a new case associated with de novo balanced autosomal translocation [46,XY,t(3;7)(q23;q32)]. Am J Med Genet 1994; 51(3):258-259.

[233] De Baere E, Fukushima Y, Small K, Udar N, Van Camp G, Verhoeven K, Palotie A, De Paepe A, Messiaen L. Identification of BPESC1, a novel gene disrupted by a balanced chromosomal translocation, t(3;4)(q23;p15.2), in a patient with BPES. Genomics 2000; 68(3):296-304.

[234] De Baere E, Dixon MJ, Small KW, Jabs EW, Leroy BP, Devriendt K, Gillerot Y, Mortier G, Meire F, Van Maldergem L, Courtens W, Hjalgrim H, Huang S, Liebaers I, Van Regemorter N, Touraine P, Praphanphoj V, Verloes A, Udar N, Yellore V, Chalukya M, Yelchits S, De Paepe A, Kuttenn F, Fellous M, Veitia R, Messiaen L. Spectrum of FOXL2 gene mutations in blepharophimosis-ptosis-epicanthus inversus (BPES) families demonstrates a genotype--phenotype correlation. Hum Mol Genet 2001; 10(15):1591-1600.

[235] Toomes C, Dixon MJ. Refinement of a translocation breakpoint associated with blepharophimosis-ptosis-epicanthus inversus syndrome to a 280-kb interval at chromosome 3q23. Genomics 1998; 53(3):308-314.

[236] Fukushima Y, Wakui K, Nishida T, Ueoka Y. Blepharophimosis sequence and de novo balanced autosomal translocation [46,XY,t(3;4)(q23;p15.2)]: possible assignment of the trait to 3q23. Am J Med Genet 1991; 40(4):485-487.

[237] Praphanphoj V, Goodman BK, Thomas GH, Niel KM, Toomes C, Dixon MJ, Geraghty MT. Molecular cytogenetic evaluation in a patient with a translocation (3;21) associated with blepharophimosis, ptosis, epicanthus inversus syndrome (BPES). Genomics 2000; 65(1):67-69.

[238] Wunderle VM, Critcher R, Hastie N, Goodfellow PN, Schedl A. Deletion of long-range regulatory elements upstream of SOX9 causes campomelic dysplasia. Proc Natl Acad Sci U S A 1998; 95(18):10649-10654.

[239] Wunderle VM, Critcher R, Hastie N, Goodfellow PN, Schedl A. Deletion of long-range regulatory elements upstream of SOX9 causes campomelic dysplasia. Proc Natl Acad Sci U S A 1998; 95(18):10649-10654.

[240] Mansour S, Hall CM, Pembrey ME, Young ID. A clinical and genetic study of campomelic dysplasia. J Med Genet 1995; 32(6):415-420.

[241] Velagaleti GV, Bien-Willner GA, Northup JK, Lockhart LH, Hawkins JC, Jalal SM, Withers M, Lupski JR, Stankiewicz P. Position effects due to chromosome breakpoints that map approximately 900 Kb upstream and approximately 1.3 Mb downstream of SOX9 in two patients with campomelic dysplasia. Am J Hum Genet 2005; 76(4):652-662.

[242] Velagaleti GV, Bien-Willner GA, Northup JK, Lockhart LH, Hawkins JC, Jalal SM, Withers M, Lupski JR, Stankiewicz P. Position effects due to chromosome breakpoints that map approximately 900 Kb upstream and approximately 1.3 Mb downstream of SOX9 in two patients with campomelic dysplasia. Am J Hum Genet 2005; 76(4):652-662.

[243] Fernandez B, Siegel-Bartelt J, Herbrick JA, Teshima I, Scherer S. Holoprosencephaly and cleidocranial dysplasia in a patient due to two position-effect mutations: case report and review of the literature. Clin Genet 2005; 68(4):349-359.

[244] de Chadarevian JP, Dunn S, Malatack JJ, Ganguly A, Blecker U, Punnett HH. Chromosome rearrangement with no apparent gene mutation in familial adenomatous polyposis and hepatocellular neoplasia. Pediatr Dev Pathol 2002; 5(1):69-75.

[245] Fernandez B, Siegel-Bartelt J, Herbrick JA, Teshima I, Scherer S. Holoprosencephaly and cleidocranial dysplasia in a patient due to two position-effect mutations: case report and review of the literature. Clin Genet 2005; 68(4):349-359.

[246] Nishimura DY, Swiderski RE, Alward WL, Searby CC, Patil SR, Bennet SR, Kanis AB, Gastier JM, Stone EM, Sheffield VC. The forkhead transcription factor gene FKHL7 is responsible for glaucoma phenotypes which map to 6p25. Nat Genet 1998; 19(2):140-147.

[247] Bovie C, Holden ST, Schroer A, Smith E, Trump D, Raymond FL. Neurofibromatosis 2 in a patient with a de novo balanced reciprocal translocation 46,X,t(X;22)(p11.2;q11.2). J Med Genet 2003; 40(9):682-684.

[248] Trembath DG, Semina EV, Jones DH, Patil SR, Qian Q, Amendt BA, Russo AF, Murray JC. Analysis of two translocation breakpoints and identification of a negative regulatory element in patients with Rieger's syndrome. Birth Defects Res A Clin Mol Teratol 2004; 70(2):82-91.

[249] Datson NA, Semina E, van Staalduinen AA, Dauwerse HG, Meershoek EJ, Heus JJ, Frants RR, den Dunnen JT, Murray JC, van Ommen GJ. Closing in on the Rieger syndrome gene on 4q25: mapping translocation breakpoints within a 50-kb region. Am J Hum Genet 1996; 59(6):1297-1305.

[250] Semina EV, Datson NA, Leysens NJ, Zabel BU, Carey JC, Bell GI, Bitoun P, Lindgren C, Stevenson T, Frants RR, van Ommen G, Murray JC. Exclusion of epidermal growth factor and high-resolution physical mapping across the Rieger syndrome locus. Am J Hum Genet 1996; 59(6):1288-1296.

[251] Datson NA, Semina E, van Staalduinen AA, Dauwerse HG, Meershoek EJ, Heus JJ, Frants RR, den Dunnen JT, Murray JC, van Ommen GJ. Closing in on the Rieger syndrome gene on 4q25: mapping translocation breakpoints within a 50-kb region. Am J Hum Genet 1996; 59(6):1297-1305.

[252] Semina EV, Datson NA, Leysens NJ, Zabel BU, Carey JC, Bell GI, Bitoun P, Lindgren C, Stevenson T, Frants RR, van Ommen G, Murray JC. Exclusion of epidermal growth factor and high-resolution physical mapping across the Rieger syndrome locus. Am J Hum Genet 1996; 59(6):1288-1296.

[253] Trembath DG, Semina EV, Jones DH, Patil SR, Qian Q, Amendt BA, Russo AF, Murray JC. Analysis of two translocation breakpoints and identification of a negative regulatory element in patients with Rieger's syndrome. Birth Defects Res A Clin Mol Teratol 2004; 70(2):82-91.

[254] Cai J, Goodman BK, Patel AS, Mulliken JB, Van Maldergem L, Hoganson GE, Paznekas WA, Ben Neriah Z, Sheffer R, Cunningham ML, Daentl DL, Jabs EW. Increased risk for developmental delay in Saethre-Chotzen syndrome is associated with TWIST deletions: an improved strategy for TWIST mutation screening. Hum Genet 2003; 114(1):68-76.

[255] Reid CS, McMorrow LE, McDonald-McGinn DM, Grace KJ, Ramos FJ, Zackai EH, Cohen MM, Jr., Jabs EW. Saethre-Chotzen syndrome with familial translocation at chromosome 7p22. Am J Med Genet 1993; 47(5):637-639.

[256] Krebs I, Weis I, Hudler M, Rommens JM, Roth H, Scherer SW, Tsui LC, Fuchtbauer EM, Grzeschik KH, Tsuji K, Kunz J. Translocation breakpoint

maps 5 kb 3' from TWIST in a patient affected with Saethre-Chotzen syndrome. Hum Mol Genet 1997; 6(7):1079-1086.

[257] Cai J, Goodman BK, Patel AS, Mulliken JB, Van Maldergem L, Hoganson GE, Paznekas WA, Ben Neriah Z, Sheffer R, Cunningham ML, Daentl DL, Jabs EW. Increased risk for developmental delay in Saethre-Chotzen syndrome is associated with TWIST deletions: an improved strategy for TWIST mutation screening. Hum Genet 2003; 114(1):68-76.

[258] Marlin S, Blanchard S, Slim R, Lacombe D, Denoyelle F, Alessandri JL, Calzolari E, Drouin-Garraud V, Ferraz FG, Fourmaintraux A, Philip N, Toublanc JE, Petit C. Townes-Brocks syndrome: detection of a SALL1 mutation hot spot and evidence for a position effect in one patient. Hum Mutat 1999; 14(5):377-386.

[259] Serville F, Lacombe D, Saura R, Billeaud C, Sergent MP. Townes-Brocks syndrome in an infant with translocation t (5;16). Genet Couns 1993; 4(2):109-112.

[260] Dlugaszewska B, Silahtaroglu A, Menzel C, Kubart S, Cohen M, Mundlos S, Tumer Z, Kjaer K, Friedrich U, Ropers HH, Tommerup N, Neitzel H, Kalscheuer VM. Breakpoints around the HOXD cluster result in various limb malformations. J Med Genet 2006; 43(2):111-118.

[261] Dlugaszewska B, Silahtaroglu A, Menzel C, Kubart S, Cohen M, Mundlos S, Tumer Z, Kjaer K, Friedrich U, Ropers HH, Tommerup N, Neitzel H, Kalscheuer VM. Breakpoints around the HOXD cluster result in various limb malformations. J Med Genet 2006; 43(2):111-118.

[262] Dlugaszewska B, Silahtaroglu A, Menzel C, Kubart S, Cohen M, Mundlos S, Tumer Z, Kjaer K, Friedrich U, Ropers HH, Tommerup N, Neitzel H, Kalscheuer VM. Breakpoints around the HOXD cluster result in various limb malformations. J Med Genet 2006; 43(2):111-118.

[263] Muncke N, Wogatzky BS, Breuning M, Sistermans EA, Endris V, Ross M, Vetrie D, Catsman-Berrevoets CE, Rappold G. Position effect on PLP1 may cause a subset of Pelizaeus-Merzbacher disease symptoms. J Med Genet 2004; 41(12):e121.

[264] Johnson D, Horsley SW, Moloney DM, Oldridge M, Twigg SR, Walsh S, Barrow M, Njolstad PR, Kunz J, Ashworth GJ, Wall SA, Kearney L, Wilkie AO. A comprehensive screen for TWIST mutations in patients with craniosynostosis identifies a new microdeletion syndrome of chromosome band 7p21.1. Am J Hum Genet 1998; 63(5):1282-1293.

[265] Krantz ID, Rand EB, Genin A, Hunt P, Jones M, Louis AA, Graham JM, Jr., Bhatt S, Piccoli DA, Spinner NB. Deletions of 20p12 in Alagille syndrome: frequency and molecular characterization. Am J Med Genet 1997; 70(1):80-86.

[266] Spinner NB, Rand EB, Fortina P, Genin A, Taub R, Semeraro A, Piccoli DA. Cytologically balanced t(2;20) in a two-generation family with alagille

syndrome: cytogenetic and molecular studies. Am J Hum Genet 1994; 55(2):238-243.

[267] Krantz ID, Colliton RP, Genin A, Rand EB, Li L, Piccoli DA, Spinner NB. Spectrum and frequency of jagged1 (JAG1) mutations in Alagille syndrome patients and their families. Am J Hum Genet 1998; 62(6):1361-1369.

[268] Oda T, Elkahloun AG, Meltzer PS, Okajima K, Sugiyama K, Wada Y, Chandrasekharappa SC. Identification of a larger than 3 Mb deletion including JAG1 in an Alagille syndrome patient with a translocation t(3;20)(q13.3;p12.2). Hum Mutat 2000; 16(1):92.

[269] Mundlos S, Otto F, Mundlos C, Mulliken JB, Aylsworth AS, Albright S, Lindhout D, Cole WG, Henn W, Knoll JH, Owen MJ, Mertelsmann R, Zabel BU, Olsen BR. Mutations involving the transcription factor CBFA1 cause cleidocranial dysplasia. Cell 1997; 89(5):773-779.

[270] Nienhaus H, Mau U, Zang KD, Henn W. Pericentric inversion of chromosome 6 in a patient with cleidocranial dysplasia. Am J Med Genet 1993; 46(6):630-631.

[271] Fantes J, Ragge NK, Lynch SA, McGill NI, Collin JR, Howard-Peebles PN, Hayward C, Vivian AJ, Williamson K, van Heyningen V, FitzPatrick DR. Mutations in SOX2 cause anophthalmia. Nat Genet 2003; 33(4):461-463.

[272] Driggers RW, Macri CJ, Greenwald J, Carpenter D, Avallone J, Howard-Peebles PN, Levin SW. Isolated bilateral anophthalmia in a girl with an apparently balanced de novo translocation: 46,XX,t(3;11)(q27;p11.2). Am J Med Genet 1999; 87(3):201-202.

[273] Krepischi-Santos AC, Carneiro JD, Svartman M, Bendit I, Odone-Filho V, Vianna-Morgante AM. Deletion of the factor IX gene as a result of translocation t(X;1) in a girl affected by haemophilia B. Br J Haematol 2001; 113(3):616-620.

[274] Journel H, Melki J, Turleau C, Munnich A, de Grouchy J. Rett phenotype with X/autosome translocation: possible mapping to the short arm of chromosome X. Am J Med Genet 1990; 35(1):142-147.

[275] Ellison KA, Roth EJ, McCabe ER, Chinault AC, Zoghbi HY. Isolation of a yeast artificial chromosome contig spanning the X chromosomal translocation breakpoint in a patient with Rett syndrome. Am J Med Genet 1993; 47(7):1124-1134.

[276] Zoghbi HY, Ledbetter DH, Schultz R, Percy AK, Glaze DG. A de novo X;3 translocation in Rett syndrome. Am J Med Genet 1990; 35(1):148-151.

[277] Borg I, Freude K, Kubart S, Hoffmann K, Menzel C, Laccone F, Firth H, Ferguson-Smith MA, Tommerup N, Ropers HH, Sargan D, Kalscheuer VM. Disruption of Netrin G1 by a balanced chromosome translocation in a girl with Rett syndrome. Eur J Hum Genet 2005.

[278] Simonic I, Gericke GS, Lippert M, Schoeman JF. Additional clinical and cytogenetic findings associated with Rett syndrome. Am J Med Genet 1997; 74(3):331-337.

[279] Wahlstrom J, Anvret M. Chromosome findings in the Rett syndrome and a test of a two-step mutation theory. Am J Med Genet Suppl 1986; 1:361-368.

[280] Scala E, Ariani F, Mari F, Caselli R, Pescucci C, Longo I, Meloni I, Giachino D, Bruttini M, Hayek G, Zappella M, Renieri A. CDKL5/STK9 is mutated in Rett syndrome variant with infantile spasms. J Med Genet 2005; 42(2):103-107.

[281] Siu VM, Gonder JR, Jung JH, Sergovich FR, Flintoff WF. Choroideremia associated with an X-autosomal translocation. Hum Genet 1990; 84(5):459-464.

[282] Lindenbaum RH, Clarke G, Patel C, Moncrieff M, Hughes JT. Muscular dystrophy in an X; 1 translocation female suggests that Duchenne locus is on X chromosome short arm. J Med Genet 1979; 16(5):389-392.

[283] Cohen MM, Lin CC, Sybert V, Orecchio EJ. Two human X-autosome translocations identified by autoradiography and fluorescence. Am J Hum Genet 1972; 24(5):583-597.

[284] Hodgson SV, Heckmatt JZ, Hughes E, Crolla JA, Dubowitz V, Bobrow M. A balanced de novo X/autosome translocation in a girl with manifestations of Lowe syndrome. Am J Med Genet 1986; 23(3):837-847.

[285] Kapur S, Higgins JV, Delp K, Rogers B. Menkes syndrome in a girl with X-autosome translocation. Am J Med Genet 1987; 26(2):503-510.

[286] Bienvenu T, Der-Sarkissian H, Billuart P, Tissot M, des Portes V, Bruls T, Chabrolle JP, Chauveau P, Cherry M, Kahn A, Cohen D, Beldjord C, Chelly J, Cherif D. Mapping of the X-breakpoint involved in a balanced X;12 translocation in a female with mild mental retardation. Eur J Hum Genet 1997; 5(2):105-109.

[287] Punnett HH. Simpson-Golabi-Behmel syndrome (SGBS) in a female with an X-autosome translocation. Am J Med Genet 1994; 50(4):391-393.

[288] Punnett HH, Kistermacher ML, Greene AE, Coriell LL. An (X;1) translocation, balanced, 46 chromosomes. Repository identification no. GM-97. Cytogenet Cell Genet 1974; 13(4):406-407.

[289] Van Maldergem L, Espeel M, Roels F, Petit C, Dacremont G, Wanders RJ, Verloes A, Gillerot Y. X-linked recessive chondrodysplasia punctata with XY translocation in a stillborn fetus. Hum Genet 1991; 87(6):661-664.

[290] Seidel J, Schiller S, Kelbova C, Beensen V, Orth U, Vogt S, Claussen U, Zintl F, Rappold GA. Brachytelephalangic dwarfism due to the loss of ARSE and SHOX genes resulting from an X;Y translocation. Clin Genet 2001; 59(2):115-121.

[291] Cremers FP, van de Pol DJ, van Kerkhoff LP, Wieringa B, Ropers HH. Cloning of a gene that is rearranged in patients with choroideraemia. Nature 1990; 347(6294):674-677.

[292] Ray PN, Belfall B, Duff C, Logan C, Kean V, Thompson MW, Sylvester JE, Gorski JL, Schmickel RD, Worton RG. Cloning of the breakpoint of an X;21 translocation associated with Duchenne muscular dystrophy. Nature 1985; 318(6047):672-675.

[293] Srivastava AK, Montonen O, Saarialho-Kere U, Chen E, Baybayan P, Pispa J, Limon J, Schlessinger D, Kere J. Fine mapping of the EDA gene: a translocation breakpoint is associated with a CpG island that is transcribed. Am J Hum Genet 1996; 58(1):126-132.

[294] Gleeson JG, Allen KM, Fox JW, Lamperti ED, Berkovic S, Scheffer I, Cooper EC, Dobyns WB, Minnerath SR, Ross ME, Walsh CA. Doublecortin, a brain-specific gene mutated in human X-linked lissencephaly and double cortex syndrome, encodes a putative signaling protein. Cell 1998; 92(1):63-72.

[295] Attree O, Olivos IM, Okabe I, Bailey LC, Nelson DL, Lewis RA, McInnes RR, Nussbaum RL. The Lowe's oculocerebrorenal syndrome gene encodes a protein highly homologous to inositol polyphosphate-5-phosphatase. Nature 1992; 358(6383):239-242.

[296] Billuart P, Bienvenu T, Ronce N, des Portes V, Vinet MC, Zemni R, Roest CH, Carrie A, Fauchereau F, Cherry M, Briault S, Hamel B, Fryns JP, Beldjord C, Kahn A, Moraine C, Chelly J. Oligophrenin-1 encodes a rhoGAP protein involved in X-linked mental retardation. Nature 1998; 392(6679):923-926.

[297] Pilia G, Hughes-Benzie RM, MacKenzie A, Baybayan P, Chen EY, Huber R, Neri G, Cao A, Forabosco A, Schlessinger D. Mutations in GPC3, a glypican gene, cause the Simpson-Golabi-Behmel overgrowth syndrome. Nat Genet 1996; 12(3):241-247.

[298] Xu W, Robert C, Thornton PS, Spinner NB. Complete androgen insensitivity syndrome due to X chromosome inversion: a clinical report. Am J Med Genet A 2003; 120(3):434-436.

[299] Krepischi-Santos AC, Carneiro JD, Svartman M, Bendit I, Odone-Filho V, Vianna-Morgante AM. Deletion of the factor IX gene as a result of translocation t(X;1) in a girl affected by haemophilia B. Br J Haematol 2001; 113(3):616-620.

[300] Schroder W, Poetsch M, Gazda H, Werner W, Reichelt T, Knoll W, Rokicka-Milewska R, Zieleniewska B, Herrmann FH. A de novo translocation 46,X,t(X;15) causing haemophilia B in a girl: a case report. Br J Haematol 1998; 100(4):750-757.

[301] Imai K, Shimadzu M, Kubota T, Morio T, Matsunaga T, Park YD, Yoshioka A, Nonoyama S. Female hyper IgM syndrome type 1 with a chromosomal translocation disrupting CD40LG. Biochim Biophys Acta 2006; 1762(3):335-340.

[302] Verloes A, David A, Odent S, Toutain A, Andre MJ, Lucas J, Le Marec B. Opitz GBBB syndrome: chromosomal evidence of an X-linked form. Am J Med Genet 1995; 59(1):123-128.

[303] Zenker M, Wermuth B, Trautmann U, Knerr I, Kraus C, Rauch A, Reis A. Severe, neonatal-onset OTC deficiency in twin sisters with a de novo balanced reciprocal translocation t(X;5)(p21.1;q11). Am J Med Genet 2004.

[304] Simonic I, Gericke GS, Lippert M, Schoeman JF. Additional clinical and cytogenetic findings associated with Rett syndrome. Am J Med Genet 1997; 74(3):331-337.

[305] Borg I, Freude K, Kubart S, Hoffmann K, Menzel C, Laccone F, Firth H, Ferguson-Smith MA, Tommerup N, Ropers HH, Sargan D, Kalscheuer VM. Disruption of Netrin G1 by a balanced chromosome translocation in a girl with Rett syndrome. Eur J Hum Genet 2005.

[306] Zoghbi HY, Ledbetter DH, Schultz R, Percy AK, Glaze DG. A de novo X;3 translocation in Rett syndrome. Am J Med Genet 1990; 35(1):148-151.

[307] Ellison KA, Roth EJ, McCabe ER, Chinault AC, Zoghbi HY. Isolation of a yeast artificial chromosome contig spanning the X chromosomal translocation breakpoint in a patient with Rett syndrome. Am J Med Genet 1993; 47(7):1124-1134.

[308] Journel H, Melki J, Turleau C, Munnich A, de Grouchy J. Rett phenotype with X/autosome translocation: possible mapping to the short arm of chromosome X. Am J Med Genet 1990; 35(1):142-147.

[309] Hearn T, Renforth GL, Spalluto C, Hanley NA, Piper K, Brickwood S, White C, Connolly V, Taylor JF, Russell-Eggitt I, Bonneau D, Walker M, Wilson DI. Mutation of ALMS1, a large gene with a tandem repeat encoding 47 amino acids, causes Alstrom syndrome. Nat Genet 2002; 31(1):79-83.

[310] Gessler M, Simola KO, Bruns GA. Cloning of breakpoints of a chromosome translocation identifies the AN2 locus. Science 1989; 244(4912):1575-1578.

[311] Fukushima Y, Wakui K, Nishida T, Ueoka Y. Blepharophimosis sequence and de novo balanced autosomal translocation [46,XY,t(3;4)(q23;p15.2)]: possible assignment of the trait to 3q23. Am J Med Genet 1991; 40(4):485-487.

[312] Young ID, Zuccollo JM, Maltby EL, Broderick NJ. Campomelic dysplasia associated with a de novo 2q;17q reciprocal translocation. J Med Genet 1992; 29(4):251-252.

[313] Maraia R, Saal HM, Wangsa D. A chromosome 17q de novo paracentric inversion in a patient with campomelic dysplasia; case report and etiologic hypothesis. Clin Genet 1991; 39(6):401-408.

[314] Nienhaus H, Mau U, Zang KD, Henn W. Pericentric inversion of chromosome 6 in a patient with cleidocranial dysplasia. Am J Med Genet 1993; 46(6):630-631.

[315] Tonkin ET, Wang TJ, Lisgo S, Bamshad MJ, Strachan T. NIPBL, encoding a homolog of fungal Scc2-type sister chromatid cohesion proteins and fly Nipped-B, is mutated in Cornelia de Lange syndrome. Nat Genet 2004; 36(6):636-641.

[316] Gustavsson P, Skeppner G, Johansson B, Berg T, Gordon L, Kreuger A, Dahl N. Diamond-Blackfan anaemia in a girl with a de novo balanced reciprocal X;19 translocation. J Med Genet 1997; 34(9):779-782.

[317] Tommerup N, Nielsen F. A familial reciprocal translocation t(3;7) (p21.1;p13) associated with the Greig polysyndactyly-craniofacial anomalies syndrome. Am J Med Genet 1983; 16(3):313-321.

[318] Schell U, Wienberg J, Kohler A, Bray-Ward P, Ward DE, Wilson WG, Allen WP, Lebel RR, Sawyer JR, Campbell PL, Aughton DJ, Punnett HH, Lammer EJ, Kao FT, Ward DC, Muenke M. Molecular characterization of breakpoints in patients with holoprosencephaly and definition of the HPE2 critical region 2p21. Hum Mol Genet 1996; 5(2):223-229.

[319] Terrett JA, Newbury-Ecob R, Smith NM, Li QY, Garrett C, Cox P, Bonnet D, Lyonnet S, Munnich A, Buckler AJ, Brook JD. A translocation at 12q2 refines the interval containing the Holt-Oram syndrome 1 gene. Am J Hum Genet 1996; 59(6):1337-1341.

[320] Erickson RP, Hudgins L, Stone JF, Schmidt S, Wilke C, Glover TW. A "balanced" Y;16 translocation associated with Turner-like neonatal lymphedema suggests the location of a potential anti-Turner gene on the Y chromosome. Cytogenet Cell Genet 1995; 71(2):163-167.

[321] Ogle RF, Dalzell P, Turner G, Wass D, Yip MY. Multiple exostoses in a patient with t(8;11)(q24.11;p15.5). J Med Genet 1991; 28(12):881-883.

[322] Duba HC, Erdel M, Loffler J, Wirth J, Utermann B, Utermann G. Nail patella syndrome in a cytogenetically balanced t(9;17)(q34.1;q25) carrier. Eur J Hum Genet 1998; 6(1):75-79.

[323] Imaizumi K, Kuroki Y. Rubinstein-Taybi syndrome with de novo reciprocal translocation t(2;16)(p13.3;p13.3). Am J Med Genet 1991; 38(4):636-639.

[324] Tommerup N, van der Hagen CB, Heiberg A. Tentative assignment of a locus for Rubinstein-Taybi syndrome to 16p13.3 by a de novo reciprocal translocation, t(7;16)(q34;p13.3). Am J Med Genet 1992; 44(2):237-241.

[325] Lacombe D, Saura R, Taine L, Battin J. Confirmation of assignment of a locus for Rubinstein-Taybi syndrome gene to 16p13.3. Am J Med Genet 1992; 44(1):126-128.

[326] Lai CS, Fisher SE, Hurst JA, Levy ER, Hodgson S, Fox M, Jeremiah S, Povey S, Jamison DC, Green ED, Vargha-Khadem F, Monaco AP. The SPCH1 region on human 7q31: genomic characterization of the critical interval and localization of translocations associated with speech and language disorder. Am J Hum Genet 2000; 67(2):357-368.

[327] Curran ME, Atkinson DL, Ewart AK, Morris CA, Leppert MF, Keating MT. The elastin gene is disrupted by a translocation associated with supravalvular aortic stenosis. Cell 1993; 73(1):159-168.

[328] Ishikiriyama S, Tonoki H, Shibuya Y, Chin S, Harada N, Abe K, Niikawa N. Waardenburg syndrome type I in a child with de novo inversion (2)(q35q37.3). Am J Med Genet 1989; 33(4):505-507.

[329] Pfeiffer RA, Ott R, Gilgenkrantz S, Alexandre P. Deficiency of coagulation factors VII and X associated with deletion of a chromosome 13 (q34). Evidence from two cases with 46,XY,t(13;Y)(q11;q34). Hum Genet 1982; 62(4):358-360.

[330] Walder RY, Shalev H, Brennan TM, Carmi R, Elbedour K, Scott DA, Hanauer A, Mark AL, Patil S, Stone EM, Sheffield VC. Familial hypomagnesemia maps to chromosome 9q, not to the X chromosome: genetic linkage mapping and analysis of a balanced translocation breakpoint. Hum Mol Genet 1997; 6(9):1491-1497.

[331] Whelan AJ, Watson MS, Porter FD, Steiner RD. Klippel-Trenaunay-Weber syndrome associated with a 5:11 balanced translocation. Am J Med Genet 1995; 59(4):492-494.

[332] Maroun C, Schmerler S, Hutcheon RG. Child with Sotos phenotype and a 5:15 translocation. Am J Med Genet 1994; 50(3):291-293.

[333] Imaizumi K, Kimura J, Matsuo M, Kurosawa K, Masuno M, Niikawa N, Kuroki Y. Sotos syndrome associated with a de novo balanced reciprocal translocation t(5;8)(q35;q24.1). Am J Med Genet 2002; 107(1):58-60.

[334] Driggers RW, Macri CJ, Greenwald J, Carpenter D, Avallone J, Howard-Peebles PN, Levin SW. Isolated bilateral anophthalmia in a girl with an apparently balanced de novo translocation: 46,XX,t(3;11)(q27;p11.2). Am J Med Genet 1999; 87(3):201-202.

[335] Kurbasic M, Jones FV, Cook LN. Bilateral microphthalmos with colobomatous orbital cyst and de-novo balanced translocation t(3;5). Ophthalmic Genet 2000; 21(4):239-242.

[336] Chong SS, Pack SD, Roschke AV, Tanigami A, Carrozzo R, Smith AC, Dobyns WB, Ledbetter DH. A revision of the lissencephaly and Miller-Dieker syndrome critical regions in chromosome 17p13.3. Hum Mol Genet 1997; 6(2):147-155.

[337] Tonkin ET, Wang TJ, Lisgo S, Bamshad MJ, Strachan T. NIPBL, encoding a homolog of fungal Scc2-type sister chromatid cohesion proteins and fly Nipped-B, is mutated in Cornelia de Lange syndrome. Nat Genet 2004; 36(6):636-641.

[338] Draptchinskaia N, Gustavsson P, Andersson B, Pettersson M, Willig TN, Dianzani I, Ball S, Tchernia G, Klar J, Matsson H, Tentler D, Mohandas N, Carlsson B, Dahl N. The gene encoding ribosomal protein S19 is mutated in Diamond-Blackfan anaemia. Nat Genet 1999; 21(2):169-175.

[339] Vortkamp A, Gessler M, Grzeschik KH. GLI3 zinc-finger gene interrupted by translocations in Greig syndrome families. Nature 1991; 352(6335):539-540.

[340] Wallis DE, Roessler E, Hehr U, Nanni L, Wiltshire T, Richieri-Costa A, Gillessen-Kaesbach G, Zackai EH, Rommens J, Muenke M. Mutations in the homeodomain of the human SIX3 gene cause holoprosencephaly. Nat Genet 1999; 22(2):196-198.

[341] Belloni E, Muenke M, Roessler E, Traverso G, Siegel-Bartelt J, Frumkin A, Mitchell HF, Donis-Keller H, Helms C, Hing AV, Heng HH, Koop B, Martindale D, Rommens JM, Tsui LC, Scherer SW. Identification of Sonic hedgehog as a candidate gene responsible for holoprosencephaly. Nat Genet 1996; 14(3):353-356.

[342] Basson CT, Bachinsky DR, Lin RC, Levi T, Elkins JA, Soults J, Grayzel D, Kroumpouzou E, Traill TA, Leblanc-Straceski J, Renault B, Kucherlapati R, Seidman JG, Seidman CE. Mutations in human TBX5 [corrected] cause limb and cardiac malformation in Holt-Oram syndrome. Nat Genet 1997; 15(1):30-35.

[343] Nishimura DY, Swiderski RE, Alward WL, Searby CC, Patil SR, Bennet SR, Kanis AB, Gastier JM, Stone EM, Sheffield VC. The forkhead transcription factor gene FKHL7 is responsible for glaucoma phenotypes which map to 6p25. Nat Genet 1998; 19(2):140-147.

[344] Ahn J, Ludecke HJ, Lindow S, Horton WA, Lee B, Wagner MJ, Horsthemke B, Wells DE. Cloning of the putative tumour suppressor gene for hereditary multiple exostoses (EXT1). Nat Genet 1995; 11(2):137-143.

[345] Narahara K, Baker E, Ito S, Yokoyama Y, Yu S, Hewitt D, Sutherland GR, Eccles MR, Richards RI. Localisation of a 10q breakpoint within the PAX2 gene in a patient with a de novo t(10;13) translocation and optic nerve coloboma-renal disease. J Med Genet 1997; 34(3):213-216.

[346] Higgins MJ, Hansen MF, Cavenee WK, Lalande M. Molecular detection of chromosomal translocations that disrupt the putative retinoblastoma susceptibility locus. Mol Cell Biol 1989; 9(1):1-5.

[347] Semina EV, Datson NA, Leysens NJ, Zabel BU, Carey JC, Bell GI, Bitoun P, Lindgren C, Stevenson T, Frants RR, van Ommen G, Murray JC. Exclusion of epidermal growth factor and high-resolution physical mapping across the Rieger syndrome locus. Am J Hum Genet 1996; 59(6):1288-1296.

[348] Petrij F, Giles RH, Dauwerse HG, Saris JJ, Hennekam RC, Masuno M, Tommerup N, van Ommen GJ, Goodman RH, Peters DJ, . Rubinstein-Taybi syndrome caused by mutations in the transcriptional co-activator CBP. Nature 1995; 376(6538):348-351.

[349] Lai CS, Fisher SE, Hurst JA, Vargha-Khadem F, Monaco AP. A forkhead-domain gene is mutated in a severe speech and language disorder. Nature 2001; 413(6855):519-523.

[350] Curran ME, Atkinson DL, Ewart AK, Morris CA, Leppert MF, Keating MT. The elastin gene is disrupted by a translocation associated with supravalvular aortic stenosis. Cell 1993; 73(1):159-168.

[351] Tsukamoto K, Tohma T, Ohta T, Yamakawa K, Fukushima Y, Nakamura Y, Niikawa N. Cloning and characterization of the inversion breakpoint at chromosome 2q35 in a patient with Waardenburg syndrome type I. Hum Mol Genet 1992; 1(5):315-317.

[352] Hearn T, Renforth GL, Spalluto C, Hanley NA, Piper K, Brickwood S, White C, Connolly V, Taylor JF, Russell-Eggitt I, Bonneau D, Walker M, Wilson DI. Mutation of ALMS1, a large gene with a tandem repeat encoding 47 amino acids, causes Alstrom syndrome. Nat Genet 2002; 31(1):79-83.

[353] Sun Y, Nicholls RD, Butler MG, Saitoh S, Hainline BE, Palmer CG. Breakage in the SNRPN locus in a balanced 46,XY,t(15;19) Prader-Willi syndrome patient. Hum Mol Genet 1996; 5(4):517-524.

[354] Tian XL, Kadaba R, You SA, Liu M, Timur AA, Yang L, Chen Q, Szafranski P, Rao S, Wu L, Housman DE, DiCorleto PE, Driscoll DJ, Borrow J, Wang Q. Identification of an angiogenic factor that when mutated causes susceptibility to Klippel-Trenaunay syndrome. Nature 2004; 427(6975):640-645.

[355] Kurotaki N, Imaizumi K, Harada N, Masuno M, Kondoh T, Nagai T, Ohashi H, Naritomi K, Tsukahara M, Makita Y, Sugimoto T, Sonoda T, Hasegawa T, Chinen Y, Tomita Ha HA, Kinoshita A, Mizuguchi T, Yoshiura KK, Ohta T, Kishino T, Fukushima Y, Niikawa N, Matsumoto N. Haploinsufficiency of NSD1 causes Sotos syndrome. Nat Genet 2002; 30(4):365-366.

[356] Fantes J, Ragge NK, Lynch SA, McGill NI, Collin JR, Howard-Peebles PN, Hayward C, Vivian AJ, Williamson K, van Heyningen V, FitzPatrick DR. Mutations in SOX2 cause anophthalmia. Nat Genet 2003; 33(4):461-463.

[357] Chong SS, Pack SD, Roschke AV, Tanigami A, Carrozzo R, Smith AC, Dobyns WB, Ledbetter DH. A revision of the lissencephaly and Miller-Dieker syndrome critical regions in chromosome 17p13.3. Hum Mol Genet 1997; 6(2):147-155.

[358] Hoovers JM, Kalikin LM, Johnson LA, Alders M, Redeker B, Law DJ, Bliek J, Steenman M, Benedict M, Wiegant J, Lengauer C, Taillon-Miller P, Schlessinger D, Edwards MC, Elledge SJ, Ivens A, Westerveld A, Little P, Mannens M, Feinberg AP. Multiple genetic loci within 11p15 defined by Beckwith-Wiedemann syndrome rearrangement breakpoints and subchromosomal transferable fragments. Proc Natl Acad Sci U S A 1995; 92(26):12456-12460.

[359] Pueschel SM, Padre-Mendoza T. Chromosome 11 and Beckwith-Wiedemann syndrome. J Pediatr 1984; 104(3):484-485.

[360] Tommerup N, Brandt CA, Pedersen S, Bolund L, Kamper J. Sex dependent transmission of Beckwith-Wiedemann syndrome associated with a reciprocal translocation t(9;11)(p11.2;p15.5). J Med Genet 1993; 30(11):958-961.

[361] Boccone L, Meloni A, Falchi AM, Usai V, Cao A. Blepharophimosis, ptosis, epicanthus inversus syndrome, a new case associated with de novo balanced autosomal translocation [46,XY,t(3;7)(q23;q32)]. Am J Med Genet 1994; 51(3):258-259.

[362] De Baere E, Fukushima Y, Small K, Udar N, Van Camp G, Verhoeven K, Palotie A, De Paepe A, Messiaen L. Identification of BPESC1, a novel gene disrupted by a balanced chromosomal translocation, t(3;4)(q23;p15.2), in a patient with BPES. Genomics 2000; 68(3):296-304.

[363] De Baere E, Dixon MJ, Small KW, Jabs EW, Leroy BP, Devriendt K, Gillerot Y, Mortier G, Meire F, Van Maldergem L, Courtens W, Hjalgrim H, Huang S, Liebaers I, Van Regemorter N, Touraine P, Praphanphoj V, Verloes A, Udar N, Yellore V, Chalukya M, Yelchits S, De Paepe A, Kuttenn F, Fellous M, Veitia R, Messiaen L. Spectrum of FOXL2 gene mutations in blepharophimosis-ptosis-epicanthus inversus (BPES) families demonstrates a genotype--phenotype correlation. Hum Mol Genet 2001; 10(15):1591-1600.

[364] Toomes C, Dixon MJ. Refinement of a translocation breakpoint associated with blepharophimosis-ptosis-epicanthus inversus syndrome to a 280-kb interval at chromosome 3q23. Genomics 1998; 53(3):308-314.

[365] Fukushima Y, Wakui K, Nishida T, Ueoka Y. Blepharophimosis sequence and de novo balanced autosomal translocation [46,XY,t(3;4)(q23;p15.2)]: possible assignment of the trait to 3q23. Am J Med Genet 1991; 40(4):485-487.

[366] Cabral de Almeida JC, Llerena JC, Jr., Neto JBG, Jung M, Martins RR. Another example favouring the location of BPES at 3q2. J Med Genet 1993; 30:86-88.

[367] Praphanphoj V, Goodman BK, Thomas GH, Niel KM, Toomes C, Dixon MJ, Geraghty MT. Molecular cytogenetic evaluation in a patient with a translocation (3;21) associated with blepharophimosis, ptosis, epicanthus inversus syndrome (BPES). Genomics 2000; 65(1):67-69.

[368] Karimi-Nejad A, Karimi-Nejad R, Najafi H, Karimi-Nejad MH. Blepharophimosis syndrome (BPES) and additional abnormalities in a female with a balanced X:3 translocation. Clin Dysmorphol 1996; 5(3):259-261.

[369] Die-Smulders CE, Engelen JJ, Donk JM, Fryns JP. Further evidence for the location of the BPES gene at 3q2. J Med Genet 1991; 28(10):725.

[370] Johnson DS, Morrison N, Grant L, Turner T, Fantes J, Connor JM, Murday VA. Confirmation of CHD7 as a cause of CHARGE association identified by mapping a balanced chromosome translocation in affected monozygotic twins. J Med Genet 2005.

[371] Mundlos S, Otto F, Mundlos C, Mulliken JB, Aylsworth AS, Albright S, Lindhout D, Cole WG, Henn W, Knoll JH, Owen MJ, Mertelsmann R, Zabel BU, Olsen BR. Mutations involving the transcription factor CBFA1 cause cleidocranial dysplasia. Cell 1997; 89(5):773-779.

[372] Sawada A, Takihara Y, Kim JY, Matsuda-Hashii Y, Tokimasa S, Fujisaki H, Kubota K, Endo H, Onodera T, Ohta H, Ozono K, Hara J. A congenital mutation of the novel gene LRRC8 causes agammaglobulinemia in humans. J Clin Invest 2003; 112(11):1707-1713.

[373] Price N, Bahra M, Griffin D, Hanna G, Stock A. Cornelia de Lange Syndrome in association with a balanced reciprocal translocation involving chromosomes 3 and 5. Prenat Diagn 2005; 25(7):602-603.

[374] Muncke N, Jung C, Rudiger H, Ulmer H, Roeth R, Hubert A, Goldmuntz E, Driscoll D, Goodship J, Schon K, Rappold G. Missense mutations and gene interruption in PROSIT240, a novel TRAP240-like gene, in patients with congenital heart defect (transposition of the great arteries). Circulation 2003; 108(23):2843-2850.

[375] Salomon-Nguyen F, Coniat-Busson M, Heilig R, Campion D, Weissenbach J, Berger R. Evidence of chromosomal inversion using fluorescence in situ hybridization to stretched DNA. C R Acad Sci III 1998; 321(6):447-452.

[376] Toriello HV, Glover TW, Takahara K, Byers PH, Miller DE, Higgins JV, Greenspan DS. A translocation interrupts the COL5A1 gene in a patient with Ehlers-Danlos syndrome and hypomelanosis of Ito. Nat Genet 1996; 13(3):361-365.

[377] van der Luijt RB, Tops CM, Khan PM, van der Klift HM, Breukel C, Leeuwen-Cornelisse IS, Dauwerse HG, Beverstock GC, van Noort E, Snel P, . Molecular, cytogenetic, and phenotypic studies of a constitutional reciprocal translocation t(5;10)(q22;q25) responsible for familial adenomatous polyposis in a Dutch pedigree. Genes Chromosomes Cancer 1995; 13(3):192-202.

[378] Nadal M, Valiente A, Domenech A, Pritchard M, Estivill X, Ramos-Arroyo MA. Hereditary neuropathy with liability to pressure palsies: two cases with a reciprocal translocation t(16;17)(q12;11.2) interrupting the PMP22 gene. J Med Genet 2000; 37(5):396-398.

[379] Faisal AS, Marsh DJ, Weremowicz S, Morton CC, Williams DM, Eng C. Balanced translocation of 10q and13q, including the PTEN gene, in a boy with a human chorionic gonadotropin-secreting tumor and the Bannayan-Riley-Ruvalcaba syndrome. J Clin Endocrinol Metab 1999; 84(12):4665-4670.

[380] Kehrer-Sawatzki H, Assum G, Hameister H. Molecular characterisation of t(17;22)(q11.2;q11.2) is not consistent with NF1 gene duplication. Hum Genet 2002; 111(4-5):465-467.

[381] Bovie C, Holden ST, Schroer A, Smith E, Trump D, Raymond FL. Neurofibromatosis 2 in a patient with a de novo balanced reciprocal translocation 46,X,t(X;22)(p11.2;q11.2). J Med Genet 2003; 40(9):682-684.

[382] Arai E, Ikeuchi T, Karasawa S, Tamura A, Yamamoto K, Kida M, Ichimura K, Yuasa Y, Tonomura A. Constitutional translocation t(4;22) (q12;q12.2)

associated with neurofibromatosis type 2. Am J Med Genet 1992; 44(2):163-167.

[383] Tsilchorozidou T, Menko FH, Lalloo F, Kidd A, De Silva R, Thomas H, Smith P, Malcolmson A, Dore J, Madan K, Brown A, Yovos JG, Tsaligopoulos M, Vogiatzis N, Baser M, Wallace AJ, Evans DG. Constitutional rearrangements of chromosome 22 as a cause of neurofibromatosis 2. J Med Genet 2004; 41(7):529-534.

[384] Rose CS, King AA, Summers D, Palmer R, Yang S, Wilkie AO, Reardon W, Malcolm S, Winter RM. Localization of the genetic locus for Saethre-Chotzen syndrome to a 6 cM region of chromosome 7 using four cases with apparently balanced translocations at 7p21.2. Hum Mol Genet 1994; 3(8):1405-1408.

[385] Wilkie AO, Yang SP, Summers D, Poole MD, Reardon W, Winter RM. Saethre-Chotzen syndrome associated with balanced translocations involving 7p21: three further families. J Med Genet 1995; 32(3):174-180.

[386] Reid CS, McMorrow LE, McDonald-McGinn DM, Grace KJ, Ramos FJ, Zackai EH, Cohen MM, Jr., Jabs EW. Saethre-Chotzen syndrome with familial translocation at chromosome 7p22. Am J Med Genet 1993; 47(5):637-639.

[387] Johnson D, Horsley SW, Moloney DM, Oldridge M, Twigg SR, Walsh S, Barrow M, Njolstad PR, Kunz J, Ashworth GJ, Wall SA, Kearney L, Wilkie AO. A comprehensive screen for TWIST mutations in patients with craniosynostosis identifies a new microdeletion syndrome of chromosome band 7p21.1. Am J Hum Genet 1998; 63(5):1282-1293.

[388] Krebs I, Weis I, Hudler M, Rommens JM, Roth H, Scherer SW, Tsui LC, Fuchtbauer EM, Grzeschik KH, Tsuji K, Kunz J. Translocation breakpoint maps 5 kb 3' from TWIST in a patient affected with Saethre-Chotzen syndrome. Hum Mol Genet 1997; 6(7):1079-1086.

[389] Marchau FE, Van Roy BC, Parizel PM, Lambert JR, De Canck I, Leroy JG, Gevaert CM, Willems PJ, Dumon JE. Tricho-rhino-phalangeal syndrome type I (TRP I) due to an apparently balanced translocation involving 8q24. Am J Med Genet 1993; 45(4):450-455.

[390] Hou J, Parrish J, Ludecke HJ, Sapru M, Wang Y, Chen W, Hill A, Siegel-Bartelt J, Northrup H, Elder FF, . A 4-megabase YAC contig that spans the Langer-Giedion syndrome region on human chromosome 8q24.1: use in refining the location of the trichorhinophalangeal syndrome and multiple exostoses genes (TRPS1 and EXT1). Genomics 1995; 29(1):87-97.

[391] Duba HC, Doll A, Neyer M, Erdel M, Mann C, Hammerer I, Utermann G, Grzeschik KH. The elastin gene is disrupted in a family with a balanced translocation t(7;16)(q11.23;q13) associated with a variable expression of the Williams-Beuren syndrome. Eur J Hum Genet 2002; 10(6):351-361.

[392] Puissant H, Azoulay M, Serre JL, Piet LL, Junien C. Molecular analysis of a reciprocal translocation t(5;11) (q11;p13) in a WAGR patient. Hum Genet 1988; 79(3):280-282.

[393] Krantz ID, Rand EB, Genin A, Hunt P, Jones M, Louis AA, Graham JM, Jr., Bhatt S, Piccoli DA, Spinner NB. Deletions of 20p12 in Alagille syndrome: frequency and molecular characterization. Am J Med Genet 1997; 70(1):80-86.

[394] Spinner NB, Rand EB, Fortina P, Genin A, Taub R, Semeraro A, Piccoli DA. Cytologically balanced t(2;20) in a two-generation family with alagille syndrome: cytogenetic and molecular studies. Am J Hum Genet 1994; 55(2):238-243.

[395] Oda T, Elkahloun AG, Meltzer PS, Okajima K, Sugiyama K, Wada Y, Chandrasekharappa SC. Identification of a larger than 3 Mb deletion including JAG1 in an Alagille syndrome patient with a translocation t(3;20)(q13.3;p12.2). Hum Mutat 2000; 16(1):92.

[396] Pichon B, Vankerckhove S, Bourrouillou G, Duprez L, Abramowicz MJ. A translocation breakpoint disrupts the ASPM gene in a patient with primary microcephaly. Eur J Hum Genet 2004; 12(5):419-421.

[397] Bache I, Hjorth M, Bugge M, Holstebroe S, Hilden J, Schmidt L, Brondum-Nielsen K, Bruun-Petersen G, Jensen PK, Lundsteen C, Niebuhr E, Rasmussen K, Tommerup N. Systematic re-examination of carriers of balanced reciprocal translocations: a strategy to search for candidate regions for common and complex diseases. Eur J Hum Genet 2006.

[398] Fritz B, Kunz J, Knudsen GP, Louwen F, Kennerknecht I, Eiben B, Orstavik KH, Friedrich U, Rehder H. Situs ambiguus in a female fetus with balanced (X;21) translocation - evidence for functional nullisomy of the ZIC3 gene? Eur J Hum Genet 2004.

[399] Cooke CT, Mulcahy MT, Cullity GJ, Watson M, Srague P. Campomelic dysplasia with sex reversal: morphological and cytogenetic studies of a case. Pathology 1985; 17(3):526-529.

[400] Winer N, Le Caignec C, Quere MP, David A, Boceno M, Aubron F, Joubert M, Boog G, Philippe HJ, Rival JM. Prenatal diagnosis of a cleidocranial dysplasia-like phenotype associated with a de novo balanced t(2q;6q)(q36;q16) translocation. Ultrasound Obstet Gynecol 2003; 22(6):648-651.

[401] Narahara K, Tsuji K, Yokoyama Y, Seino Y. Cleidocranial dysplasia associated with a t(6;18)(p12;q24) translocation. Am J Med Genet 1995; 56(1):119-120.

[402] Brueton LA, Reeve A, Ellis R, Husband P, Thompson EM, Kingston HM. Apparent cleidocranial dysplasia associated with abnormalities of 8q22 in three individuals. Am J Med Genet 1992; 43(3):612-618.

[403] Wilson WG, Kennaugh JM, Kugler JP, Wyandt HE. Reciprocal translocation 14q;21q in a patient with the Brachmann-de Lange syndrome. J Med Genet 1983; 20(6):469-471.

[404] Ireland M, English C, Cross I, Houlsby WT, Burn J. A de novo translocation t(3;17)(q26.3;q23.1) in a child with Cornelia de Lange syndrome. J Med Genet 1991; 28(9):639-640.

[405] Tonkin ET, Smith M, Eichhorn P, Jones S, Imamwerdi B, Lindsay S, Jackson M, Wang TJ, Ireland M, Burn J, Krantz ID, Carr P, Strachan T. A giant novel gene undergoing extensive alternative splicing is severed by a Cornelia de Lange-associated translocation breakpoint at 3q26.3. Hum Genet 2004; 115(2):139-148.

[406] Stefanova M, Zemke K, Dimitrov B, Has C, Kern JS, Bruckner-Tuderman L, Kutsche K. Disruption of ERBB2IP is not associated with dystrophic epidermolysis bullosa in both father and son carrying a balanced 5;13 translocation. J Invest Dermatol 2005; 125(4):700-704.

[407] Balestrazzi P, Baeteman MA, Mattei MG, Mattei JF. Franceschetti syndrome in a child with a de novo balanced translocation (5;13)(q11;p11) and significant decrease of hexosaminidase B. Hum Genet 1983; 64(3):305-308.

[408] Dixon MJ, Haan E, Baker E, David D, McKenzie N, Williamson R, Mulley J, Farrall M, Callen D. Association of Treacher Collins syndrome and translocation 6p21.31/16p13.11: exclusion of the locus from these candidate regions. Am J Hum Genet 1991; 48(2):274-280.

[409] Peng HW, Chou CF, Liang DC. Hereditary cyclic neutropenia in the male members of a Chinese family with inverted Y chromosome. Br J Haematol 2000; 110(2):438-440.

[410] Cousin J, Creusy C, Croquette MF, Vittu G. [Major malformation syndrome and apparently balanced chromosomal abnormality: holoprosencephaly and 5p; 12q translocation]. J Genet Hum 1988; 36(1-2):83-88.

[411] Benzacken B, Siffroi JP, Le Bourhis C, Krabchi K, Joye N, Maschino F, Viguie F, Soulie J, Gonzales M, Migne G, Bucourt M, Encha-Razavi F, Carbillon L, Taillemite JL. Different proximal and distal rearrangements of chromosome 7q associated with holoprosencephaly. J Med Genet 1997; 34(11):899-903.

[412] Petek E, Kroisel PM, Wagner K. Isolation of a 370 kb YAC fragment spanning a translocation breakpoint at 3p14.1 associated with holoprosencephaly. Clin Genet 1998; 54(5):406-412.

[413] Yang SP, Sherman S, Derstine JB, Schonberg SA. Holt-Oram syndrome gene may be on chromosome 20. Pediat.Res. 27, 137A. 1990.
Ref Type: Abstract

[414] Kullmann F, Koch R, Feichtinger W, Giesen H, Schmid M, Grimm T. [Holt-Oram syndrome in combination with reciprocal translocation, lung hypoplasia and cardiomyopathy]. Klin Padiatr 1993; 205(3):185-189.

[415] Froster-Iskenius UG, Hayden MR, Wang HS, Kalousek DK, Horsman D, Pfeiffer RA, Schottky A, Schwinger E. A family with Huntington disease and reciprocal translocation 4;5. Am J Hum Genet 1986; 38(5):759-767.

[416] Holm IA, Huang X, Kunkel LM. Mutational analysis of the PEX gene in patients with X-linked hypophosphatemic rickets. Am J Hum Genet 1997; 60(4):790-797.

[417] Israel J, Lessick M, Szego K, Wong P. Translocation 19;Y in a child with Bannayan-Zonana phenotype. J Med Genet 1991; 28(6):427-428.

[418] Balestrazzi P, Mattei MG, Baeteman MA, Mattei JF, Giraud F. Bilateral retinoblastoma with de novo constitutional balanced translocation t(2;9)(q11;p11). Eur J Pediatr 1984; 141(4):250-251.

[419] Ponzio G, Savin E, Cattaneo G, Ghiotti MP, Marra A, Zuffardi O, Danesino C. Translocation X;13 in a patient with retinoblastoma. J Med Genet 1987; 24(7):431-434.

[420] Hersh JH, Yen FF, Peiper SC, Barch MJ, Yacoub OA, Voss DH, Roberts JL. De novo 1;10 balanced translocation in an infant with thanatophoric dysplasia: a clue to the locus of the candidate gene. J Med Genet 1995; 32(4):293-295.

[421] Sanchez LM, Labarta JD, De Negrotti TC, Migliorini AM. Complex translocation in a boy with trichorhinophalangeal syndrome. J Med Genet 1985; 22(4):314-316.

[422] Booth C, Maurer W. De novo 9:11 translocation in a sporadic case of trichorhinophalangeal syndrome. Pediat.Res. 15, 559. 1981.
Ref Type: Abstract

[423] Dundar M, Lowther G, Colgan J, Ozkul Y, Candemir Z, Saatci C, Kurtoglu S, Watt J, Morrison N. A case with Waardenburg syndrome presenting with two separate translocations--one reciprocal and one complex. Clin Dysmorphol 2001; 10(1):65-66.

[424] Reynolds PA, Powlesland RM, Keen TJ, Inglehearn CF, Cunningham AF, Green ED, Brown KW. Localization of a novel t(1;7) translocation associated with Wilms' tumor predisposition and skeletal abnormalities. Genes Chromosomes Cancer 1996; 17(3):151-155.

[425] Mujica P, Morali A, Vidailhet M, Pierson M, Gilgenkrantz S. A case of Alagille's syndrome with translocation (4;14) (q21;q21). Ann Genet 1989; 32(2):117-119.

[426] Novelli A, Valente EM, Bernardini L, Ceccarini C, Sinibaldi L, Caputo V, Cavalli P, Dallapiccola B. Autosomal dominant Brody disease cosegregates with a chromosomal (2;7)(p11.2;p12.1) translocation in an Italian family. Eur J Hum Genet 2004; 12(7):579-583.

[427] Tuck-Muller CM, Dyken PR, Li S, Chen H, Labbe E, Wertelecki W. Translocation 10;18 in a patient with juvenile neuronal ceroid-lipofuscinosis (Batten disease). Am J Med Genet 1995; 57(2):168-171.

[428] Fryns JP, Kleczkowska A, Smeets E, Thiry P, Geutjens J, Van den Berghe H. Cohen syndrome and de novo reciprocal translocation t(5;7)(q33.1;p15.1). Am J Med Genet 1990; 37(4):546-547.

[429] Van Hove JL, Damme-Lombaerts R, Grunewald S, Peters H, Van Damme B, Fryns JP, Arnout J, Wevers R, Baumgartner ER, Fowler B. Cobalamin disorder Cbl-C presenting with late-onset thrombotic microangiopathy. Am J Med Genet 2002; 111(2):195-201.

[430] Walder RY, Shalev H, Brennan TM, Carmi R, Elbedour K, Scott DA, Hanauer A, Mark AL, Patil S, Stone EM, Sheffield VC. Familial hypomagnesemia maps to chromosome 9q, not to the X chromosome: genetic linkage mapping and analysis of a balanced translocation breakpoint. Hum Mol Genet 1997; 6(9):1491-1497.

[431] Chery M, Biancalana V, Philippe C, Malpuech G, Carla H, Gilgenkrantz S, Mandel JL, Hanauer A. Hypomagnesemia with secondary hypocalcemia in a female with balanced X;9 translocation: mapping of the Xp22 chromosome breakpoint. Hum Genet 1994; 93(5):587-591.

[432] Goobie S, Morrison J, Ginzberg H, Ellis L, Corey M, Masuno M, Imaizumi K, Kuroki Y, Fujiwara TM, Morgan K, Durie PR, Rommens JM. Exclusion of linkage of Shwachman-Diamond syndrome to chromosome regions 6q and 12q implicated by a de novo translocation. Am J Med Genet 1999; 85(2):171-174.

[433] Ikegawa S, Masuno M, Kumano Y, Okawa A, Isomura M, Koyama K, Okui K, Makita Y, Sasaki M, Kohdera U, Okuda M, Koyama H, Ohashi H, Tajiri H, Imaizumi K, Nakamura Y. Cloning of translocation breakpoints associated with Shwachman syndrome and identification of a candidate gene. Clin Genet 1999; 55(6):466-472.

[434] Alley TL, Scherer SW, Huizenga JJ, Tsui LC, Wallace MR. Physical mapping of the chromosome 7 breakpoint region in an SLOS patient with t(7;20) (q32.1;q13.2). Am J Med Genet 1997; 68(3):279-281.

[435] Scherer SW, Soder S, Duvoisin RM, Huizenga JJ, Tsui LC. The human metabotropic glutamate receptor 8 (GRM8) gene: a disproportionately large gene located at 7q31.3-q32.1. Genomics 1997; 44(2):232-236.

[436] Karadeniz N, Zenciroglu A, Gurer YK, Senbil N, Karadeniz Y, Topalolu H. De novo translocation t(5;6)(q35;q21) in an infant with Walker-Warburg syndrome. Am J Med Genet 2002; 109(1):67-69.

[437] Laml T, Preyer O, Umek W, Huber J, Hengstschlager M. Chromosomal translocation t(10;11)(q26;q13) in a woman with combined pituitary hormone deficiency. Gynecol Obstet Invest 2004; 58(2):114-116.

[438] Wang Q, Timur AA, Szafranski P, Sadgephour A, Jurecic V, Cowell J, Baldini A, Driscoll DJ. Identification and molecular characterization of de novo translocation t(8;14)(q22.3;q13) associated with a vascular and tissue overgrowth syndrome. Cytogenet Cell Genet 2001; 95(3-4):183-188.

[439] Clarke RA, Singh S, McKenzie H, Kearsley JH, Yip MY. Familial Klippel-Feil syndrome and paracentric inversion inv(8)(q22.2q23.3). Am J Hum Genet 1995; 57(6):1364-1370.

[440] Schrander-Stumpel CT, Fryns JP, Hamers GG. Sotos syndrome and de novo balanced autosomal translocation (t(3;6)(p21;p21)). Clin Genet 1990; 37(3):226-229.

[441] Tamaki K, Horie K, Go T, Okuno T, Mikawa H, Hua ZY, Abe T. Sotos syndrome with a balanced reciprocal translocation t(2;12)(q33.3;q15). Ann Genet 1989; 32(4):244-246.

[442] Ireland M, English C, Cross I, Houlsby WT, Burn J. A de novo translocation t(3;17)(q26.3;q23.1) in a child with Cornelia de Lange syndrome. J Med Genet 1991; 28(9):639-640.

[443] Wilson WG, Kennaugh JM, Kugler JP, Wyandt HE. Reciprocal translocation 14q;21q in a patient with the Brachmann-de Lange syndrome. J Med Genet 1983; 20(6):469-471.

[444] Steinbach P, Adkins WN, Jr., Caspar H, Dumars KW, Gebauer J, Gilbert EF, Grimm T, Habedank M, Hansmann I, Herrmann J, Kaveggia EG, Langenbeck U, Meisner LF, Najafzadeh TM, Opitz JM, Palmer CG, Peters HH, Scholz W, Tavares AS, Wiedeking C. The dup(3q) syndrome: report of eight cases and review of the literature. Am J Med Genet 1981; 10(2):159-177.

[445] Wilson GN, Dasouki M, Barr M, Jr. Further delineation of the dup(3q) syndrome. Am J Med Genet 1985; 22(1):117-123.

[446] Tonkin ET, Smith M, Eichhorn P, Jones S, Imamwerdi B, Lindsay S, Jackson M, Wang TJ, Ireland M, Burn J, Krantz ID, Carr P, Strachan T. A giant novel gene undergoing extensive alternative splicing is severed by a Cornelia de Lange-associated translocation breakpoint at 3q26.3. Hum Genet 2004; 115(2):139-148.

[447] Tonkin ET, Wang TJ, Lisgo S, Bamshad MJ, Strachan T. NIPBL, encoding a homolog of fungal Scc2-type sister chromatid cohesion proteins and fly Nipped-B, is mutated in Cornelia de Lange syndrome. Nat Genet 2004; 36(6):636-641.

[448] Krantz ID, McCallum J, DeScipio C, Kaur M, Gillis LA, Yaeger D, Jukofsky L, Wasserman N, Bottani A, Morris CA, Nowaczyk MJ, Toriello H, Bamshad MJ, Carey JC, Rappaport E, Kawauchi S, Lander AD, Calof AL, Li HH, Devoto M, Jackson LG. Cornelia de Lange syndrome is caused by mutations in NIPBL, the human homolog of Drosophila melanogaster Nipped-B. Nat Genet 2004; 36(6):631-635.

[449] Gillis LA, McCallum J, Kaur M, DeScipio C, Yaeger D, Mariani A, Kline AD, Li HH, Devoto M, Jackson LG, Krantz ID. NIPBL mutational analysis in 120 individuals with Cornelia de Lange syndrome and evaluation of genotype-phenotype correlations. Am J Hum Genet 2004; 75(4):610-623.

[450] Gillis LA, McCallum J, Kaur M, DeScipio C, Yaeger D, Mariani A, Kline AD, Li HH, Devoto M, Jackson LG, Krantz ID. NIPBL mutational analysis in 120 individuals with Cornelia de Lange syndrome and evaluation of genotype-phenotype correlations. Am J Hum Genet 2004; 75(4):610-623.

[451] Guan XY, Zhang H, Bittner M, Jiang Y, Meltzer P, Trent J. Chromosome arm painting probes. Nat Genet 1996; 12(1):10-11.

[452] Boyle S, Gilchrist S, Bridger JM, Mahy NL, Ellis JA, Bickmore WA. The spatial organization of human chromosomes within the nuclei of normal and emerin-mutant cells. Hum Mol Genet 2001; 10(3):211-219.

[453] Fantes J, Ragge NK, Lynch SA, McGill NI, Collin JR, Howard-Peebles PN, Hayward C, Vivian AJ, Williamson K, van Heyningen V, FitzPatrick DR. Mutations in SOX2 cause anophthalmia. Nat Genet 2003; 33(4):461-463.

[454] Liehr T, Grehl H, Rautenstrauss B. FISH analysis of interphase nuclei extracted from paraffin-embedded tissue . Techincal Tips Online 1, T00027. 1996.
Ref Type: Abstract

[455] Guan XY, Zhang H, Bittner M, Jiang Y, Meltzer P, Trent J. Chromosome arm painting probes. Nat Genet 1996; 12(1):10-11.

[456] Lorentz CP, Jalal SM, Thompson DM, Babovic-Vuksanovic D. Mosaic r(13) resulting in large deletion of chromosome 13q in a newborn female with multiple congenital anomalies. Am J Med Genet 2002; 111(1):61-67.

[457] Ohashi H, Ishikiriyama S, Fukushima Y. New diagnostic method for Pallister-Killian syndrome: detection of i(12p) in interphase nuclei of buccal mucosa by fluorescence in situ hybridization. Am J Med Genet 1993; 45(1):123-128.

[458] Firth HV, Boyd PA, Chamberlain PF, MacKenzie IZ, Morriss-Kay GM, Huson SM. Analysis of limb reduction defects in babies exposed to chorionic villus sampling. Lancet 1994; 343(8905):1069-1071.

[459] Tomkins D, Hunter A, Roberts M. Cytogenetic findings in Roberts-SC phocomelia syndrome(s). Am J Med Genet 1979; 4(1):17-26.

[460] Murray RS, Keeling JW, Ellis PM, FitzPatrick DR. Symmetrical upper limb peromelia and lower limb phocomelia associated with a de novo apparently balanced reciprocal translocation: 46,XX,t(2; 12)(p25.1;q24.1). Clin Dysmorphol 2002; 11(2):87-90.

[461] Bamshad M, Lin RC, Law DJ, Watkins WC, Krakowiak PA, Moore ME, Franceschini P, Lala R, Holmes LB, Gebuhr TC, Bruneau BG, Schinzel A, Seidman JG, Seidman CE, Jorde LB. Mutations in human TBX3 alter limb,

apocrine and genital development in ulnar-mammary syndrome. Nat Genet 1997; 16(3):311-315.

[462] Bamshad M, Lin RC, Law DJ, Watkins WC, Krakowiak PA, Moore ME, Franceschini P, Lala R, Holmes LB, Gebuhr TC, Bruneau BG, Schinzel A, Seidman JG, Seidman CE, Jorde LB. Mutations in human TBX3 alter limb, apocrine and genital development in ulnar-mammary syndrome. Nat Genet 1997; 16(3):311-315.

[463] Basson CT, Huang T, Lin RC, Bachinsky DR, Weremowicz S, Vaglio A, Bruzzone R, Quadrelli R, Lerone M, Romeo G, Silengo M, Pereira A, Krieger J, Mesquita SF, Kamisago M, Morton CC, Pierpont ME, Muller CW, Seidman JG, Seidman CE. Different TBX5 interactions in heart and limb defined by Holt-Oram syndrome mutations. Proc Natl Acad Sci U S A 1999; 96(6):2919-2924.

[464] HOLT M, ORAM S. Familial heart disease with skeletal malformations. Br Heart J 1960; 22:236-242.

[465] Basson CT, Bachinsky DR, Lin RC, Levi T, Elkins JA, Soults J, Grayzel D, Kroumpouzou E, Traill TA, Leblanc-Straceski J, Renault B, Kucherlapati R, Seidman JG, Seidman CE. Mutations in human TBX5 [corrected] cause limb and cardiac malformation in Holt-Oram syndrome. Nat Genet 1997; 15(1):30-35.

[466] Li QY, Newbury-Ecob RA, Terrett JA, Wilson DI, Curtis AR, Yi CH, Gebuhr T, Bullen PJ, Robson SC, Strachan T, Bonnet D, Lyonnet S, Young ID, Raeburn JA, Buckler AJ, Law DJ, Brook JD. Holt-Oram syndrome is caused by mutations in TBX5, a member of the Brachyury (T) gene family. Nat Genet 1997; 15(1):21-29.

[467] Basson CT, Bachinsky DR, Lin RC, Levi T, Elkins JA, Soults J, Grayzel D, Kroumpouzou E, Traill TA, Leblanc-Straceski J, Renault B, Kucherlapati R, Seidman JG, Seidman CE. Mutations in human TBX5 [corrected] cause limb and cardiac malformation in Holt-Oram syndrome. Nat Genet 1997; 15(1):30-35.

[468] Takeuchi JK, Koshiba-Takeuchi K, Suzuki T, Kamimura M, Ogura K, Ogura T. Tbx5 and Tbx4 trigger limb initiation through activation of the Wnt/Fgf signaling cascade. Development 2003; 130(12):2729-2739.

[469] Witters I, Delattin P, Moerman P, Fryns JP. Symmetrical tetraphocomelia without associated congenital malformations: a nosological dilemma. Am J Med Genet 2002; 113(2):227-228.

[470] Witters I, Delattin P, Moerman P, Fryns JP. Symmetrical tetraphocomelia without associated congenital malformations: a nosological dilemma. Am J Med Genet 2002; 113(2):227-228.

[471] Saunders J. The proximo-distal sequence of origin of the parts of the chick wing and the role of the ectoderm. J Exp Zool 1948; 108:363-403.

[472] Summerbell D. Interaction between the proximo-distal and antero-posterior co-ordinates of positional value during the specification of positional information in the early development of the chick limb-bud. J Embryol Exp Morphol 1974; 32(1):227-237.

[473] Summerbell D, Lewis JH, Wolpert L. Positional information in chick limb morphogenesis. Nature 1973; 244(5417):492-496.

[474] Wolpert L. Positional information revisited. Development 1989; 107 Suppl:3-12.

[475] Summerbell D, Lewis JH, Wolpert L. Positional information in chick limb morphogenesis. Nature 1973; 244(5417):492-496.

[476] Summerbell D. A quantitative analysis of the effect of excision of the AER from the chick limb-bud. J Embryol Exp Morphol 1974; 32(3):651-660.

[477] Dudley AT, Ros MA, Tabin CJ. A re-examination of proximodistal patterning during vertebrate limb development. Nature 2002; 418(6897):539-544.

[478] Saunders J, Gasseling M. Ectoderm-mesenchymal interactions in the origin of limb symmetry. Epithelial-Mesencymal interactions. Baltimore: Williams and Wilkins, 1968: 78-97.

[479] MacCabe JA, Errick J, Saunders JW, Jr. Ectodermal control of the dorsoventral axis in the leg bud of the chick embryo. Dev Biol 1974; 39(1):69-82.

[480] Thumkeo D, Keel J, Ishizaki T, Hirose M, Nonomura K, Oshima H, Oshima M, Taketo MM, Narumiya S. Targeted disruption of the mouse rho-associated kinase 2 gene results in intrauterine growth retardation and fetal death. Mol Cell Biol 2003; 23(14):5043-5055.

[481] Thumkeo D, Keel J, Ishizaki T, Hirose M, Nonomura K, Oshima H, Oshima M, Taketo MM, Narumiya S. Targeted disruption of the mouse rho-associated kinase 2 gene results in intrauterine growth retardation and fetal death. Mol Cell Biol 2003; 23(14):5043-5055.

[482] Gantz I, Konda Y, Yang YK, Miller DE, Dierick HA, Yamada T. Molecular cloning of a novel receptor (CMKLR1) with homology to the chemotactic factor receptors. Cytogenet Cell Genet 1996; 74(4):286-290.

[483] Martensson UE, Owman C, Olde B. Genomic organization and promoter analysis of the gene encoding the mouse chemoattractant-like receptor, CMKLR1. Gene 2004; 328:167-176.

[484] Meder W, Wendland M, Busmann A, Kutzleb C, Spodsberg N, John H, Richter R, Schleuder D, Meyer M, Forssmann WG. Characterization of human circulating TIG2 as a ligand for the orphan receptor ChemR23. FEBS Lett 2003; 555(3):495-499.

[485] Wittamer V, Franssen JD, Vulcano M, Mirjolet JF, Le Poul E, Migeotte I, Brezillon S, Tyldesley R, Blanpain C, Detheux M, Mantovani A, Sozzani S,

Vassart G, Parmentier M, Communi D. Specific recruitment of antigen-presenting cells by chemerin, a novel processed ligand from human inflammatory fluids. J Exp Med 2003; 198(7):977-985.

[486] Adams AE, Abu-Amer Y, Chappel J, Stueckle S, Ross FP, Teitelbaum SL, Suva LJ. 1,25 dihydroxyvitamin D3 and dexamethasone induce the cyclooxygenase 1 gene in osteoclast-supporting stromal cells. J Cell Biochem 1999; 74(4):587-595.

[487] Meder W, Wendland M, Busmann A, Kutzleb C, Spodsberg N, John H, Richter R, Schleuder D, Meyer M, Forssmann WG. Characterization of human circulating TIG2 as a ligand for the orphan receptor ChemR23. FEBS Lett 2003; 555(3):495-499.

[488] Methner A, Hermey G, Schinke B, Hermans-Borgmeyer I. A novel G protein-coupled receptor with homology to neuropeptide and chemoattractant receptors expressed during bone development. Biochem Biophys Res Commun 1997; 233(2):336-342.

[489] Methner A, Hermey G, Schinke B, Hermans-Borgmeyer I. A novel G protein-coupled receptor with homology to neuropeptide and chemoattractant receptors expressed during bone development. Biochem Biophys Res Commun 1997; 233(2):336-342.

[490] Methner A, Hermey G, Schinke B, Hermans-Borgmeyer I. A novel G protein-coupled receptor with homology to neuropeptide and chemoattractant receptors expressed during bone development. Biochem Biophys Res Commun 1997; 233(2):336-342.

[491] Summerbell D. The effect of local application of retinoic acid to the anterior margin of the developing chick limb. J Embryol Exp Morphol 1983; 78:269-289.

[492] Brockes JP. Amphibian limb regeneration: rebuilding a complex structure. Science 1997; 276(5309):81-87.

[493] Crawford K, Stocum DL. Retinoic acid proximalizes level-specific properties responsible for intercalary regeneration in axolotl limbs. Development 1988; 104(4):703-712.

[494] Maden M. Vitamin A and pattern formation in the regenerating limb. Nature 1982; 295(5851):672-675.

[495] Tamura K, Yokouchi Y, Kuroiwa A, Ide H. Retinoic acid changes the proximodistal developmental competence and affinity of distal cells in the developing chick limb bud. Dev Biol 1997; 188(2):224-234.

[496] Mercader N, Leonardo E, Piedra ME, Martinez A, Ros MA, Torres M. Opposing RA and FGF signals control proximodistal vertebrate limb development through regulation of Meis genes. Development 2000; 127(18):3961-3970.

[497] Niederreither K, Vermot J, Schuhbaur B, Chambon P, Dolle P. Embryonic retinoic acid synthesis is required for forelimb growth and anteroposterior patterning in the mouse. Development 2002; 129(15):3563-3574.

[498] Niederreither K, Vermot J, Schuhbaur B, Chambon P, Dolle P. Embryonic retinoic acid synthesis is required for forelimb growth and anteroposterior patterning in the mouse. Development 2002; 129(15):3563-3574.

[499] Mic FA, Sirbu IO, Duester G. Retinoic acid synthesis controlled by Raldh2 is required early for limb bud initiation and then later as a proximodistal signal during apical ectodermal ridge formation. J Biol Chem 2004; 279(25):26698-26706.

[500] Mic FA, Sirbu IO, Duester G. Retinoic acid synthesis controlled by Raldh2 is required early for limb bud initiation and then later as a proximodistal signal during apical ectodermal ridge formation. J Biol Chem 2004; 279(25):26698-26706.

[501] Niederreither K, Vermot J, Schuhbaur B, Chambon P, Dolle P. Embryonic retinoic acid synthesis is required for forelimb growth and anteroposterior patterning in the mouse. Development 2002; 129(15):3563-3574.

[502] Niederreither K, Vermot J, Schuhbaur B, Chambon P, Dolle P. Embryonic retinoic acid synthesis is required for forelimb growth and anteroposterior patterning in the mouse. Development 2002; 129(15):3563-3574.

[503] Abu-Abed S, Dolle P, Metzger D, Beckett B, Chambon P, Petkovich M. The retinoic acid-metabolizing enzyme, CYP26A1, is essential for normal hindbrain patterning, vertebral identity, and development of posterior structures. Genes Dev 2001; 15(2):226-240.

[504] MacLean G, Abu-Abed S, Dolle P, Tahayato A, Chambon P, Petkovich M. Cloning of a novel retinoic-acid metabolizing cytochrome P450, Cyp26B1, and comparative expression analysis with Cyp26A1 during early murine development. Mech Dev 2001; 107(1-2):195-201.

[505] Yashiro K, Zhao X, Uehara M, Yamashita K, Nishijima M, Nishino J, Saijoh Y, Sakai Y, Hamada H. Regulation of retinoic acid distribution is required for proximodistal patterning and outgrowth of the developing mouse limb. Dev Cell 2004; 6(3):411-422.

[506] Niederreither K, Vermot J, Schuhbaur B, Chambon P, Dolle P. Embryonic retinoic acid synthesis is required for forelimb growth and anteroposterior patterning in the mouse. Development 2002; 129(15):3563-3574.

[507] Yashiro K, Zhao X, Uehara M, Yamashita K, Nishijima M, Nishino J, Saijoh Y, Sakai Y, Hamada H. Regulation of retinoic acid distribution is required for proximodistal patterning and outgrowth of the developing mouse limb. Dev Cell 2004; 6(3):411-422.

[508] Lee CT, Li L, Takamoto N, Martin JF, Demayo FJ, Tsai MJ, Tsai SY. The nuclear orphan receptor COUP-TFII is required for limb and skeletal muscle development. Mol Cell Biol 2004; 24(24):10835-10843.

[509] Potter E. Bilateral renal agenesis. J Pediatr 1946; 26:68-76.

[510] Potter E. Facial characteristics of infants with bilateral renal agenesis. Am J Obstet Gynecol 1946; 51:885-888.

[511] Joss S, Howatson A, Trainer A, Whiteford M, FitzPatrick DR. De novo translocation (1;2)(q32; p25) associated with bilateral renal dysplasia. Clin Genet 2003; 63(3):239-240.

[512] Biri A, Karaoguz MY, Ince GD, Ergun MA, Menevse S, Bingol B. Double aneuploidy involving trisomy 7 with Potter sequence. Eur J Med Genet 2005; 48(1):67-73.

[513] Yunis E, Ramirez E, Uribe JG. Full trisomy 7 and Potter syndrome. Hum Genet 1980; 54(1):13-18.

[514] Pflueger SM, Scott CI, Jr., Moore CM. Trisomy 7 and Potter syndrome. Clin Genet 1984; 25(6):543-548.

[515] Devriendt K, Moerman P, Van Schoubroeck D, Vandenberghe K, Fryns JP. Chromosome 22q11 deletion presenting as the Potter sequence. J Med Genet 1997; 34(5):423-425.

[516] Fryns JP, Kleczkowska A, Jaeken J, Van den Berghe H. Ring chromosome 4 mosaicism and Potter sequence. Ann Genet 1988; 31(2):120-122.

[517] Su PH, Kuo PL, Chen SJ, Hung HM, Yi TH, Chen JY. De novo 4p-syndrome with oligohydramnios sequence. J Formos Med Assoc 2003; 102(9):647-649.

[518] Clark RD. Del(15)(q22q24) syndrome with Potter sequence. Am J Med Genet 1984; 19(4):703-705.

[519] Brewer C, Holloway S, Zawalnyski P, Schinzel A, FitzPatrick D. A chromosomal deletion map of human malformations. Am J Hum Genet 1998; 63(4):1153-1159.

[520] Schinzel A. Human Cytogenetics Database. Oxford Medical Databases Series. Oxford Univ. Press, Electronic Publishing (pub.), 1994.

[521] Yosypiv IV, El Dahr SS. Role of the renin-angiotensin system in the development of the ureteric bud and renal collecting system. Pediatr Nephrol 2005; 20(9):1219-1229.

[522] Pearsall N, Bhattacharya G, Wisecarver J, Adams J, Cosgrove D, Kimberling W. Usherin expression is highly conserved in mouse and human tissues. Hear Res 2002; 174(1-2):55-63.

[523] Bhattacharya G, Miller C, Kimberling WJ, Jablonski MM, Cosgrove D. Localization and expression of usherin: a novel basement membrane protein defective in people with Usher's syndrome type IIa. Hear Res 2002; 163(1-2):1-11.

[524] Heard DJ, Norby PL, Holloway J, Vissing H. Human ERRgamma, a third member of the estrogen receptor-related receptor (ERR) subfamily of orphan nuclear receptors: tissue-specific isoforms are expressed during development and in the adult. Mol Endocrinol 2000; 14(3):382-392.

[525] Huppunen J, Wohlfahrt G, Aarnisalo P. Requirements for transcriptional regulation by the orphan nuclear receptor ERRgamma. Mol Cell Endocrinol 2004; 219(1-2):151-160.

[526] Sanyal S, Matthews J, Bouton D, Kim HJ, Choi HS, Treuter E, Gustafsson JA. Deoxyribonucleic acid response element-dependent regulation of transcription by orphan nuclear receptor estrogen receptor-related receptor gamma. Mol Endocrinol 2004; 18(2):312-325.

[527] Hatini V, Huh SO, Herzlinger D, Soares VC, Lai E. Essential role of stromal mesenchyme in kidney morphogenesis revealed by targeted disruption of Winged Helix transcription factor BF-2. Genes Dev 1996; 10(12):1467-1478.

[528] Qiao J, Uzzo R, Obara-Ishihara T, Degenstein L, Fuchs E, Herzlinger D. FGF-7 modulates ureteric bud growth and nephron number in the developing kidney. Development 1999; 126(3):547-554.

[529] Shen LX, Basilion JP, Stanton VP, Jr. Single-nucleotide polymorphisms can cause different structural folds of mRNA. Proc Natl Acad Sci U S A 1999; 96(14):7871-7876.

[530] Capon F, Allen MH, Ameen M, Burden AD, Tillman D, Barker JN, Trembath RC. A synonymous SNP of the corneodesmosin gene leads to increased mRNA stability and demonstrates association with psoriasis across diverse ethnic groups. Hum Mol Genet 2004; 13(20):2361-2368.

[531] Titorenko VI, Rachubinski RA. The peroxisome: orchestrating important developmental decisions from inside the cell. J Cell Biol 2004; 164(5):641-645.

[532] Kersten S, Desvergne B, Wahli W. Roles of PPARs in health and disease. Nature 2000; 405(6785):421-424.